THE PREDICTION OF PILOT OPINION RATINGS USING OPTIMAL AND SUB-OPTIMAL PILOT MODELS

THESIS

Craig R. Edkins, Captain, USAF
AFIT/GAE/ENY/94M-2

Approved for public release; distribution unlimited

DEPARTMENT OF THE AIR FORCE
AIR UNIVERSITY
AIR FORCE INSTITUTE OF TECHNOLOGY

Wright-Patterson Air Force Base, Ohio

AFIT/GAE/ENY/94M-2

THE PREDICTION OF PILOT OPINION RATINGS USING OPTIMAL AND SUB-OPTIMAL PILOT MODELS

THESIS

Craig R. Edkins, Captain, USAF
AFIT/GAE/ENY/94M-2

REPORT DOCUMENTATION PAGE

March 1994 | Master's Thesis

THE PREDICTION OF PILOT OPINION RATINGS USING OPTIMAL AND SUB-OPTIMAL PILOT MODELS

Craig R. Edkins, Captain, USAF

Air Force Institute of Technology
Wright-Patterson AFB OH 45433-6583

AFIT/GAE/ENY/94M-2

Air Force Flight Dynamics Directorate
WL/FIGC
Wright-Patterson AFB OH 45433-6503

N/A

APPROVED FOR PUBLIC RELEASE;
DISTRIBUTION UNLIMITED

This study details the development of a sub-optimal pilot model that blended the classical and optimal pilot model approaches in an attempt to achieve the advantages of each. This model used a numerical solution to the linear quadratic Gaussian problem to find the pilot gain, lead, and lag values that minimized a performance index consisting of task error and control usage. This development was conducted in four phases. First, an optimal pilot model developed by Systems Technology, Incorporated, was analyzed in detail. This analysis included a step-by-step example problem to clarify the model's logic and an in-depth sensitivity analysis of the model's parameters. Second, a ground and airborne evaluation of human pilot response was conducted using the Calspan variable stability Lear II aircraft. Primary pilot response parameters were recorded and examined using statistical and Fourier transform analysis in an attempt to provide insight into human pilot response. Third, a numerical solution to the linear quadratic Gaussian control problem that allows the compensator form to be predetermined was derived. Finally, the sub-optimal pilot model was developed and an analysis of the model's parameters was conducted.

PILOT MODELING; OPTIMAL PILOT MODELING; FLYING QUALITIES
HUMAN PILOT RESPONSE; REDUCED ORDER COMPENSATION

218

UNCLASSIFIED | UNCLASSIFIED | UNCLASSIFIED | UL

NOTICE

When government drawings, specifications, or other data are used for any purpose other than in connection with a definitely government-related procurement, the United States government incurs no responsibility or any obligation whatsoever. The fact that the government may have formulated or in any way supplied the said drawing, specification, or other data, is not to be regarded by implication, or otherwise in any manner construed, as licensing the holder, or any other person or corporation; or as conveying any rights or permission to manufacture, use, or sell any patented invention that may in any way be related thereto.

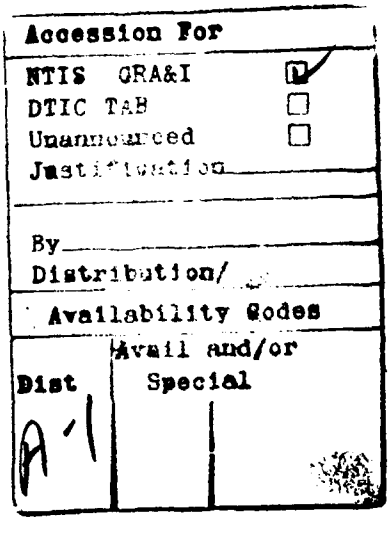

AFIT/GAE/ENY/94M-2

THE PREDICTION OF PILOT OPINION RATINGS USING OPTIMAL AND SUB-OPTIMAL PILOT MODELS

THESIS

Presented to the Faculty of the School of Graduate Engineering

of the Air Force Institute of Technology

Air University

In Partial Fulfillment of the

Requirements for the Degree of

Master of Science in Aeronautical Engineering

Craig R. Edkins, B.S., M.B.A.

Captain, USAF

March 1994

Preface

The purpose of this thesis was to develop a pilot model that combined the intuitive nature of classical pilot models with the optimal nature of modern pilot models. This thesis is divided into six sections. First, general background information is given. Second, an optimal pilot model, developed by Systems Technology, Incorporated, is analyzed in detail. Third, a flight test designed to provide insight into human pilot behavior during ground and airborne tracking tasks is described in detail. Fourth, a numerical solution to the linear quadratic Gaussian (LQG) problem is derived. This technique allows the compensator form to be predetermined. Fifth, a sub-optimal pilot model is presented. This model uses the numerical LQG approach to restrict the optimal pilot model solution to the classical pilot model form. Finally, the conclusions and recommendations of this thesis are summarized.

This research was accomplished under the joint Air Force Institute of Technology -- USAF Test Pilot School program. I am grateful for the unique opportunity this program provided. This effort would not have been possible without the assistance of several people. I would like to thank my advisors, Dr. Brad Liebst and Lt. Col. (Dr.) Daniel Gleason, for providing assistance and motivation during this extended program. I also wish to thank the members of my test management project team, Capt. Benjamin Coffey, Capt. Darcy Granley (CF), Capt. John Kruzinauskas, Jr., and Capt. Mary McNeely, for their invaluable flight test assistance. Finally, and most importantly, I wish to thank my wife, Karen, and daughter, Aubrey, for their support and understanding during this three year ordeal.

Table of Contents

Page

Page

Page

List of Figures

Figure **Page**

Figure **Page**

Figure **Page**

Figure **Page**

Figure **Page**

List of Tables

Table **Page**

List of Symbols

General

deg	Degree
g	Acceleration Due to Gravity (32.2 feet per second per second)
in	Inch
lb	Pound
t	Time
$\forall$	All
λ_i (A)	Eigenvalues of A

Pilot Modeling

Y_p	Pilot Describing Function
Y_C	Controlled Element (Aircraft) Dynamics
s, jω	Laplace Variable for Random Input
K_p	Pilot Gain
T_L	Pilot Lead Time Constant
T_I	*Pilot* Lag Time Constant
τ	Pilot Delay
T_K	Very Low Frequency Pilot Lead Time Constant
T'_K	Very Low Frequency Pilot Lag Time Constant
T_{N1}	Neuromuscular Time Constant
ω_N	High Frequency Neuromuscular Natural Frequency
ζ_N	High Frequency Neuromuscular Damping Ratio
T_N	First Order Approximation of Neuromuscular Time Constant
T_{wp}	Washout Time Constant in Error Feedback Loop
T_{wr}	Washout Time Constant in Error Rate Feedback Loop
K_{p1}	Error Feedback Gain
K_{p2}	Error Rate Feedback Gain
ξ_m	Muscular Noise
ξ_o	Observation Noise
F_s	Stick Force
δ_s	Stick Deflection
δ_c	Commanded Stick Deflection
F_{es}	Longitudinal Stick Force
δ_{es}	Longitudinal Stick Displacement
F_{as}	Lateral Stick Force
δ_{as}	Lateral Stick Displacement
ζ_{sp}	Short Period Damping Ratio

ω_{sp}	Short Period Natural Frequency
T_R	Roll Mode Time Constant
δ_e	Elevator Position
δ_a	Aileron Position
θ	Pitch Angle
θ_c	Commanded Pitch Angle
e	Task Error
$\dot{e}$	Task Error Rate
$\dot{\beta}$	Sideslip Rate
r	Input

Sum-of-Sines Task

K	Task Gain
A_i	Task Amplitudes
ω_i	Task Frequencies
ϕ_i	Task Phases

Regression Analysis

C_{x1}	Root Mean Square Tracking Error Coefficient
C_{x2}	Normalized Root Mean Square Stick or Stick Rate Coefficient
C	Regression Constant
R^2	Regression Variance

State Space Theory

A,B,C,D,E	State Space Matrices where: $\dot{x} = Ax + Bu + Ew$ *and* $y = Cx + Du$
P_i	State Space Representation: $P_i = \left[\begin{array}{c\|c} A_i & B_i \\ \hline C_i & D_i \end{array}\right]$
Y_C	Controlled Element (Plant) Describing Function
A_C, B_C, C_C, D_C	Controlled Element (Plant) State Space Matrices
$Y_\Gamma(s)$, $\Gamma(s)$	Task or Forcing Function Dynamics
A_Γ, B_Γ, C_Γ, D_Γ	Coloring Filoter State Space Matrices
Γ	Disturbance Noise Distribution Matrix (No Coloring Filter)
$Y_{KLQG}(s)$	Optimal LQG Compensator
K	Compensator
A_K, B_K, C_K, D_K	Compensator State Space Matrices
x(t)	State Vector
$\hat{x}(t)$	Estimated State Vector
u(t)	Control Vector

$\dot{u}(t)$	Control Rate Vector
y(t)	Output Vector
x_C	Controlled Element (Plant) State Vector
x_G	Plant and Filter State Vector
x_K	Compensator State Vector
J	Performance Index
J_{min}	Minimum Performance Index
Q,Q'	State Deviation or Error Weighting Matrix
R	Control or Control Rate Weighting Matrix
Q_c	State Deviation Weighting (Linear Quadratic Regulator Problem)
R_c	Control Weighting (Linear Quadratic Regulator Problem)
Q_o	Disturbance Noise Intensity
R_o,R_f	Measurement Noise Intensity
Q_n	Noise Intensity Matrix = diag{Q_o,R_o}
Q_f	Standard LQG Noise Intensity Matrix (C^TQ_oC)
η	Measurement or Observation Noise
V_η	Measurement or Observation Noise Intensity
$\xi(t)$	Process or Disturbance Noise
Σ_y	Forcing Function Power Spectral Density
Σ_v,W_w,w(t)	Zero Mean, Uncorrelated White Gaussian Noise
W_c	Colored Noise
E{ }	Expected Value
X	Covariance Matrix
X,Y	Autocorrelation Matrices
Σ,P	Algebraic Riccati Equation Solutions
K_c, K_{c1}, K_{c2}	Linear Quadratic Regulator Gains
f	Number of Filter States
m	Number of Compensator States
n	Number of Plant and Filter States
o	Length of Control Vector
p	Number of Plant States
I	Identity Matrix
c(i)	Compensator Coefficient Vector
cmin	Optimal Compensator Coefficient Vector
c0	Initial Compensator Coefficient Vector
σ_e^2	Root Mean Square Magnitude of Task Error
G^*	Augmented Plant

STI Optimal Pilot Model

Y_P	Pilot Describing Function
Y_C	Controlled Element (Aircraft) Dynamics
Y_w	Task Forcing Function

q	Error Weighting - Scalar
g	Control Rate Weighting - Scalar
g_i	Initial Guess for Control Rate Weighting
V_w	Task Forcing Function Driving Noise Intensity
V_{yi}	Driving Noise Intensity of i^{th} Output
V_{y1i}	Initial Noise Intensity for Error
V_{y2i}	Initial Noise Intensity for Error Rate
V_u	Motor Noise Intensity
V_{ui}	Initial Motor Noise Intensity
ρ_{yi}	Observation Noise Ratio of i^{th} Output
ρ_{y1}	Observation Noise Ratio for Error
ρ_{y2}	Observation Noise Ratio for Error Rate
ρ_u	Motor Noise Ratio
σ_{yi}	Standard Deviation of i^{th} Output
σ_u	Standard Deviation of Control
σ^2_c	Task Forcing Function Root Mean Square Amplitude
ω_w	Forcing Function Bandwidth (Zero dB Crossover Frequency)
T_i	Visual Indifference Threshold of i^{th} Output
T_{y1}	Visual Indifference Threshold for Task Error
T_{y2}	Visual Indifference Threshold for Task Error Rate
f	Fractional Attention Parameter
E	Error Function (erf)
δ'_e	Control Input Before Muscular Lag

List of Abbreviations

AFB	Air Force Base
AFFTC	Air Force Flight Test Center
CF	Canadian Forces
C-H Rating	Cooper-Harper Rating
dB	decibels
HUD	Head-Up Display
IBM	International Business Machines
KIAS	Knots, Indicated Airspeed
LAMARS	Large Amplitude Multi-Mode Aerospace Research Simulator
LQG	Linear Quadratic Gaussian
LQR	Linear Quadratic Regulator
MSL	Mean Seal Level
NRMS	Normalized Root Mean Square
PC	Personal Computer
PIO	Pilot Induced Oscillation
PSD	Power Spectral Density
RMS	Root Mean Square
STI	Systems Technology, Incorporated
TLR	Technical Letter Report
USAF	United States Air Force
VMC	Visual Meteorological Conditions
WL/FIGC	Air Force Flight Dynamics Directorate

ABSTRACT

This study details the development of a sub-optimal pilot model that blended the classical and optimal pilot model approaches in an attempt to achieve the advantages of each. This model used a numerical solution to the linear quadratic Gaussian problem to find the pilot gain, lead, and lag values that minimized a performance index consisting of task error and control usage. This development was conducted in four phases.

First, an optimal pilot model developed by Systems Technology, Incorporated, was analyzed in detail. This analysis included a step-by-step example problem to clarify the model's logic and an in-depth sensitivity analysis of the model's parameters. This study found that when the proper choices were made for these parameters, the model accurately predicted Cooper-Harper ratings. The pilot describing functions predicted by this model, however, were not consistent with the classical pilot model form.

Second, a ground and airborne evaluation of human pilot response was conducted using the Calspan variable stability Lear II aircraft. Four different pitch and four different roll axis dynamics cases were evaluated using three different tracking tasks. Primary pilot response parameters were recorded and examined using statistical and Fourier transform analysis in an attempt to provide insight into human pilot response. Except for the presence of large amounts of pure phase lead at high frequency, the frequency responses of the pilots were consistent with the gain, lead, and lag form of the classical pilot model. In all cases, the pilot applied compensation so that the response of

the combined pilot-aircraft system resembled and integrator near the cross-over frequency.

Third, a numerical solution to the linear quadratic Gaussian control problem that allowed the compensator form to be predetermined was derived. This method used the covariance matrix to compute the performance index, element by element, and a Nelder-Meade simplex search algorithm to find the coefficients of the compensator that minimized the performance index. When the desired compensator form was the same as the standard linear quadratic Gaussian solution, the two methods produced identical results.

Finally, the sub-optimal pilot model was developed and an analysis of the model's parameters was conducted. This model was restricted to single axis dynamics due to the assumptions necessary to numerically compute the performance index value. By design, the pilot describing functions predicted by the sub-optimal pilot model were consistent with the flight test results and classical pilot modeling theory. There was an excellent correlation between the performance indices and the actual Cooper-Harper ratings, but the model lacked the maturity necessary for consistent Cooper-Harper ratings prediction.

THE PREDICTION OF PILOT OPINION RATINGS USING OPTIMAL AND SUB-OPTIMAL PILOT MODELS

1. INTRODUCTION

Motivation

Even before Charles Manley was twice catapulted into the Potomac River at the controls of the Langley *Aerodrome,* engineers were concerned about the handling qualities of aircraft. Early designs relied on instinct and trial and error, often with disastrous results. Today, it is critical that we know as much about an aircraft's handling qualities as early in the design process as possible. This analysis must include some sort of pilot-in-the-loop evaluation. The optimal and sub-optimal pilot models are powerful tools for performing this analysis.

Pilot model development has not kept pace with the advances in flight control design. Modern day performance and stealth requirements often dictate the geometry of the aircraft, and assume that a digital flight-control system can be built to make the aircraft exhibit *good* handling qualities. For this reason pilot model analysis is critical in all phases of an aircraft's design. Unfortunately, the handling qualities of these complex flight-control systems usually cannot be accurately predicted by currently accepted pilot models.

Historically, every advance in control theory has led to an attempt to understand human pilot behavior in terms of the advance. The development of classical control theory after World War II led to a continuing effort to model the human pilot with transfer functions. The development of modern control theory and linear quadratic Gaussian techniques in the early 1970s led to the on-going attempts to model the human pilot with an optimal regulator, filter, and estimator. This thesis proposes a numerical approach to pilot modeling that was made possible by an exponential growth in computer speed and availability. This numerical approach blends the classical and optimal pilot modeling theories in an effort to achieve the advantages of each.

Objectives

The overall objective of this project was to develop a pilot model that combines the intuitive nature of classical pilot modeling theory with the optimizing nature of modern pilot modeling theory. The specific objectives were:

1. Study existing classical pilot models.
   A. Implement the MIL-STD-1797A pilot models on MATLAB™[1].
   B. Include important aspects of these models into the pilot model developed for this thesis.

2. Analyze the optimal pilot model developed by Systems Technology, Incorporated, (STI) for use with *Program CC*.
   A. Supplement the guidance provided by STI for the use of this model.
   B. Conduct a sensitivity analysis of the parameters used by this model.
   C. Use insights from this model to develop the sub-optimal pilot model.

[1] MATLAB is a trademark of The MathWorks, Inc.

3. Record and examine pilot response parameters during ground and airborne tracking tasks that can be used as a data base for pilot model development and validation.
   A. Gather Cooper-Harper ratings and pilot comments for a range of aircraft dynamics.
   B. Using frequency response analysis techniques, examine the relationship between stick displacement and task error for single axis sum-of-sines tracking tasks.
   C. Use the insight into human pilot response provided by this experiment in the development of the sub-optimal pilot model.

4. Derive a numerical solution to the linear quadratic Gaussian control problem that allows the compensator form to be predetermined.

5. Implement the sub-optimal pilot model on MATLAB™ for single axis analysis.
   A. Expand the numerical linear quadratic Gaussian solution in Objective 4 to include the output disturbance structure necessary for the evaluation of single axis tracking tasks.
   B. Restrict the optimal pilot model solution to the classical pilot model form.
   C. Compare the predictions of this model with flight test frequency response analysis data.
   D. Compare the predictions of this model with those of the STI optimal pilot model and the classical pilot models accepted in MIL-STD-1797A.

Thesis Overview

The following procedures were used to accomplish the objectives presented above. Results are summarized at the end of each chapter.

1. This thesis conducted an analysis of the crossover pilot model (Reference 17) and the longitudinal and lateral handling qualities models described in MIL-STD-1797A (Reference 5). The results of this analysis are reported in Chapter 2 of this thesis. Additionally, all of the longitudinal and lateral models accepted in MIL-STD-1797A

were implemented in a *Handling Qualities Toolbox* for MATLAB™. This toolbox was used for much of the classical pilot model analysis conducted in this thesis. Copies of the MATLAB™ programs (.m files) and user's guide are available from the author.

2. The optimal pilot model developed by Systems Technology, Incorporated, was analyzed in detail. This effort is detailed in Chapter 3. A model overview is provided and a simple example is worked step-by-step using the program's logic. The sensitivity of the model results to the required parameter choices is also examined and recommended values are presented.

3. A ground and airborne evaluation of human pilot response was conducted using the Calspan variable stability Lear II aircraft. The results of this flight test are presented in Chapter 4. Four different pitch and four different roll axis dynamics were evaluated using three different types of compensatory tracking tasks. Primary pilot response parameters were recorded and examined using Fourier transform analysis in an attempt to provide insight into human pilot response. The flight test data gathered during this project are maintained at the Flight Dynamics Directorate (WL/FIGC), Wright-Patterson AFB, Ohio, and are available for research purposes. A companion report to this thesis, AFFTC-TLR-93-41 (Reference 7) serves as a detailed guide for this flight test data base and provides an initial look a the test results.

4. A numerical solution to the linear quadratic Gaussian (LQG) control problem that allows the compensator form to be predetermined is derived in Chapter 5. This method uses the covariance matrix to compute the performance index value, element by element. A Nelder-Meade simplex algorithm then finds the coefficients of compensator

that minimize the performance index. This method is not only useful in the optimal pilot model problem. It may be beneficial for any situation when reduced order compensation is desired.

5. The sub-optimal pilot model is described in Chapter 6. This model uses the numerical LQG method to restrict the optimal pilot model solution to the classical pilot model form. The results of this new pilot model were compared with the flight test frequency response analysis data as well as the predictions of the STI optimal pilot model and the classical pilot models accepted in MIL-STD-1797A.

6. Finally, the conclusions and recommendations of thesis are summarized in Chapter 7.

Limitations

This thesis had several limitations. First, only single axis, compensatory tracking tasks were evaluated or considered. Valid multi-axis analysis is not possible without the legitimate single-axis framework this thesis was meant to advance. Second, the effects of feel system characteristics were not considered. A thorough analysis of this important factor was beyond the scope of this thesis. Finally, the pilots used in the flight-test portion of this study were not entirely linear, and they did not employ the ratings scale with perfect consistency. While every attempt was made to reduce pilot variations, these restrictions are impossible to avoid and should be considered when studying any handling qualities experiment.

2. Background

General

This chapter provides the background information essential to this thesis. It includes five sections. The first section, *Handling Qualities,* discusses the Cooper-Harper rating scale and defines some important handling qualities terms. The next three sections, *The Pilot as a Linear Element, Pilot-in-the-Loop Analysis,* and *Pilot Models,* provide a brief description of linear pilot modeling fundamentals. The final section, *Feel System Considerations,* discusses the relationship between force and displacement controllers, and the impact of each on handling qualities.

Handling Qualities

The goal of this thesis is to develop a pilot model that will, under certain conditions, predict an aircraft's handling qualities. Cooper and Harper defined handling qualities as, " . . . *those qualities or characteristics of an aircraft that govern the ease and precision with which a pilot is able to perform the tasks required* (2:2)." Central to this definition are the concepts of performance, workload, and task.

Aircraft handling qualities can not be based on performance alone. A pilot can achieve the same performance for a wide range of aircraft characteristics. As the aircraft characteristics degrade, however, this performance can be attained only at the expense of a reduction in the pilot's capacity to perform other duties. Thus, handling qualities also depend on workload, defined to include both mental and physical effort (2:6).

Additionally, the same aircraft may exhibit different handling qualities for different tasks. For example, if the task is overly simple to perform, the poor handling qualities of an aircraft may not be apparent to the pilot. Cooper and Harper define *task* as the work assigned to the pilot. *Task* does not include all aspects of the mission or intended use of the aircraft (2:4).

The Cooper-Harper rating scale, shown in Figure 2-1 on the following page and described in Reference 2, was the basis for all of the handling qualities ratings used in this thesis[1]. This scale requires the pilot to answer a series of questions concerning controllability, performance, and workload to arrive at a rating. Each rating is merely a shorthand for a set of handling qualities characteristics. Additionally, assigning Cooper-Harper ratings is a subjective process and variability in the pilot ratings is unavoidable. Because of this, predicting precise Cooper-Harper ratings with mathematical models is problematic at best[2]. The pilot models examined in this thesis were considered successful when they consistently predicted the ratings trends.

The Pilot as a Linear Element

Pilot behavior has eluded understanding since the earliest days of aviation. Not only is the human pilot non-linear and adaptive, but his behavior varies over time. No single existing model can imitate the complexities of human behavior. Instead, simplifying assumptions must be made and the range of the model's application

---

[1] The term *handling qualities rating* and *pilot opinion rating* are interchangeable in this thesis. Both refer to the Cooper-Harper rating.

[2] Cooper and Harper warn against attempting to treat pilot rating data with mathematical operations that are rigorously applicable only to a linear, interval scale.

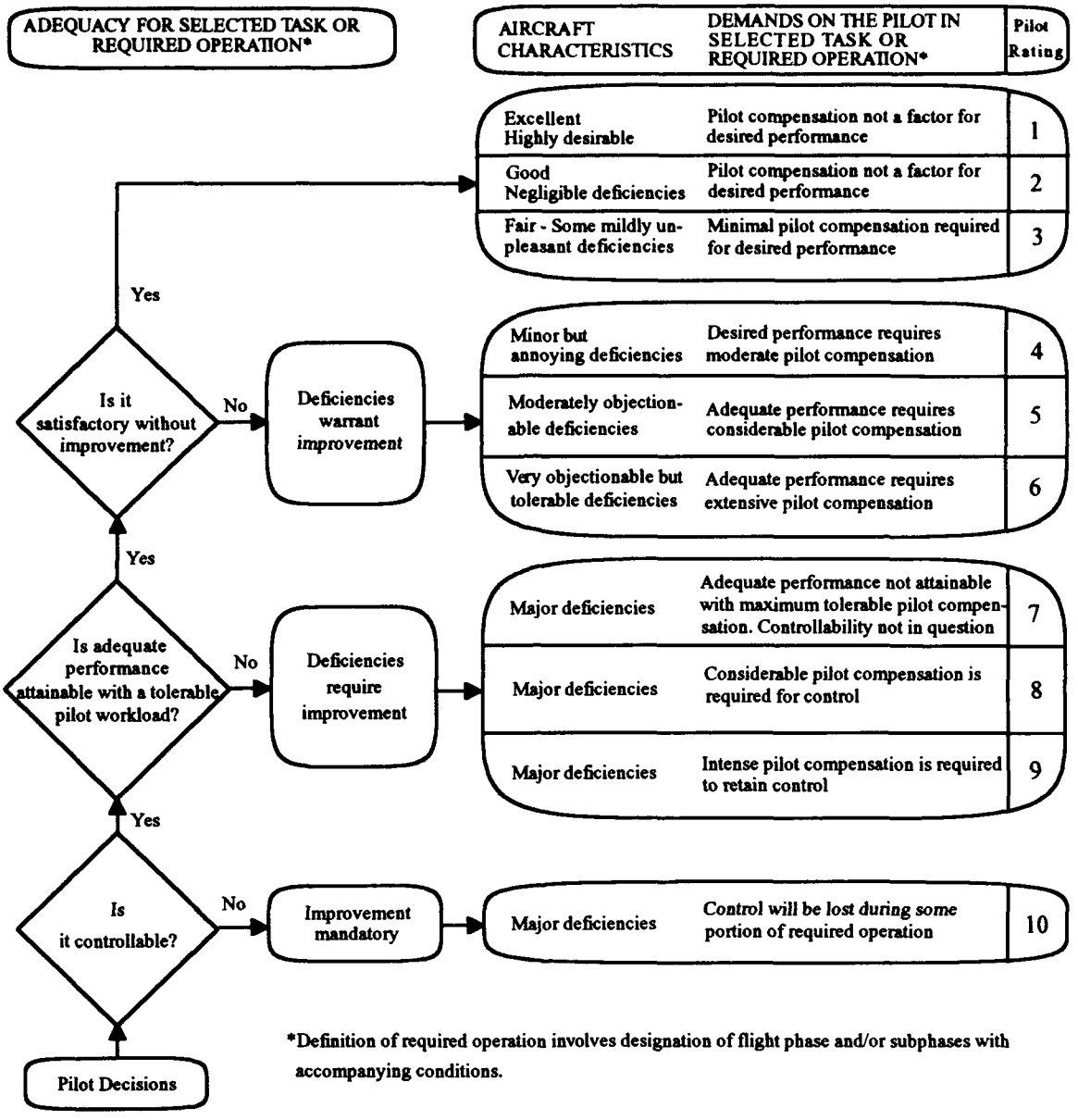

Figure 2-1. Cooper-Harper Rating Scale

appropriately limited. The most significant assumption made throughout this thesis is that the human pilot is a linear element.

The response of a non-linear system can be divided into two parts. The first part is linearly coherent with the input and generally taking a describing function form. The

second part, the remnant, is not linearly coherent with the input. To accurately make the linear modeling assumption, this remnant must be minimized (14:4).

McRuer found that when modeling the human pilot, the remnant is primarily due to four sources (14:37).

1. Non-Linear Operations
2. Non-Steady Behavior
3. Operator Response to Other Inputs
4. Injection of Noise

The first two sources, non-linear operations and non-steady behavior, result primarily from the pilot's ability to learn and adapt. To minimize their effects, both the task and the pilot must be carefully chosen.

The task must be random appearing and within the capabilities of the pilot. This prevents the pilot from learning the task and adapting his behavior accordingly. McRuer found that the remnant also increased with task bandwidth, but the effect was minor for bandwidths between 1.5 and 4.0 radians per second (15:128). When the bandwidth of the task approached 8.0 radians per second, however, the pilot ignored the high frequency commands and adopted a more open-loop, non-linear behavior (17:246-248). Additionally, the task must have an appropriate length. It has to be long enough to allow the pilot time to become actively involved, but not so long that he becomes fatigued. McRuer found no evidence of excessive non-linear behavior for task lengths between twenty seconds and four minutes (17:240).

Finally, the pilot must be carefully chosen. McRuer found that using highly trained and motivated subjects reduced pilot variability and non-linear behavior (15:12).

Smith, in Reference 24 disagrees. He suggests that highly experienced pilots use their skill and experience to avoid closed loop control when necessary (24:20). While Smith may be correct, it is the goal of this thesis to develop a pilot model that will predict an aircraft's handling qualities. The traditional evaluator of an aircraft's handling qualities is the experienced test pilot.

The final two remnant sources, operator response to other inputs and injection of noise, are primarily affected by experimental procedures. To minimize the remnant, the task must be clearly and carefully defined. For example, if a pure single axis roll tracking task is desired, the lateral and directional axes should be uncoupled, or the pilot will have to divide his attention between the two. These final two remnant sources are often mutually exclusive. If a vision restriction device is used so that the only pilot visual cue is task error, for example, his response to other inputs may be minimized. The injection of noise may greatly increase, however, due to the resulting disorientation.

The only task examined in this thesis was the compensatory tracking task. For this task, the error between a command and the actual aircraft condition was displayed to the pilot and he acted to minimize this error. This task was considered representative of several important flight phases, such as air-to-air and air-to-ground gunnery, aerial refueling, and approach and landing in gusty winds. The tasks used during both the analysis and the actual experiment in this thesis were random appearing with a bandwidth of 2.0 radians per second. Highly trained pilots from the USAF Test Pilot School were used as subjects in the experimental portion of this thesis. Additionally, uncoupled,

linear vehicle dynamics were simulated, and the effects of the dutch roll and phugoid modes of motion were minimized.

Pilot-in-the-Loop Analysis

For a large class of tracking tasks, the pilot acts to minimize the error between some aircraft parameter and a task command. Using pitch (θ) and pitch command (θ_c), for example, this compensatory tracking task is illustrated in Figure 2-2.

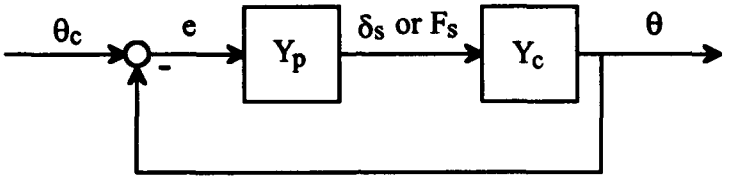

Figure 2-2. Compensatory Tracking Task Block Diagram

where

θ	= Pitch Angle	Y_p	= Pilot
θ_c	= Pitch Command	Y_c	= Aircraft
e	= Task Error	F_s	= Stick Force
δ_s	= Stick Deflection		

Through block diagram manipulation this can be re-drawn such that the pilot senses the task error and applies compensation to minimize it as shown in Figure 2-3. This form will be used in the remainder of this thesis for all model development. The salient question is, "*What is Y_p?*"

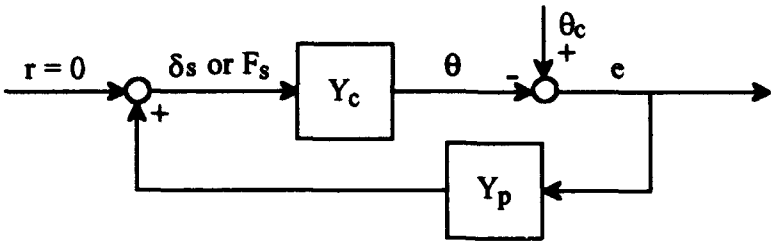

Figure 2-3. Compensatory Tracking Task Block Diagram - Feedback Compensation

In 1965 McRuer and Krendel conducted a controlled measurement of human pilot behavior using frequency response methods. Using a pitch axis tracking task generated on a laboratory oscilloscope, they found that for very simple dynamics, the quasi-linear[1] pilot can be represented by the following describing function (15:14-17).

$$Y_P = K_P \cdot e^{-j\omega\tau} \cdot \underbrace{\frac{(T_L \cdot j\omega + 1)}{(T_I \cdot j\omega + 1)}}_{\text{Series Equalization}} \cdot \underbrace{\frac{[T_K \cdot j\omega + 1]}{[T'_K \cdot j\omega + 1]}}_{\text{Very Low Frequency Lag-Lead}} \cdot \underbrace{\frac{1}{(T_{N1} \cdot j\omega + 1) \cdot \left[(\frac{j\omega}{\omega_n})^2 + \frac{2\zeta_n}{\omega_n} j\omega + 1 \right]}}_{\text{Neuromuscular System}} \quad (2\text{-}1)$$

Gain — Pure Delay

where

$j\omega$ = Laplace Variable for Random Input[2]
Y_p = Pilot Describing Function
K_p = Pilot Gain
τ = Pilot Delay
T_L = Pilot Lead Time Constant
T_I = Pilot Lag Time Constant
T_K = Very Low Frequency Pilot Lead Time Constant
T'_K = Very Low Frequency Pilot Lag Time Constant
T_{N1} = Neuro-Muscular Time Constant
ω_n = High Frequency Neuro-Muscular Natural Frequency
ζ_n = High Frequency Neuro-Muscular Damping Ratio

[1] McRuer used the term, *quasi-linear,* because the pilot can be modeled as a linear element only if specific conditions are satisfied.

[2] $j\omega$ is used instead of the general Laplace variable, $s = \sigma + j\omega$, to emphasize that this equation is strictly valid only in the frequency domain with continuous, random-like inputs. It should not be used for system responses to deterministic inputs such as step commands.

Limiting the frequency range of interest to 0.1 to 10 radians per second, the influence of the very low frequency lag-lead is minimal. Additionally, the neuro-muscular system can be modeled as a first order lag as shown in Equation 2-2 (16:29).

$$\frac{1}{(T_{N1}\cdot j\omega+1)\cdot\left[(\frac{j\omega}{\omega_n})^2+\frac{2\zeta_n}{\omega_n}j\omega+1\right]}\approx\frac{1}{T_N\cdot j\omega+1}\quad\text{if}\quad T_N\approx T_{N1}+\frac{2\zeta_n}{\omega_n}\qquad(2\text{-}2)$$

where

T_N = First Order Approximation of Neuro-Muscular Time Constant

and typical values are (15:171):

$T_{N1} = 0.1$ $\qquad$ $\zeta_n = 0.12$

$\omega_n = 16.5$ $\qquad$ $T_N \approx 0.115$

Making these assumptions leaves the classical pilot model shown in Equation 2-3.

$$Y_P = K_P\cdot e^{-j\omega\tau}\cdot\frac{(T_L\cdot j\omega+1)}{(T_I\cdot j\omega+1)\cdot(T_N\cdot j\omega+1)}\qquad(2\text{-}3)$$

As shown in this equation, the pilot can be modeled by a gain, a lead, a lag, a delay, and a first order muscular lag.

Using the classical pilot model and including measurement and muscular noise the block diagram of Figure 2-3 can be re-drawn as in Figure 2-4 on the following page. As shown in this figure, the pilot makes an imperfect, or noisy (ξ_o), measurement of the task error and applies a delayed compensation to minimize this error. The desired stick deflection (δ_c) is corrupted by both the muscular lag and a random muscular noise (ξ_m).

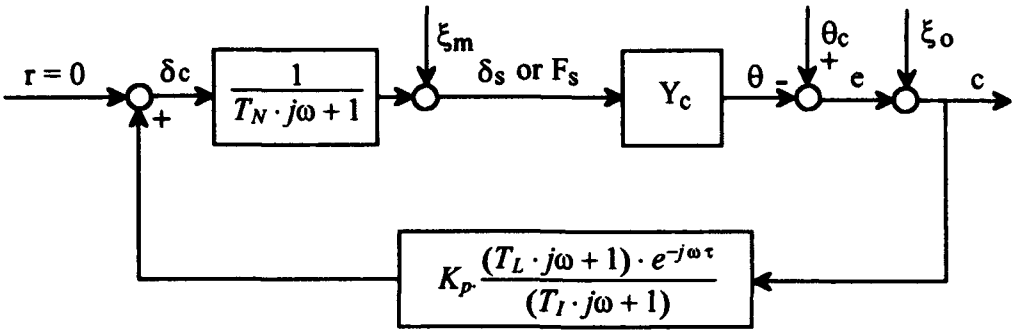

Figure 2-4. Classical Pilot Model Block Diagram

where

θ	= Pitch Angle	ξ_o	= Observation Noise
θ_c	= Pitch Command	ξ_m	= Muscular Noise
e	= Task Error	δ_c	= Commanded Stick Deflection
K_p	= Pilot Gain	δ_s	= Stick Deflection
T_L	= Pilot Lead Time Constant	F_s	= Stick Force
T_I	= Pilot Lag Time Constant	Y_c	= Aircraft Transfer Function
τ	= Pilot Delay	$j\omega$	= Laplace Variable
T_N	= Muscular Time Constant	c/r	= Output/Input

While pilot *lead* makes practical sense, pilot *lag* is not intuitively obvious. Smith proposed a more intuitive approach. In Reference 24 Smith theorized that the pilot measures both error and error rate and applies a gain to each, resulting in lead compensation. Thus, the larger the error or error rate, the larger the compensating stick movement, but only to a point. As the error or error rate grow large, the pilot will no longer proportionally increase the stick deflection by the same amount. In other words the pilot will apply washout to the error and error rate signals. It is this washout of the error and error rate signals that produces the lag in Equation 2-3, not some mentally computed lag compensation (24:37-40). This can be drawn as shown in Figure 2-5.

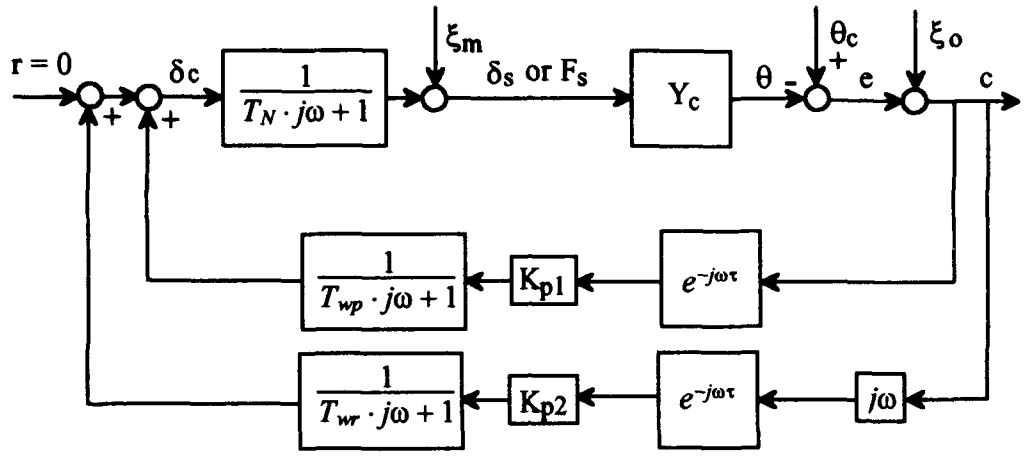

Figure 2-5. Multi-Loop Pilot Model Block Diagram

where

T_{wp} = Washout Time Constant in Error Feedback Loop
T_{wr} = Washout Time Constant in Error Rate Feedback Loop
K_{p1} = Error Feedback Gain
K_{p2} = Error Rate Feedback Gain

It is interesting to note that the multi-loop model in Figure 2-5 and the classical pilot model in Figure 2-4 are equivalent if the washout time constants in the error and error rate feedback loops are equal ($T_{wp} = T_{wr}$). To make this illustration simpler, the identical forward paths in each figure were replaced with the variable, G. Using block algebra, the closed-loop transfer function for Figure 2-4 is:

$$\frac{c}{r} = \frac{G \cdot (T_I \cdot j\omega + 1)}{T_I \cdot j\omega + 1 - G \cdot K_p \cdot (T_L \cdot j\omega + 1) \cdot e^{-j\omega \cdot \tau}} \qquad (2\text{-}4)$$

while the closed-loop transfer function of Figure 2-5 is:

$$\frac{c}{r} = \frac{G \cdot (T_{wp} \cdot j\omega + 1) \cdot (T_{wr} \cdot j\omega + 1)}{(T_{wp} \cdot j\omega + 1 - G \cdot K_{p1} \cdot e^{-j\omega \cdot \tau}) \cdot (T_{wr} \cdot j\omega + 1) - G \cdot (T_{wp} \cdot j\omega + 1) \cdot j\omega \cdot K_{p2} \cdot e^{-j\omega \cdot \tau}} \qquad (2\text{-}5)$$

If the washout time constants in both the error and error rate feedback loops are equal ($T_{wp} = T_{wr} = T_w$), then Equation 2-5 reduces to:

$$\frac{c}{r} = \frac{G \cdot (T_w \cdot j\omega + 1)}{T_w \cdot j\omega + 1 - G \cdot K_{p1} \cdot e^{-j\omega \cdot \tau} - G \cdot j\omega \cdot K_{p2} \cdot e^{-j\omega \cdot \tau}} \tag{2-6}$$

which can be rewritten as:

$$\frac{c}{r} = \frac{G \cdot (T_w \cdot j\omega + 1)}{T_w \cdot j\omega + 1 - G \cdot K_{p1} \cdot \left(\frac{K_{p2}}{K_{p1}} \cdot j\omega + 1\right) \cdot e^{-j\omega \cdot \tau}} \tag{2-7}$$

This transfer function is equivalent to that in Equation 2-4 found using the classical pilot model. Several important insights can be gained from comparing Equations 2-4 and 2-7. The classical pilot modeling approach and the multi-loop approach are identical if:

1. The washout time constant in both the error and error rate feedback loops of the multi-loop model are equal to the lag time constant of the classical pilot model ($T_{wp} = T_{wr} = T_w = T_I$).
2. The gain on error feedback in both models are equal ($K_{p1} = K_p$).
3. The ratio of error rate to error feedback gain in the multi-loop model equals the lead time constant in the classical pilot model ($K_{p2} / K_{p1} = T_L$).

Pilot Models

There are currently three broad categories of pilot models. The first category, *open loop pilot models,* uses the aircraft response to open loop commands to predict handling qualities. These models are based on statistical fits to past data and make no attempt to model human pilot behavior. The second category, *classical pilot models,*

model the pilot as a gain, lead, lag, and delay as shown in Equation 2-3. The final category, *optimal pilot models,* model the pilot so that some performance index is minimized. These models generally take the form of a linear quadratic regulator and Kalman filter.

The majority of pilot models in use are open loop models. Because these models do not directly consider human pilot behavior, they are comparatively simple to develop. Five of the six pitch axis and all of the roll axis models in MIL-STD-1797A are open-loop models (5:171-256, 377-427).

Classical and optimal pilot models face three obstacles. First, a form for the pilot must be chosen. For example, the classical pilot models use gain, lead, lag, and delay. Second, the constants in the pilot model forms must be found. The optimal pilot model computes these values so that a performance index is minimized. Finally, the resulting pilot describing function must be related to the aircraft's handling qualities through some metric.

The primary advantage of classical pilot models is that the form used by these models is based on experimental results. The gain, lead, lag, and delay behavior of the human pilot during compensatory tracking tasks is well documented (References 14, 15, 16, 17, and 21). Choosing values for these variables and then using them to predict a handling qualities rating, however, can be quite difficult.

Classical pilot model parameter selection does have some experimental basis. McRuer found that the pilot uses gain, lead, and lag so that just within and beyond the task bandwidth the combined aircraft-pilot system has a slope of -20 dB per decade and

adequate stability margins. Changes in aircraft gain are offset by changes in pilot gain so that the crossover frequency is largely invariant (17:234-238). McRuer also found that the generation of second order lead was difficult or impossible with only visual random appearing inputs. While several of the systems he tested could have used second order compensation to advantage, this behavior was not noted (14:218). Finally, McRuer measured pilot delay between 0.2 and 0.3 seconds (14:217).

The crossover pilot model used this behavior-based approach to form a series of rules for selecting pilot gain, lead, and lag (Reference 17). The problem of accurately and consistently relating these variables to a handling qualities rating still remains. As a result, classical models are not in wide use. The Neal-Smith model is currently the only classical pilot model accepted in MIL-STD-1797A.

Optimal pilot models are based on the assumption that the well-trained, well-motivated human controller will perform in a near optimal manner subject to certain internal constraints. Optimal pilot models have two advantages over classical pilot models. First, selection of the describing function constants is not difficult. The values are chosen so that the linear quadratic Gaussian performance index is minimized. Second, relating the pilot describing function to a handling qualities rating is more straight forward than with classical pilot models. Usually, the performance index is directly related to a handling qualities rating.

The optimal pilot model suffers from two deficiencies. First, optimal pilot models are complicated, both in the order of the predicted pilot describing function and in their implementation. Due to the nature of linear quadratic Gaussian theory, the

predicted pilot describing function has an order of at least twice that of the aircraft dynamics. This is not consistent with the gain, lead, lag, and delay behavior observed by McRuer. Additionally, implementing the internal constraints of the human pilot, delay and muscular lag for example, within a standard linear quadratic Gaussian structure is complicated. The second deficiency is over parameterization. When implementing an optimal pilot model, the engineer has to make numerous parameter choices, such as noise intensities, performance index weightings, and forcing function form and intensity. The predicted handling qualities rating and pilot describing function is normally sensitive to these choices.

Feel System Considerations

It is difficult to imagine any pilot-in-the-loop analysis without considering control stick characteristics. Controller sensitivity, or stick force gradient, can have a huge effect on an aircraft's handling qualities. In one experiment, a Cooper-Harper rating was changed from a *seven* to a *two* only by changing the roll-rate sensitivity (18:19). Control stick dynamics and control stick type -- force versus position command -- are also important factors in an aircraft's handling qualities.

The position command feel system dynamics include the spring, mass, and damper characteristics that translate the pilot's stick force input into stick position. There are two different approaches to analyzing this type of feel system. It can be considered as another flight control system filter, or it can be treated as a unique dynamic element. If the feel system is treated as another flight control system filter, the stick dynamics are

included in the analytical model as a linear element between stick force and aircraft response as shown in Figure 2-6 (18:36).

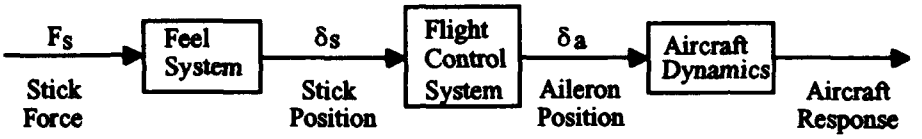

Figure 2-6. Position Command Feel System

If the feel system is treated as a unique element, it is assumed that the pilot uses his direct access to the input force and the output stick displacement to form an inner loop around the feel system. Thus, the stick dynamics become internal to the pilot and do not need to be included in the analytical model (23:582-583). MIL-STD-1797A advocates the latter approach (5:172).

The force command feel system acts in parallel as shown in Figure 2-7 (18:36).

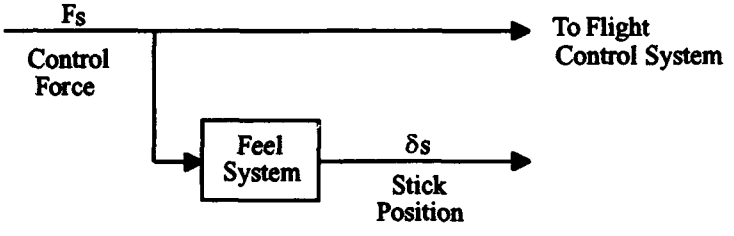

Figure 2-7. Force Command Feel System

The traditional approach is to exclude the feel system dynamics for force controllers since they act in parallel. Without the feel system dynamics, the system will exhibit less phase lag and therefore better closed-loop performance (18:14).

Mitchell found that including the feel system as an equivalent delay, regardless of the feel system type, improved the correlation between handling qualities ratings and feel system dynamics. In other words, an aircraft with a "bad" feel system should receive

poor ratings whether position or force command is used. The systems could be modeled as an equivalent delay due to the neuromuscular reaction of the pilot to both types of feel systems. Mitchell emphasized that the effect of the feel system was not identical to a pure time delay. It was possible, however, to estimate the effects of the feel system on pilot ratings by considering it as such (18:24).

This thesis only studied position command systems, and the feel system dynamics were generally analyzed as a linear element in the command path. An in-flight analysis of both position and force command systems was not feasible because of the numerous additional flight test combinations it would have required.

3. *The Optimal Pilot Model*

General

While the gain, lead, lag, and delay form of the classical pilot model is well documented, choosing values for these variables and then using them to predict a handling qualities rating remains a daunting task. The optimal pilot model was developed in an attempt to overcome these deficiencies. The optimal pilot model is based on linear quadratic Gaussian (LQG) stochastic control theory which appears intuitively suited to the solution of the human pilot modeling problem. The human pilot adapts his control strategy so that the trade-off between performance and workload results in the optimal handling qualities rating (6:7). Likewise, the optimal pilot model finds the control strategy that minimizes a performance index consisting of average tracking error *(performance)* and control usage *(workload)*. This performance index can be used to estimate a handling qualities rating based on statistical fits to past data.

This chapter focuses on an optimal pilot model developed by Systems Technology, Incorporated (STI), for use with *Program CC* (Reference 25). The STI model was selected for several reasons. First, it incorporates nearly every important aspect of other optimal pilot models, making it a good candidate for study. Second, it can be implemented on the personal computer and is therefore widely available. Finally, this model has had some success in predicting Cooper-Harper ratings, but lacks parameter selection guidance.

This chapter is divided into three sections. The first section gives a brief overview of optimal pilot modeling theory. The second section analyzes the STI optimal pilot model in detail. This analysis includes a description of the model, a step-by-step example problem, and a detailed sensitivity analysis. Finally, the conclusions and recommendations of this chapter are summarized.

Background

Kleinman, Baron and Levison made the first integrated attempt to describe the behavior of the human pilot in the framework of optimal control theory in 1970 (Reference 10). The theory involved has not changed significantly since the Kleinman study was completed. The basic assumption implicit in the optimal pilot model is that the well-trained and motivated pilot behaves in an optimal manner subject to his inherent limitations (8:464). These limitations include neuromuscular lag, internal motor noise, perceptual threshold, and processing delay.

A block diagram of the standard optimal pilot model is shown in Figure 3-1 (6:15). The aircraft dynamics are represented by a linear state vector and vector-matrix equations. The task forcing function is input as a disturbance and modeled as white Gaussian noise shaped by coloring filters. Because the human pilot is able to obtain both displacement and rate information from a single display, the feedback vector normally consists of the error and error rates of the displayed variables. If the error or error rates are smaller than a threshold value, the pilot will neither observe them nor take any corrective action.

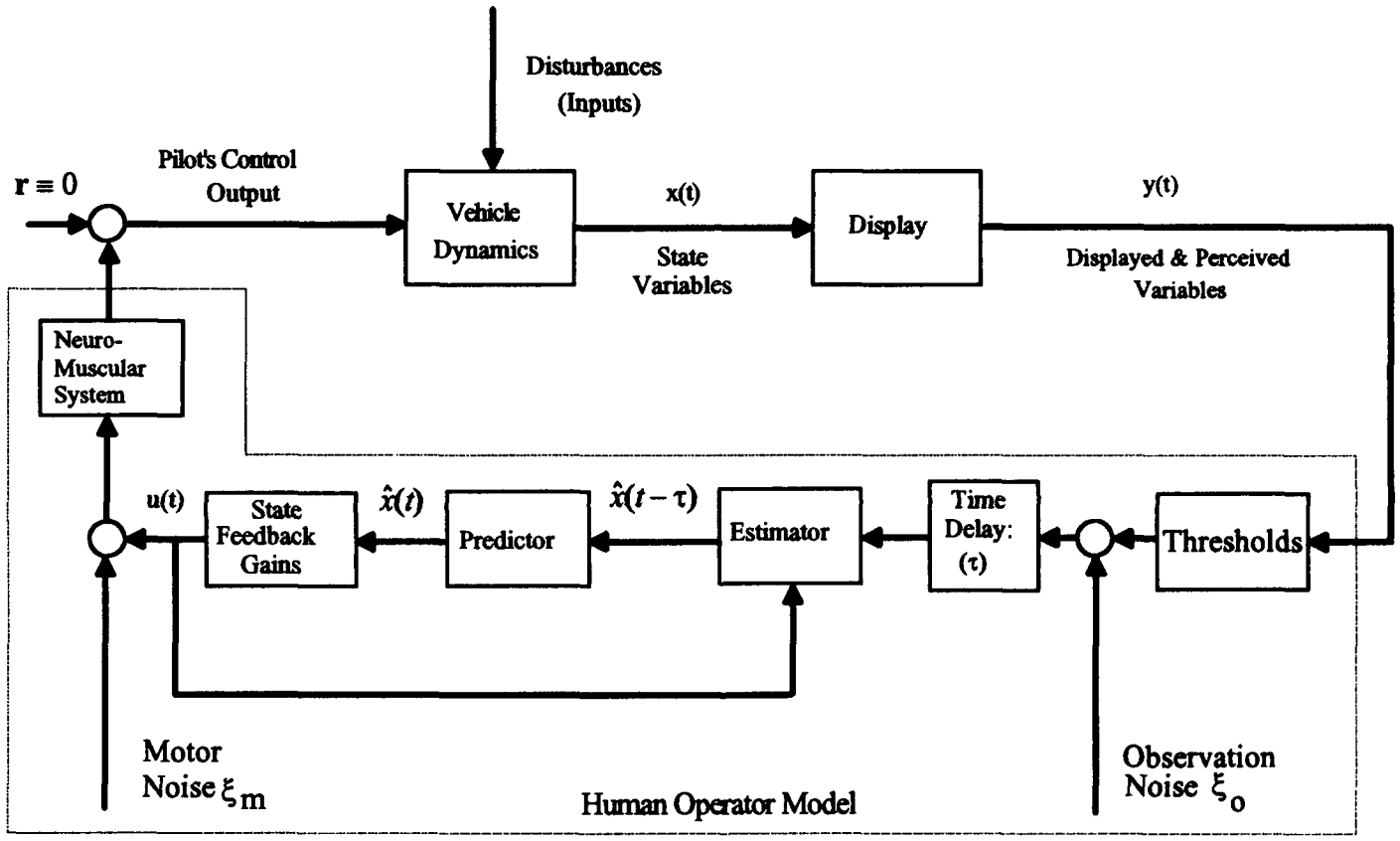

Figure 3-1. Block Diagram of Optimal Pilot Model

Pilot induced, uncorrelated white noise is added to each observation. This noise represents the nonlinear remnant of the pilot as well as his random error in observing the displayed variables. If more than one variable and its derivative are observed, sampling must also be considered (6:16).

The many internal time delays inherent to the human pilot are modeled by a single perceptual delay. A Kalman filter and least-squares predictor are used to produce a non-delayed, optimal estimate of the observation vector. The linear quadratic regulator (LQR) gains are then determined to minimize an appropriate performance index[1]. For the optimal pilot model, this performance index generally takes the form of Equation 3-1.

$$J = \int_0^\infty [x^T(t)\,Q\,x(t) + \dot{u}^T(t)\,R\,\dot{u}(t)]\,dt \tag{3-1}$$

where

$x(t)$ = State Vector
$\dot{u}(t)$ = Control Rate Vector
J = Performance Index
t = Time
Q = State Deviation Weighting Matrix
R = Control Rate Weighting Matrix

The first part of this integral $(x^T Q\,x)$ is directly related to performance, while the second part $(\dot{u}^T R\,\dot{u})$ represents physical and mental workload (8:475). The state weightings can be difficult to pick *a priori*. Hess found success by choosing the weighting coefficients as the squares of the reciprocals of the maximum allowable deviation of the state variables (8:470). These weightings can also be used to make the model task dependent (6:11).

[1] Background information on control rate weighting is provided in Appendix A. For more detailed information on LQG theory consult References 13 and 20.

The neuromuscular lag is not normally explicitly modeled. Kleinman, Baron, and Levison showed that the neuromuscular dynamics did not need to be introduced if the performance index, Equation 3-1, includes a penalty on control rate instead of control (8:465). The neuromuscular noise, or motor noise, and the observation noise have spectral densities proportional to the mean squared operator output. Thus, they must be found in an iterative fashion.

Finally, the performance index is used to estimate a handling qualities rating based on statistical fits to experimental data (6:24). This relationship normally accounts for the strength of the forcing function as well as the forcing function bandwidth.

STI Optimal Pilot Model

This section presents a detailed analysis of the optimal pilot model developed by Systems Technology, Incorporated, for use with *Program CC*. Reference 25 explains the theory behind this model. This section is intended to supplement Reference 25 by providing an extended discussion of the model as well as the user-selected model parameters. The discussion that follows is divided into three parts. The first section provides an overview of the model. The second section follows the model's computational flow using an integrator example. The final section contains a detailed sensitivity analysis of the modeling parameters and provides guidance for their selection.

Model Overview. The flow diagram for the STI optimal pilot model is shown in Figure 3-2 on the following page (25:7). This model was only designed to handle one

Where

T_N = Muscular Time Constant

g = Control Rate Weighting

q = State Deviation Weighting

τ = Pilot Delay

V_w = Intensity of Driving Noise

ρ_{yi} = Observation Noise Ratio

ρ_u = Motor Noise Ratio

T_i = Visual Indifference Threshold

f = Fractional Attention Parameter

V_{yi} = Observation Noise Intensity

V_u = Motor Noise Intensity

σ_{yi} = Standard Deviation of Error or Error Rate

σ_u = Standard Deviation of Control Rate

E = Error Function

J = Performance Index

Y_p = Predicted Pilot Transfer Function

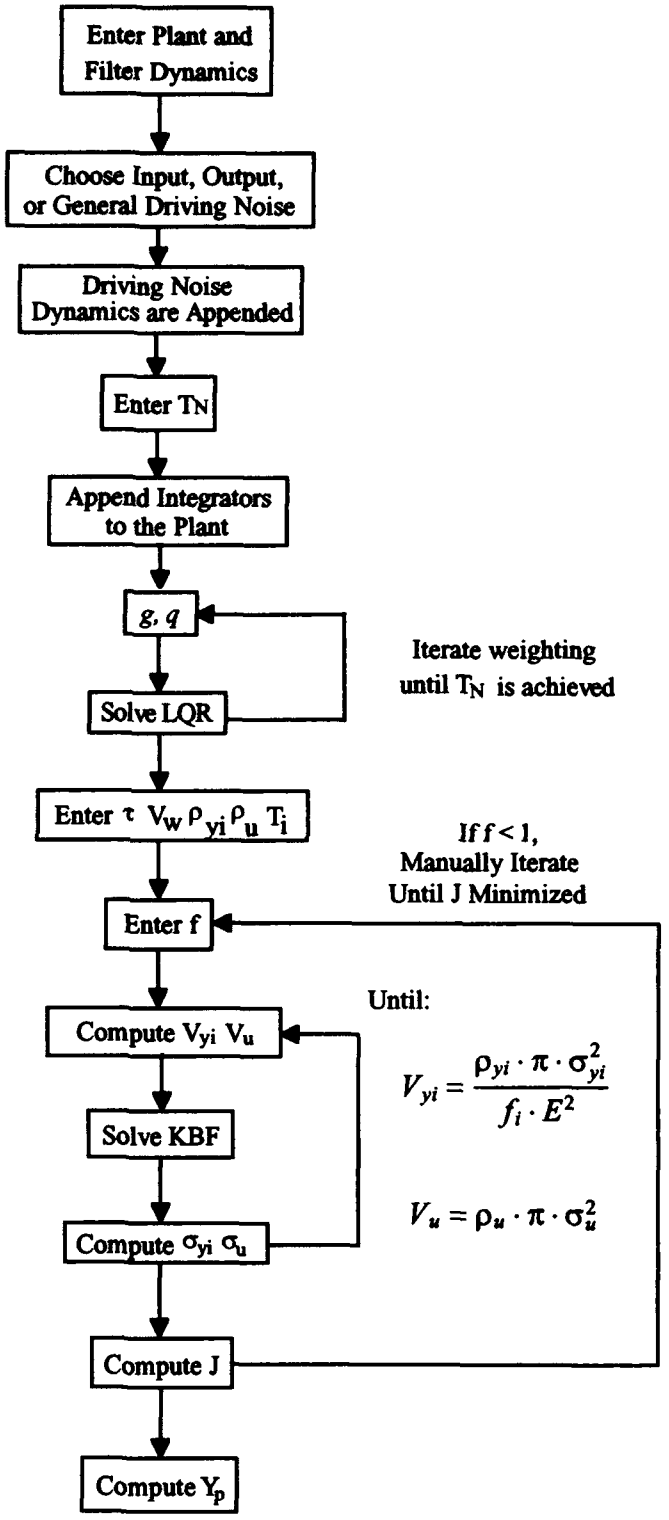

Figure 3-2. Computational Flow for the STI Optimal Pilot Model

feedback channel and its derivative. If there is more than one channel, each must be analyzed separately. This model can be divided into three parts.

First the aircraft dynamics are input in either transfer-function or state-space form and appended with the necessary coloring filters[1]. Because this model allows the feedback of only one variable and its derivative, single-input-single-output (SISO) aircraft and shaping filter dynamics must be used. Once these dynamics are entered, the aircraft states are augmented with the driving noise filter states in one of three different manners. The noise can be injected at the aircraft output, at the aircraft input, or in the middle of the aircraft. Finally, the state-space representation of the augmented aircraft is configured so that error and error rate are used for feedback.

Second, the linear quadratic regulator problem is solved so that the neuromuscular dynamics are modeled. The user enters the state deviation penalty, q. This weighting applies only to the error channel since the penalty on error rate is always zero in this model. Integrators are then appended to the aircraft dynamics. Finally, the weighting on control rate, g, is iterated until the neuromuscular dynamics are modeled. Because the STI optimal pilot model is restricted to single-input-single-output dynamics, q and g are scalar weightings and are used in the STI documentation instead of the standard weighting matrices, Q and R, in Equation 3-1.

[1] The tracking task forcing function must be modeled as a white Gaussian noise shaped by coloring filters.

Finally, the Kalman filter problem is solved. The user must enter several parameters:

τ	Pilot Delay
V_w	Intensity of the Driving Noise
ρ_{y1}, ρ_{y2}	Observation Noise Ratios for Error and Error Rate
ρ_u	Motor Noise Ratio
V_{y1i}, V_{y2i}	Intensity of the Observation Noise -- Starting Values
V_{ui}	Intensity of the Motor Noise -- Starting Value
T_{y1}, T_{y2}	Visual Indifference Thresholds
f	Fractional Attention Parameter

The starting values for the noise intensities are used to find the Kalman filter solution. From this solution σ_{yi} and σ_u, the standard deviations of y_i and u, are determined. The noise intensities are then iterated until the equations for V_{yi} and V_u shown in Figure 3-2 are satisfied. For multi-axis tasks this entire model must be repeated and the fractional attention parameter manually iterated until the combination that produces the minimum performance index is found. Finally, the model computes the performance index value and a pilot describing function. The performance index can be used in Equation 3-2 to estimate a Cooper-Harper rating (19:40).

$$Rating = 5.5 + 3.7 \cdot \log_{10}\left(\frac{J}{\sigma_c^2 \cdot \omega_w^2}\right) \tag{3-2}$$

where

σ_c = Forcing Function Root Mean Square Error Amplitude
ω_w = Forcing Function Bandwidth

Integrator Example. The easiest way to understand how this model works is to follow the computational flow using a simple example. This example will also give insight into the parameter selection process that will be discussed in the next section.

The simplest choice is to assume the aircraft dynamics can be modeled by an integrator and the forcing-function can be modeled by a first order lag. The following values parallel a sample problem presented in Reference 25.

State Space Realization

$$Y_c = \frac{\theta}{\delta e} = \frac{1}{s} \quad \Rightarrow \quad [\dot{x}_1] = [0]x_1 + [1]\delta e$$

$$y = \theta = [1]x_1 \tag{3-3}$$

$$Y_w = \frac{W_c}{W_w} = \frac{\sqrt{8.8}}{s+2} \quad \Rightarrow \quad [\dot{x}_2] = [-2]x_2 + [1]W_w$$

$$y = W_c = \left[\sqrt{8.8}\right]x_2 \tag{3-4}$$

where

Y_c = Aircraft Dynamics
Y_w = Tracking Task Forcing Function
x_1 = Pitch State (θ)
x_2 = Coloring Filter State
W_w = Zero Mean White Gaussian Noise
W_c = Colored Noise

The filter states are now augmented to the aircraft states in one of three ways. The advantages and disadvantages of each method will be discussed in the sensitivity analysis section of this chapter. The first option is to inject the noise at the aircraft output according to Figure 3-3.

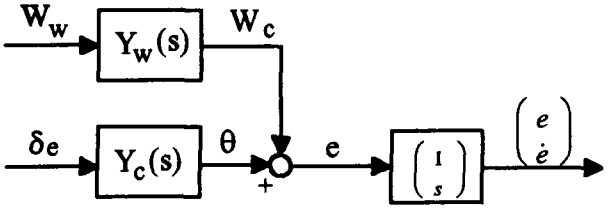

Figure 3-3. Noise Injected at Aircraft Output

Because the coloring filter and aircraft dynamics operate in parallel, their states can simply be appended together as shown in Equation 3-5.

$$\begin{bmatrix} \dot{x}_1 \\ \dot{x}_2 \end{bmatrix} = \begin{bmatrix} 0 & 0 \\ 0 & -2 \end{bmatrix} \cdot \begin{bmatrix} x_1 \\ x_2 \end{bmatrix} + \begin{bmatrix} 1 & 0 \\ 0 & 1 \end{bmatrix} \cdot \begin{bmatrix} \delta_e \\ Ww \end{bmatrix} \tag{3-5}$$

The output vector, *y*, contains the error and error rate where this error can be written as:

$$\begin{matrix} e = W_c + \theta \\ \dot{e} = \dot{W}_c + \dot{\theta} \end{matrix} \quad \text{but} \quad \begin{matrix} \theta = x_1 \\ \dot{\theta} = \dot{x}_1 = \delta_e \end{matrix} \quad \text{and} \quad \begin{matrix} W_c = \sqrt{8.8}\, x_2 \\ \dot{W}_c = \sqrt{8.8}\,(-2x_2 + W_w) \end{matrix} \tag{3-6}$$

The output can now be written in the following state space form:

$$y = \begin{bmatrix} e \\ \dot{e} \end{bmatrix} = \begin{bmatrix} 1 & \sqrt{8.8} \\ 0 & -2\sqrt{8.8} \end{bmatrix} \cdot \begin{bmatrix} x_1 \\ x_2 \end{bmatrix} + \begin{bmatrix} 0 & 0 \\ 1 & \sqrt{8.8} \end{bmatrix} \cdot \begin{bmatrix} \delta_e \\ W_w \end{bmatrix} \tag{3-7}$$

The second augmentation option is to inject the driving noise at the aircraft input as shown in Figure 3-4.

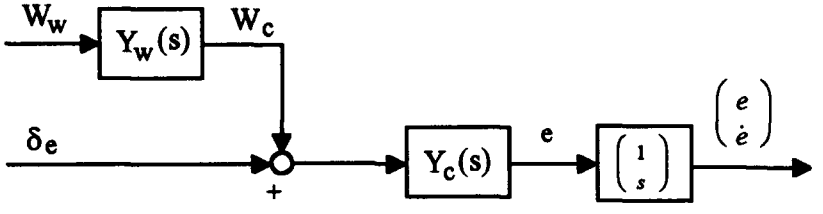

Figure 3-4. Noise Injected at Aircraft Input

Because the two transfer functions act in series, they require some manipulation. The state-space equation of the filter remains:

$$\dot{x}_2 = -2x_2 + W_w \quad \text{and} \quad y = W_c = \sqrt{8.8}\, x_2 \tag{3-8}$$

The aircraft input, however, is now $\delta + Wc$, and Y_c becomes:

$$\dot{x}_1 = \delta_e + W_c \quad \text{and} \quad y = e = x_1 \tag{3-9}$$

Combining Equations 3-8 and 3-9 gives the state-space representation shown below:

$$\begin{bmatrix} \dot{x}_1 \\ \dot{x}_2 \end{bmatrix} = \begin{bmatrix} 0 & \sqrt{8.8} \\ 0 & -2 \end{bmatrix} \cdot \begin{bmatrix} x_1 \\ x_2 \end{bmatrix} + \begin{bmatrix} 1 & 0 \\ 0 & 1 \end{bmatrix} \cdot \begin{bmatrix} \delta_e \\ Ww \end{bmatrix} \tag{3-10}$$

To find the output vector note that

$$e = \theta = x_1 \quad \text{and} \quad \dot{e} = \dot{\theta} = \dot{x}_1 = \sqrt{8.8}\, x_2 + \delta_e \tag{3-11}$$

Using Equation 3-11, the output vector can be written in the following form:

$$y = \begin{bmatrix} e \\ \dot{e} \end{bmatrix} = \begin{bmatrix} 1 & 0 \\ 0 & \sqrt{8.8} \end{bmatrix} \cdot \begin{bmatrix} x_1 \\ x_2 \end{bmatrix} + \begin{bmatrix} 0 & 0 \\ 1 & 0 \end{bmatrix} \cdot \begin{bmatrix} \delta_e \\ W_w \end{bmatrix} \tag{3-12}$$

The final augmentation option requires splitting the aircraft into two separate transfer functions, one before and one after the noise as shown in Figure 3-5.

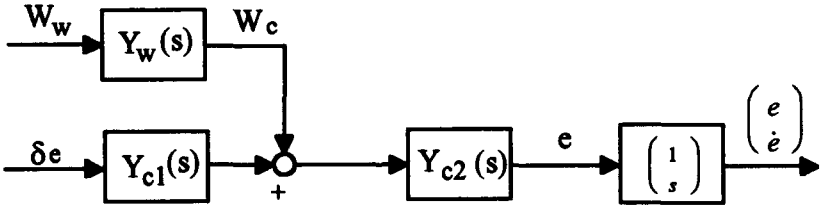

Figure 3-5. Noise Injected in the Middle of the Aircraft Dynamics

This form is not practical to implement for the integrator example, and will not be considered further in this section.

The linear quadratic regulator (LQR) problem must now be solved so that the muscular system is modeled. This is accomplished by augmenting the aircraft with integrators and iterating the control-rate weighting in the performance index[1]. For this analysis, the noise will be injected at the aircraft input, and Equations 3-10 and 3-12 will be used. The noises (including W_w) can be set to zero for the LQR solution, and the resulting state-space is:

$$\begin{bmatrix} \dot{x}_1 \\ \dot{x}_2 \end{bmatrix} = \begin{bmatrix} 0 & \sqrt{8.8} \\ 0 & -2 \end{bmatrix} \cdot \begin{bmatrix} x_1 \\ x_2 \end{bmatrix} + \begin{bmatrix} 1 \\ 0 \end{bmatrix} \cdot \delta_e$$

$$y = \begin{bmatrix} e \\ \dot{e} \end{bmatrix} = \begin{bmatrix} 1 & 0 \\ 0 & \sqrt{8.8} \end{bmatrix} \cdot \begin{bmatrix} x_1 \\ x_2 \end{bmatrix} + \begin{bmatrix} 0 \\ 1 \end{bmatrix} \cdot \delta_e \qquad (3\text{-}13)$$

This state space equation can be augmented with integrators by adding a third state, $x_3 = \delta_e$, and driving the system with $\dot{\delta}_e$. The resulting state-space is:

$$\begin{bmatrix} \dot{x}_1 \\ \dot{x}_2 \\ \dot{x}_3 \end{bmatrix} = \begin{bmatrix} 0 & \sqrt{8.8} & 1 \\ 0 & -2 & 0 \\ 0 & 0 & 0 \end{bmatrix} \cdot \begin{bmatrix} x_1 \\ x_2 \\ x_3 \end{bmatrix} + \begin{bmatrix} 0 \\ 0 \\ 1 \end{bmatrix} \dot{\delta}_e$$

$$y = \begin{bmatrix} e \\ \dot{e} \end{bmatrix} = \begin{bmatrix} 1 & 0 & 0 \\ 0 & \sqrt{8.8} & 1 \end{bmatrix} \cdot \begin{bmatrix} x_1 \\ x_2 \\ x_3 \end{bmatrix} + \begin{bmatrix} 0 \\ 0 \end{bmatrix} \dot{\delta}_e \qquad (3\text{-}14)$$

Equation 3-14 is now used to find the LQR solution. Because output weighting is desired, the user must select a state deviation weighting matrix, Q, where

$$Q = C^T Q_y C \qquad (3\text{-}15)$$

$$Q_y = diag\{q, 0\} \qquad (3\text{-}16)$$

[1] Consult the discussion in Appendix A for further information on this method.

q is always a scalar value. In this example q = 1 will be used. The weighting on error rate is automatically set to zero in this model.

Now the control weighting is iterated until the gain on the last state equals the inverse of the desired neuromuscular time constant. The optimal control law from the LQR solution of Equation 3-14 is:

$$u = \dot{\delta}_e = -K_c \bar{x} \tag{3-17}$$

Partitioning the gain and state matrices results in

$$\dot{\delta}_e = -\begin{bmatrix} K_{c1} & K_{c2} \end{bmatrix} \begin{bmatrix} \mathbf{x} \\ \delta_e \end{bmatrix} \tag{3-18}$$

$$\dot{\delta}_e = -K_{c1} \cdot \mathbf{x} - K_{c2} \cdot \delta_e \tag{3-19}$$

$$K_{c2}^{-1} \cdot \dot{\delta}_e + \delta_e = -K_{c2}^{-1} \cdot K_{c1} \cdot \mathbf{x} \tag{3-20}$$

Equivalently, the following relationship exists between the control input before and after the neuromuscular system:

$$\frac{\delta_e}{\delta'_e} = \frac{1}{\tau_n s + 1} \tag{3-21}$$

δ'_e is the control input before the muscular lag and δ_e is the control input after the lag. Equation 3-21 can be rewritten as:

$$\tau_n \dot{\delta}_e + \delta_e = \delta'_e \tag{3-22}$$

The terms in Equations 3-20 and 3-22 can be equated. This results in the following relationships:

$$\tau_n = K_{c2}^{-1} \quad \text{and} \quad \delta'_e = -K_{c2}^{-1} \cdot K_{c1} \cdot \mathbf{x} \tag{3-23}$$

In Equation 3-18, K_{c2} is the gain on the last state. Thus, the neuromuscular lag can be modeled by iterating the weighting on control rate until $K^{-1}_{c2} = T_n$ (2:10).

Continuing with the integrator example, with q = 1 and T_n = 0.08, the STI model will return a value for *g* of 0.00017. Further insight can be gained by solving this problem using the MATLAB™ command, *lqr*. Using Equation 3-14 and the weighting:

$$Q_y = \begin{bmatrix} 1 & 0 \\ 0 & 0 \end{bmatrix} \quad \text{and} \quad Q = C^T Q_y C = \begin{bmatrix} 1 & 0 & 0 \\ 0 & 0 & 0 \\ 0 & 0 & 0 \end{bmatrix} \tag{3-24}$$

yields the gain matrix:

$$K = \begin{bmatrix} 76.70 & 31.03 & 12.39 \end{bmatrix} \tag{3-25}$$

The inverse of the last gain is 0.08, the desired muscular lag[1]. The corresponding closed-loop transfer functions are:

$$\begin{bmatrix} \frac{e}{u} \\ \frac{\dot{e}}{u} \end{bmatrix} = \begin{bmatrix} \frac{(s+2)}{(s+2)(s^2+12.4s+76.7)} \\ \frac{s(s+2)}{(s+2)(s^2+12.4s+76.7)} \end{bmatrix} \tag{3-26}$$

The complex pole has a natural frequency of 8.76 radians per second and represents the neuromuscular dynamics. The iterative method used by this model will always return a pair of complex poles slightly below the desired neuromuscular break frequency.

Compare this result with the results achieved by appending the neuromuscular dynamics directly to the aircraft dynamics. The first order muscular lag can be written as shown in Equation 3-27.

---

[1] The STI literature refers to the *Time Constant* (τ_N) using the form: ($\tau_N s + 1$).

$$\frac{\delta_e}{\delta'^e} = \frac{1}{\tau_n s + 1} \Rightarrow \dot{x}_3 = -\frac{1}{\tau_n} x + \frac{1}{\tau_n} \delta'_e \quad \text{and} \quad \delta_e = x_3 \tag{3-27}$$

Placing Equations 3-13 and 3-27 in series and using the identity

$$P_3 = P_2 \cdot P_1 = \left[\begin{array}{cc|c} A_2 & B_2 C_1 & B_2 D_1 \\ 0 & A_1 & B_1 \\ \hline C_2 & D_2 C_1 & D_2 D_1 \end{array}\right] \tag{3-28}$$

where

$$P_i = \left[\begin{array}{c|c} A_i & B_i \\ \hline C_i & D_i \end{array}\right]$$

results in the following state-space representation:

$$\frac{1}{\tau_n s + 1} \cdot G_p \Rightarrow \begin{bmatrix} \dot{x}_1 \\ \dot{x}_2 \\ \dot{x}_1 \end{bmatrix} = \begin{bmatrix} 0 & \sqrt{8.8} & 1 \\ 0 & -2 & 0 \\ 0 & 0 & -\frac{1}{\tau_n} \end{bmatrix} \cdot \begin{bmatrix} x_1 \\ x_2 \\ x_3 \end{bmatrix} + \begin{bmatrix} 0 \\ 0 \\ \frac{1}{\tau_n} \end{bmatrix} \delta'_e$$

$$y = \begin{bmatrix} e \\ \dot{e} \end{bmatrix} = \begin{bmatrix} 1 & 0 & 0 \\ 0 & \sqrt{8.8} & 1 \end{bmatrix} \cdot \begin{bmatrix} x_1 \\ x_2 \\ x_3 \end{bmatrix} \tag{3-29}$$

Using Equation 3-29, $T_n = 0.08$, and $q = g = 1$, the LQR solution is:

$$K = \begin{bmatrix} 1 & 1.0563 & .0770 \end{bmatrix} \tag{3-30}$$

$$\begin{bmatrix} \frac{e}{u} \\ \frac{\dot{e}}{u} \end{bmatrix} = \begin{bmatrix} \frac{12.5 \cdot (s+2)}{(s+2)(s+1)(s+12.46)} \\ \frac{12.5 \cdot s(s+2)}{(s+2)(s+1)(s+12.46)} \end{bmatrix} \tag{3-31}$$

While this approach places a pole very near the desired muscular lag frequency (12.5), it allows the other pole to float well inside the pilot bandwidth. The iterative method

produced a 40 dB per decade roll-off slightly below the desired muscular frequency. This approach produced a 20 dB per decade roll-off at the desired muscular frequency. The first choice best models the human pilot and is used in the STI optimal pilot model.

The Kalman filter problem must now be solved. Since this is a single axis example, the fractional attention parameter, *f*, is one. For simplicity, this example will assume the indifference thresholds are zero. The noise intensity equations from Figure 3-2 take the following form:

$$V_{yi} = diag\{v_{y1}, v_{y2}\} \tag{3-32}$$

$$v_{yi} = \rho_{yi} \cdot \pi \cdot \sigma_{yi}^2 \quad \text{and} \quad V_u = \rho_u \cdot \pi \cdot \sigma_u^2 \tag{3-33}$$

In these equations the noise ratios (ρ) are user-defined, constant values. These values are entered in dB, but it should be noted that this model uses power spectra dB according to the following relationship.

$$dB = 10 \cdot \log_{10}(x) \tag{3-34}$$

This example uses the experimentally estimated noise ratios of 0.01 and 0.003 (6:18), or:

$$\rho_{yi} = -20\,dB \qquad \text{and} \qquad \rho_u = -25\,dB \tag{3-35}$$

When the program is initiated, an initial guess for the noise intensities must be made. The LQG problem is solved and the variances of the states are computed. The noise intensities are then iterated until Equations 3-33 is satisfied within some tolerance. Assuming a pilot delay of 0.15 seconds and unit-intensity driving noise (V_w), the optimal pilot model converged after seven iterations. The information in Figure 3-6 was displayed.

Iteration # 7

Optimal cost:	q,	g,	output,	input rate,	total
	1.0000E+00	1.7000E-04	1.1803E-01	4.1207E-02	1.5923E-01
Performance:	E{y_1^2},	E{y_2^2},	E{u_a^2},	E{u^2},	E{(du/dt)^2}
	1.1803E-01	3.0834E+00	4.8469E+00	3.8633E+00	2.4240E+02

Old noise intensities (V_y1, V_y2, V_ua):	3.7167E-03	9.6967E-02	4.8176E-02
New noise intensities (V_y1, V_y2, V_ua):	3.7079E-03	9.6869E-02	4.8152E-02
Noise ratios dB (rho_y1, rho_y2, rho_ua):	-19.9897	-19.9956	-24.9978

Max. noise ratio difference = 1.028061E-02 dB, Threshold = .1 dB
Finished with iterations

Figure 3-6. STI Optimal Pilot Model Output Display

The performance index value in the top right-hand portion of the display (1.5923E-01) was found from the following relationship:

$$J = E\{y_1^2\} \cdot q + E\{\dot{u}^2\} \cdot g \tag{3-36}$$

Note that by converting the noise ratios (ρ) back into decimal form (0.01, 0.01, and 0.001), the noise intensities can be verified using the following equations.

$$V_{y1} = E\{y_1^2\}\rho_1\pi \qquad V_{y2} = E\{y_2^2\}\rho_2\pi \qquad V_{ua} = E\{u_a^2\}\rho_{ua}\pi \tag{3-37}$$

Unfortunately, due to the way the display code was written, the above equations only hold when the *Old noise intensities* line is used. The final solution and performance index value are unaffected by this oddity, however.

This model requires a non-zero pilot delay. It finds the LQG solution in the digital domain using a sampling period equal to the pilot delay. If the delay is zero, the numerical algorithm called by the model will give an error message and the optimal pilot model will display erroneous data.

The STI optimal pilot model uses the compensator gains to form a transfer-function representation of the pilot. This is accomplished by modeling the pilot delay with a second order Pade approximation.

The performance index can be used to estimate an Cooper-Harper rating using Equation 3-2. In this equation, the rating is scaled by the forcing function bandwidth, ω_w, as well as the forcing function root mean square (RMS) error amplitude, σ_c. The RMS value is found by noting that for linear systems driven by white noise w(t):

$$\begin{aligned} \dot{x} &= A \cdot x + E \cdot w(t) \\ y &= C \cdot x \end{aligned} \tag{3-38}$$

where

$$\begin{aligned} E\{w(t)\} &= 0 \\ E\{w(t) \cdot w^T(t+\tau)\} &= Q \cdot \delta(\tau) \end{aligned}$$

w(t) = Zero Mean Stationary White Gaussian
E{w(t)}= Gaussian Probability Density
Q = Constant Intensity Matrix for w(t)

The covariance matrix X is defined as:

$$X = E\{x(t) \cdot x^T(t)\} \tag{3-39}$$

and is the solution of the following Lyapunov equation:

$$A \cdot X + X \cdot A^T + E \cdot Q \cdot E = 0 \tag{3-40}$$

The output covariance matrix is then

$$Y = E\{y(t) \cdot y^T(t)\} = C \cdot X \cdot C^T \tag{3-41}$$

Because the STI optimal pilot model requires single-input-single-output dynamics, Y is a scalar and is the output variance, σ^2, of the forcing function filter (11:97-111). The

Program CC command - *MEAN,Yw* - will compute this value as long as the task forcing function coloring filter is driven by unit intensity white noise ($V_w = 1$).

In this example the RMS, σ_c, is 1.48 and the filter bandwidth, ω_w, is 2.2 radians per second. Substituting these values into Equation 3-2 result in the following equation.

$$Rating = 1.7 + 3.7 \cdot \log_{10}(J) \tag{3-42}$$

For a performance index value of 0.159 (see Figure 3-6), the predicted Cooper-Harper rating is -1.25. Obviously, this is not a practical handling qualities rating. The aircraft dynamics and tracking task forcing function used for this example were overly simplified. More importantly, the parameters used when running this model were chosen to parallel an example in Reference 25. As shown in the next section, these parameters must be more carefully selected.

Sensitivity Analysis. The pilot describing function and Cooper-Harper rating predicted by the STI optimal pilot model are sensitive to the many parameters the user must select. This section conducts a sensitivity analysis of the pilot model parameters and offers some selection guidance in an effort to make this model more practicable.

The following pitch-attitude transfer functions were used to conduct the sensitivity analysis.

$$\text{Case 1:} \quad \frac{\theta}{\delta_e} = \frac{100}{s(s+100)} \tag{3-43}$$

$$\text{Case 2:} \quad \frac{\theta}{\delta_e} = \frac{20(s+1.25)}{s(s^2+8s+25)} \cdot e^{-.033s} \tag{3-44}$$

$$\text{Case 3:} \quad \frac{\theta}{\delta_e} = \frac{20(s+1.25)}{s(s^2+8s+25)} \cdot e^{-.2s} \tag{3-45}$$

$$\text{Case 4:}\quad \frac{\theta}{\delta_e} = \frac{20(s+1.25)}{s(s^2+1.8s+25)} \cdot e^{-.033s} \tag{3-46}$$

$$\text{Case 5:}\quad \frac{\theta}{\delta_e} = \frac{20(s+1.25)}{s(s^2+1.8s+25)} \cdot e^{-.2s} \tag{3-47}$$

These equations of motion were chosen for two reasons. First, they represent a broad range of aircraft dynamics and are therefore well suited for the sensitivity analysis. Second, these dynamics were evaluated in a previous experiment using the Large Amplitude Multi-Mode Aerospace Research Simulator (LAMARS) (Reference 19).

All of the dynamics have fighter type responses. Case 1 is nearly an integrator. The other cases have the characteristics shown in Table 3-1.

Table 3-1
STI Optimal Pilot Model Evaluation Dynamics

	Short Period Damping Ratio, ζ_{sp}	Short Period Natural Frequency, ω_{sp}	Delay, τ
Case 2	0.8	5	0.033
Case 3	0.8	5	0.2
Case 4	0.18	5	0.033
Case 5	0.18	5	0.2

These dynamics were evaluated by McRuer using a sum-of-sines tracking task generated on the LAMARS head-up display (HUD), and were assigned the Cooper-Harper ratings shown in Table 3-2 (19:19).

Table 3-2
Cooper-Harper Ratings Used for Sensitivity Analysis

	Case 1	Case 2	Case 3	Case 4	Case 5
Rating	2	3	4	4	6

The user must choose the following parameters before running the STI optimal pilot model.

1. Aircraft Model Order (Y_c)
2. Task Forcing Function (Y_w)
3. Intensity of the Driving Noise (V_w)
4. Filter Augmentation Method (Aircraft Output or Input)
5. Neuromuscular Time Constant (T_n)
6. State Deviation Weighting (q)
7. Initial Guesses and Convergence Thresholds for Control Rate Weighting and Noise Intensities (g, V_y, and V_u)
8. Pilot Delay (τ)
9. Observation and Motor Noise Ratios (ρ_{y1}, ρ_{y2}, and ρ_u)
10. Visual Indifference Thresholds (T_{y1} and T_{y2})
11. Fractional Attention Parameter (f)

The data gathered in this thesis indicates that the values in Table 3-3 should be used.

Table 3-3
Recommended Parameters for STI Optimal Pilot Model

Parameter	Symbol	Recommended Value
Aircraft Model Order	Y_c	Lowest Feasible
Task Forcing Function	Y_w	$\frac{\sqrt{2}}{6.25 \cdot s^2 + 3.54 \cdot s + 1}$
Intensity of the Driving Noise	V_w	1
Filter Augmentation Method	-----	Output
Neuromuscular Time Constant	τ_n	0.08
State Deviation Weighting	q	1
Initial Guesses for Control Rate Weighting and Noises	g_i, V_{yi}, V_{ui}	$g_i = 0.1$ V_{yi}, $V_{ui} = 1$
Convergence Thresholds for Control Rate Weighting and Noises	-----	g: 0.001 V_y, V_u: 0.1
Pilot Delay	τ	0.2 seconds
Observation and Motor Noise Ratios	ρ_{y1}, ρ_{y2}, ρ_u	-20 dB for All
Visual Indifference Thresholds	T_{y1}, T_{y2}	0
Fractional Attention Parameter	f	1

In the following discussion each of these parameters is evaluated individually with the others held constant at the values shown in this table[1].

Aircraft Model Order. The lowest model order consistent with the task should be used. High-order dynamics should be modeled by an equivalent delay if possible using a lower order equivalent system[2]. The STI optimal pilot model computes a predicted pilot describing function of order $2n+5$ where n is the number of aircraft and filter states. For example, the model returned a fifteenth order pilot describing function when the short period approximation of Case 2, was analyzed.

Task Forcing Function. The task forcing function recommended by this thesis is a second order Butterworth filter, shown in Equation 3-48, with a break frequency of 0.4 radians per second. The numerator gain $(\sqrt{2})$ makes the filter bandwidth, ω_ω, equal to the break frequency.

$$Y_w = \frac{\sqrt{2}}{\left(\frac{s}{\omega_w}\right)^2 + \frac{\sqrt{2}}{\omega_w}s + 1} \tag{3-48}$$

Table 3-4 shows the relationship between filter bandwidth and predicted Cooper-Harper rating. The forcing function root mean square (RMS) errors were computed using the *Program CC* command -- *Mean,yw* -- and the predicted Cooper-Harper ratings were computed using Equation 3-2. The pure delays in Equations 3-44 through 3-47 were added to the pilot delay, τ. When modeled instead by a first order Pade approximation, the results were within one-hundredth of a rating.

[1] A macro containing typical *Program CC* commands used for this analysis is presented at the end of Appendix B.

[2] The lower order equivalent system match routine described in MIL-STD-1797 was implemented on PC MatLab in a *Handling Qualities Toolbox* for this thesis. Copies of this toolbox are available from the author.

Table 3-4
The Effects of Forcing Function Bandwidth on Predicted Cooper-Harper Rating
-- STI Optimal Pilot Model

Bandwidth, ω_w	RMS Error, σ_c	Case 1 (2)[1]	Case 2 (3)[1]	Case 3 (4)[1]	Case 4 (4)[1]	Case 5 (6)[1]	*Legend*[2]
0.1	0.266	3.99E-5	1.17E-4	1.86E-4	3.50E-4	4.33E-4	*J*
		0.9	2.6	3.4	4.4	4.7	*Rating*
0.4	0.532	4.73E-3	9.72E-3	1.66E-2	2.33E-2	3.09E-2	*J*
		1.9	3.0	3.9	4.4	4.9	*Rating*
0.5	0.595	1.00E-2	1.92E-2	3.24E-2	4.30E-2	5.7E-2	*J*
		2.0	3.0	3.9	4.3	4.8	*Rating*
0.8	0.752	4.62E-2	7.45E-2	1.23E-1	1.41E-1	1.86E-1	*J*
		2.2	3.0	3.8	4.0	4.4	*Rating*
1	0.841	9.23E-2	1.38E-1	2.21E-1	2.35E-1	3.09E-1	*J*
		2.2	2.9	3.6	3.7	4.2	*Rating*
2	1.19	6.63E-1	7.73E-1	1.07	9.35E-1	1.15	*J*
		2.1	2.3	2.8	2.6	2.9	*Rating*
5	1.88	4.16	3.76	3.69	3.61	3.60	*J*
		0.6	0.4	0.4	0.4	0.4	*Rating*

[1] Cooper-Harper rating assigned during simulator tracking task in Reference 24

[2] Where *J* is the performance index and *Rating* is the predicted Cooper-Harper rating

The data from Table 3-4 is plotted in Figure 3-7 for clarity. Close examination of this figure reveals that the STI optimal pilot model responded to the forcing function characteristics in much the same way as a human pilot would. As the bandwidth of the forcing function approached the pilot bandwidth, the difference between the predicted ratings became negligible. Likewise, the human pilot will not attempt to follow the commands as this frequency is approached, and is therefore not able to distinguish between the different dynamics.

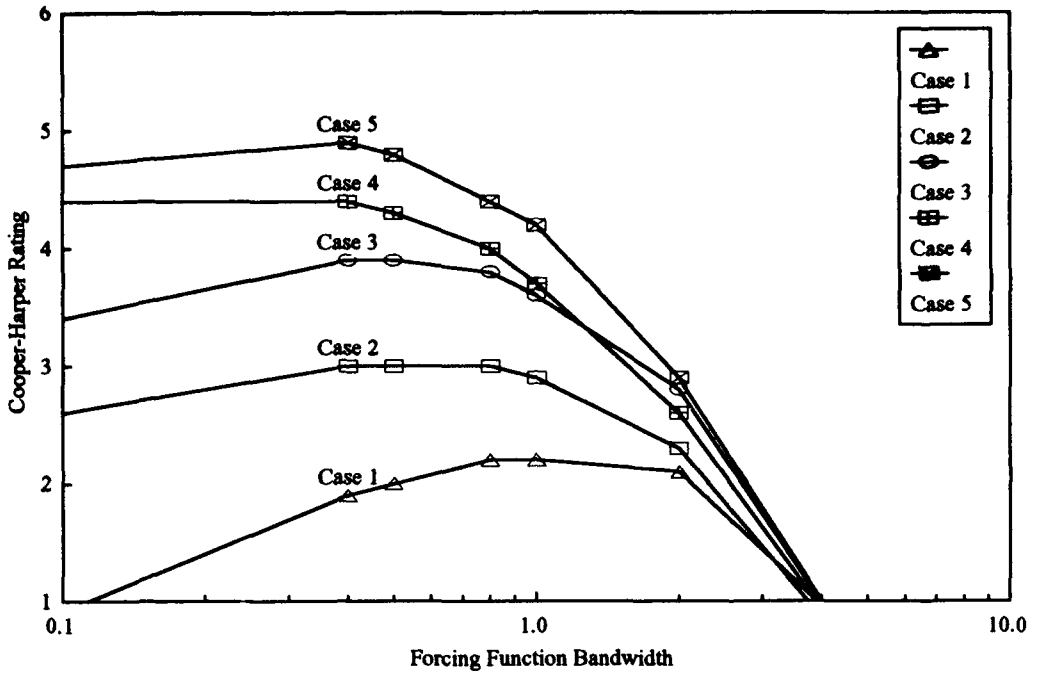

Figure 3-7. The Effects of Forcing Function Bandwidth on Predicted Cooper-Harper Ratings -- STI Optimal Pilot Model

The logical first choice for forcing function bandwidth is one that mirrors that of the actual tracking task. The STI optimal pilot model does not work well when this choice is made. McRuer's evaluation of these dynamics used a forcing-function bandwidth of 2 radians per second which is typical for compensatory tracking tasks. As shown in Figure 3-7 the ratings in this region are tightly grouped and are not good predictors of the experimental ratings. Instead, the best results will be obtained if each case is evaluated for a range of forcing function bandwidths, and the one producing the worst Cooper-Harper rating is used. Note that in Figure 3-7 this maximum occurs over a broad frequency making the top of each curve fairly flat. A break frequency of 0.4 radians per second worked well for all five cases examined in this chapter.

Driving Noise Intensity. The intensity of the driving noise, V_w, can be included either as a numerator gain in the task forcing function, Y_w, or directly by

varying the noise intensity value, V_w. Both methods yield identical results. In either case the predicted rating is independent of the noise intensity.

The method for finding the forcing function root mean square (RMS) error amplitude, σ_c, described in Equations 3-38 through 3-41 and the *Program CC* command that implements this method -- *Mean, Y_w* -- assume a unit intensity driving noise, V_w. If the driving noise is not unit intensity, the numerator of the task forcing function, Y_w, must be multiplied by the square root of the driving noise intensity, V_w, to form an equivalent system. It is therefore easier to always use unit intensity driving noise.

Because the Cooper-Harper rating formula, Equation 3-2, is normalized for σ_c, the predicted Cooper-Harper rating is independent of the numerator gain of the task forcing function, Y_w. Table 3-5 shows the predicted Cooper-Harper ratings for a range of numerator values. Note that while the performance index, *J*, increased with the forcing function RMS error amplitude, σ_c, the predicted Cooper-Harper ratings did not change.

Table 3-5
The Effects of Task Forcing Function Numerator on Predicted Cooper-Harper Rating
-- STI Optimal Pilot Model

Y_w Numerator	RMS Error[1], σ_c	Case 1 (2)[2]	Case 2 (3)[2]	Case 3 (4)[2]	Case 4 (4)[2]	Case 5 (6)[2]	*Legend*[3]
$\sqrt{2}$	0.532	4.73E-3	9.72E-3	1.66E-2	2.33E-2	3.09E-2	*J*
		1.9	3.0	3.9	4.4	4.9	*Rating*
2	0.752	9.43E-3	1.94E-2	3.32E-2	4.68E-2	6.17E-2	*J*
		1.9	3.0	3.9	4.4	4.9	*Rating*
4	1.50	3.78E-2	7.79E-2	1.33E-1	1.87E-1	2.47E-1	*J*
		1.9	3.0	3.9	4.4	4.9	*Rating*

[1] Forcing function bandwidth was 0.4 radians per second for all runs in this table.

[2] Cooper-Harper rating assigned during simulator tracking task in Reference 24

[3] Where *J* is the performance index and *Rating* is the predicted Cooper-Harper rating

Since the numerator gain of the task forcing function, Y_w, has no effect on the predicted Cooper-Harper rating, the square root of two was used. This value makes the bandwidth -- defined as the zero magnitude (dB) frequency -- equal to the filter break frequency.

Filter Augmentation Method. As discussed earlier in this chapter, the driving noise can be added at the aircraft input, output, or between to parts of the aircraft dynamics. This study chose output augmentation for two reasons. First, it makes better physical sense. Second, the Cooper-Harper ratings predicted using the output augmentation method better matched the experimental results.

The STI optimal pilot model uses only error and error rate for feedback. When the output augmentation method of Figure 3-3 (page 3-9) is chosen, this error is the difference between the colored, forcing function driving noise and the aircraft output. This is similar to an actual tracking task, including the LAMARS task, where the pilot perceives a difference between his actual condition and his desired position and acts to minimize this error. If the noise is injected at the aircraft input as shown in Figure 3-4 (page 3-10), this physical significance is lost. Injecting the noise between two parts of the aircraft dynamics, as shown in Figure 3-5 (page 3-11), is for specialized analysis and not considered further in this thesis.

The Cooper-Harper ratings predicted using the output augmentation method better matched experimental results. The predicted Cooper-Harper ratings for both input and output noise injection are shown in Table 3-6. Notice that input injection values are overly pessimistic when compared to experimentally obtained values.

Table 3-6
The Effects of Noise Injection Method on Predicted Cooper-Harper Rating
-- STI Optimal Pilot Model

Noise Injection Method	Case 1 (2)[1]	Case 2 (3)[1]	Case 3 (4)[1]	Case 4 (4)[1]	Case 5 (6)[1]	*Legend*[2]
Input	1.20E-2	5.13E-2	8.28E-2	1.67E-1	2.11E-1	*J*
	3.3	5.7	6.5	7.6	8.0	*Rating*
Output	4.73E-3	9.72E-3	1.66E-2	2.33E-2	3.09E-2	*J*
	1.9	3.0	3.9	4.4	4.9	*Rating*

[1] Cooper-Harper rating assigned during simulator tracking task in Reference 24
[2] Where *J* is the performance index and *Rating* is the predicted Cooper-Harper rating

Neuromuscular Time Constant. The neuromuscular time constant is used to limit the pilot model bandwidth. The actual bandwidth for this model was lower than the time constant choice should have produced. Thus, a time constant, T_n, of 0.08, or a muscular lag at 12.5 radians per second, is recommended.

The iterative method of using control rate weighting to model the neuromuscular lag always produces a pair of complex poles at a frequency less than the desired muscular lag frequency. As shown with the integrator example in Equation 3-26 (page 3-14), a neuromuscular time constant, T_n, of 0.08 placed a pair of complex poles at 8.76 radians per second. The actual human neuromuscular time constant has been experimentally measured between 0.08 and 0.12, resulting in a first order lag between 8.3 and 12.5 radians per second (16:29). The high end of this range ($T_n = 0.08$) was chosen.

State Deviation Weighting. It makes no difference what value is used for the state deviation weighting. The STI model results are independent of this value.

Because the STI optimal pilot model requires single-input-single-output aircraft dynamics, the state deviation weighting matrix is formed by selecting a scalar value, q, as

shown in Equation 3-16 (page 3-12). The model then finds the control rate weighting, g, that establishes the desired neuromuscular lag. The ratio between the control-rate and state deviation weighting is fixed by this process.

The gain matrix shown in Equation 3-25 (page 3-14), was computed in the integrator example presented earlier in this chapter. In this example, the state deviation weighting, q, was one and the state deviation weighting, g, used to model the neuromuscular lag was 0.00017. When the same problem was repeated with a state deviation weighting of 5, the model set the control rate penalty, g, at *0.00085* to model the muscular dynamics and computed the same gain matrix. This weighting was five times the previous value, just as the state deviation penalty was five times that in the previous example.

Initial Guesses and Convergence Thresholds. Because the STI optimal pilot model finds the control rate weighting, g, and the noise, V_{yi} and V_u, iteratively, the model requires initial guesses and convergence thresholds for each. Within reason, it does not matter what values are chosen for the initial guesses. The number of iterations required for convergence does not increase significantly if a poor initial guess is made. This thesis used the convergence thresholds recommended in Reference 25 (25:29).

Pilot Delay. The delay time of the human pilot has been measured experimentally between 0.15 and 0.3 seconds (6:18). A pilot delay of 0.2 seconds was used in this analysis.

The effects of pilot delay on predicted Cooper-Harper rating are shown in Table 3-7.

Table 3-7
The Effects of Pilot Delay on Predicted Cooper-Harper Rating
-- STI Optimal Pilot Model

Pilot Delay (seconds)	0.10	0.15	0.20	0.25	0.30	*Legend*[2]
Case 1 (2)[1]	2.53E-3	3.52E-3	4.73E-3	6.15E-3	7.80E-3	*J*
	0.9	1.4	1.9	2.3	2.7	*Rating*
Case 2 (3)[1]	6.28E-3	7.93E-3	9.72E-3	1.16E-2	1.37E-2	*J*
	2.3	2.7	3.0	3.3	3.6	*Rating*
Case 4 (4)[1]	1.75E-2	2.06E-2	2.33E-2	2.59E-2	2.82E-2	*J*
	4.0	4.2	4.4	4.6	4.7	*Rating*

[1] Cooper-Harper rating assigned during simulator tracking task in Reference 24
[2] Where *J* is the performance index and *Rating* is the predicted Cooper-Harper rating

Cases 3 and 5 are not included in this table because their dynamics are identical to those of Cases 2 and 4. Note that the relationship is fairly linear with every ten milliseconds of added delay producing no more than a tenth of a rating increase. Also note that added delay does not affect the ratings of the *poor* dynamics as much as *good* dynamics. For the same added delay, the predicted rating for Case 1 dropped from 0.9 to 2.7 while the predicted rating for Case 4 went from 4.0 to 4.7.

Noise Ratios. The noise ratios are perhaps the most difficult pilot model parameters to select. The predicted Cooper- ratings and estimated pilot describing functions are especially sensitive to these values. For this reason it is desirable to stay as close as possible to experimentally measured values. Reference 6 recommended using the following values (6:18).

$$\rho_{yi} = -20\,dB \quad \text{and} \quad \rho_u = -25\,dB \tag{3-49}$$

The STI optimal pilot model results in Table 3-8 were found using these values.

Table 3-8
The Effects of Noise Ratios on Predicted Cooper-Harper Rating
-- STI Optimal Pilot Model (ρ_u = -25 dB)

Bandwidth, ω_w	RMS Error, σ_c	Case 1 (2)[1]	Case 2 (3)[1]	Case 3 (4)[1]	Case 4 (4)[1]	Case 5 (6)[1]	*Legend*[2]
0.1	0.266	1.87E-5	4.99E-5	9.04E-5	1.41E-4	2.00E-4	*J*
		----	1.2	2.3	2.9	3.5	*Rating*
0.4	0.532	2.79E-3	5.35E-3	1.02E-2	1.13E-2	1.75E-2	*J*
		1.0	2.1	3.1	3.3	4.0	*Rating*
0.5	0.595	6.11E-3	1.11E-2	2.11E-2	2.11E-2	3.38E-2	*J*
		1.2	2.2	3.2	3.2	4.0	*Rating*
0.8	0.752	3.04E-2	4.88E-2	8.80E-2	7.99E-2	1.23E-1	*J*
		1.5	2.3	3.2	3.1	3.8	*Rating*
1	0.841	6.31E-2	9.55E-2	1.67E-1	1.42E-1	2.16E-1	*J*
		1.6	2.0	2.6	2.2	2.7	*Rating*
2	1.19	5.00E-1	6.30E-1	9.20E-1	7.20E-1	9.80E-1	*J*
		1.6	2.0	2.6	2.2	2.7	*Rating*
5	1.88	3.50	3.50	3.60	3.50	3.50	*J*
		0.3	0.3	0.4	0.3	0.3	*Rating*

[1] Cooper-Harper rating assigned during simulator tracking task in Reference 24
[2] Where *J* is the performance index and *Rating* is the predicted Cooper-Harper rating

As in Table 3-4, the results are displayed for range of forcing function bandwidths. The data from Table 3-8 is plotted in Figure 3-8 on the following page for clarity. In all cases the predicted Cooper-Harper ratings were overly optimistic when compared with experimentally obtained ratings.

Increasing the motor noise ratio, ρ_u, from -25 dB to -20 dB improved the model's predictions. The results in Table 3-4 and Figure 3-7 (page 3-24) were obtained with a motor noise ratio of -20 dB, and were more in line with the experimentally obtained ratings. The motor noise ratio, ρ_u, was used in this thesis to fine tune the STI optimal pilot model predictions, and -20 dB seemed to do this well.

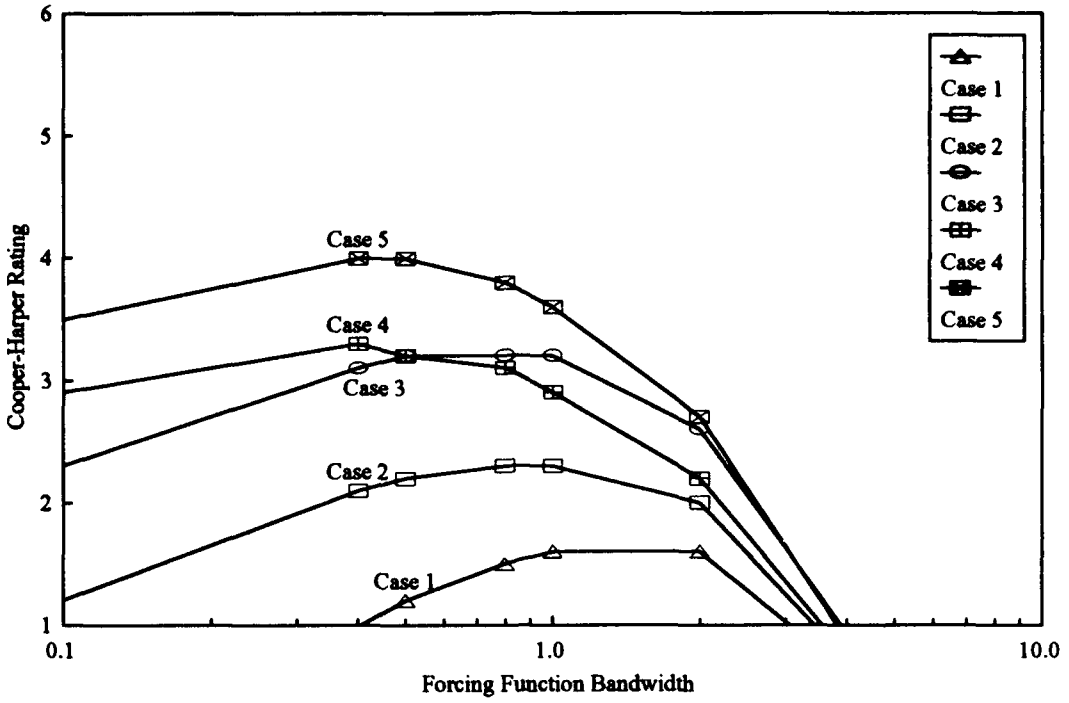

Figure 3-8. The Effects of Noise Ratios on Predicted Cooper-Harper Ratings -- STI Optimal Pilot Model (ρ_u = -25 dB)

Visual Indifference Thresholds. Visual indifference thresholds in the STI optimal pilot model tended to excessively penalize *good* dynamics, and this thesis recommends using thresholds of zero unless display effects are being specifically studied.

The visual indifference thresholds of the human pilot are dependent on the task display. Dillow and Picha used 0.05 degrees and 0.18 degrees per second as typical values for pitch axis error and error rate, visual indifference thresholds (6:18). The STI optimal pilot model results found using these values are presented in Table 3-9. As shown in this table, the predictions obtained using indifference thresholds of zero better matched experimental results.

Table 3-9
The Effects of Visual Indifference Thresholds on Predicted Cooper-Harper Rating
-- STI Optimal Pilot Model

Visual Indifference Thresholds	Case 1 (2)[1]	Case 2 (3)[1]	Case 3 (4)[1]	Case 4 (4)[1]	Case 5 (6)[1]	*Legend*[2]
Error, $T_{y1} = 0$ Error Rate, $T_{y2} = 0$	4.73E-3	9.72E-3	1.66E-2	2.33E-2	3.09E-2	*J*
	1.9	3	3.9	4.4	4.9	*Rating*
Error, $T_{y1} = 0.05$ Error Rate, $T_{y2} = 0.18$	1.14E-2	1.60E-2	2.32E-2	2.78E-2	3.51E-2	*J*
	3.3	3.8	4.4	4.7	5.1	*Rating*

[1] Cooper-Harper rating assigned during simulator tracking task in Reference 24

[2] Where *J* is the performance index and *Rating* is the predicted Cooper-Harper rating

Fractional Attention Parameter. The fractional attention parameter is used to predict multi-axis Cooper-Harper ratings. Each axis is assigned a fraction of the pilot's attention so that the fractions total one. Because the STI optimal pilot model requires single axis dynamics, the fractional attention parameters must be manually iterated.

In a two axis problem, for example, the user must find the performance index in each axis for a range of fractional attention parameters. The performance indices for those combinations of fractional attention parameters that total one must then be summed. The lowest total performance index is then used to find the predicted multi-axis rating using Equation 3-2. Obviously, this procedure becomes more complicated and lengthy as additional axes are added.

Pilot Describing Function. The STI optimal pilot model computes a pilot describing function along with a predicted Cooper-Harper rating. This transfer function enhances the model's abilities as a predictive tool. Unfortunately, these transfer functions are very high order and often do not reduce to the classical lead-lag-delay pilot model with acceptable accuracy.

Using the values in Table 3-3, the STI optimal pilot model predicted the following pilot describing functions for Cases 1 through 5 (Y_{p1}- Y_{p5})[1].

$$Y_{p1} = \frac{174(0)(.0448)[.707,.4](1.65)(5.79)(12.63)(12.91)[-.866,17.3](100)^2}{(0)[.707,.4]^2(6.02)(12.57)(12.63)[.274,18.96](45.4)(94)(100)} \quad (3\text{-}50)$$

$$Y_{p2} = \frac{92.6(0)(.032)[.707,.4](1.45)[.814,4.56][.8,5](5.08)(12.5)^2[-.866,14.9]}{(0)[.707,.4]^2(1.25)(4.96)[.8,5](12.43)(12.46)[.146,14.2][.84,27.3]} \quad (3\text{-}51)$$

$$Y_{p3} = \frac{92.7(0)(.035)[.707,.4](1.19)(4.1)[.79\ \ 6,4.78][.8,5][-.866,8.66](12.5)^2}{(0)[.707,.4]^2(1.25)(4.02)[.8,5][.043,11.5](12.36)(12.46)[.81,23.5]} \quad (3\text{-}52)$$

$$Y_{p4} = \frac{46.2(0)(.028)[.707,.4](1.18)[.06,4.4](4.56)[.18,5](12.5)(12.6)[-.866,14.9]}{(0)[.707,.4]^2(1.25)(4.6)[.18,5](12.49)(12.52)[.157,12.8][.846,23.3]} \quad (3\text{-}53)$$

$$Y_{p5} = \frac{40.4(0)(.028)[.707,.4](1.04)(3.74)[.025,4.96],[.18,5],[-.866,8.66](12.5)^2}{(0)[.707,.4]^2(1.25)(3.77)[.182,5][.082,10.7](12.4)(12.5)[.818,19.12]} \quad (3\text{-}54)$$

The pilot delay was modeled with a second order Pade approximation. There are several near pole-zero cancellations in the above transfer functions. Thompson also recommends grouping the high-frequency poles, those above 5 radians per second, into an equivalent delay (25:38). An alternative approach is to use a lower order equivalent system match routine similar to that used in MIL-STD-1797A for aircraft dynamics (Reference 5). The following equivalent systems were computed by finding the best fit to the classical gain, lead, lag, and delay pilot model between 0.1 and 10 radians per second[2].

$$Y_{p1} = \frac{3.756(s+2.921)}{(s+1.546)} \cdot e^{-.154s} \quad (3\text{-}55)$$

[1] Where the brackets denote $[\zeta, \omega_n]$ as in $s^2 + 2\zeta\omega_n + \omega_n^2$, and the parentheses denote (τ) as in $s + \tau$.

[2] This lower order equivalent system match routine was implemented on PC MatLab in a *Handling Qualities Toolbox* for this thesis and is available from the author.

$$Y_{p2} = \frac{1.29(s+3.248)}{(s+0.973)} \cdot e^{-.106s} \tag{3-56}$$

$$Y_{p3} = \frac{1.294(s+2.253)}{(s+1.036)} \cdot e^{-.198s} \tag{3-57}$$

$$Y_{p4} = \frac{0.347(s+5.42)}{(s+0.682)} \cdot e^{-.0123s} \tag{3-58}$$

$$Y_{p5} = \frac{0.295(s+5.31)}{(s+0.765)} \cdot e^{-.13s} \tag{3-59}$$

The Bode plots of the predicted pilot describing function and their lower order equivalent systems matches are shown in Appendix B. These matches were especially poor for the lightly damped dynamics (Cases 4 and 5). For these cases, shown in Figures B-4 and B-5, the STI optimal pilot model predicted a pilot describing function that essentially notched out the aircraft short period dynamics. This behavior is not possible using only a gain, lead, lag, and delay model, and is inconsistent with McRuer's experimental observations (14:218)[1].

Summary

The optimal pilot model was developed in an attempt to overcome deficiencies in the classical pilot model approach. This chapter focused on an optimal pilot model developed by Systems Technology, Incorporated (STI), for use with *Program CC* (Reference 25). This model incorporates nearly every important aspect of other optimal pilot models and can be implemented on the personal computer, but it lacks parameter selection guidance.

---

[1] Consult the discussion on page 2-13.

This model allows the feedback of only one variable and its derivative, therefore single-input-single-output dynamics must be used for both the aircraft and forcing function dynamics. The model solves the linear quadratic regulator (LQR) problem by adjusting the control rate weighting, *g*, so that the neuromuscular dynamics are modeled. The model then iteratively solves the Kalman filter problem so that the desired noise ratios are obtained. Finally, a predicted pilot describing function is computed and the performance index is used to predict a Cooper-Harper rating.

The user must choose several parameters before running the STI optimal pilot model. A sensitivity analysis of these parameters was conducted using five different pitch axis dynamics. Based on this analysis, the parameters in Table 3-3 (page 3-21) should be used when running the STI optimal pilot model. Additionally, the following conclusions were reached.

1. Include aircraft delays in the pilot delay or model them with a first order Pade approximation. The results are the same for both methods (page 3-22)[1].
2. Model the task forcing function, Y_w, as a second order Butterworth filter. Evaluate the dynamics for a range of forcing function bandwidths, and use the one that predicts the worst Cooper-Harper rating. A bandwidth of 0.4 radians per second worked well for all five cases examined in this chapter (page 3-24).
3. The predicted Cooper-Harper ratings are independent of the driving noise intensity, V_w (page 3-25).
4. Injecting the forcing function driving noise at the aircraft output makes better physical sense and produces more accurate predictions (page 3-26).
5. Use a neuromuscular time constant, T_n, of 0.08, producing a lag at 12.5 radians per second. The optimal pilot model establishes the model bandwidth slightly lower than it should, and 12.5 is at the high end of the experimentally measured range (page 3-27).

[1] Refers to the page in this thesis containing this conclusion.

6. The STI optimal pilot model results are independent of the state deviation weighting, q (page 3-28).

7. The STI optimal pilot model is insensitive to initial guess values for the control-rate weighting and the noise intensities (page 3-28).

8. Use -20 dB for all noise intensities, ρ_{y1}, ρ_{y2}, and ρ_u. The motor noise intensity, ρ_u, was increased from its experimentally measured value (-25 dB) to fine tune the model's predictions (page 3-30).

9. Set the visual indifference thresholds, T_{y1} and T_{y2}, to zero unless display effects are being studied. Non-zero values overly penalize good dynamics (page 3-31).

10. The predicted pilot describing functions are not consistent with the classical pilot model form or the experimental observations of McRuer in Reference 14 (page 3-34).

4. Flight Test

General

As shown in the previous chapter, the high order pilot transfer functions predicted by the STI optimal pilot model were not consistent with classical pilot model theory. In an effort to resolve this and other important pilot modeling issues, a limited evaluation of human pilot response was sponsored in support of this thesis by the Air Force Flight Dynamics Directorate. This flight test is detailed in AFFTC-TLR-93-41 (Reference 7). The applicable aspects of the test are presented in this chapter.

This chapter is divided into three sections. The first section, *Test Procedures,* provides a description of the flight test. The second section, *Test Results,* emphasizes those results applicable to optimal pilot modeling theory. This section focuses on single axis tasks and contains statistical and frequency response analysis not published in AFFTC-TLR-93-41. Finally, the important conclusions of this chapter are summarized.

Test Procedures

The flight test was conducted at Calspan Corporation, Buffalo, New York by a five member team from the USAF Test Pilot School between 8 and 11 October 1993. Five sorties totaling 7.6 hours were flown in the Calspan variable stability Lear II aircraft. Ground simulations in Lear II were also performed. Four different pitch and four different roll axis dynamics were evaluated using three different tracking tasks. For each set of dynamics, primary pilot response parameters were recorded and examined

using Fourier transform analysis in an attempt to provide an insight into human pilot behavior. Pilot comments and Cooper-Harper ratings were also recorded. The flight test data gathered during this project are maintained at the Air Force Flight Dynamics Directorate (WL/FIGC), Wright-Patterson AFB, OH 45433, and are available for research purposes. AFFTC-TLR-93-41 serves as a guide for the flight test data base and provides an initial look at the test results.

Research Vehicle Description. The pilot was the true test item for this test program. The three test pilots used for this evaluation had a variety of operational backgrounds. Two of the pilots had multi-engine backgrounds. One had extensive KC-10 experience and the other had extensive C-130 experience. The third pilot was an experienced test pilot with considerable F-15 and F-16 experience.

The Calspan Variable-Stability Lear II was used as the research vehicle for this evaluation. It was a production Learjet 25 aircraft that was extensively modified for use as an in-flight simulator. The basic aircraft is shown in Figure 4-1.

The safety pilot's (left seat) control column was connected directly to the aircraft's control surfaces through the production, reversible push rod system and mirrored the surface positions. The evaluation pilot's (right seat) controls were removed and replaced with a variable, center-stick feel system that was part of the in-flight simulation system.

A digital computer system was located in the main cabin. It was designed to model aircraft and artificial feel systems and record in-flight data. Real time monitoring of up to 64 selected parameters at a sampling rate of 100 hertz was possible. The data

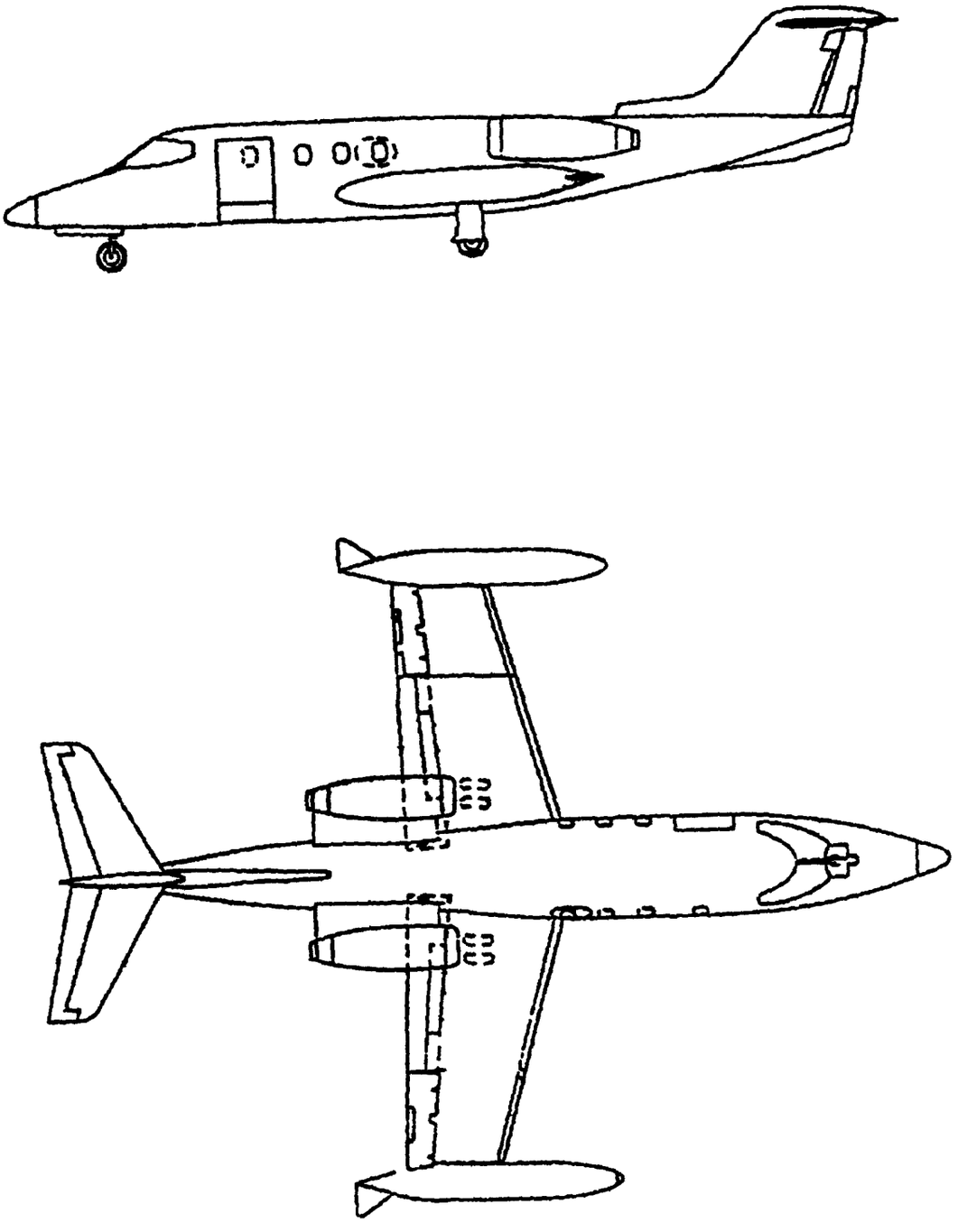

Figure 4-1. Two Plan View of Lear 25B

were stored on 90 megabyte personal computer (PC) compatible, removable Bernoulli drive cartridges in a MATLAB™ compatible format.

A color flat panel display, located on the main instrument panel in front of the evaluation pilot's station, displayed the tracking tasks. The display is shown in Figure 4-2.

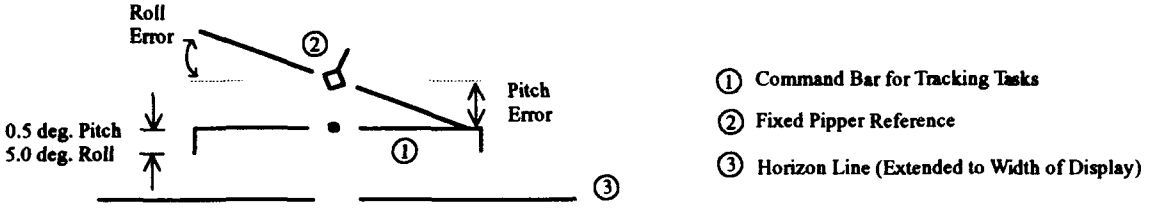

Figure 4-2. Tracking Task Display

Pitch and roll errors were indicated to the pilot by the angular deviation between the command bar and the extended fixed-pipper attitude reference. The lengths of the subtends on the attitude reference corresponded to 0.5 degree of pitch error and 5 degrees of roll error. A horizon line was also displayed to reduce the potential for pilot disorientation. A 0.025 second delay arose from the display process. A detailed description of the Lear II and the flat panel display is given in AFFTC-TLR-93-41 (7:33).

Tracking Tasks. Three different types of tracking tasks were used for this test, a discrete tracking task, a sum-of-sines tracking task, and a regulator task. To lessen the pilot's ability to memorize the tasks, two different tasks of each type were used during testing. Each task was 53 seconds long.

Discrete Tracking Task. The discrete tracking task consisted of a series of steps and ramps. A representative task is shown in Figure 4-3. The initial command in each axis was a step. The maximum commanded input was ±2.25 degrees from the initial condition in pitch and ±35 degrees in roll.

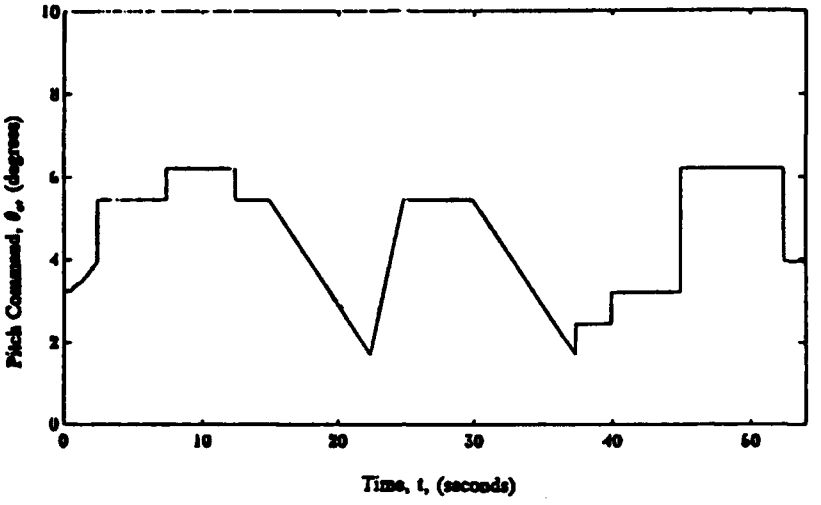

Figure 4-3. Discrete Pitch Axis Tracking Task

Sum-of-Sines Tracking Task. The sum-of-sines tracking task was a random appearing, frequency-based function computed using the following formula:

$$Command = K \cdot \sum_{i=1}^{n} A_i \cdot \sin(\omega_i + \phi_i) \qquad (4\text{-}1)$$

The tasks used in this test were formed by summing 13 sine waves. The phases (ϕ_i) were randomly chosen and the task gain (K) was set to achieve the desired task amplitude. The frequencies (ω_i) were evenly spaced between 0.1 and 30 radians per second. The amplitudes (A_i) were selected using a corner frequency of 2 radians per second and a second-order roll off producing the power spectral density magnitudes shown in

Figure 4-4. A typical task is shown in Figure 4-5. While this task appeared random, the power spectral density was concentrated only at the selected frequencies (ω_i) as shown in Figure 4-4:

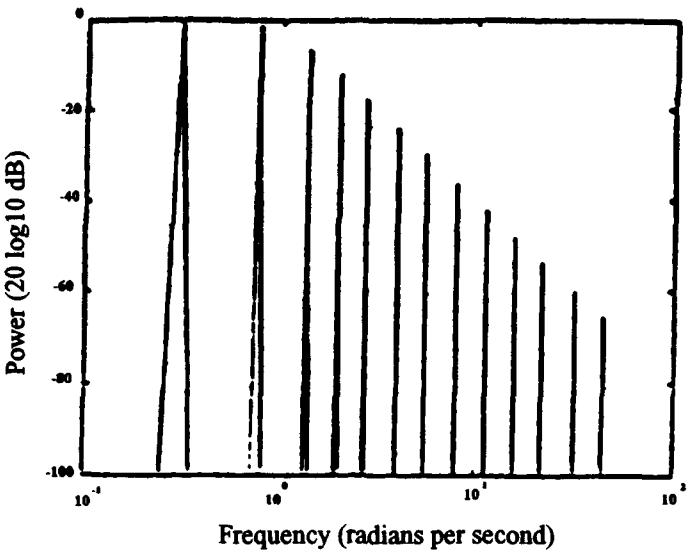

Figure 4-4. Power Spectral Density of Sum-of-Sines Tracking Task

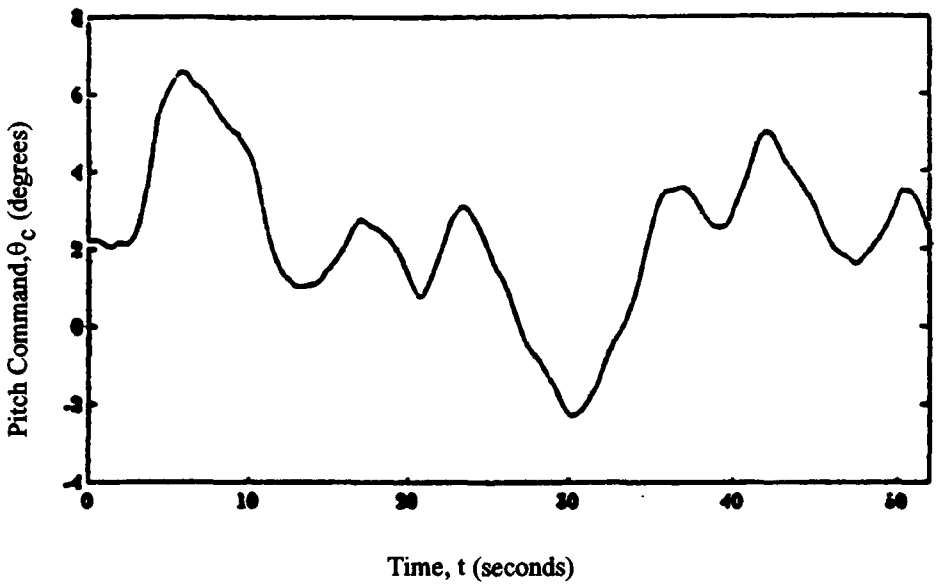

Figure 4-5. Sum-of-Sines Pitch Axis Tracking Task

Regulator Task. The regulator task was computed in the same manner as the sum-of-sines task. Instead of driving a command bar, however, this task was input as an additive to the pilot's stick command. It had the effect of simulating turbulence. The pilot's objective during this task was to maintain wings level, zero pitch flight. This tracking task had the same frequency content as the sum-of-sines task.

Desired And Adequate Criteria. Each airborne test case was examined using all three types of tracking tasks. Only the discrete and sum-of-sines tracking tasks were used during ground simulation runs. Cooper-Harper ratings were assigned for each run in accordance with the following criteria:

> Desired Criteria: Pilot induced oscillations (PIO) tendencies do not compromise tracking task. Commanded attitude maintained within 0.5 degrees in pitch and 5 degrees in bank (measured at end of command bar) for 50 percent of the time except immediately following step command changes. See Figure 4-6.
>
> Adequate Criteria: Commanded attitude maintained within 1 degrees in pitch and 10 degrees in bank (measured at end of command bar) for 50 percent of the time except immediately following step command change.

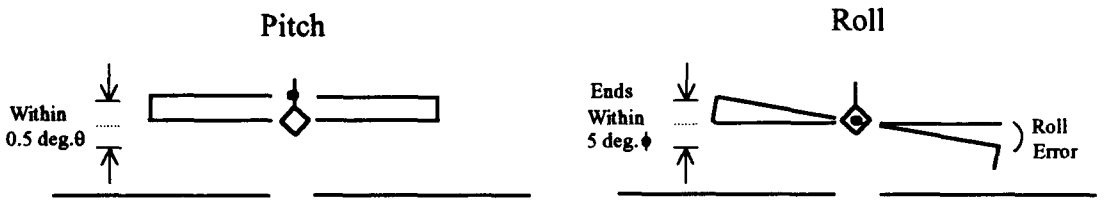

Figure 4-6. Tracking Task Desired Criteria

Dynamics. The following dynamics were selected based on past Calspan flight test experience so that Cases 1 and A would produce a level 1 aircraft. Subsequent cases

degraded either the damping, roll mode time constant, or system delay to produce the desired spread in aircraft handling qualities.

Longitudinal Dynamics:		Lateral Dynamics:		
Case 1:	$\frac{20(s+1.8)e^{-0.04s}}{s(s^2+8.4s+36)}$	Case A:	$\frac{2.5e^{-0.04s}}{s(s+2.5)}$	(4-2)
Case 2:	$\frac{20(s+1.8)e^{-0.04s}}{s(s^2+4.8s+36)}$	Case B:	$\frac{e^{-0.04s}}{s(s+1)}$	(4-3)
Case 3:	$\frac{20(s+1.8)e^{-0.24s}}{s(s^2+8.4s+36)}$	Case C:	$\frac{2.5e^{-0.24s}}{s(s+2.5)}$	(4-4)
Case 4:	$\frac{20(s+1.8)e^{-0.24s}}{s(s^2+4.8s+36)}$	Case D:	$\frac{e^{-0.24s}}{s(s+1)}$	(4-5)

These cases have the characteristics summarized in Table 4-1.

Table 4-1
Case Definition Table

	Longitudinal		Lateral	
	Short Period Damping, ζ_{sp}	Delay, τ_e	Roll Mode Time Constant, T_R	Delay, τ_e
Case 1	0.7	0.04		
Case 2	0.4	0.04		
Case 3	0.7	0.24		
Case 4	0.4	0.24		
Case A			0.4	0.04
Case B			1.0	0.04
Case C			0.4	0.24
Case D			1.0	0.24

These dynamics were implemented as a stick position command system as described in Appendix C.

During the simulations, sideslip angle rate $(\dot{\beta})$ was driven to zero by the simulation computers. Additionally, the roll and yaw axes were de-coupled so the pilot could fly the simulations with feet on the floor.

Data Collection. Both ground and airborne evaluations were conducted. For the ground evaluations, the Lear II was operated in the ground simulation mode inside the Calspan hanger. In-flight testing was conducted under day, visual meteorological conditions (VMC) with no more than occasional light turbulence.

All single axis ground simulation cases were flown twice. All of the airborne single axis cases were evaluated three times. In planning the specific test points, project engineers ensured adequate pilot variability checks by assigning some pilots the same cases twice and by assigning some cases to more than one pilot. The dynamics cases were also evaluated in a random order.

For each case, the test pilots flew the discrete tracking task, followed by the sum-of-sines tracking task and the regulator task. Each task was 53 seconds long. The regulator tasks were only evaluated during airborne simulations since these tasks were designed to evaluate normal acceleration feedback cues.

Immediately after each task, the pilot and flight test engineer completed the test point comment card shown in Figure C-3. The pilots then assigned a pilot induced oscillation (PIO) rating, using the scale in Figure C-4, and a Cooper-Harper rating using the scale in Figure 2-1.

Twenty-two parameters were recorded with a sampling rate of 100 hertz for each test case. These parameters included commanded and actual pitch and roll angle as well as longitudinal and lateral stick force and deflection (7:3-4). The percentage of time the desired and adequate criteria were met as computed by the Lear II simulation computer were saved in separate scoring files.

Data Reduction. In an effort to gain insight into human pilot response, a frequency response analysis of the relationship between the pilot's input (task error) and the pilot output (stick force and displacement) was conducted. This analysis was accomplished using the MATLAB™ fast Fourier transform software described in AFFTC-TLR-93-41 (7:55-58). This software converted time domain data to frequency domain data. In doing so, it yielded the power spectral densities of the input and output parameters, a Bode plot of the transfer function, and a coherence function. This coherence function provided a measure of how much of the output at each frequency was caused by the input rather than by noise or other inputs. A coherence value of 1.0 meant that the output was completely a function of the input, whereas as value of 0.0 meant that the output was not a function of the input. This software was included in the data base described in Reference 7 and can be distributed freely.

Validation. The frequency response analysis software was based on code written for the Air Force Flight Test Center (AFFTC) CYBER computer system. The CYBER code was previously validated by numerous AFFTC projects. The MATLAB™ version of the software was validated by analyzing data from several ground simulations

on both systems and comparing the results. For the frequency range of interest (0.1 to 10 radians per second) the results produced by the two versions agreed to within 0.1 percent.

The data reduction software was further validated by running an example problem. The following dynamics were simulated on MATLAB™ and Simulink:

$$Y_c = \frac{(s+2)\cdot e^{-0.25s}}{(s+5)\cdot(s+.2)} \tag{4-6}$$

A random, normal input vector was generated using the command, *rand('normal')*, and the output of the simulation analyzed. The Bode and coherence plots are shown in Figure C-5. Notice that the coherence is nearly perfect, especially at higher frequencies. Additionally, the 95% confidence bounds, represented by the dashed lines in all three plots, are tight. This frequency response and the bode plot of the actual system are shown in Figure C-6. Notice that except for the lowest frequency, phase point, the two are nearly identical.

Windowing and Overlap. A common frequency response analysis technique is ensemble averaging. Ensemble averaging improves the reliability of the frequency response calculations for time histories of data corrupted by measurement noise, such as flight test data (Reference 9).

Overlap ensemble averaging was used both in this thesis and in AFFTC-TLR-93-41. The first five seconds, or five hundred data samples, of each task were not considered so that the pilot could become actively involved in the task. The next 4,096 samples (40.96 seconds) were divided into seven ensembles, each with fifty percent overlap. The data from several tasks were analyzed using different percent

overlap and numbers of ensembles. In all cases the computed frequency response points were the same. The confidence intervals, however, grew tighter as the overlap and number of ensembles increased.

Test Results

There are four areas of analysis that have implications for the optimal pilot model analysis conducted in this thesis. They are *Pilot Ratings and Comments, Pilot Delay, Statistical Analysis,* and *Frequency Response Analysis.* The following sections present the important results from each of these areas.

Pilot Ratings and Comments. The Cooper-Harper ratings and pilot comments are presented in Tables C-1 and C-2 for the ground and airborne evaluations, respectively. These tables also include the pilot induced oscillation (PIO) rating and the percentage of time the pilot met desired and adequate criteria during each task. Only the single axis sum-of-sines data were included in this thesis.

The Cooper-Harper ratings are presented graphically in Figure C-7. The dynamics evaluated in AFFTC-TLR-93-41 produced a wide range of pilot response, as evidenced by the spread in Cooper-Harper ratings. These ratings ranged from 1 to 6 on the ground and 1 to 7 for the airborne evaluations. Pilot variability was fairly low. In most cases the Cooper-Harper Ratings were within one rating of each other. Ratings for the airborne evaluations of Case D were the exception, ranging from 4 to 7. No significant differences between ground and airborne ratings were noted.

Pilot Delay. The delay between task command and pilot response was estimated in AFFTC-TLR-93-41 using the airborne, single axis discrete tracking tasks. This tracking task consisted of a series of steps and ramps separated by as much as five seconds. Pilot delay was estimated by measuring the time between the command change and the stick force or deflection (7:127-128).

The pilot delay between task command and stick force was estimated at 0.27 seconds. The delay times did not vary significantly by pilot, dynamics case, or axis. This estimate is consistent with the 0.2 to 0.3 second delay observed by McRuer (14:217). In all cases, stick deflection lagged stick force by 0.1 ($\pm$ 0.01) seconds, reflecting the lag inherent in the stick dynamics. Thus, the total delay between task command and stick deflection was 0.37 seconds, well above the value normally used for pilot model analysis (7:13-14). It is also important to note that the dynamics evaluated in AFFTC-TLR-93-41 were implemented as a position command system.

Statistical Analysis. The standard optimal control problem minimizes a performance index that weights state deviation and control usage. The optimal pilot model minimizes a performance index that weights tracking error and control rate usage. Control rate usage is included in the optimal pilot model performance index to implement the muscular dynamics as described in Chapter 3 and Appendix A of this thesis (pages A-1, 3-5, and 3-13). This section examines the statistical validity of both weightings in the prediction of Cooper-Harper ratings.

Root mean square (RMS) tracking error, control deflection, and control rate values were computed from the flight test data base produced by AFFTC-TLR-93-41 and

are presented in Tables C-3 and C-4. Only the single axis, sum-of-sines data were included in this thesis.

The root mean square (RMS) values in Tables C-3 and C-4 were computed using the following formula:

$$RMS(x) = \sqrt{\frac{\Sigma |x|^2}{n}} \tag{4-7}$$

In this equation, n is the number of samples in the vector, x. The RMS tracking error *(RMS Error)* was determined by computing the difference between the task command and the actual aircraft position ($e_\theta = \theta_c - \theta$) and then applying Equation 4-7 to this error vector. The normalized RMS stick deflection *(NRMS Stick)* was found by subtracting the mean stick deflection from each element in the vector before applying Equation 4-7. Finally, the stick deflection rate was estimated by computing the difference between each sequential element in the stick deflection vector and dividing the differences by the sampling rate, 0.01 seconds. The RMS stick deflection rate *(RMS Stick Rate)* was found by applying Equation 4-7 to this stick rate estimate.

The results of the regression analysis of these parameters is presented in Table 4-2 on the following page. In all of the runs the first independent variable was RMS tracking error and the dependent variable was the Cooper-Harper rating. The second independent variable was either normalized RMS stick deflection or RMS stick deflection rate. The last column, variance, was used to evaluate the quality of the least squares fits.

Weighting either normalized stick deflection or stick rate produced similar correlations in all but two cases. For the airborne pitch axis cases, normalized stick

Table 4-2
Regression Analysis of Optimal Pilot Model Weightings

	Axis	Independent Variable[1], X_1	Independent Variable[1], X_2	Coefficient, C_{X1}	Coefficient, C_{X2}	Constant, C	Variance, R^2
Flight	Pitch	RMS Error	NRMS Stick	7.1936	32.4729	-12.7970	0.8206
		RMS Error	RMS Stick Rate	4.4283	3.9928	-2.6624	0.6193
	Roll	RMS Error	NRMS Stick	1.7082	2.2877	-3.9951	0.7201
		RMS Error	RMS Stick Rate	1.7371	0.6798	-4.4372	0.7233
Ground	Pitch	RMS Error	NRMS Stick	4.4451	13.0161	-3.8750	0.5491
		RMS Error	RMS Stick Rate	1.5746	3.4441	0.0993	0.9583
	Roll	RMS Error	NRMS Stick	0.8013	7.1414	-3.4535	0.8246
		RMS Error	RMS Stick Rate	0.7280	1.8389	-2.7809	0.7658
Both Air and Ground	Pitch	RMS Error	NRMS Stick	6.0179	21.1914	-8.0429	0.7311
		RMS Error	RMS Stick Rate	4.7125	3.1204	-2.0751	0.7320
	Roll	RMS Error	NRMS Stick	0.9224	7.4571	-3.8638	0.6877
		RMS Error	RMS Stick Rate	1.1075	1.4758	-3.8931	0.6946

[1] The dependent variable was the Cooper-Harper Rating such that: $C\text{-}H\ Rating = C_{X1}X_1 + C_{X2}X_2 + C$.

deflection weighting was significantly better than stick rate weighting. The reverse was true for the pitch axis ground evaluations. It appears that both weighting schemes were statistically valid. Normalized stick deflection weighting may be more appropriate, however, for two reasons. First, the airborne sample size was nearly twice that of the ground evaluations (12 versus 7). Second, the pilots may have exhibited singular

behavior during the ground simulations due to the lack of motion cues. For example, they may have been more apt to move the stick rapidly when evaluating poor dynamics on the ground where there were no uncomfortable acceleration forces to discourage such behavior.

The normalized stick deflection regression coefficients from the airborne evaluations were used to draw the regression analysis lines in Figures C-8 and C-9. Each airborne test point was plotted as a function of RMS error and normalized RMS stick deflection. The number above each data point is the Cooper-Harper rating assigned during the task. As shown in these figures, there was a strong relationship between these two variables and the Cooper-Harper rating, but this relationship was by no means perfect.

Frequency Response Analysis

From a linear systems perspective, the primary input to the pilot was assumed to be task error. The pilot's primary outputs were assumed to be stick force and deflection. A frequency response analysis of these input and output variables was performed for all of the single axis, sum-of-sines tracking tasks. This section presents the applicable results of this analysis.

Stick Force Versus Stick Deflection. As described previously in this chapter, the evaluated dynamics were implemented as a position command system. Stick force and displacement were related by a high frequency stick dynamics term and a force gradient as shown in Figure C-1. The only difference between the frequency responses

of stick force and stick deflection was the frequency response of these stick dynamics. In other words, when the frequency responses of stick force to task error were summed with the Bode plot of the stick dynamics, the result was identical to the stick deflection frequency responses in Appendix D. As a result, the same insights could have been gained by studying either variable. The analysis in AFFTC-TLR-93-41 and this thesis focused on stick deflection (7:14-15).

Ground Simulation. As discussed in AFFTC-TLR-93-41, there were no significant differences between the pilot's airborne and ground frequency response. The phase lead at higher frequencies, however, was slightly greater on the ground than in the air. There were no consistent trends for the magnitude (7:18).

Stick Deflection to Task Error. A frequency response analysis of stick deflection to tracking task error for all single axis sum-of-sines tracking tasks was completed for AFFTC-TLR-93-41. A representative cross-section of this data is presented in Appendix D.

The power spectral densities (PSD) of the pilot input and the pilot output for two of the worst dynamics cases, Cases 4 and D, are presented in Figures D-1 and D-2. Even for these two highly oscillatory cases there were no notches in the PSD magnitude.

Likewise, the Bode plots of the pilot response did not reveal any higher order compensation, or *notching* behavior. One representative frequency response plot for each dynamics case is presented in Figures D-3 through D-10. As shown in these figures, the magnitudes were consistent with the classical gain, lead, and lag pilot model form described previously in this thesis and in Reference 15. The phase, however, was not

consistent with this form of pilot compensation due to the large amount of phase lead present at higher frequencies. As shown in Figure D-10, this high frequency phase lead is especially noticeable for cases with delay. Despite this phase lead, no higher order compensation was noted in any of the evaluations.

The pilot response appears to be strongly related to the aircraft dynamics. To see this relationship, the frequency responses of the combined pilot-aircraft systems are presented in Figures D-11 through D-18. These plots were formed by adding the frequency response of the pilot (stick deflection to task error) with that of the aircraft (pitch or roll angle to stick deflection). As shown in these figures, the combined system responses resembled integrators near the cross-over frequency in all cases. This is consistent with McRuer's crossover pilot model theory (Reference 17). Note also that the cross-over frequency of the combined system dropped from 1.9 radians per second for the best pitch case (Figure D-11) to 1.6 radians per second for the worst pitch case (Figure D-14) and from 1.6 radians per second for the best roll case (Figure D-15) to 1.0 radians per second for the worst roll case (Figure D-18).

Gain Effects. The effect of command path gain was briefly evaluated during the ground simulation phase. The frequency response analysis of stick deflection to task error for the ground evaluation of Case 1 is shown in Figure D-19. The command path gain for Case 1 was increased from 8 to 16 and re-evaluated by the same pilot. The resulting frequency response is shown in Figure D-20. As shown in this figure, the pilot decreased his *gain* by about 6 dB to compensate. This behavior is even more apparent when examining the combined pilot-aircraft systems in Figures D-21 and D-22. Even

though the aircraft command path gain for Figure D-22 was twice that in Figure D-21, the frequency responses of the combined systems were nearly the same.

Conventional Pilot Model Predictions

The dynamics cases described in Appendix C were evaluated using the STI optimal pilot model and all of the applicable pitch and roll axis pilot models in MIL-STD-1797 (Reference 5).

The results of the pitch axis pilot model analysis are presented in Table C-6. As shown in this table, the MIL-STD-1797A pitch models were unsatisfactory for predicting the handling qualities ratings of the pitch dynamics used for this evaluation. Three of the five models predicted Level II handling qualities for Case 1 which actually had Level I handling qualities. All of the models predicted Level III handling qualities for Cases 3 and 4, and both of these cases had Level II handling qualities.

The optimal pilot model was moderately successful in predicting the Cooper-Harper ratings, but the predicted pilot describing functions were not consistent with the observed behavior. Bode plots of the predicted pilot describing functions and the resulting pilot-aircraft systems are shown in Figures C-10 through C-13 for Cases 1 and 4. Due to the higher order pilot compensation, or *notching,* present in these figures, they do not resemble the corresponding flight test responses in Figures D-3, D-6, D-11, and D-14.

The roll axis pilot model predictions are presented in Table C-7. These models adequately predicted the Cooper-Harper ratings and handling qualities levels of the roll

axis dynamics. Due to the simplicity of the MIL-STD-1797A roll axis models, however, these models had to be used together in a checklist fashion to gain adequate insight into the aircraft's predicted handling qualities. The optimal pilot model predictions were slightly pessimistic, while the bandwidth criterion predictions were slightly optimistic. Both were accurate enough to be useful. As with the pitch axis, the pilot describing functions predicted by the STI optimal pilot model were not consistent with observed behavior.

Summary

In an effort to provide insight into human pilot behavior, a limited evaluation of human pilot response was conducted. This evaluation consisted of ground and airborne simulations in the variable stability Lear II aircraft. Four different pitch and four different roll axis dynamics were evaluated using three different tracking tasks. For each set of dynamics, primary pilot response parameters were recorded and examined using Fourier transform analysis.

The dynamics evaluated produced a wide range of pilot response as evidenced by the spread in Cooper-Harper ratings. Pilot variability was fairly low. In all but one case the Cooper-Harper ratings were within one rating of each other. No significant difference between ground and airborne ratings were noted (page 4-12)[1].

Using the discrete tracking task time histories, the pilot delay between task command and stick force was estimated at 0.27 seconds. In all cases, stick displacement lagged stick force by 0.1 seconds due to the lag inherent in the stick dynamics. Thus, the

[1] Refers to the page in this thesis containing this conclusion.

total delay between command and stick displacement was 0.37 seconds, well above the value normally used for pilot model analysis (page 4-13).

The statistical validity of using root mean square (RMS) tracking error and stick deflection or deflection rate to predict Cooper-Harper ratings was examined. A regression analysis revealed that task error and normalized stick deflection weighting produced the best correlation with airborne pilot ratings (page 4-15).

A frequency response analysis of stick force and displacement to task error was conducted for all single axis, sum-of-sines tracking tasks. The following conclusions were made.

1. The only difference between the frequency responses of stick force and stick deflection was the frequency response of the stick dynamics. Thus, the same insights could have been gained by examining either variable. Because the evaluated dynamics were implemented as a position command system, stick deflection was chosen (page 4-16).

2. There were no significant differences between the pilot's airborne and ground frequency response (page 4-17).

3. No notches were observed in any of the stick displacement power spectral densities (page 4-17).

4. No higher order pilot compensation, or *notching* behavior, was noted in any of the single axis frequency responses. The magnitude plots in both axes were consistent with the classical gain, lead, and lag pilot model form. The phases were not consistent with this form due to large amounts of pure phase lead present at higher frequencies (page 4-17).

5. In all cases, the pilot applied compensation so that the combined pilot-aircraft system resembled an integrator near the cross-over frequency (page 4-18).

6. When the aircraft command path gain was doubled, the pilot reduced his gain so that the response of the combined pilot-aircraft system remained unchanged (page 4-18).

All of the dynamics were evaluated by the pilot models in MIL-STD-1797A and by the STI optimal pilot model. The MIL-STD-1797A roll axis pilot models adequately predicted the Cooper-Harper ratings and handling qualities levels of the dynamic used for this project. The MIL-STD-1797A pitch axis models, however, were unsatisfactory for predicting the handling qualities levels or ratings. The STI optimal pilot model successfully predicted the Cooper-Harper ratings in both axes. The pilot describing functions predicted by this model were not consistent with observed behavior because they contained higher order compensation (page 4-19).

5. *A Numerical Solution to the Linear Quadratic Gaussian Problem*

General

The standard solution to the linear quadratic Gaussian (LQG) problem is a compensator of the same order as the controlled element. Because the optimal pilot model is based on LQG theory, the high order pilot describing functions it predicts are generally not consistent with classical pilot modeling theory or observed behavior. The method detailed in this chapter was developed to provide a way around this problem.

The numerical LQG solution described in this chapter allows the user to select a compensator form. It then uses a Nelder-Meade simplex algorithm to find the coefficients of the compensator that minimize the standard LQG performance index. This method is not only useful in the optimal pilot model problem. It may apply to all situations when reduced order compensation is desired.

This chapter is divided into four section. The first section of this chapter gives general background information. The second section describes the numerical LQG solution method. This method is then demonstrated by solving two example problems. Finally, the results of this chapter are summarized.

Background

Reduced Order Controllers. There are three principal approaches to reduced order LQG controller design as shown in Figure 5-1 (1:253). One method is to reduce the order of the controlled element. For the optimal pilot model problem this alone is not

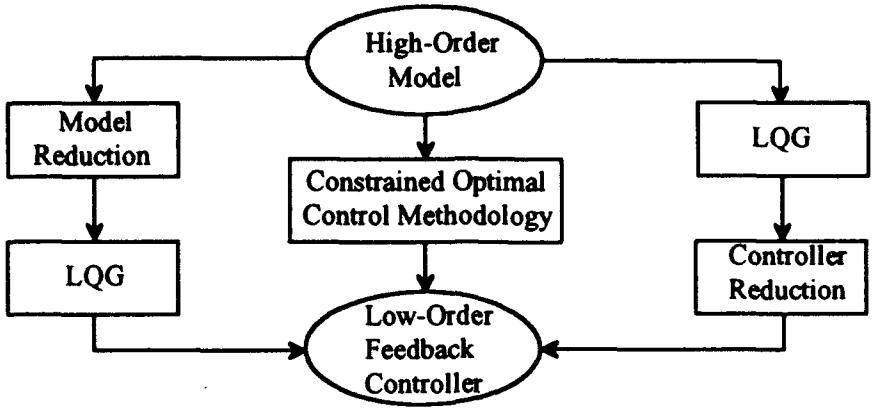

Figure 5-1. Reduced Order Controller Design

a practical solution. The second approach requires the application of a controller reduction algorithm to the standard LQG solution. As shown in Chapter 3 and Appendix B, however, accurate first order approximations of optimal pilot model results are not always attainable. The more direct approach is to use a constrained optimal control methodology similar to the one described in this chapter. For a detailed discussion of constrained optimization theory consult Bernstein and Hyland (Reference 1).

The Standard Linear Quadratic Gaussian Problem. A general form of the standard LQG problem is shown in Figure 5-2.

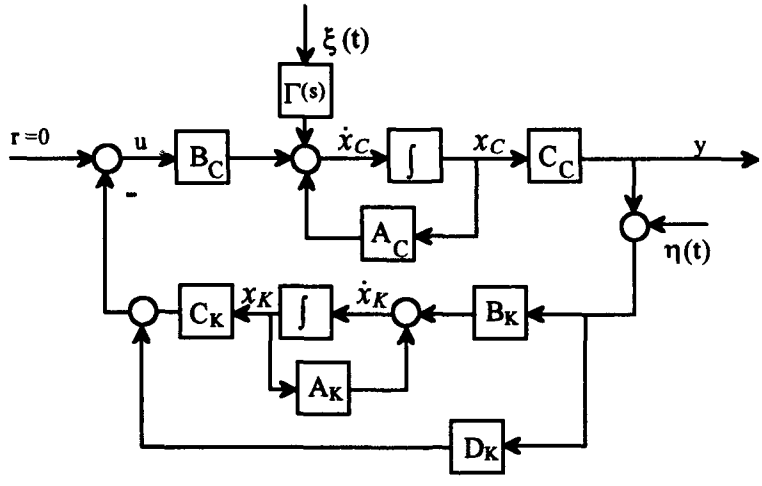

Figure 5-2. General Linear Quadratic Gaussian Problem

where

A_C, B_C, C_C	Controlled Element State Space Matrices
x_C	Controlled Element State Vector
A_K, B_K, C_K, D_K	Compensator State Space Matrices
x_K	Compensator State Vector
u	Control Vector
y	Controlled Element Output Vector
$\eta(t)$	Measurement Noise
$\xi(t)$	Disturbance Noise
$\Gamma(s)$	Disturbance Noise Coloring Filter (Laplace)

The methods developed in this thesis assumed the controlled element was time-invariant and strictly proper (no D_C term)[1]. These assumptions were not considered limiting.

The standard LQG solution is the compensator that minimizes the following performance index:

$$J = \int_0^\infty [x^T Q x + u^T R u]\, dt \tag{5-1}$$

Where R is the control weighting and Q is the state deviation weighting. If the system is driven only by random noises as shown in Figure 5-2, this performance index can be rewritten as an expected value rather than an integral as shown.

$$J = E\{x^T Q x + u^T R u\} \tag{5-2}$$

From Figure 5-2, the control vector, u, is:

$$u = -[C_K x_K + D_K C_C x_C + D_K \eta] \tag{5-3}$$

Notice that the last part of this expression, $D_K \eta$, contains a linear combination of the sensor noises. If this expression is substituted into Equation 5-2, the performance index

[1] This assumption was made to simplify the numerical solution derivation.

will contain the following term:

$$E\{\eta^T D_K^T R D_K \eta\} \tag{5-4}$$

Unless this value is zero, the performance index will be infinite. For illustration purposes, assume there is only one feedback channel. The matrices, D_K and R, become scalars, and Equation 5-4 can be written as:

$$D_K^2 \cdot R \cdot E\{\eta^2\} \tag{5-5}$$

The sensor noises in the LQG problem are defined as:

$$\mathrm{E}\{\eta(t) \cdot \eta^T(t-\tau)\} = R_o \cdot \delta(\tau) \qquad \forall\, t, \tau \tag{5-6}$$

where R_o is the intensity of the measurement noise. Combining terms, Equation 5-5 can be written as:

$$D_K^2 \cdot R \cdot R_o \cdot \delta(\tau) \tag{5-7}$$

Because of the delta function, the magnitude of Equation 5-7 is infinite. Thus, the magnitude of the performance index, which contains this term, is also infinite.
The most obvious solution to this problem is to require the compensator feed-through term, D_K, to be zero. In other words, the compensator must be strictly proper.

Assuming a proper compensator, the LQG problem can be represented by the block diagram in Figure 5-3. Also, the frequency content of the disturbance noise, $\Gamma(s)$, is now written in state space form.

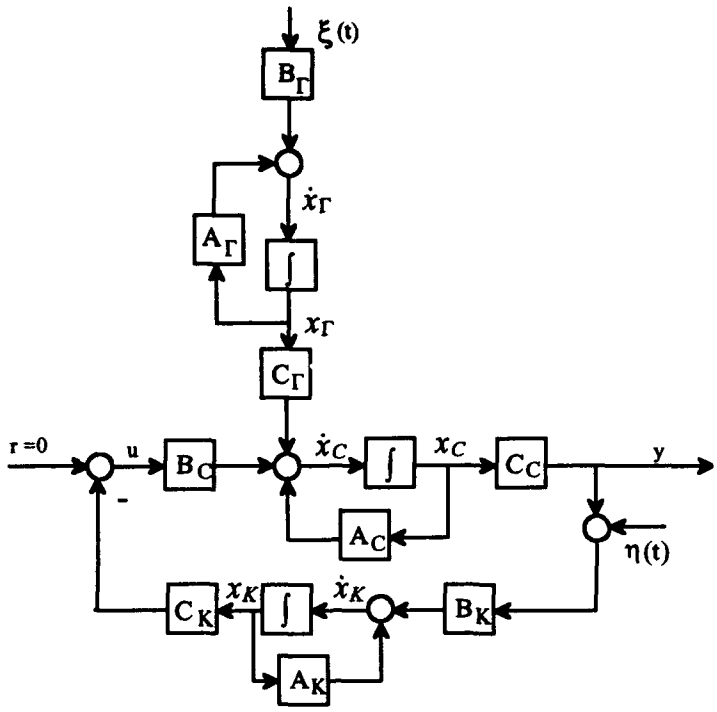

Figure 5-3. Linear Quadratic Gaussian Problem
-- Proper Compensator

Assuming the controlled element disturbance noise filter is also strictly proper[1], the equations of state for this system are:

$$\dot{x}_C = A_C x_C + B_C u + C_\Gamma x_\Gamma \qquad y = C_C x_C \tag{5-8}$$

$$\dot{x}_\Gamma = A_\Gamma x_\Gamma + B_\Gamma \xi \tag{5-9}$$

$$\dot{x}_K = A_K x_K + B_K(\eta + y) \qquad u = -C_K x_K \tag{5-10}$$

Substituting and combining terms yields the following state-space representation driven only by white noises:

$$\begin{bmatrix} \dot{x}_C \\ \dot{x}_\Gamma \\ \dot{x}_K \end{bmatrix} = \begin{bmatrix} A_C & C_\Gamma & -B_C C_K \\ 0 & A_\Gamma & 0 \\ B_K C_C & 0 & A_K \end{bmatrix} \cdot \begin{bmatrix} x_C \\ x_\Gamma \\ x_K \end{bmatrix} + \begin{bmatrix} 0 & 0 \\ B_\Gamma & 0 \\ 0 & B_K \end{bmatrix} \cdot \begin{bmatrix} \xi \\ \eta \end{bmatrix} \tag{5-11}$$

[1] This assumption was made to simplify the numerical solution derivation.

This system is in the form of:

$$\dot{x} = Ax + Ew \tag{5-12}$$

where the noise intensities are:

$$E\{\xi(t) \cdot \xi^T(t-\tau)\} = Q_o \cdot \delta(\tau) \tag{5-13}$$

$$E\{\eta(t) \cdot \eta^T(t-\tau)\} = R_o \cdot \delta(\tau) \tag{5-14}$$

and the constant intensity noise matrix, Q_n, is defined as:

$$Q_n = \begin{bmatrix} Q_o & 0 \\ 0 & R_o \end{bmatrix} \tag{5-15}$$

One important point should be made. When there is no driving noise coloring filter, the filter states should be removed. If A_Γ, B_Γ, and C_Γ are simply set to zero, the matrices in Equation 5-11 will not form a minimum realization. The state space representation of the system without coloring filters is given in Equation 5-16.

$$\begin{bmatrix} \dot{x}_C \\ \dot{x}_K \end{bmatrix} = \begin{bmatrix} A_C & -B_C C_K \\ B_K C_C & A_K \end{bmatrix} \cdot \begin{bmatrix} x_C \\ x_K \end{bmatrix} + \begin{bmatrix} \Gamma & 0 \\ 0 & B_K \end{bmatrix} \cdot \begin{bmatrix} \xi \\ \eta \end{bmatrix} \tag{5-16}$$

Where Γ is now a gain matrix that distributes the driving noise into the controlled element states.

The Numerical Solution

As mentioned earlier, for systems driven by random noises, the standard LQG performance index can be written as the sum of two expected values.

$$J = E\{x^T Q x\} + E\{u^T R u\} \tag{5-17}$$

The expected value of the state vector can be found from the covariance matrix, X, such that:

$$X = E\{x \cdot x^T\} \tag{5-18}$$

where the covariance matrix is the solution to the following Lyapunov equation (11:106-111).

$$AX + XA^T + EQ_nE^T = 0 \tag{5-19}$$

The matrices, E and A, correspond to those in Equation 5-12, and Q_n is the noise matrix defined in Equation 5-15.

The covariance matrix can be used to find the value of the performance index, Equation 5-17, by defining the following matrices.

$$x_G = [I_n \mid 0_{nxm}]\underline{x} = \begin{bmatrix} \underline{x}_C \\ \underline{x}_\Gamma \end{bmatrix} \tag{5-20}$$

$$x_K = [0_{mxn} \mid I_m]\underline{x} \tag{5-21}$$

$$u = -C_K x_K \tag{5-22}$$

where

x_G = Forward Loop State Vector (Controlled Element and Filter)
n = Number of Controlled Element and Filter States
m = Number of Compensator States
I = Identity Matrix

Combining Equations 5-20 to 5-22 and Equation 5-17 yields:

$$J = E\{x_G^T Q x_G\} + E\{x_K^T C_K^T R C_K x_K\} \tag{5-23}$$

Assuming Q is a diagonal matrix, the first term of Equation 5-23 can be expanded as follows.

$$E\left\{x_G^T Q x_G\right\} = E\{x_{G1} Q_{11} x_{G1} + x_{G2} Q_{22} x_{G2} + ...x_{Gi} Q_{ii} x_{Gi}\} \tag{5-24}$$

Grouping terms, Equation 5-23 can be written as:

$$E\left\{x_G^T Q x_G\right\} = \sum_{i=1}^{n} Q_{ii} \cdot E\left\{x_{Gi}^2\right\}$$

$$= \sum_{i=1}^{n} Q_{ii} \cdot X_{ii} \tag{5-25}$$

where

n = Number of Controlled Element and Filter States
Q = State Deviation Weighting Matrix from Equation 5-17
X = Covariance Matrix from Equation 5-18

The second term of Equation 5-23 is a little more convoluted. If, for example, there are two compensator states and two feedback channels, this term expands to:

$$\begin{bmatrix} x_{K1} \\ x_{K2} \end{bmatrix} \cdot \begin{bmatrix} C_{K11} & C_{K21} \\ C_{K12} & C_{K22} \end{bmatrix} \cdot \begin{bmatrix} R_{11} & 0 \\ 0 & R_{22} \end{bmatrix} \cdot \begin{bmatrix} C_{K11} & C_{K12} \\ C_{K21} & C_{K22} \end{bmatrix} \cdot \begin{bmatrix} x_{K1} \\ x_{K2} \end{bmatrix}$$

$$= R_{11}\left[x_{K1}^2 C_{K11}^2 + x_{K2}^2 C_{K12}^2 + 2x_{K1} x_{K2} C_{K11} C_{K12}\right] +$$

$$R_{22}\left[x_{K1}^2 C_{K21}^2 + x_{K2}^2 C_{K22}^2 + 2x_{K1} x_{K2} C_{K21} C_{K22}\right] \tag{5-26}$$

Grouping terms, the general form of this expression is:

$$E\left\{x_K^T C_K^T R C_K x_K\right\} = \sum_{h=1}^{o} \sum_{i=1}^{m} \sum_{j=1}^{m} R_{hh} \cdot C_{K(hi)} \cdot C_{K(hj)} \cdot E\{x_{K(i)} \cdot x_{K(j)}\}$$

$$= \sum_{h=1}^{o} \sum_{i=1}^{m} \sum_{j=1}^{m} R_{hh} \cdot C_{K(hi)} \cdot C_{K(hj)} \cdot X_{(n+i,n+j)} \tag{5-27}$$

where

o = Length of Control Vector, u (number of rows in C_K)
m = Number of Compensator States
n = Number of Controlled Element and Filter States
R = Control Weighting from Equation 5-17 (Diagonal)
C_K= Compensator State Space Matrix
X = Covariance Matrix from Equation 5-18

Equations 5-25 and 5-27 are the central equations in the numerical solution of the LQG problem. Using these equations the performance index can be computed for any controlled element and compensator. A numerical minimization routine can then search all of the compensator parameters for the combination that returns the minimum performance index. Additionally, the performance index can be modified to include side constraints, such as gain or phase margin.

Equations 5-25 and 5-27 are implemented in the MATLAB™ routines, or ".M" files listed in Appendix E. *PIFIND.M* computes the performance index value for problems with driving noise coloring filters. *PIFINDNF.M* computes the performance index value for problems without coloring filters.

Example Problems

This numerical solution is illustrated in the following examples. The first example consists of a low order plant augmented with a disturbance noise coloring filter. The second example uses a high order plant with no disturbance noise coloring filter. These examples are not necessarily meant to mimic aircraft dynamics. This numerical method can apply to any type of LQG problem.

Low Order Plant with Coloring Filter. Assume the controlled element is an integrator and the driving noise is filtered as follows:

State Space Representation

$$Y_C = \frac{1}{s} \quad \Rightarrow \quad [\dot{x}_C] = [0]x_C + [1]u$$

$$y = [1]x_C \tag{5-28}$$

$$Y_\Gamma = \frac{W_c}{\xi} = \frac{\sqrt{8.8}}{s+2} \quad \Rightarrow \quad [\dot{x}_\Gamma] = [-2]x_\Gamma + [1]\xi$$

$$W_c = \left[\sqrt{8.8}\right]x_\Gamma \tag{5-29}$$

where ξ is the random disturbance noise and W_c is this noise after the coloring filter. Assume the state deviation weighting is one and the control usage weighting is two. The state deviation weighting matrix, Q, must be diagonal due to the assumptions made in the development of the numerical solution. Because the controlled element states must be augmented with the filter states, the state deviation weighting matrix, Q, must have the same number of rows as the total number of filter and controlled element states. There is normally no penalty on filter state deviations, making their weightings zero. The control usage weighting matrix, R, must be diagonal with the same number of rows as in the control vector, u. In this example, there are two total controlled element and filter states and only one control channel. The weighting matrices are shown in Equation 5-30.

$$Q = \begin{bmatrix} 1 & 0 \\ 0 & 0 \end{bmatrix} \qquad R = \begin{bmatrix} 2 \end{bmatrix} \tag{5-30}$$

The noises, ξ and η, will have unit intensity for this example such that the noise intensity matrix, Q_n, is as shown in Equation 5-31.

$$Q_n = \begin{bmatrix} 1 & 0 \\ 0 & 1 \end{bmatrix} \tag{5-31}$$

In this example, assume the optimal second order compensator of the form in Equation 5-32 is desired.

$$K(s) = \frac{c(1) \cdot s + c(2)}{s^2 + c(3) \cdot s + c(4)} \tag{5-32}$$

The Nelder-Meade simplex algorithm, *fmins,* on MATLAB™ will now be used to search for the combination of compensator variables, *c(i),* that produces the minimum performance index. An additional function (*.m file*) containing the compensator form must be written. The routine for solving this problem is:

```
function[J]=comp(c,Ac,Bc,Cc,Ag,Bg,Cg,Q,R,Noise)

    [Ak,Bk,Ck,Dk]=tf2ss([c(1),c(2)],abs([1,c(3),c(4)]));
    J=PIFIND(Ak,Bk,Ck,Ac,Bc,Cc,Ag,Bg,Cg,Q,R,Noise);
```

The first line lists the input and output arguments. The second line converts the desired compensator form into state space, and the final line finds the performance index, *J,* using the file, *PIFIND,* listed in Appendix E. This function, *comp,* is minimized by typing the following MATLAB™ command.

```
cmin=fmins('comp',c0,[],[],Ac,Bc,Cc,Ag,Bg,Cg,Q,R,Noise)
```

In this command, *c0* is the initial guess and the rest of the matrices are as shown in Equations 5-28 through 5-31. *Noise* refers to the matrix, Q_n, shown in Equation 5-31.

Due to the nature of the Nelder-Meade simplex search routine, the initial guess requires some consideration. If any evaluated compensator has poles in the right half plane or on the imaginary axis, the simplex search may not be successful. Thus, restricting the denominator values in the search vector, *c,* to positive values greatly improves the robustness of the numerical search. Likewise, the Lyapunov solution must be unique. The necessary and sufficient condition for this is:

$$\lambda_i(A) + \lambda_j(A) \neq 0 \quad for \quad \forall i,j = 1 \ldots n \tag{5-33}$$

where A is from Equation 5-12 and λ is the eigenvector of A. A sufficient condition for a unique Lyapunov solution is that the real part of all eigenvectors be negative (3:30). Thus, the search may not converge for compensators, controlled elements, or filter dynamics with entire state space matrices of zeros. As the number of parameters to search increases, the importance of the initial guess increases. Additionally, the Nelder-Meade routine is best for finding the minimum of functions with five or fewer unknown parameters (4:116-122). For complex compensator forms a different numerical search routine may be appropriate. For this example, any initial condition vector, *c0,* with values between approximately 0.1 and 100 will return the proper solution.

In this example, the initial guess was

$$Y_{Ki} = \frac{s+1}{s^2+s+1} \quad \text{or} \quad c0 = \begin{bmatrix} 1 & 1 & 1 & 1 \end{bmatrix} \tag{5-34}$$

and the following compensator was computed:

$$c_{min} = \begin{bmatrix} 0.9876 & 2.0977 & 3.8588 & 4.2075 \end{bmatrix} \tag{5-35}$$

$$Y_k = \frac{0.9876s + 2.0977}{s^2 + 3.8588s + 4.2075} \tag{5-36}$$

with a resulting performance index, J, of 3.9252.

As a check, the same problem was worked using the conventional LQG solution methods described in Appendix A. First, the system had to be put into the following form.

$$\dot{x} = Ax + Bu + \Gamma\xi$$

$$y = Cx + D\eta \tag{5-37}$$

This was accomplished using the following formulas.

$$\begin{bmatrix} \dot{x}_C \\ \dot{x}_\Gamma \end{bmatrix} = \begin{bmatrix} A_C & C_\Gamma \\ 0 & A_\Gamma \end{bmatrix} \cdot \begin{bmatrix} x_C \\ x_\Gamma \end{bmatrix} + \begin{bmatrix} B_C \\ 0 \end{bmatrix} \cdot u + \begin{bmatrix} 0 \\ B_\Gamma \end{bmatrix} \cdot \xi \tag{5-38}$$

$$Y = [\, C_C \;\; 0] \cdot \begin{bmatrix} x_C \\ x_\Gamma \end{bmatrix} + [0] \cdot u + \eta \tag{5-39}$$

For this example these equations were:

$$\begin{bmatrix} \dot{x}_C \\ \dot{x}_\Gamma \end{bmatrix} = \begin{bmatrix} 0 & \sqrt{8.8} \\ 0 & -2 \end{bmatrix} \cdot \begin{bmatrix} x_C \\ x_\Gamma \end{bmatrix} + \begin{bmatrix} 1 \\ 0 \end{bmatrix} \cdot u + \begin{bmatrix} 0 \\ 1 \end{bmatrix} \cdot \xi \tag{5-40}$$

$$Y = [\, 1 \;\; 0] \cdot \begin{bmatrix} x_C \\ x_\Gamma \end{bmatrix} + [0] \cdot u + \eta \tag{5-41}$$

In the previous method, the system was only driven by random noises and was in the form of Equation 5-12. Now the system is driven both by noise and the control input, u. Because of this, the disturbance noise matrix is now:

$$Q_f = \Gamma \cdot Q_o \cdot \Gamma^T \tag{5-42}$$

where Q_o is the noise intensity from Equation 5-13, and Γ is the disturbance distribution gain matrix in Equation 5-37. The state deviation matrix, Q, control weighting matrix, R, and measurement noise matrix, R_o, are the same as in the numerical solution.

For the *lqg* command in MATLAB™, the control weightings and noises must be grouped as shown in Equations 5-43 and 5-44.

$$W = \begin{bmatrix} Q & 0 \\ 0 & R \end{bmatrix} = \begin{bmatrix} 1 & 0 & 0 \\ 0 & 0 & 0 \\ 0 & 0 & 2 \end{bmatrix} \tag{5-43}$$

$$V = \begin{bmatrix} Q_f & 0 \\ 0 & R_o \end{bmatrix} = \begin{bmatrix} 0 & 0 & 0 \\ 0 & 1 & 0 \\ 0 & 0 & 1 \end{bmatrix} \tag{5-44}$$

The following command returned the same solution as that found in Equation 5-36 using the numerical method.

```
[Ak,Bk,Ck,Dk]=lqg(A,B,C,D,W,V)
```

where A, B, C, and D are from Equations 5-40 and 5-41 and W and V are from Equations 5-43 and 5-44.

High Order Plant with No Coloring Filter. This example is presented to illustrate the application of this method to reduced order compensator design. In this example the following controlled element state space was used:

$$\dot{x}_C = \begin{bmatrix} -4 & -10 & -12 & -5 \\ 1 & 0 & 0 & 0 \\ 0 & 1 & 0 & 0 \\ 0 & 0 & 1 & 0 \end{bmatrix} \cdot x_C + \begin{bmatrix} 1 \\ 0 \\ 0 \\ 0 \end{bmatrix} \cdot u + \begin{bmatrix} 1 \\ 0 \\ 0 \\ 0 \end{bmatrix} \cdot \xi \tag{5-45}$$

$$y = \begin{bmatrix} 0 & 1 & 6 & 8 \end{bmatrix} \cdot x_C + [0] \cdot u \tag{5-46}$$

This is a single-input-single-output system (SISO) as shown. Unit intensity weightings were applied to the control usage and state deviations such that:

$$R = \begin{bmatrix} 1 \end{bmatrix} \quad \text{and} \quad Q = \begin{bmatrix} 1 & 0 & 0 & 0 \\ 0 & 1 & 0 & 0 \\ 0 & 0 & 1 & 0 \\ 0 & 0 & 0 & 1 \end{bmatrix} \tag{5-47}$$

The control and state deviation weighting matrices, R and Q, must be diagonal for the numerical solution to be valid. The noises, ξ and η, were assumed to be unit intensity, random white noises such that:

$$Q_n = \begin{bmatrix} Q_o & 0 \\ 0 & Ro \end{bmatrix} = \begin{bmatrix} 1 & 0 \\ 0 & 1 \end{bmatrix} \tag{5-48}$$

and the standard LQG noise intensity matrix was:

$$Q_f = \Gamma Q_o \Gamma^T = \begin{bmatrix} 1 & 0 & 0 & 0 \\ 0 & 0 & 0 & 0 \\ 0 & 0 & 0 & 0 \\ 0 & 0 & 0 & 0 \end{bmatrix} \tag{5-49}$$

Using the MATLAB™ command, *lqg,* described in the previous example, the resulting standard LQG solution was:

$$Y_{k_{LQG}}(s) = \frac{-0.0163s^3 - 0.1413s^2 - 0.1929s - .0680}{s^4 + 4.7837\,s^3 + 12.9420\,s^2 + 17.8484\,s + 9.7295} \tag{4-50}$$

The numerical LQG solutions were found using the same method as in the previous example. The routine *PIFINDNF,* listed in Appendix E, computed the compensators listed in Table 5-1.

Table 5-1
Sub-Optimal Compensator Example

Order	Compensator	PI[1]	Time[2,3]
4	$\frac{-0.0163s^3 - 0.1415s^2 - 0.1949s - .0689}{s^4 + 4.7981\ s^3 + 13.0013\ s^2 + 17.9841\ s + 9.8708}$	0.23694	2:20
3	$\frac{-0.0162s^2 - 0.1284s - 0.0620}{s^3 + 3.8922\ s^2 + 9.0063\ s + 8.9584}$	0.23694	1:57
2	$\frac{-0.0237s - 0.0398}{s^2 + 1.3466s + 4.3805}$	0.23695	0:45
1	$\frac{-0.0335}{s + 2.6522}$	0.23713	0:10

[1] Performance Index
[2] Processing time (minutes:seconds) on IBM compatible 486DX (50 MHz)
[3] Computing time for the standard LQG solution method was five seconds on the same computer.

Two conclusions can be drawn from these examples. First, the performance index computation routines are valid. When the desired compensator order was equal to the LQG compensator order, the numerical method and the standard LQG solution method produced the same results, within the tolerance of the numerical search. Second, reducing the compensator order did not significantly affect the resulting performance index value. For less than one tenth of a percent increase in the performance index, a first order compensator could have been used in this example instead of the fourth order, standard LQG solution.

For higher order compensators (more than six unknown variables), this simplex search algorithm was not satisfactory and an alternative numerical minimization routine may be necessary. As the number of unknown variables increased above six, the solution became sensitive to the initial guess for some problems. For the second example problem, the third order solution was found using the following initial condition:

$$C_0 = \begin{bmatrix} -0.1 & -0.1 & -0.1 & 4 & 4 & 4 \end{bmatrix} \tag{5-51}$$

The fourth order solution was found using a small perturbation of the standard LQG solution. If a higher order compensator is desired, the MATLAB™ Lyapunov routine should be rewritten so that it does not return an error message and interrupt the program when the Lyapunov solution is not unique. A large, arbitrary performance index should be assigned instead. The Nelder-Meade simplex algorithm was satisfactory for the lower order compensators. The first and second order compensators were not sensitive to the initial guesses. Any initial condition with values between *1* and *100* allowed convergence to the same optimal solution. Additionally, the computing time for the first and second order compensators was not significant.

Bode plots of the four compensators are shown in Figures E-1 through E-10. As shown in Figures E-9 and E-10, the second, third, and fourth order compensators are roughly equivalent. From a low order equivalent system standpoint, the first order compensator was not a good approximation of the others. However, this compensator only increased the LQG performance index 0.08 percent over the fourth order solution as shown in Table 5-1.

Summary

A numerical solution to the LQG problem was developed. This method allowed the user to select a compensator form. It then used a Nelder-Meade simplex algorithm to find the coefficients of the compensator that minimized the standard LQG performance index. This method is valid for situations when reduced order LQG compensation is desired.

Several assumptions were made in the development of the numerical LQG solution.

1. The controlled element is time invariant (page 5-3)[1].
2. The controlled element is proper (page 5-3).
3. The compensator is proper (page 5-4).
4. The system is driven only by random noises (page 5-3).
5. The frequency content of the driving noise is proper (page 5-5).
6. The state deviation weighting matrix, Q, is diagonal (page 5-8).
7. The control usage weighting matrix, R, is diagonal (page 5-9).

Given these assumptions, Equations 5-25 and 5-27 were derived. These equations compute the LQG performance index value for any controlled element and compensator. Two routines that implement these equations were provided in Appendix E.

Two example problems were worked using the Nelder-Meade simplex search routine to find the minimum performance index. When the desired compensator order was equal to the LQG compensator order, the numerical method and the standard LQG solution method produced the same results. Reducing the compensator from fourth order to first order in the second example only increased the performance index by 0.08 percent (page 5-17).

---

[1] Refers to the page in this thesis containing this conclusion.

The solution was overly sensitive to the initial guess for higher order compensators (more than six unknown variables). Additionally, the MATLAB™ Lyapunov routine should be rewritten so that it does not return an error message and interrupt the program when the Lyapunov solution is not unique. A large, arbitrary performance index should be assigned instead.

The numerical solution technique developed in this chapter was satisfactory for lower order compensators. The solution was not sensitive to the initial guess and the computing time was not significant (page 5-17).

6. *The Sub-Optimal Pilot Model*

General

The primary advantage of classical pilot models is that their gain, lead, lag, and delay form is based on experimental observations of human pilot behavior. Choosing values for these variables and then using them to predict a Cooper-Harper rating, however, is difficult. The primary advantage of optimal pilot models is that they, like the pilot, find the control strategy that minimizes a combination of average tracking error (performance) and control usage (workload). This weighted combination, or performance index, can be directly related to a predicted Cooper-Harper rating based on statistical fits to historical data. Because they are based on linear quadratic Gaussian (LQG) theory, however, the pilot describing functions predicted by optimal pilot models tend to be high order and therefore inconsistent with experimentally observed behavior. Additionally, when the constraints of the human pilot are implemented within the LQG structure, the intuitive nature of the model is lost.

The sub-optimal pilot model developed in this chapter uses the numerical LQG solution method described in Chapter 5 to restrict the optimal pilot model solution to the classical pilot model form. While this solution may be *sub-optimal* in comparison to the standard LQG solution, it more accurately models observed human pilot behavior. The sub-optimal pilot model is not presented as a solution to the pilot modeling problem. To do so would require the examination of a broad handling qualities data base, requiring

years of experience and model development. Rather, it is a unique and promising approach, offered as a prototype for future study.

This chapter is divided into four sections. The first section, *Model Development,* describes the sub-optimal pilot model. The next section, *Parameter Analysis,* examines the model's input parameters. In the third section, *Results,* the Cooper-Harper ratings and pilot describing functions predicted by the sub-optimal pilot model are compared with flight test results as well as the predictions of other pilot models. Finally, the conclusions of this chapter are summarized.

Model Development

Model Structure. The sub-optimal pilot model is based on the classical pilot model structure. This can be represented for the pitch axis as shown in Figure 6-1[1].

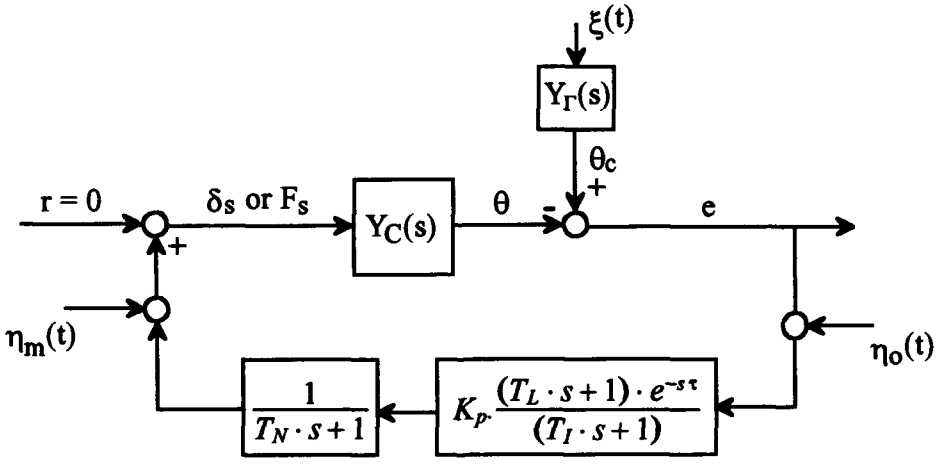

Figure 6-1. Classical Pilot Model Structure

[1] The standard Laplace variable, *s,* is used in this chapter for convenience. However, all Laplace transform representations of the human pilot used in this thesis are strictly valid only in the frequency domain with continuous, random-like inputs. They should not be used for system responses to deterministic inputs.

where

ξ	= Task Driving Noise	θ	= Pitch Angle
η_m	= Muscular Noise	θ_c	= Pitch Command
η_o	= Observation Noise	e	= Task Error
K_p	= Pilot Gain	F_s	= Stick Force
T_L	= Pilot Lead Time Constant	δ_s	= Stick Deflection
T_I	= Pilot Lag Time Constant	Y_C	= Aircraft Dynamics
τ	= Pilot Delay	Y_Γ	= Task Dynamics
T_N	= Muscular Time Constant		

This classical pilot model structure is equivalent to that shown in Figure 2-5 (page 2-10), where the pilot applies gain and washout to the error and error rate signals. This structure is not identical, however, to that used for the development of the numerical solution to the general LQG problem. The numerical method developed in Chapter 5 must therefore be adapted slightly.

For the sub-optimal pilot model, the aircraft and task forcing function dynamics will be assumed to be single-input-single-output systems. As a result, Figure 6-1 can be redrawn for the pitch axis as shown in Figure 6-2. Notice that the motor noise was removed from the model. Also, unlike the general LQG problem presented in Chapter 5, the disturbance noise is now injected at the controlled element output so that the error vector (θ_c-θ) can be formed.

Motor noise was not included in the sub-optimal pilot model for two reasons. First, it was assumed that the observation noise would adequately account for its effects. Second, if motor noise is added to the control vector, the problem cannot be solved

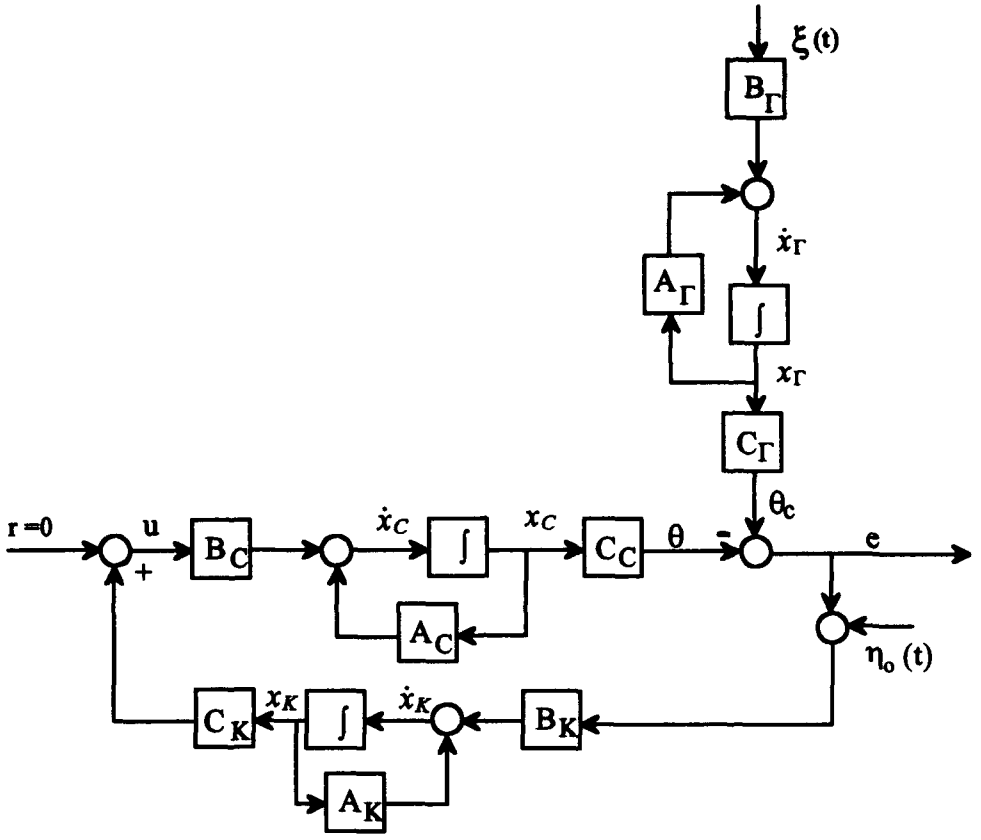

Figure 6-2. Sub-Optimal Pilot Model Structure

directly. The sub-optimal pilot model weights control and tracking error in the following performance index.

$$J = \int_0^\infty [e^T Q e + u^T R u]\, dt \tag{6-1}$$

The numerical solution assumes that the system is driven by random noises such that:

$$J = E\{e^T Q e + u^T R u\} \tag{6-2}$$

If noise is added to the control vector, u, it can be written as:

$$u = [C_K x_K + \eta_m] \tag{6-3}$$

Substituting Equation 6-3 into the second term in Equation 6-2 results in Equation 6-4.

$$E\{u^T R u\} = R \cdot E\{u^T u\} = R \cdot E\{(C_k x_k + \eta_m)^2\} \tag{6-4}$$

Because of the single-input-single-output nature of the sub-optimal pilot model, u is a scalar, and several simplifying assumptions were made as shown. Equation 6-4 expands to:

$$E\{(C_k x_k + \eta_m)^2\} = E\left\{(C_k x_k)^2\right\} + E\left\{(\eta_m)^2\right\} + E\{2C_k x_K \cdot \eta_m\} \tag{6-5}$$

The first term can be computed as shown in the previous chapter. The third term contains cross-correlations that can only be solved for the single-input-single-output case. Finally, the second term drives the performance index to infinity. The reasons for this are the same as for requiring a proper compensator (page 5-4). By definition, the expected value of the motor noise is as shown in Equation 6-6.

$$E\{\eta_m \eta_m^T\} = R_o \cdot \delta(\tau) \tag{6-6}$$

Because of the delta function, the magnitude of Equation 6-6 and the performance index that contains this term is infinite.

The equations of state for the sub-optimal pilot model system in Figure 6-2 are:

$$\dot{x}_C = A_C x_C + B_C u \qquad \theta = C_C x_C \tag{6-7}$$

$$u = C_K x_k \tag{6-8}$$

$$\dot{x}_\Gamma = A_\Gamma x_\Gamma + B_\Gamma \xi \qquad \theta_c = C_\Gamma x_\Gamma \tag{6-9}$$

$$\dot{x}_K = A_K x_K + B_K(\eta_o + e) \qquad e = \theta_c - \theta \tag{6-10}$$

Substituting and combining terms yields the following state-space representation driven only by white noises.

$$\begin{bmatrix} \dot{x}_C \\ \dot{x}_\Gamma \\ \dot{x}_K \end{bmatrix} = \begin{bmatrix} A_C & 0 & B_C C_K \\ 0 & A_\Gamma & 0 \\ -B_K C_C & B_K C_\Gamma & A_K \end{bmatrix} \cdot \begin{bmatrix} x_C \\ x_\Gamma \\ x_K \end{bmatrix} + \begin{bmatrix} 0 & 0 \\ B_\Gamma & 0 \\ 0 & B_K \end{bmatrix} \cdot \begin{bmatrix} \xi \\ \eta \end{bmatrix} \tag{6-11}$$

where

$$e = \begin{bmatrix} -C_C & C_\Gamma & 0 \end{bmatrix} \cdot \begin{bmatrix} x_C \\ x_\Gamma \\ x_K \end{bmatrix} \tag{6-12}$$

The filter state space matrix, A_Γ, must have all eigenvalues in the open left half plane since x_Γ is not controllable from u. This system is in the form:

$$\dot{x} = Ax + Ew \tag{6-13}$$

The autocorrelation matrix, X, can be found by solving the following Lyapunov equation.

$$AX + XA^T + EQ_n E^T = 0 \tag{6-14}$$

where Q_n contains the noise intensities, ξ and η, on the diagonals. The autocorrelation matrix, X, is related to the expected values of the states, x, by the following identity.

$$X = E\{x^T x\} \tag{6-15}$$

Performance Index. The performance index used in the sub-optimal pilot model weights error and control such that:

$$J = E\{e^T Q e\} + E\{u^T R u\} \tag{6-16}$$

Because this model is restricted to single-input-single-output systems, this equation can be rewritten as:

$$J = Q \cdot E\{e^T e\} + R \cdot E\{u^T u\} \tag{6-17}$$

where Q and R are the scalar weightings. Using Equations 6-7 through 6-10, and assuming the single-input-single-output case, this becomes:

$$J = Q \cdot E\{(C_\Gamma x_\Gamma - C_C x_C)^2\} + R \cdot E\left\{x_K^T C_K^T C_K x_K\right\} \tag{6-18}$$

The second term is identical to that in Chapter 5 and can be written for the single-input-single-output case as:

$$R \cdot \sum_{i=1}^{m} \sum_{j=1}^{m} C_{K_{1,i}} \cdot C_{K_{1,j}} \cdot X_{(n+i),(n+j)} \tag{6-19}$$

where m is the number of compensator states, n is the number of aircraft and filter states, and X is the autocorrelation matrix from Equation 6-15. The first term in Equation 6-18 is much more complicated, and can only be solved for the single-input-single-output case where $C_\Gamma x_\Gamma$ and $C_C x_C$ are scalars. This term can be expanded as in Equation 6-20.

$$\begin{aligned} Q \cdot E\{(C_\Gamma x_\Gamma - C_C x_C)^2\} = {} & Q \cdot E\{(C_\Gamma x_\Gamma)^2\} + Q \cdot E\{(C_C x_C)^2\} \\ & -2 \cdot Q \cdot E\{(C_C x_C) \cdot (C_\Gamma x_\Gamma)\} \end{aligned} \tag{6-20}$$

The first two expected values are similar to that in Equation 6-19. They can therefore be solved numerically using the following summations.

$$E\{(C_\Gamma x_\Gamma)^2\} = \sum_{i=1}^{f} \sum_{j=1}^{f} C_{\Gamma_{1,i}} \cdot C_{\Gamma_{1,j}} \cdot X_{(p+i),(p+j)} \tag{6-21}$$

$$E\{(C_C x_C)^2\} = \sum_{i=1}^{p}\sum_{j=1}^{p} C_{C_{1,i}} \cdot C_{C_{1,j}} \cdot X_{i,j} \tag{6-22}$$

where f is the number of filter states, p is the number of aircraft states, and X is the autocorrelation matrix from Equation 6-15. The final expected value in Equation 6-20 is not as simple to solve. However, by expanding the problem symbolically and grouping terms, the following summation can be found.

$$E\{(C_\Gamma x_\Gamma)(C_C x_C)\} = \sum_{i=1}^{f}\sum_{j=1}^{p} C_{\Gamma_{1,i}} \cdot C_{C_{1,j}} \cdot X_{(p+i),j} \tag{6-23}$$

In this equation, f is the number of filter states, p is the number of aircraft states and X is the autocorrelation matrix from Equation 6-15. Equations 6-19 and 6-21 through 6-23 were used to compute the performance index in the sub-optimal pilot model. This numerical algorithm is validated in Appendix F.

Pilot Model Form. Due to the unique nature of the numerical approach, the LQG solution can be restricted to a desired compensator form. Thus, the muscular lag and pilot delay can be modeled directly and intuitively.

The desired compensator for this model is:

$$\frac{c(1)\cdot(s+c(2))}{(s+c(3))\cdot(T_N s+1)} \cdot \frac{2-\tau s}{2+\tau s} \tag{6-24}$$

The vector, c, contains the three parameters the numerical routine will search to minimize the performance index. The first element in the vector is pilot gain, the second is lead, and the is third lag. T_N is the muscular time constant and τ is the pilot delay. In

the sub-optimal pilot model, the muscular lag time constant, T_N, can be selected by the model user, but it is not varied in the numerical search algorithm.

The pilot delay is modeled by a first order Pade approximation. Like the muscular lag time constant, the delay is selected by the model user, but it is not varied in the numerical search algorithm. A second order Pade approximation did not affect the results significantly. For the integrator example described in Chapter 3 (page 3-8), the performance index increased from 4.6309 to 4.6326 when a second order Pade approximation was used instead of a first. This 0.037 percent increase was both typical and insignificant.

As a final note, the numerical search algorithm did not consistently converge when the pilot model was written exactly as in Equation 6-24. Instead, the denominator had to be expanded as shown in Equation 6-25.

$$\frac{c(1)s+c(2)}{s^2+\left(c(3)+\frac{1}{T_N}\right)\cdot s+c(3)\cdot\frac{1}{T_N}}\cdot\frac{2-\tau s}{2+\tau s} \tag{6-25}$$

Performance Index Weightings. The standard optimal pilot model includes control rate instead of control in the performance index. It then iterates the control rate weighting until the desired muscular time constant is obtained. This establishes the ratio between the weightings as shown in Chapter 3, and makes the model's results independent of these weightings (see page 3-27 of this thesis). The sub-optimal pilot model directly includes the muscular system in the compensator form, leaving the weightings, Q and R, free to be chosen by the user.

Noise Intensities. Intensities must be selected for both the forcing function and measurement noises. Unit intensity driving noise should be used for the task forcing function, V_ξ. The observation noise intensity, V_η, is iteratively determined so that the noise ratio, ρ, input by the user is obtained.

The Cooper-Harper rating formula is normalized for unit intensity forcing function noise. The observation noise intensity, V_η, is determined by solving the numerical LQG problem repeatedly until the desired noise ratio is achieved. This is accomplished using the following relationship.

$$V_\eta = \rho\pi\sigma_e^2 \tag{6-26}$$

In this equation, V_η is the observation noise intensity, ρ is the desired noise ratio, and σ_e^2 is the root mean square magnitude of the task error (25:11-14). In the sub-optimal pilot model structure, σ_e^2 is the first term in Equation 6-18 and is found using Equations 6-21 through 6-23. A simple binary search, limited to five iterations, is used.

Cooper-Harper Rating Prediction. It would be advantageous to use the same ratings prediction formula used in the STI optimal pilot model, Equation 3-2 (page 3-8). This formula was based on the analysis of a wide range of aircraft dynamics and normalizes the predicted rating for task intensity. This equation can not be applied to the sub-optimal pilot model for two reasons. First, Equation 3-2 was formulated for an performance index that weights control rate and error. The sub-optimal pilot model weights control usage. Second, the nature of the two models is quite different. The sub-optimal pilot model solution is restricted to a compensator form with only three

variables available for optimization. This produces a much tighter spread in the performance index values than will occur in the STI optimal pilot model. Based on the limited evaluation of the sub-optimal pilot model conducted for this thesis the following equations tend to produce the best ratings correlation. Note that these equations are not normalized for task intensity or bandwidth. They are based on a regression analysis of the dynamics analyzed for this thesis, and are proposed as a course measure to enhance the parameter analysis conducted later in this chapter.

$$\begin{aligned} \textit{Pitch Rating} &= -30 + 241 \cdot \log_{10}(J) \\ \textit{Roll Rating} &= -13 + 117 \cdot \log_{10}(J) \end{aligned} \tag{6-27}$$

Flow Diagram. The equations and computational flow of the sub-optimal pilot model are summarized in the flow diagram of Figure 6-3 on the next page. The user inputs the aircraft and task forcing functions along with the error weighting, Q, the control weighting, R, the observation noise ratio, ρ, the muscular time constant, T_N, and the pilot delay, τ_D. The sub-optimal pilot model sets the task driving noise intensity at one, the initial observation noise intensity at 0.5, and all initial compensator coefficients to one. The minimum performance index is then found using the methods described previously in this chapter. The relationship between the observation noise intensity and the desired noise ratio is examined using Equation 6-26, and the process repeated (up to five times) until adequate convergence is obtained. Next, the predicted Cooper-Harper rating is computed using Equation 6-27. Finally, the resulting pilot describing function, performance index, and predicted Cooper-Harper rating are displayed. The three routines, or *.m files*, that implement this model are presented in Appendix G. The first

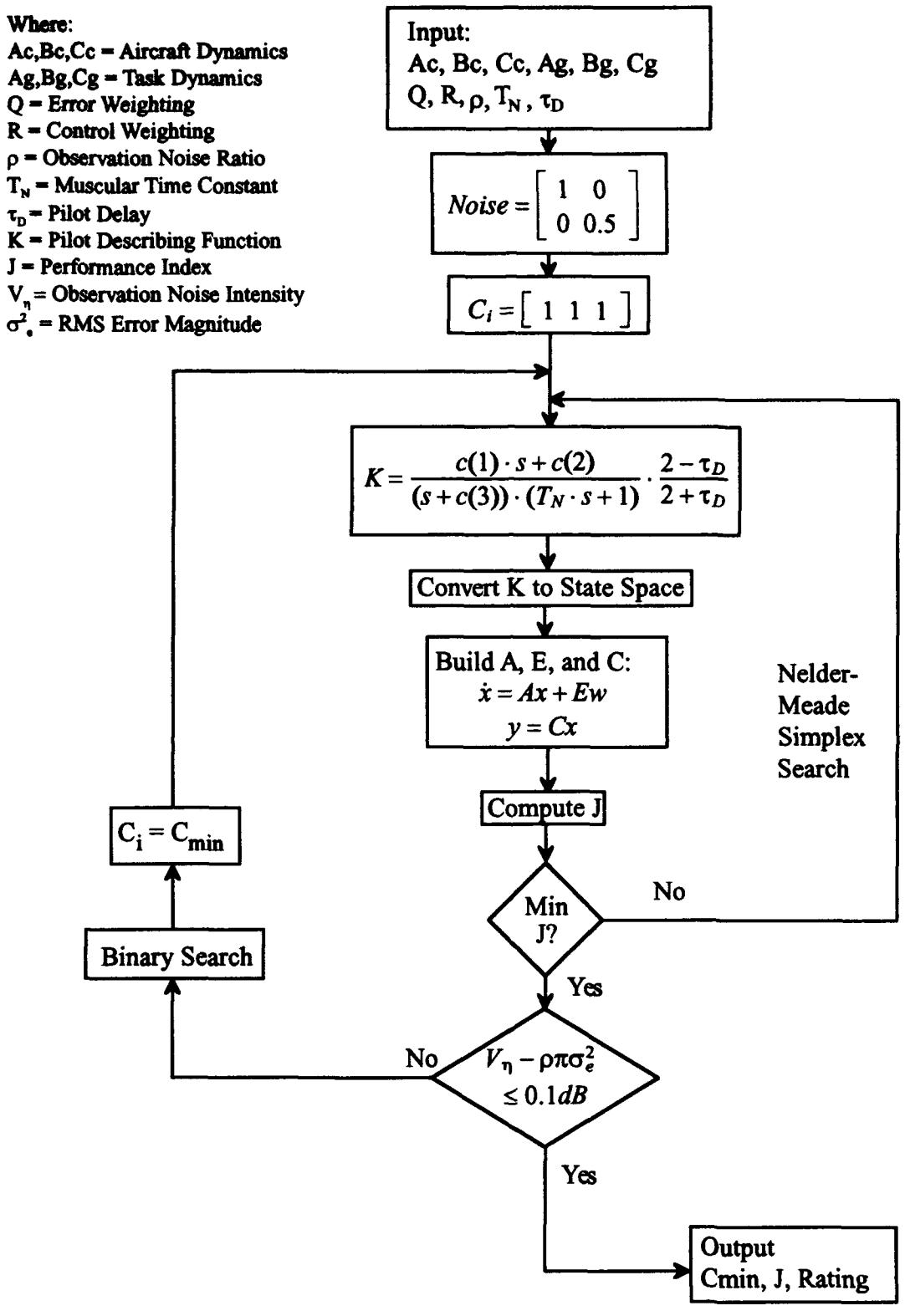

Figure 6-3. Sub-Optimal Pilot Model Flow Diagram

file, *SOPM.M,* is the master routine. It conducts the iterations and calls the other two files as necessary. The second file, *PI_SOPM.M,* finds the performance index value for the given compensator, aircraft, and pilot dynamics. The final file, *RMS_SOPM,* is identical to *PI_SOPM* except that in addition to the performance index, it also passes back the root mean square (RMS) value of the error for noise ratio computations. This file is used only after the optimal compensator is determined.

Parameter Analysis

The user must choose several parameters when using the sub-optimal pilot model.

1. Aircraft Model Order
2. Task Forcing Function (Ag, Bg, Cg)
3. Error Weighting (Q)
4. Control Weighting (R)
5. Observation Noise Ratio (ρ)
6. Muscular Time Constant (T_N)
7. Pilot Delay (τ_D)

The data gathered in the following analysis indicates that the values in Table 6-1 produce the best results.

Table 6-1
Recommended Parameters for the Sub-Optimal Pilot Model

Parameter	Symbol	Recommended Value
Aircraft Model Order	-----	Any
Task Forcing Function	Ag, Bg, Cg	$\frac{\sqrt{2}}{0.25s^2 + \frac{\sqrt{2}}{2}s + 1}$
Error Weighting	Q	1
Control Weighting	R	4.5 (pitch); 1 (roll)
Observation Noise Ratio	ρ	0.01 (-20 dB)
Muscular Time Constant	T_N	0.115
Pilot Delay	τ_D	0.37

The reasons for each of these choices are given in the following discussion. Except where noted, each of these parameters was evaluated individually with the others held at the values shown in this table. This parameter analysis is not meant to fine tune the model for use. The data base evaluated was much to small for this, and the model is only a prototype for future study. Rather, this analysis is offered for the insights it provides.

The following dynamics and Cooper-Harper ratings, shown in Table 6-2, were used for this parameter analysis. These values are from the in-flight sum-of-sines tracking task described in Chapter 4.

	Longitudinal Dynamics:		Lateral Dynamics:	
Case 1:	$\frac{20(s+1.8)e^{-0.04s}}{s(s^2+8.4s+36)}$	Case A:	$\frac{2.5e^{-0.04s}}{s(s+2.5)}$	(6-28)
Case 2:	$\frac{20(s+1.8)e^{-0.04s}}{s(s^2+4.8s+36)}$	Case B:	$\frac{e^{-0.04s}}{s(s+1)}$	(6-29)
Case 3:	$\frac{20(s+1.8)e^{-0.24s}}{s(s^2+8.4s+36)}$	Case C:	$\frac{2.5e^{-0.24s}}{s(s+2.5)}$	(6-30)
Case 4:	$\frac{20(s+1.8)e^{-0.24s}}{s(s^2+4.8s+36)}$	Case D:	$\frac{e^{-0.24s}}{s(s+1)}$	(6-31)

Table 6-2
Cooper-Harper Ratings Used for
Sub-Optimal Pilot Model Parameter Analysis

	Case 1	Case 2	Case 3	Case 4	Case A	Case B	Case C	Case D
Rating	2	2	5	5	1	2	4	6

Aircraft Model Order. Any aircraft model order can be used. Unlike the STI optimal pilot model discussed in Chapter 3, the order of the pilot describing function predicted by the sub-optimal pilot model does not depend on the aircraft model order. Additionally, increasing the aircraft model order only increases the size of the Lyapunov matrices, and does not significantly increase the computing time.

Some higher order dynamics are problematic, however. Full order dynamics, by their nature, have poorly scaled state space representations. For, example the numerator for Case 1 has a numerator gain of over 200,000 (refer to Equation C-3), but the first term in the denominator has unity gain. The numerical search routine did not converge for the full order dynamics evaluated in the flight test described in Chapter 4. However, the short period approximations of Equation 6-28 through 6-31 did not present any special problems.

Task Forcing Function. When comparing model predictions with flight test results, a task forcing function consistent with the actual task should be used. Otherwise, the following second order Butterworth filter with a break frequency, ω_b, of two radians per second is recommended.

$$Y_\Gamma(s) = \frac{\sqrt{2}}{\frac{s^2}{\omega_b^2} + \frac{\sqrt{2}}{\omega_b}s + 1} \tag{6-32}$$

This break frequency is consistent with that normally used in airborne compensatory tracking tasks. The square root of two in the numerator makes the filter bandwidth (zero dB crossover) equal to the filter break frequency.

As the break frequency was moved from two, the correlation between the performance indices and the actual aircraft handling qualities degraded rapidly. For example the effects of decreasing the break frequency to 0.4 radians per second is shown in Table 6-3.

Table 6-3
The Effects of Task Break Frequency on Sub-Optimal Pilot Model Results

	Break Frequency	Performance Index	Minimum Compensator Values[1]
Case 1	2	1.3637	0.879, 0, 1.826
Case 2	2	1.3473	1.218, 0, 1.506
Case 3	2	1.3885	0.9441, 0, 2.600
Case 4	---[2]	---[2]	---[2]
Case 1	0.4	0.1620	3.820, 0, 0.297
Case 2	0.4	0.1544	2.209, 85.212, 23.546
Case 3	0.4	0.1374	3.807, 0 0.281
Case 4	0.4	0.1333	3.809, 0, 0.263

[1] Where the pilot is in the form: (c1*s + c2) exp (-tau*s) / (s + c3)*(s +1/Tn)
[2] A "matrix poorly conditioned" warning was given while evaluating this case.

The performance indices correlate well with the Cooper-Harper ratings gathered during flight test for a break frequency of two. Notice that the trend is reversed when the lower break frequency is used. Such behavior makes this model sensitive to the task and is undesirable.

Weightings. It was concluded from the flight test described in Chapter 4, that weighting stick deflection and task error produced the best correlation with in-flight Cooper-Harper ratings. Values for the correlation coefficients were computed and are presented in Table 6-4. As shown in this table, the control weighting, *R,* should be about

4.5 times the error weighting, Q, for pitch tasks. The weightings should be roughly equal for roll tasks[1].

Table 6-4
Sub-Optimal Pilot Model Weighting Coefficients

	Pitch Axis	Roll Axis
Tracking Error Weighting, Q	7.2	1.7
Stick Deflection Weighting, R	32.5	2.2

These values also produced the best results in the sub-optimal pilot model. Each of the pitch cases were evaluated using a stick deflection weighting, R, of 4.5 and again with a weighting of one. The results of this analysis are presented in Table 6-5.

Table 6-5
The Effects of Control Weighting on Sub-Optimal Pilot Model Results

	Control Weighting	Performance Index	Minimum Compensator Values[1]
Case 1	4.5	1.3637	0.879, 0, 1.826
Case 2	4.5	1.3473	1.218, 0, 1.506
Case 3	4.5	1.3885	0.9441, 0, 2.600
Case 4	--[2]	---[2]	---[2]
Case 1	1	1.2530	4.064, 0, 2.2035
Case 2	1	1.2154	3.869, 0, 1.712
Case 3	1	1.2375	0.950, 0 1.306
Case 4	1	1.3038	3.860, 0, 2.7536

[1] Where the pilot is in the form: (c1*s + c2) exp (-tau*s) / (s + c3)*(s +1/Tn).
[2] A "matrix poorly conditioned" warning was given while evaluating this case.

Note that the performance index did not correlate as well with the handling qualities when the lower weighting was used. When a weighting of one was used, Case 3

[1] The ratio between the weightings, Q and R, is the salient issue. Any constant multiplier of the two weightings can be factored to the front of the performance index.

had better predicted handling qualities (a lower performance index) than Case 1. In the actual tracking task, Case 3 was given a Cooper-Harper rating of 5 and Case 1 was given a 2.

Observation Noise Ratio. The observation noise ratio was experimentally measured at 0.01, or -20 dB (25:12). Note that power spectra dB (10 $\log_{10}$) is normally used when referring to this value. The sub-optimal pilot model results were evaluated for noise ratios of 0.316 (-15 dB) and 0.0032 (-25 dB). The correlation between the performance indices and the actual aircraft handling qualities was not affected by the different values of noise ratios. However, as the observation noise ratio increased, the magnitude of the performance indices increased. The results of some representative runs are presented for the roll axis in Table 6-6.

Table 6-6
The Effects of Observation Noise Ratio on Sub-Optimal Pilot Model Results

	Noise Ratio	Performance Index	Minimum Compensator Values[1]
Case A	-20 dB	1.3890	2.179, 0, 3.539
Case B	-20 dB	1.4070	1.261, 0, 3.905
Case C	-20 dB	1.4046	1.564, 0, 4.677
Case D	-20 dB	1.4120	0.826, 0, 5.387
Case A	-15 dB	1.3987	1.096, 0, 2.283
Case B	-15 dB	1.4101	0.609, 0, 2.592
Case C	-15 dB	1.4089	0.728, 0, 3.168
Case D	-15 dB	1.4131	0.366, 0, 3.839
Case A	-25 dB	1.3795	4.036, 0, 5.715
Case B	-25 dB	1.4038	2.411, 0, 6.189
Case C	-25 dB	1.3998	3.097, 0, 7.345
Case D	-25 dB	1.4107	1.695, 0, 8.182

[1] Where the pilot is in the form: (c1*s + c2) exp (-tau*s) / (s + c3)*(s +1/Tn).

Muscular Time Constant. The muscular time constant was experimentally measured by McRuer at values between about 0.08 and 0.12 (15:171). The sub-optimal pilot model results were evaluated using the extremes of these values. The data used for this evaluation are presented in Table 6-7.

Table 6-7
The Effects of Muscular Time Constant on Sub-Optimal Pilot Model Results

	Time Constant	Performance Index	Minimum Compensator Values[1]
Case 1	0.115	1.3637	0.879, 0, 1.826
Case 2	0.115	1.3473	1.218, 0, 1.506
Case 3	0.115	1.3885	0.9441, 0, 2.600
Case 4	---	---[2]	---[2]
Case 1	0.083	1.3641	0.332, 0, 1.353
Case 2	0.083	1.3472	1.478, 0, 1.188
Case 3	0.083	1.3889	1.086, 0, 2.039
Case 4	0.083	1.3790	1.222, 0, 1.839

[1] Where the pilot is in the form: (c1*s + c2) exp (-tau*s) / (s + c3)*(s +1/Tn).
[2] A "matrix poorly conditioned" warning was given while evaluating this case.

As shown in this table, changing the muscular time constant had almost no effect on the performance index value or the predicted pilot describing function. A value of 0.115 was used for consistency with past research (consult the discussion in Chapter 2 of this thesis (page 2-8).

Pilot Delay. A pilot delay of 0.35 should be used for stick displacement command systems, and 0.25 seconds should be used for force command systems. These values are based on the flight test results presented in Chapter 4 (page 4-13).

The sub-optimal pilot model adds the aircraft delay to the pilot delay before minimizing the performance index. Thus, the effects of altering pilot delay values can be seen by comparing Cases 1 and 3 or 2 and 4. In all cases evaluated for this thesis, increasing the delay increased the performance index.

Results

The sub-optimal pilot model results produced using the recommended values in Table 6-1 are presented in Table 6-8.

Table 6-8
Sub-Optimal Pilot Model Results

	Performance Index	Predicted Rating	Actual Rating	Minimum Compensator Values[1]
Case 1	1.3637	2.5	2	0.879, 0, 1.826
Case 2	1.3473	1.2	2	1.218, 0, 1.506
Case 3	1.3885	4.4	5	0.9441, 0, 2.600
Case 4	1.4502[2]	8.9	5	5.438, 0, 2.941[2]
Case A	1.3890	0.8	1	2.179, 0, 3.539
Case B	1.4070	3.7	2	1.261, 0, 3.905
Case C	1.4046	3.4	4	1.564, 0, 4.677
Case D	1.4120	4.3	6	0.826, 0, 5.387

[1] Where the pilot is in the form: (c1*s + c2) exp (-tau*s) / (s + c3)*(s +1/Tn).
[2] A "matrix poorly conditioned" warning was given while evaluating this case.

As shown in this table, the trend between performance index values and the actual handling qualities ratings was reasonably consistent. The *predicted* Cooper-Harper ratings should not be given too much emphasis. These values were found using a regression formula optimized for these dynamics cases. For this reason they were

omitted from the analysis in the previous sections. They are provided here to confirm the correlation between the performance index and the actual Cooper-Harper rating.

Bode plots of the predicted pilot describing functions are presented in Figures G-1 through G-4. Notice that in all cases, the optimal pilot describing function was one with pure lead in the numerator. This equates to pure error rate feedback with washout. In other words the error gain, K_{p1}, in Figure 2-5 (page 2-10) is zero. Such compensation delays the magnitude and phase roll-offs to the maximum extent possible.

The pilot describing functions predicted by the sub-optimal pilot model are by design more consistent with flight test results than the pilot describing functions predicted by the STI optimal pilot model. The STI optimal pilot model is much more accurate predictor of Cooper-Harper ratings, however. There is a strong correlation between the sub-optimal pilot model performance index and the actual Cooper-Harper ratings, but this model lacks the maturity necessary for consistent predictions.

Conclusions

The sub-optimal pilot model developed in this chapter uses the numerical LQG solution method described in Chapter 5 to restrict the optimal pilot model solution to the classical pilot model form. This model minimizes a performance index consisting of error and control usage and is restricted to single axis use due to the assumptions necessary to numerically compute the performance index value (page 6-5)[1]. The numerical algorithm was validated in Appendix F. Additionally, motor noise was not modeled because it would drive the value of the performance index to infinity (page 6-3).

[1] Refers to the page in this thesis containing this conclusion.

The sub-optimal pilot model solution was restricted to a gain, lead, lag, delay, and neuromuscular lag. The user inputs the desired muscular time constant and delay value (modeled by a first order Pade approximation). The model then searches all values of gain, lead, and lag to minimize the performance index. The model is solved iteratively until the desired observation noise ratio is achieved. Finally, the predicted pilot describing function, Cooper-Harper rating, and minimum performance index are displayed.

A brief parameter analysis was performed in an effort to gain insight into the sub-optimal pilot model. Through this analysis, the recommended input parameters presented in Table 6-1 (6-13) were derived. More importantly this analysis lead to several conclusions concerning the model.

1. Any aircraft model order can be used as long as the state space representation is not poorly scaled. Neither the predicted pilot describing function nor the required computing time are affected by the model order (page 6-15).
2. The task forcing function should be modeled by a second order Butterworth filter with a break frequency of two. As the break frequency was moved from this value, the correlation between the performance index and the predicted Cooper-Harper rating was diminished (6-16).
3. The performance index weightings estimated from the flight test data produced the best results (6-17).
4. The correlation between the performance indices and the actual aircraft handling qualities was not affected by changes in the noise ratios. However, as the observation noise ratio increased, the magnitude of the performance indices increased (6-18).
5. The value of the muscular time constant had no significant effect on the sub-optimal pilot model results (6-19).

Finally, the results of the sub-optimal pilot model were compared to those of STI optimal pilot model. By design, the describing functions predicted by the sub-optimal

pilot model were more consistent with flight test than those of the STI optimal pilot model. The STI optimal pilot model was a much more accurate predictor of Cooper-Harper ratings, however. The sub-optimal pilot model is a unique and promising approach to pilot modeling and warrants further study.

7. Conclusions and Recommendations

The most significant assumption made throughout this thesis was that the pilot can be modeled as a linear element. As discussed in Chapter 2, this assumption is only valid when the task is random appearing and within the capabilities of the pilot. Under these conditions, past experiments found that the human pilot can be modeled as a gain, lead, lag, delay, and a first order muscular lag (Reference 15).

There are currently three broad categories of pilot models. The first category, *open loop models,* use the aircraft response to open loop commands to predict handling qualities. Because these models make no attempt to directly model the human pilot, they are relatively simple to develop and are the most commonly used. The second category, *classical pilot models,* model the pilot as a gain, lead, lag, and delay. This form is based on experimental observations, but using these models to predict Cooper-Harper ratings remains a difficult task. The final type of model, *optimal pilot models,* model the pilot as an optimal regulator and estimator. Relating the predicted pilot describing function to a predicted Cooper-Harper rating is more straight forward with these model. Their implementation is difficult, however, and the pilot describing functions they predict are generally high order, and therefore not consistent with observed human behavior.

An optimal pilot model developed by Systems Technology, Incorporated, (STI) was analyzed in detail. This model was chosen for three reasons. First, it incorporates nearly every important aspect of other optimal pilot models, making it a good candidate for study. Second it can be implemented on the personal computer and is therefore

widely available. Finally, this model has had some success in predicting Cooper-Harper ratings, but lacks parameter selection guidance.

The analysis of this model included a model overview, an integrator example, and a detailed parameter analysis. The integrator example was worked, step-by-step, to clarify the model's logic. This example paralleled an example presented in the STI documentation (Reference 25). The handling qualities rating predicted for this example was not realistic (negative), illustrating the need for proper selection of the model's parameters.

The user must select nearly twenty parameters when running the STI optimal pilot model. Most of the selections are straight forward, and some have no significant effect on the model results. Several important recommendations were made, however. First, the lowest feasible aircraft model order should be used. The STI model predicts a pilot describing function of order $2n+5$ where n is the number of aircraft and filter states. Second, the task bandwidth should be selected by running the model for a range of bandwidths and selecting the one that produces the worst Cooper-Harper rating. If the generally accepted flight test bandwidth of 2 radians per second is used, the model does not produce satisfactory results. Third, the filter should be augmented to the plant output. Finally, the experimentally estimated observation noise ratios of -20 decibels should be used. For the best results, however, the motor noise ratio should be increased from its experimentally based value of -25 decibels to -20 decibels.

When the proper model parameters were used, the STI optimal pilot model was moderately successful at predicting Cooper-Harper ratings, both for the LAMARS cases

analyzed in Chapter 3 and the flight dynamics cases described in Chapter 4. Unfortunately, the STI model predicted a fifteenth order pilot when short period dynamics were analyzed. Bode plots of these pilot describing functions had deep notches, indicative of this high order compensation. Due to their high order, the pilot describing functions predicted by the STI model were not consistent with the classical pilot model form or observed human pilot behavior.

A limited evaluation of human pilot response was sponsored in support of this thesis by the Air Force Flight Dynamics Directorate. Five sorties were flown in the Calspan variable stability Lear II aircraft. Ground simulations in Lear II were also performed. Four different pitch and four different roll axis dynamics were evaluated using three different tracking tasks. Primary pilot response parameters were recorded and examined using statistical and Fourier transform analysis in an attempt to provide insight into human pilot behavior.

The dynamics evaluated during the flight test represented a broad range of handling qualities as evidenced by the assigned Cooper-Harper ratings. Additionally, the variability in these ratings was acceptably low.

An analysis of the discrete tracking task time histories revealed that the pilot delay between task command and stick force (0.27 seconds) was consistent with previous experimental estimations. The stick deflection lagged stick force by 0.1 seconds in all cases, however, due to the lag effects of the stick dynamics. This produced a total delay between task command and stick deflection of 0.37 seconds, well above that normally used in pilot model analysis.

A regression analysis of the flight test data was conducted in an attempt to evaluate the validity of two optimal pilot model weighting schemes. First, a regression analysis of root mean square (RMS) tracking error and normalized RMS stick deflection to Cooper-Harper rating was performed. Second a regression analysis of RMS tracking error and RMS stick deflection rate to Cooper-Harper rating was performed. The task error and normalized stick deflection weighting scheme produced a much higher rating correlation for the airborne data.

A frequency response analysis of task error to stick deflection was conducted in an attempt to provide insight into human pilot response. This analysis revealed that the pilots did not exhibit higher order behavior. The frequency responses were consistent with the classical gain, lead, and lag form except for the presence of large amounts of pure phase lead at higher frequencies. In all cases the pilot acted so that the combined pilot-aircraft system resembled and integrator in the crossover region. When the aircraft command path gain was doubled, the pilot reduced his gain so that the response of the combined pilot-aircraft system was not significantly changed.

A numerical solution to the linear quadratic Gaussian (LQG) problem was derived in Chapter 5. This solution allows the compensator form to be predetermined. This method may be applicable for any situation when reduced order compensation is desired.

The numerical method assumes the aircraft, filter, and compensator dynamics are proper. Further, the LQG weighting matrices must be diagonal and the system must only be driven by random noises. The value of the standard LQG performance index is

determined numerically, using the covariance matrix and a series of summations for any compensator, controlled element, and filter. A Nelder-Meade simplex search is then used to find the compensator coefficients that minimize the performance index.

Two examples were worked using this numerical approach. The first demonstrated that when the predetermined compensator order was the same as that of the standard LQG solution, the two methods produced identical results. The second example demonstrated the potential of this method for use in finding reduced-order, sub-optimal compensators.

These examples also revealed a deficiency in the numerical search routine. The Nelder-Meade search routine was found to be unsatisfactory for complex compensator forms. When numerous parameters had to be searched the success of the routine depended greatly on the initial guess. The method was found to be satisfactory for compensators with six or less parameters to search. Further, it was recommended that the MATLAB™ Lyapunov solver be rewritten so that it returns an arbitrary and large performance index when the Lyapunov solution is not unique, rather than an error message.

Finally, the numerical LQG solution was used in a sub-optimal pilot model developed in Chapter 6. This model restricted the optimal pilot model solution to the classical pilot model form. It was sub-optimal in terms of the standard LQG performance index due to its low order form, but it was by nature more consistent with human pilot behavior. This model minimized a performance index consisting of task error and control usage.

Additional numerical summations were developed to implement the output disturbance form and error weighting of a compensatory tracking task. The model was restricted to single axis use due to the assumptions necessary to numerically compute the performance index value. These new summations were verified by example in Appendix F.

The sub-optimal pilot model solution was restricted to a gain, lead, lag, delay, and muscular lag. The user input the desired muscular time constant and delay value. The model then searched all values of gain, lead, and lag to minimize the performance index. The model was solved iteratively until the desired observation noise ratio was achieved. Finally, the predicted pilot describing function, Cooper-Harper rating, and minimum performance index were displayed.

A brief parameter analysis was performed in an effort to gain insight into the sub-optimal pilot model. Through this analysis, recommended input parameters were derived. More importantly, this analysis lead to several conclusions concerning the model. First, any aircraft model order could be used so long as the state space representations were properly scaled. Second, a task forcing function consistent with that used in flight test could be used. Third, the performance index weightings obtained from the flight test regression analysis produced good results. Finally, in all cases the predicted pilot describing function had a free s in the numerator, generating as much lead at as low frequency as possible.

By design, the describing functions predicted by the sub-optimal pilot model were more consistent with flight test than those of the STI optimal pilot model. The STI

optimal pilot model was a much more accurate predictor of Cooper-Harper ratings, however. The sub-optimal pilot model is a unique and promising approach to pilot model and warrants further analysis.

Appendix A. Nonstandard Performance Indices

The optimal pilot model discussed in Chapter 3 uses the following nonstandard performance index.

$$J = \int_0^\infty [x^T(t) Q_c x(t) + \dot{u}^T(t) R_c \dot{u}(t)] dt \qquad \text{(A-1)}$$

Notice the weighting penalty is on control rate instead of control usage. Minimizing this performance index is equivalent to augmenting all channels of the plant with integrators and minimizing the standard performance index in Equation A-2.

$$J = \int_0^\infty [x^T(t) Q_c x(t) + u^T(t) R_c u(t)] dt \qquad \text{(A-2)}$$

Consider the standard LQG diagram in Figure A-1 below with *r,* the commanded input, equal to zero and the weighting matrices, *Q* and *R,* as shown.

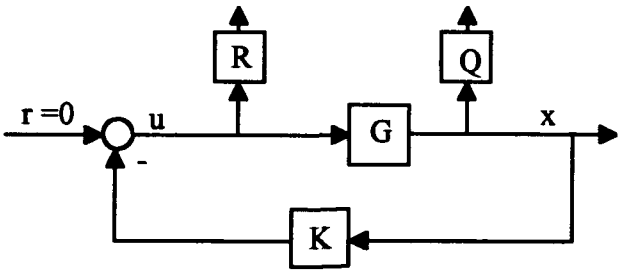

Figure A-1. Standard Control Weighting

Minimizing the standard quadratic performance index, Equation A-2, is equivalent to minimizing the two-norm of the output of the two vectors, Ru(t) and Qx(t), over an infinite time horizon. If it is desired to minimize $R\dot{u}(t)$ instead of Ru(t), the diagram can

be modified as shown in Figure A-2.

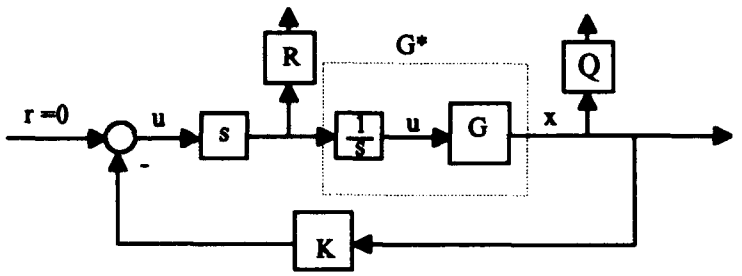

Figure A-2. Control Rate Weighting

The new plant, G*, is equivalent to the original plant augmented with integrators. The control rate weighting matrix, *R*, can now be used to establish compensator lags on the different control channels.

Appendix B. Predicted Describing Functions

General

This appendix contains Bode plots of the pilot describing functions predicted by the STI optimal pilot model during the sensitivity analysis in Chapter 3. Each figure also presents the lower order equivalent system match to the classical pilot model form.

The dynamics analyzed were:

$$\text{Case 1:}\quad \frac{\theta}{\delta_e} = \frac{100}{s(s+100)} \tag{B-1}$$

$$\text{Case 2:}\quad \frac{\theta}{\delta_e} = \frac{20(s+1.25)}{s(s^2+8s+25)} \cdot e^{-.033s} \tag{B-2}$$

$$\text{Case 3:}\quad \frac{\theta}{\delta_e} = \frac{20(s+1.25)}{s(s^2+8s+25)} \cdot e^{-.2s} \tag{B-3}$$

$$\text{Case 4:}\quad \frac{\theta}{\delta_e} = \frac{20(s+1.25)}{s(s^2+1.8s+25)} \cdot e^{-.033s} \tag{B-4}$$

$$\text{Case 5:}\quad \frac{\theta}{\delta_e} = \frac{20(s+1.25)}{s(s^2+1.8s+25)} \cdot e^{-.2s} \tag{B-5}$$

These dynamics have the following characteristics:

Table B-1
STI Optimal Pilot Model Evaluation Dynamics

	Short Period Damping Ratio, ζ_{sp}	Short Period Natural Frequency, ω_{sp}	Delay, τ
Case 1	1	100	0
Case 2	0.8	5	0.033
Case 3	0.8	5	0.2
Case 4	0.18	5	0.033
Case 5	0.18	5	0.2

The STI optimal pilot model predicted the following pilot describing functions[1]:

$$Y_{p1} = \frac{174(0)(.0448)[.707,.4](1.65)(5.79)(12.63)(12.91)[-.866,17.3](100)^2}{(0)[.707,.4]^2(6.02)(12.57)(12.63)[.274,18.96](45.4)(94)(100)} \quad \text{(B-6)}$$

$$Y_{p2} = \frac{92.6(0)(.032)[.707,.4](1.45)[.814,4.56][.8,5](5.08)(12.5)^2[-.866,14.9]}{(0)[.707,.4]^2(1.25)(4.96)[.8,5](12.43)(12.46)[.146,14.2][.84,27.3]} \quad \text{(B-7)}$$

$$Y_{p3} = \frac{92.7(0)(.035)[.707,.4](1.19)(4.1)[.79\ \ 6,4.78][.8,5][-.866,8.66](12.5)^2}{(0)[.707,.4]^2(1.25)(4.02)[.8,5][.043,11.5](12.36)(12.46)[.81,23.5]} \quad \text{(B-8)}$$

$$Y_{p4} = \frac{46.2(0)(.028)[.707,.4](1.18)[.06,4.4](4.56)[.18,5](12.5)(12.6)[-.866,14.9]}{(0)[.707,.4]^2(1.25)(4.6)[.18,5](12.49)(12.52)[.157,12.8][.846,23.3]} \quad \text{(B-9)}$$

$$Y_{p5} = \frac{40.4(0)(.028)[.707,.4](1.04)(3.74)[.025,4.96],[.18,5],[-.866,8.66](12.5)^2}{(0)[.707,.4]^2(1.25)(3.77)[.182,5][.082,10.7](12.4)(12.5)[.818,19.12]} \quad \text{(B-10)}$$

The following lower order equivalent system matches to the classical pilot model form were found:

$$Y_{p1} = \frac{3.756(s+2.921)}{(s+1.546)} \cdot e^{-.154s} \quad \text{(B-11)}$$

$$Y_{p2} = \frac{1.29(s+3.248)}{(s+0.973)} \cdot e^{-.106s} \quad \text{(B-12)}$$

$$Y_{p3} = \frac{1.294(s+2.253)}{(s+1.036)} \cdot e^{-.198s} \quad \text{(B-13)}$$

$$Y_{p4} = \frac{0.347(s+5.42)}{(s+0.682)} \cdot e^{-.0123s} \quad \text{(B-14)}$$

$$Y_{p5} = \frac{0.295(s+5.31)}{(s+0.765)} \cdot e^{-.13s} \quad \text{(B-15)}$$

[1] Where the brackets denote $[\zeta, \omega_n]$ as in $s^2+2\zeta\omega_n+\omega_n^2$, and the parentheses denote (τ) as in $s+\tau$.

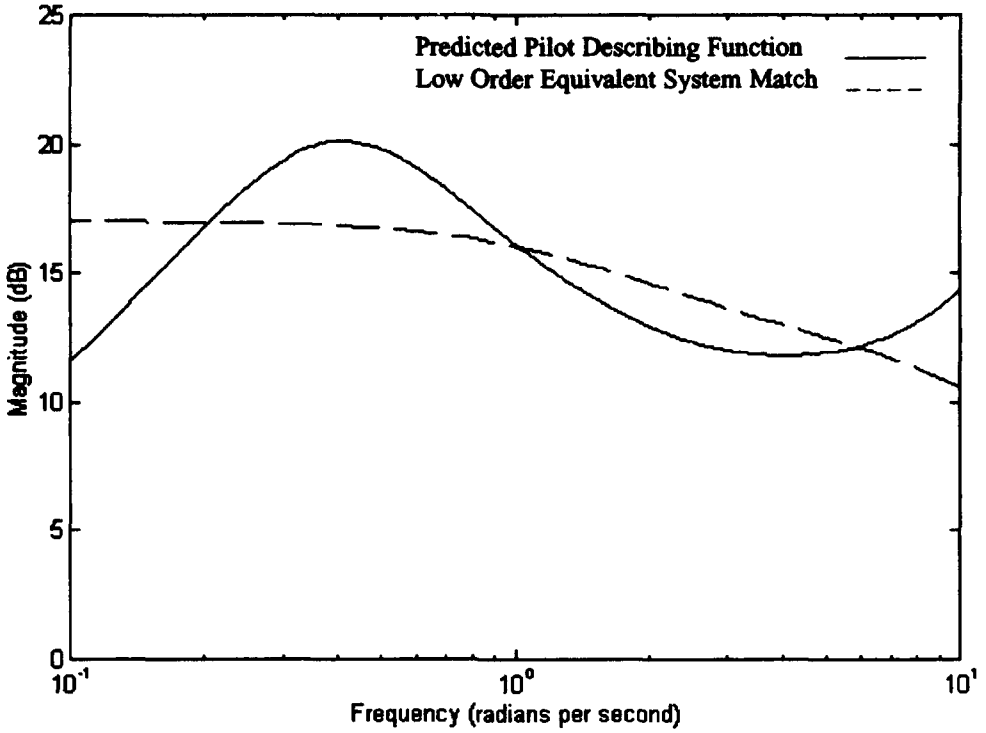

Figure B-1. Bode Magnitude Plot of Case 1

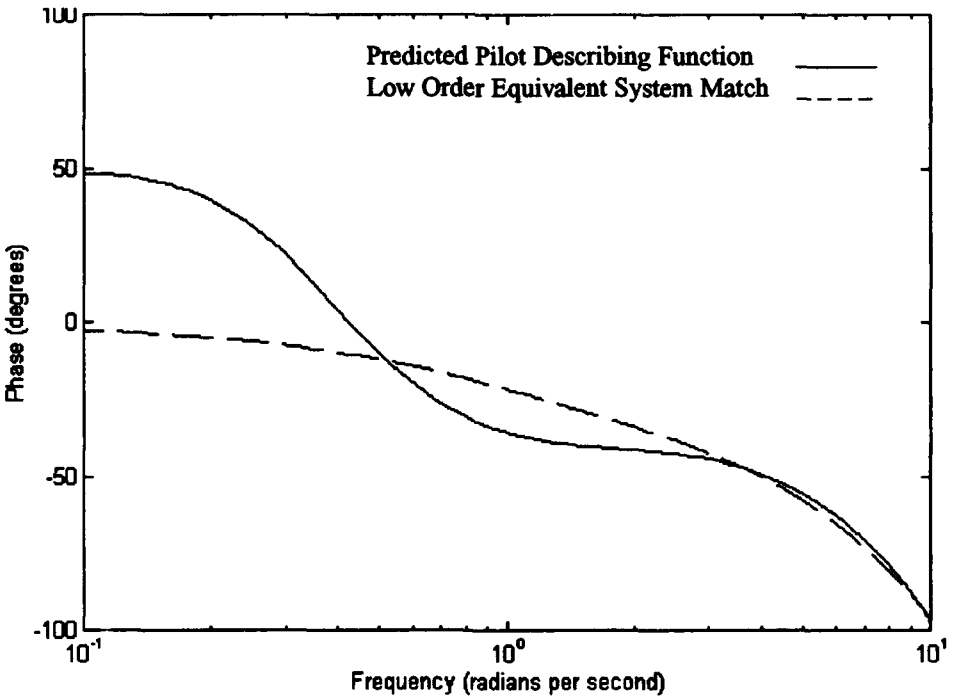

Figure B-2. Bode Phase Plot of Case 1

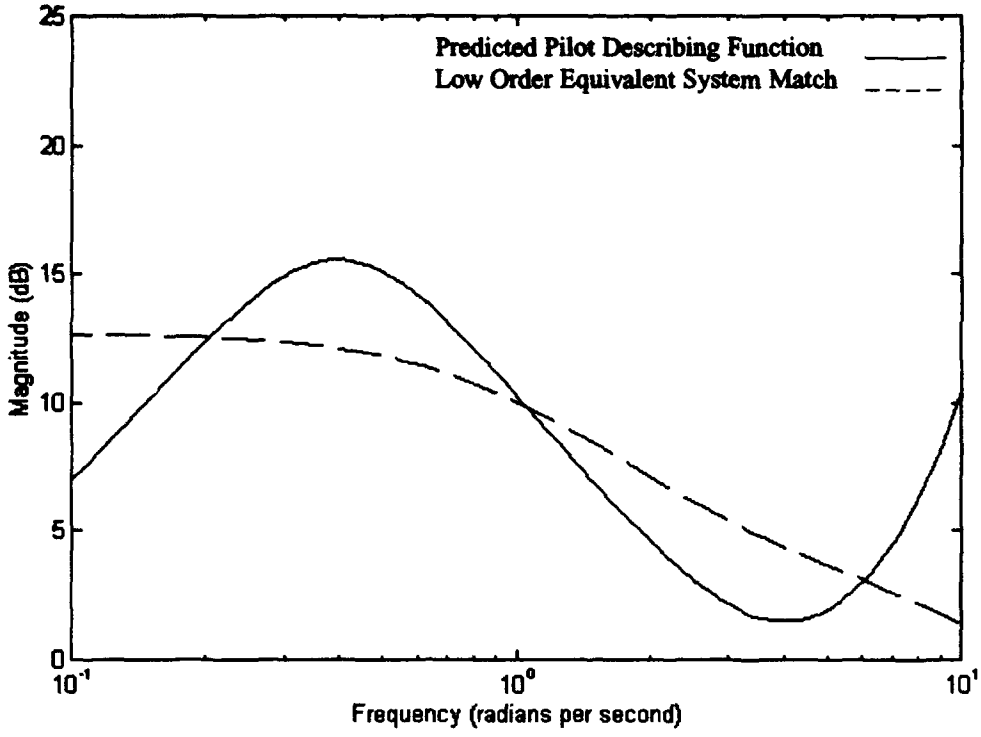

Figure B-3. Bode Magnitude Plot of Case 2

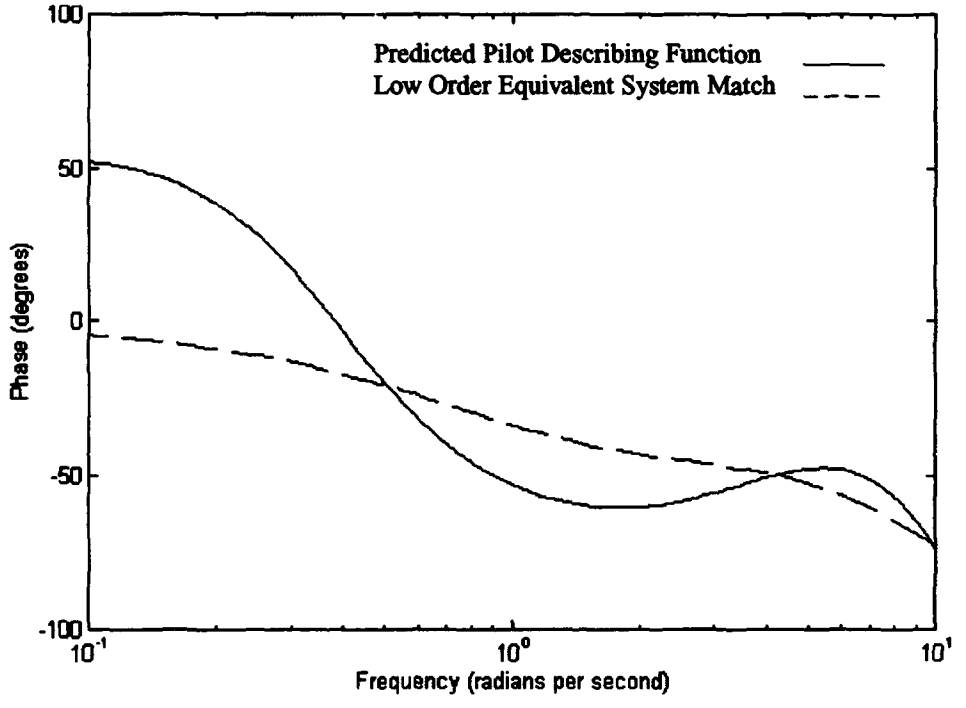

Figure B-4. Bode Phase Plot of Case 2

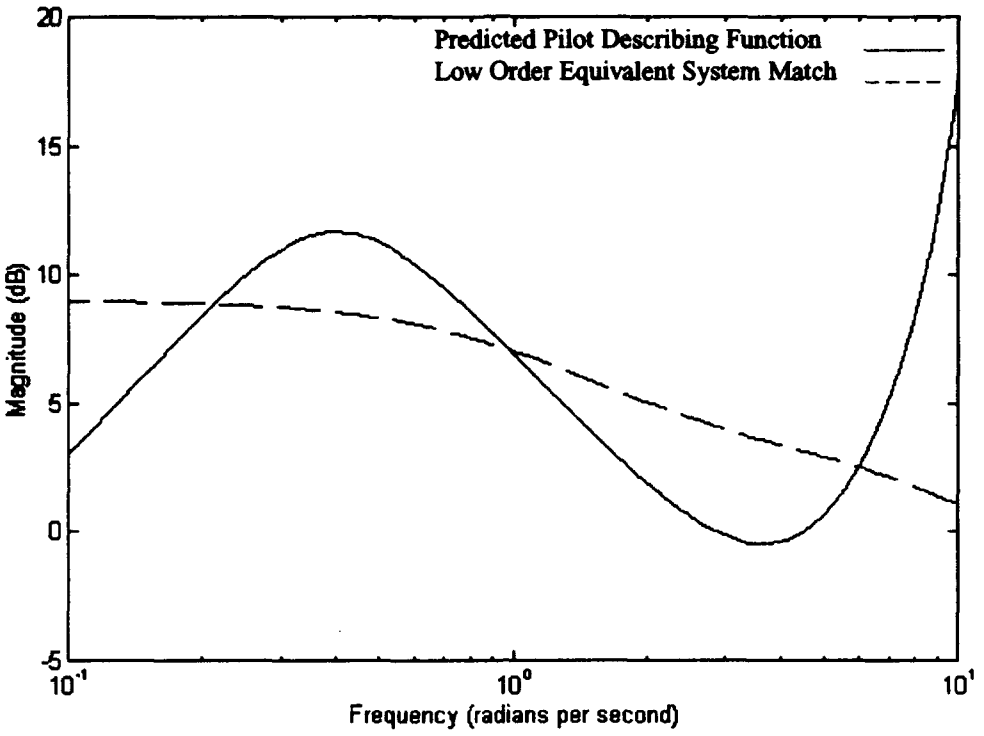

Figure B-5. Bode Magnitude Plot of Case 3

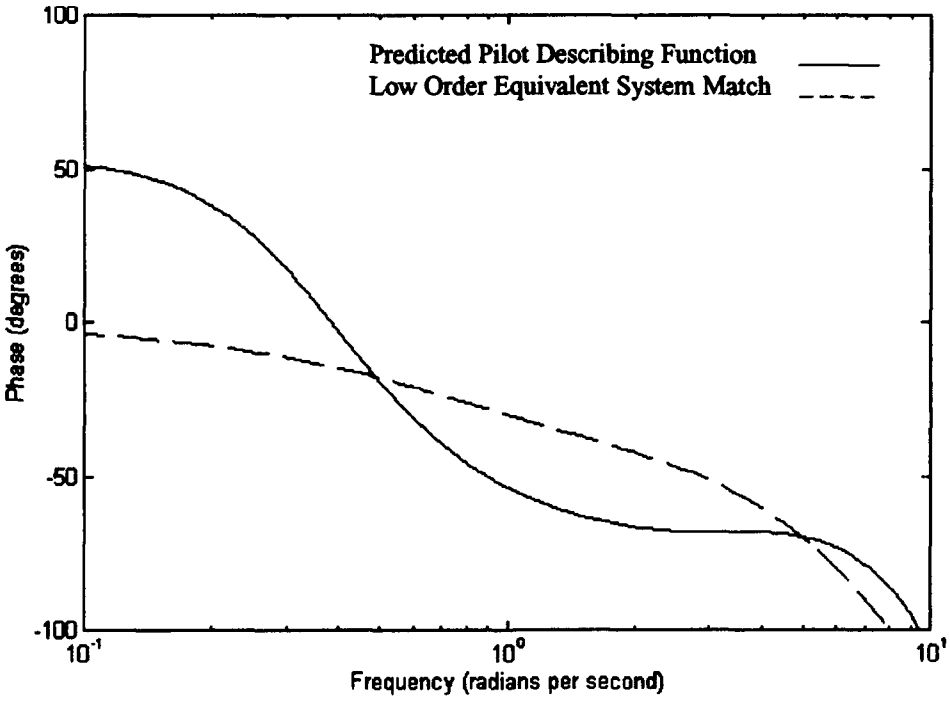

Figure B-6. Bode Phase Plot of Case 3

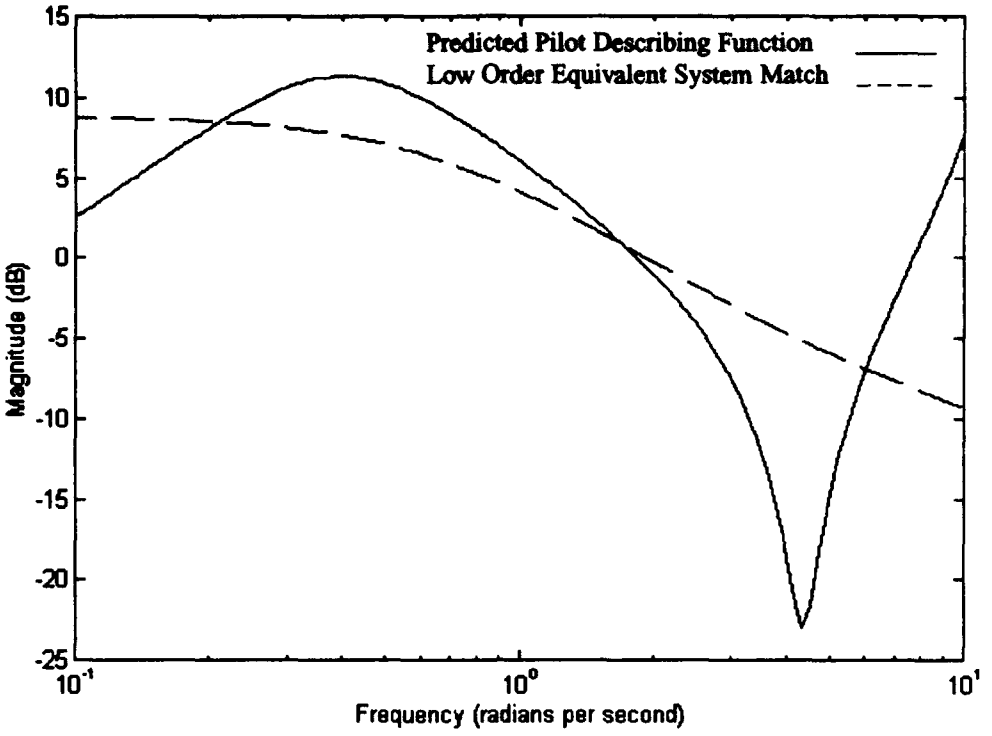

Figure B-7. Bode Magnitude Plot of Case 4

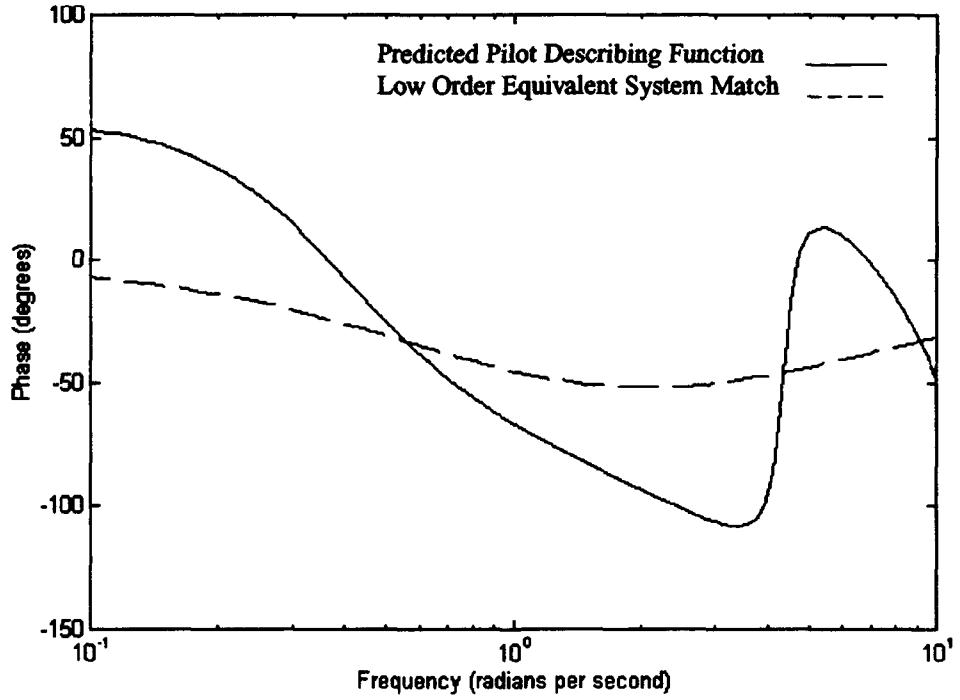

Figure B-8. Bode Phase Plot of Case 4

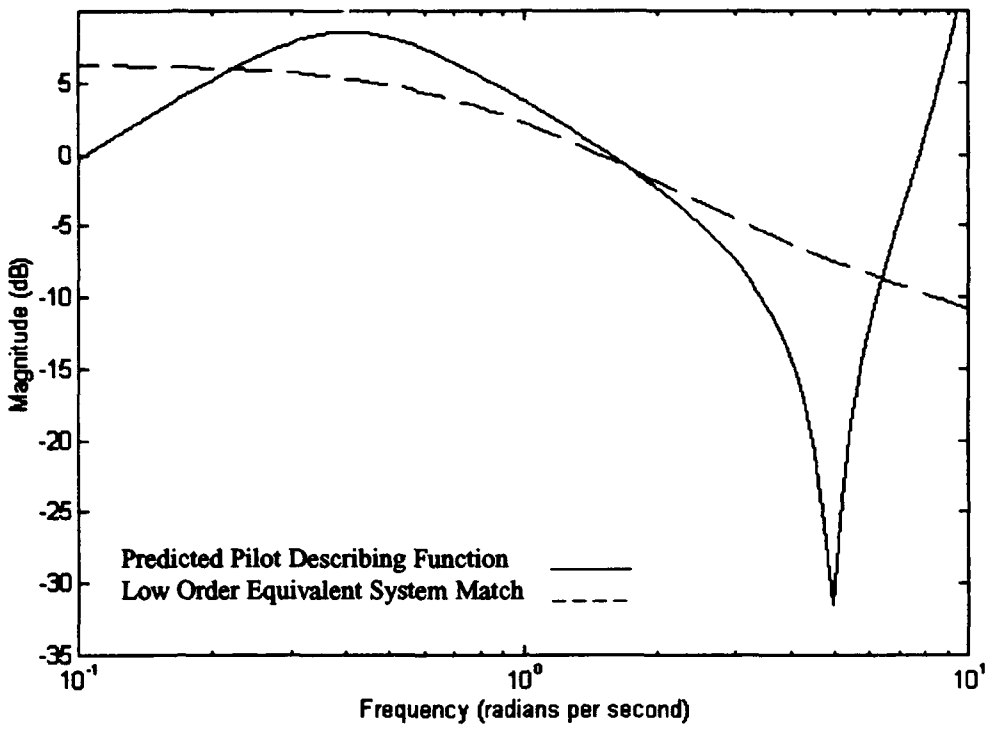

Figure B-9. Bode Magnitude Plot of Case 5

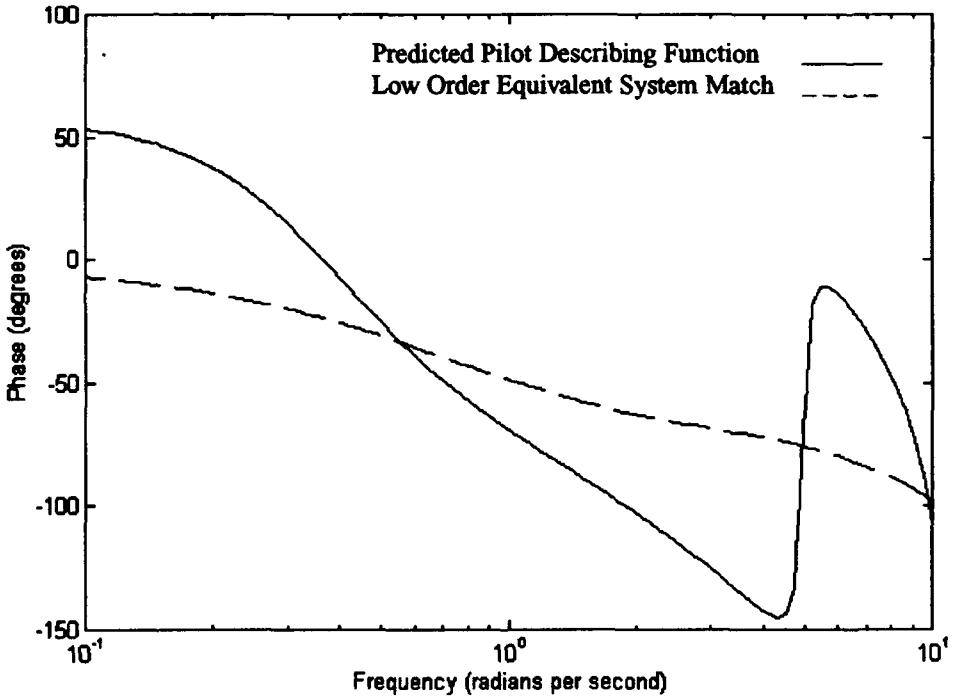

Figure B-10. Bode Phase Plot of Case 5

Program CC Macro

The following macro implements the STI optimal pilot model on *Program CC* as described in Chapter 3. These commands use the baseline parameters listed in Table 3-3 (page 3-21), where *yc1* is the aircraft transfer function and *yw* is the task forcing function.

File Name: *.MAC in OCM subdirectory

```
@ocmyc1,yc1,yw,p40
@ocmlqr,p40,1,.1,.08,.001
@ocmsetup,1,.2,-20,-20,-20,1,1,1,0,0,1
@ocmkbf,.1
@ocmpilot,.2,2
state
gep,p24,yp
cc
yp=-yp
yp
```

Appendix C. Flight Test Information

General

This appendix presents supplemental information for Chapter 4, *Flight Test.*

Dynamics Implementation

The dynamics described on page 4-8 of this thesis were implemented as a position command system as shown in Figure C-1 and C-2.

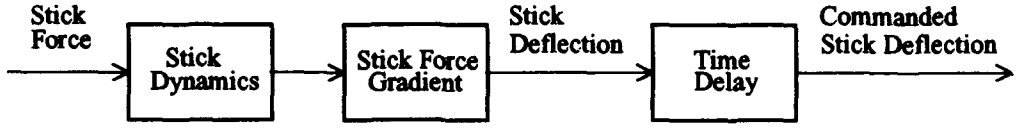

Figure C-1. Feel System

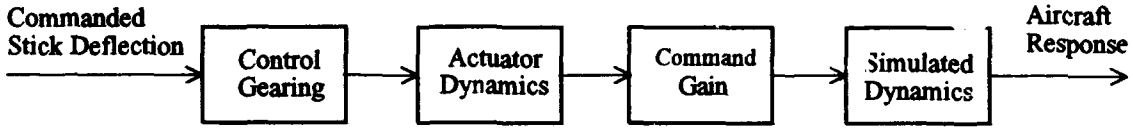

Figure C-2. Flight Control System

The elevator and aileron actuator dynamics were:

$$\frac{70^2}{s^2 + 2(.7)(70) + 70^2} \tag{C-1}$$

The longitudinal and lateral stick dynamics were:

$$\frac{16^2}{s^2 + 2(.7)(16) + 16^2} \tag{C-2}$$

The feel system characteristics were:

	Elevator:	Aileron:
Stick Force Gradient	6 lb/in	4 lb/in
Stick Breakout Force	0.75 lb	0.75 lb
Stick Force per g	7 lb/g	-----
Control Gearing	8 deg/in	12 deg/in

The following equations represent the linear implementation of these dynamics[1] (31:49-50).

$$\frac{\theta}{F_{es}} = \frac{16^2}{[.7,16]} \cdot \frac{1}{6} \cdot 8 \cdot \frac{70^2}{[.7,70]} \cdot \frac{5.5(1.8)}{(0)[\zeta_{sp},6]} \cdot e^{-\tau_D \cdot s} \qquad \text{(C-3)}$$

$$\frac{\theta}{\delta_{es}} = 8 \cdot \frac{70^2}{[.7,70]} \cdot \frac{5.5(1.8)}{(0)[\zeta_{sp},6]} \cdot e^{-\tau_D \cdot s} \qquad \text{(C-4)}$$

$$\frac{\phi}{F_{as}} = \frac{16^2}{[.7,16]} \cdot \frac{1}{4} \cdot 12 \cdot \frac{70^2}{[.7,70]} \cdot \frac{3.3}{(0)(T_R)} \cdot e^{-\tau_D \cdot s} \qquad \text{(C-5)}$$

$$\frac{\phi}{\delta_{as}} = 12 \cdot \frac{70^2}{[.7,70]} \cdot \frac{3.3}{(0)(T_R)} \cdot e^{-\tau_D \cdot s} \qquad \text{(C-6)}$$

Test Point Evaluation Cards

The test point evaluation card, presented in Figure C-3, and the pilot induced oscillation (PIO) rating scale, presented in Figure C-4, were used during the flight test described in AFFTC-TLR-93-41. They are presented here for the reader's convenience.

[1] Where *[.7,16]* denotes $[\zeta, \omega_n]$ as in $s^2+2\zeta\omega_n+\omega_n^2$ and *(1.8)* denotes (τ) as in $(s+\tau)$.

HAVE PILOT TEST CARD

CASE #	Itera-tion #	Sortie #	Longitudinal		Lateral		Pilot	Date	Filename
			ζ_{sp}	τ_e	T_R	τ_e			

PRE-BRIEF

All test points start at 15,000 feet MSL, 250 KIAS

The pilot will perform each task using any pilot compensation necessary to minimize the average tracking task error.

DESIRED: PIO tendencies do not compromise tracking task. Commanded attitude maintained within 0.5 degrees in pitch and 5 degrees in bank (measured at end of command bar) for 50% of the task except immediately following step command changes.

ADEQUATE: Commanded attitude maintained within 1 degree in pitch and 10 degrees in bank (measured at end of command bar) for 50% of the task except immediately following step command change.

POST-BRIEF

	C-H Rating	PIO Rating
1. Assign PIO rating		

2. Assign Cooper-Harper rating

3. Aircraft response to input (pitch/roll)
   Initial - Quick, Slow, Sluggish, etc
   Final - Predictable, Crisp, etc

4. Does the level of aggressiveness affect task performance (precision, accuracy, etc)?

5. Any special piloting techniques/compensation required?

6. Any undesirable aircraft motions (turbulence, disorienting)?

7. Provide actual percentage performance to pilot	Turb Rating	% in Desired	% in Adequate	C-H Re-Rating
8. Review Cooper-Harper rating				

Figure C-3. Test Point Comment Card

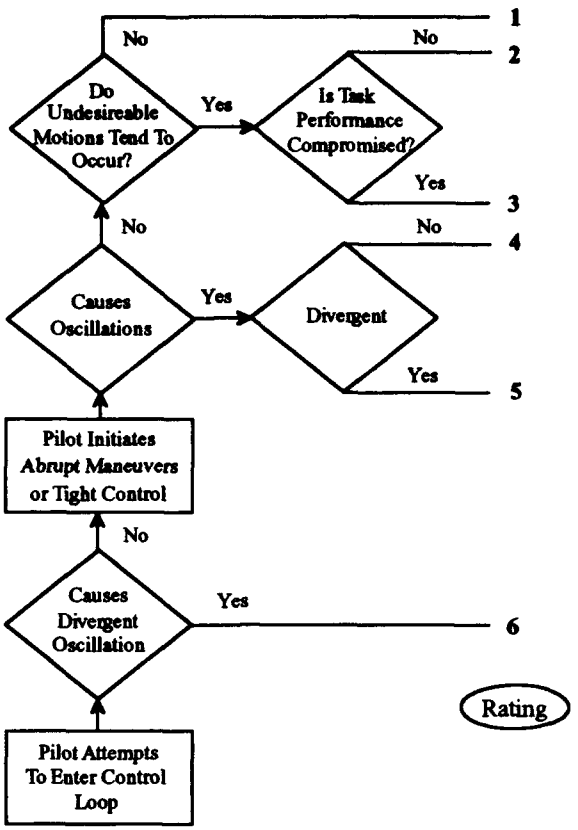

Figure C-4. Calspan Pilot Induced Oscillation Rating Scale

Software Validation Test Case

Figure C-5 presents the magnitude (top plot), phase (middle plot), and coherence (bottom plot) computed by the frequency response analysis software as described in Chapter 4 of this thesis (page 4-10). Each of these is plotted as a function of frequency. Individual data points are represented by asterisks. The dotted lines represent 95 percent confidence interval bounds (7:55).

Figure C-6 presents the Bode plot found using the frequency response analysis software along with the actual Bode plot of the linear system. Except for the lowest frequency phase point, the two plots are nearly identical.

Random Noise Simulation of: $\frac{(s+2)e^{-0.25s}}{(s+5)\cdot(s+.2)}$

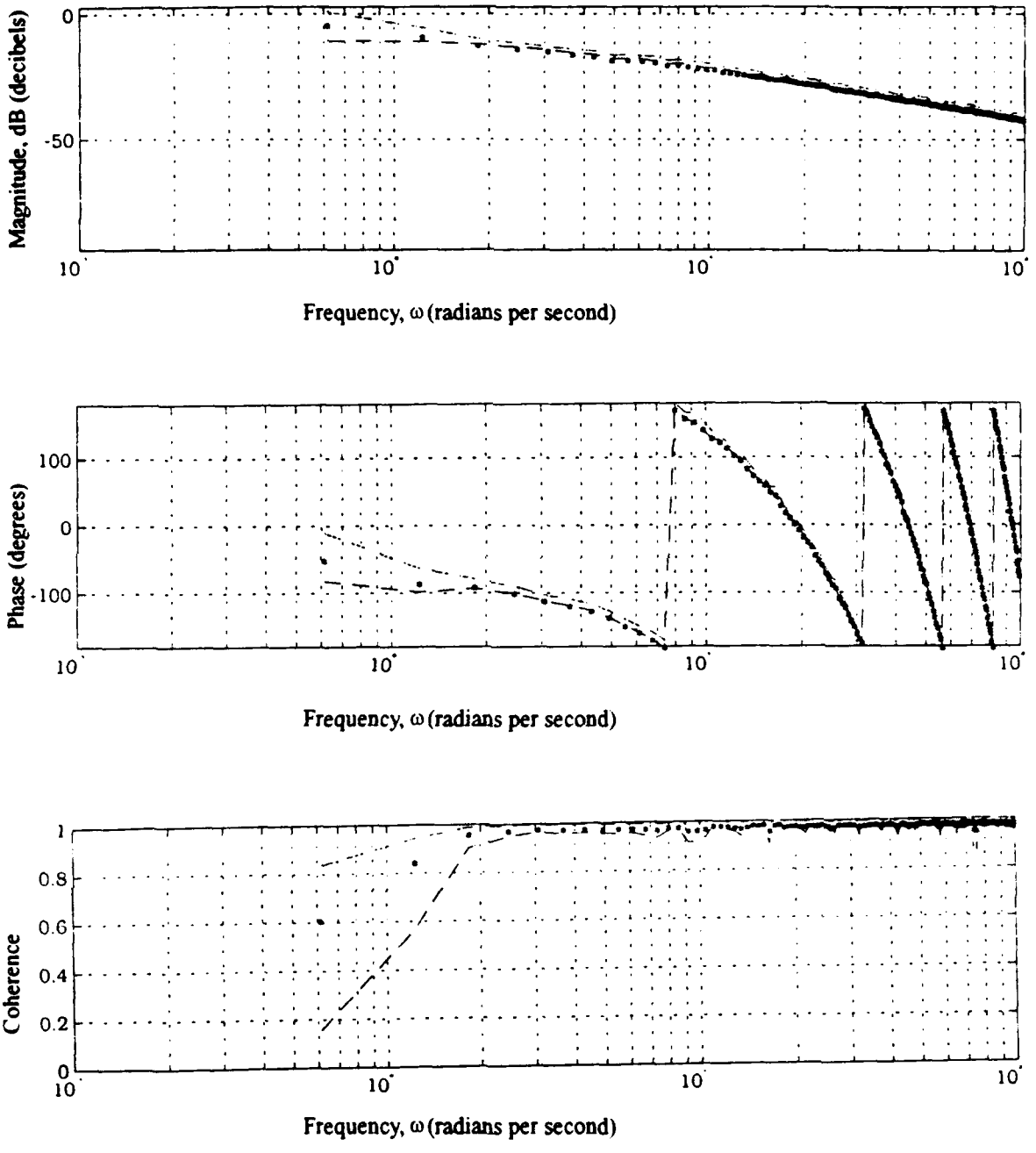

Figure C-5. Frequency Response Analysis -- Validation Case

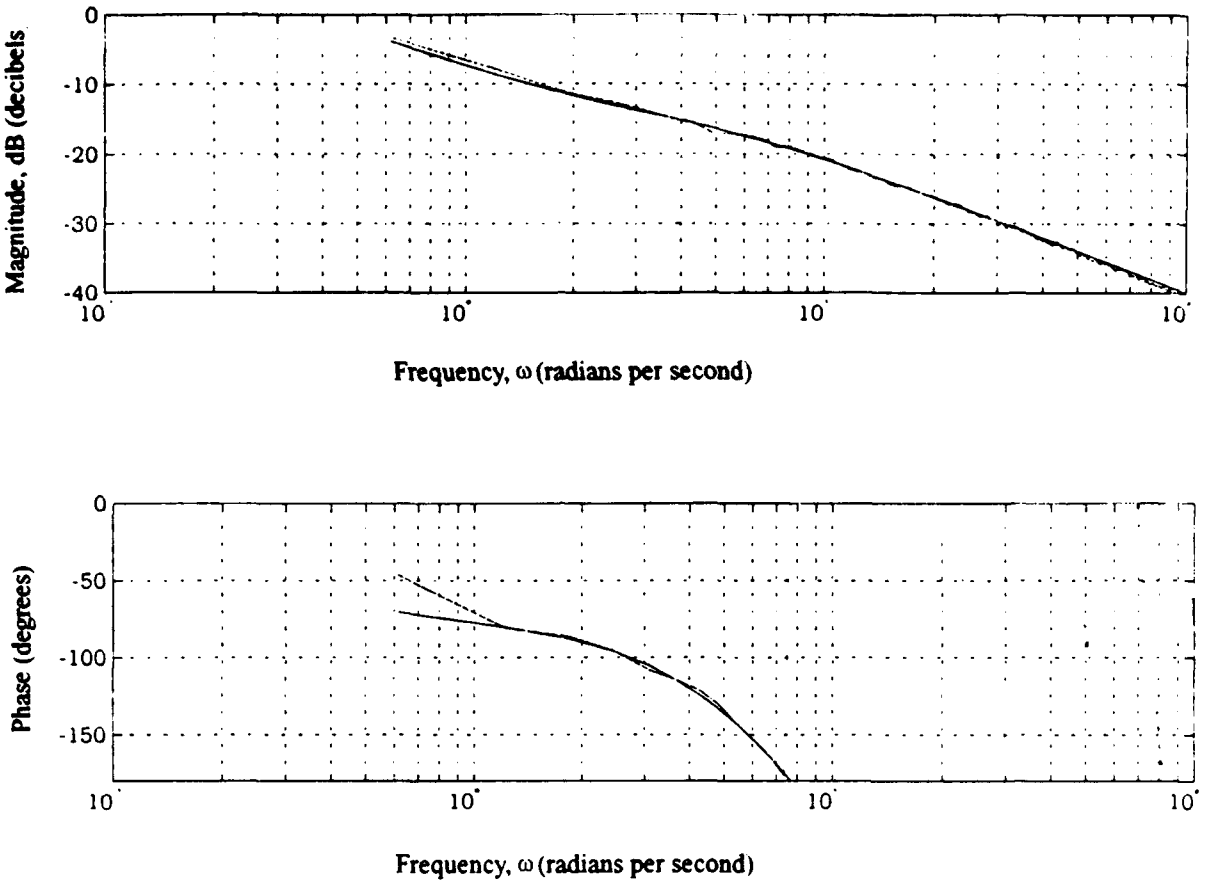

Figure C-6. Bode Comparison Plot -- Validation Case

Cooper-Harper Ratings and Pilot Comments

The Cooper-Harper ratings and pilot comments for the ground and airborne evaluations are summarized in Tables C-1 and C-2. Only the single axis, sum-of-sines evaluations from AFFTC-TLR-93-41 were analyzed in this thesis (7:73-107).

Table C-1
Cooper-Harper Ratings and Pilot Comments -- Ground Simulation

Case	Iteration (sortie)	PIO Rating	C-H Rating	Percent Desired	Percent Adequate	Comments[1]
1	1(1)	1	2	49	90	Good response in the pich axis. I didn't have to be overly aggressive.
1	2(3)	1	3	52	91	A little slow in pitch. The more aggresive I got the better I could track.
2	1(2)	2	4	54	86	Satisfactory. Initial respone was quick. Tendecny to overshoot.
2	2(3)	2	3	39	76	Easy to acquire. Couple of overshoots. Slightly sensitive. Maybe too quick.
3	1(1)	3	5	43	82	Large inputs required. Slight PIO. A little sensitive. Lead required.
3	2(6)	2	4	39	81	Slow initial response. Sluggish. Moderate compensation required.
4	1(1)	4	6	44	72	Large inputs required. PIO Tendency. Have to come out of the loop.
4	2(5)	2	4(5)	35	68	Undesireable motions. Slow. Tend to overshoot. Unpredictable. Required lead.
A	1(2)	1	1	80	99	Quick. Predictable. Fairly aggressive. Pilot compensation not a factor.
A	2(3)	2	2	88	99	Slow response. Easy to reacquire. No undesirable motions. Comp. nota factor.
B	1(4)	1	2	82	100	Initial input was good. No tendency to overshoot. Work load not too high.
B	2(5)	1	2	75	98	Quick. Predictable. Could be fairly aggressive. Stayed in the loop.
C	1(5)	2	4	63	91	Need to back out a little. Not slow, but not predictable. Slight ocillatory motion.
C	2(6)	2	3	77	99	Overshoots. A little compensation required. Tend to back out of loop. Slow.
D	1(2)	3	5	61	87	Sluggish. Tendency to overshoot. Large lead input required. Backed out of loop.
D	2(4)	2	3	77	96	Tendency to overshoot. Work load tolerable. Little oscillation, but not obj.

[1] These comments were summarized from AFFTC-TLR-93-41 (7:83-90).

Table C-2
Cooper-Harper Ratings and Pilot Comments -- Airborne Evaluation

Case	Iteration (sortie)	PIO Rating	C-H Rating	Percent Desired	Percent Adequate	Comments[1]
1	1(1)	1	2	67	98	Predictable. No PIO tendency. Good initial response. No real comp. used.
1	2(2)	2	3	68	97	Backed out of the loop to prevent oscillation tendencies.
1	3(5)	1	2	69	96	Good initial response. Slight bobble but negligible deficiencies.
2	1(1)	1	1	53	93	Didn't push as hard as I did on the ground.
2	2(2)	1	2	63	98	No PIO tendency. Compensation not a factor. Backed out a little bit.
2	3(5)	1	2	70	97	Good initial response. A little bobble. Don't have to be aggressive at all.
3	1(1)	4	5	45	86	Oscillatory tendency. Need to come out of the loop. PIO tendency. Unpredictable.
3	2(2)	4	5	48	97	Can track fairly aggressively. Moderately objectionable. Slow initial response.
3	3(5)	2	3	62	98	No tendency to oscillate. Lagging with my inputs. Initial response a bit slow.
4	1(1)	4	4	47	89	PIO tendency. Can't be too aggressive. Light on the controls. High worload.
4	2(2)	2	4	48	80	Oscillatory especilally when aggressive. Less than predictable. Tend to overshoot.
4	3(5)	3	5	41	76	Tend to overshoot. Tend to back out a little bit. Osillations. Not predictable.

[1] These comments were summarized from AFFTC-TLR-93-41 (7:83-90).

Table C-2 (Continued)
Cooper-Harper Ratings and Pilot Comments -- Airborne Evaluation

Case	Iteration (sortie)	PIO Rating	C-H Rating	Percent Desired	Percent Adequate	Comments[1]
A	1(1)	1	1	91	100	No tendency to overshoot. Predictable response. Like the way it handled.
A	2(2)	1	3	86	99	Fine tracking is simple. No oscillation at all. Response predictable.
A	3(5)	1	1	95	99	Can make prety quick inputs. Quick. Predictable. No compensation. required.
B	1(1)	1	2	86	99	Initial response OK. Put in big input then take it out. Anticipation required.
B	2(2)	2	4	82	99	Fine tracking not a problem. Slight oscillatory tendency. Lacks predictability.
B	3(5)	1	2	90	99	Response initially good. Easy to track target. Nice handling aircraft.
C	1(1)	2	3	74	100	If too aggressive, get more oscillations. Response is sluggish and unpredictable.
C	2(2)	2	4	79	99	Can't be real aggressive in fine tracking. Slight delay.
C	3(5)	2	4	79	99	Fine tracking not too bad. Tendency to over-control with large inputs.
D	1(1)	4	6	62	93	Had to back out of the loop. Required lots of lead.
D	2(2)	4	7	71	98	Practically flying this open loop. Initial response was slow. Overshoot tendency.
D	3(5)	3	4	77	98	Large lead input required. Oscillations. Came out of the loop. High work load.

[1] These comments were summarized from AFFTC-TLR-93-41 (7:83-90).

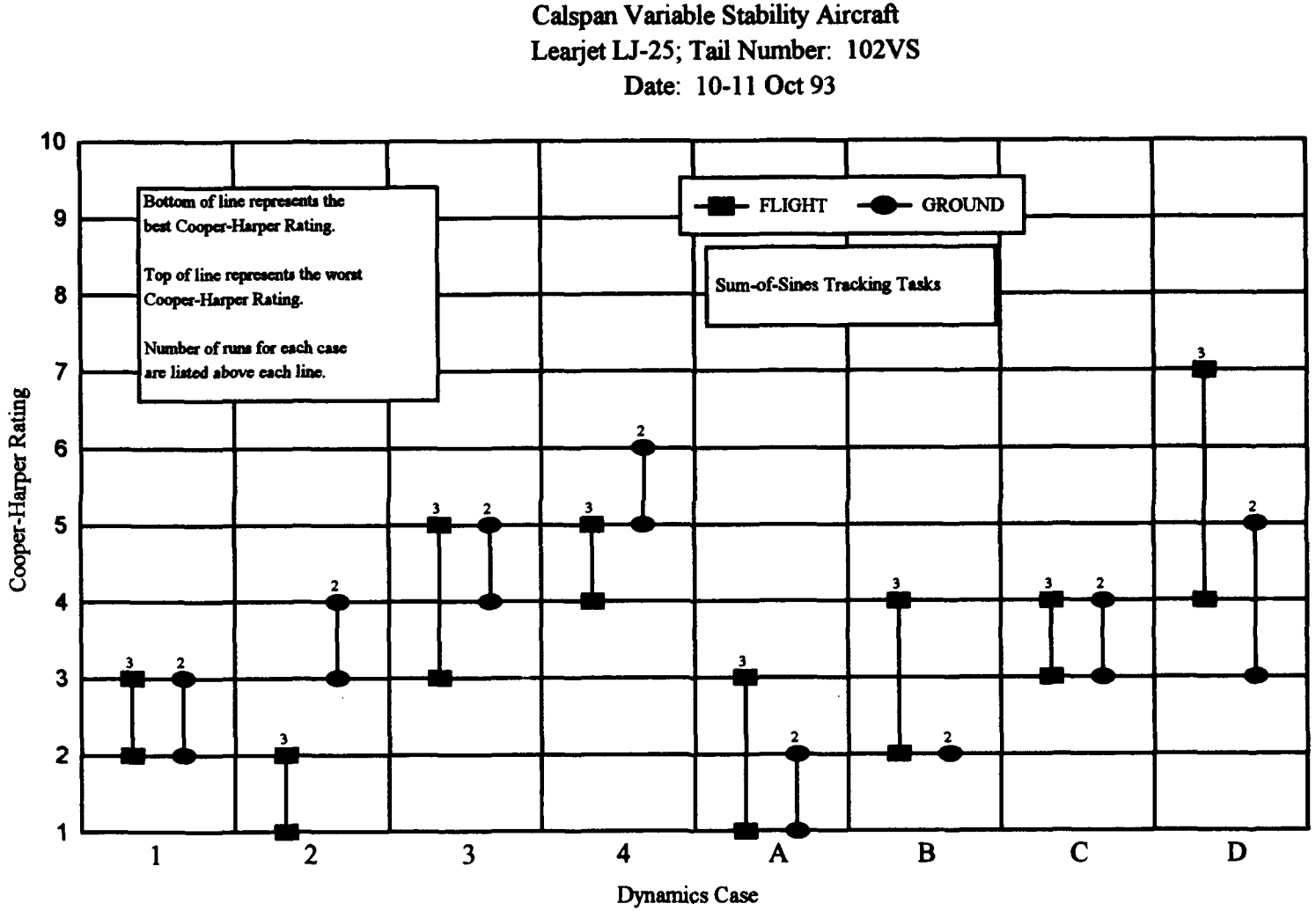

Figure C-7. Cooper-Harper Ratings

Statistical Analysis

The statistics in Tables C-3 and C-4 were computed using the flight test data base produced by AFFTC-TLR-93-41 and are summarized in Table 4-2. Only the single axis sum-of-sines data were analyzed for this thesis.

Table C-3
Optimal Pilot Model Statistical Analysis Parameters
-- Ground Simulation Single Axis Sum-of-Sines Data

Case	Sortie #	C-H Rating	RMS Error	NRMS Stick	RMS Stick Rate
1	3	3	0.5894	0.3306	0.6290
2	2	4	0.6738	0.3654	0.6853
2	3	3	0.7911	0.3374	0.5088
3	1	5	0.7506	0.3478	1.1005
3	6	4	0.7242	0.3902	0.8480
4	1	6	0.8765	0.3910	1.2988
4	5	5	0.9031	0.4135	1.0112
A	2	1	3.9868	0.3490	1.1969
A	3	2	3.1897	0.3752	1.1342
A	7	2	3.4809	0.3727	1.1294
B	4	2	3.5883	0.2947	1.0995
B	5	2	4.2318	0.3069	1.0815
C	5	4	5.4722	0.4556	1.7275
C	6	3	3.7028	0.4496	1.3451
D	2	5	6.2632	0.4538	1.4944
D	4	3	4.7876	0.3127	1.1310

where:

$$RMS(x) = \sqrt{\frac{\Sigma |x|^2}{n}} \qquad \text{(C-7)}$$

and n is the number of samples in the vector, x.

Table C-4
Optimal Pilot Model Statistical Analysis Parameters
-- Airborne Single Axis Sum-of-Sines Data

Case	Sortie #	C-H Rating	RMS Error	NRMS Stick	RMS Stick Rate
1	1	2	0.4649	0.3590	0.6647
1	2	3	0.4633	0.3931	0.6542
1	5	2	0.4694	0.3693	0.7803
2	1	1	0.6112	0.3097	0.7035
2	2	2	0.4996	0.3364	0.7024
2	5	2	0.4462	0.3546	0.6393
3	1	5	0.6715	0.3770	1.0363
3	2	5	0.6702	0.3739	0.7804
3	5	3	0.5123	0.3535	0.8920
4	1	4	0.6421	0.3626	0.8406
4	2	4	0.7262	0.3887	1.0014
4	5	5	0.8272	0.3697	1.0555
A	1	1	3.0050	0.4416	1.6112
A	2	3	3.5325	0.5116	2.1329
A	5	1	2.8450	0.4035	1.8860
B	1	2	3.2138	0.4057	2.0166
B	2	4	3.4165	0.3929	1.8709
B	5	2	2.9061	0.3533	1.8516
C	1	4	3.8592	0.7353	3.0660
C	2	4	3.8756	0.6058	2.3255
C	5	4	3.6456	0.5488	2.5740
D	1	6	5.7705	0.6105	2.4467
D	2	7	4.4030	0.5779	2.2287
D	5	4	4.0556	0.4792	2.3097

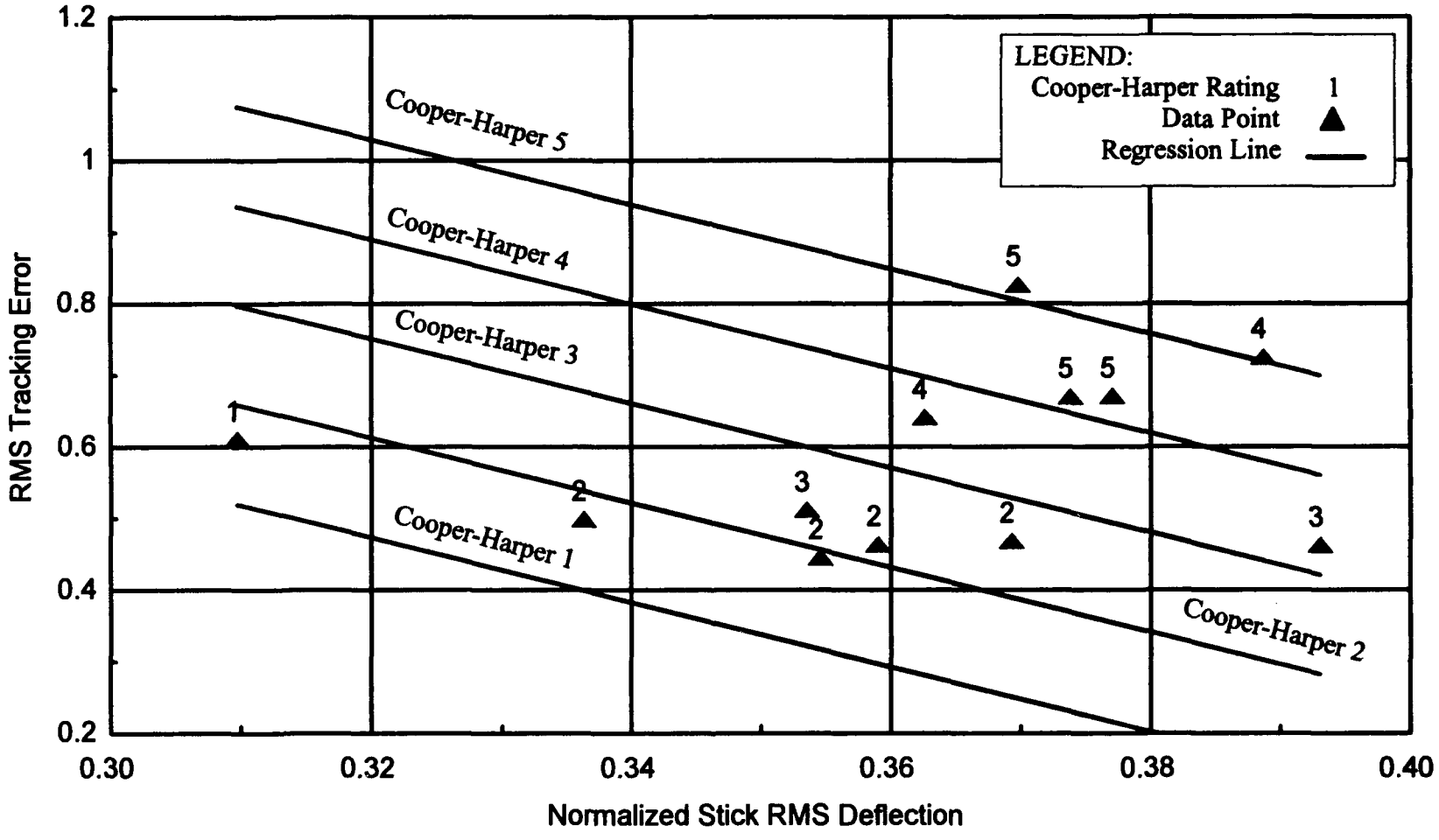

Figure C-8. Optimal Pilot Model Weightings -- Pitch Axis

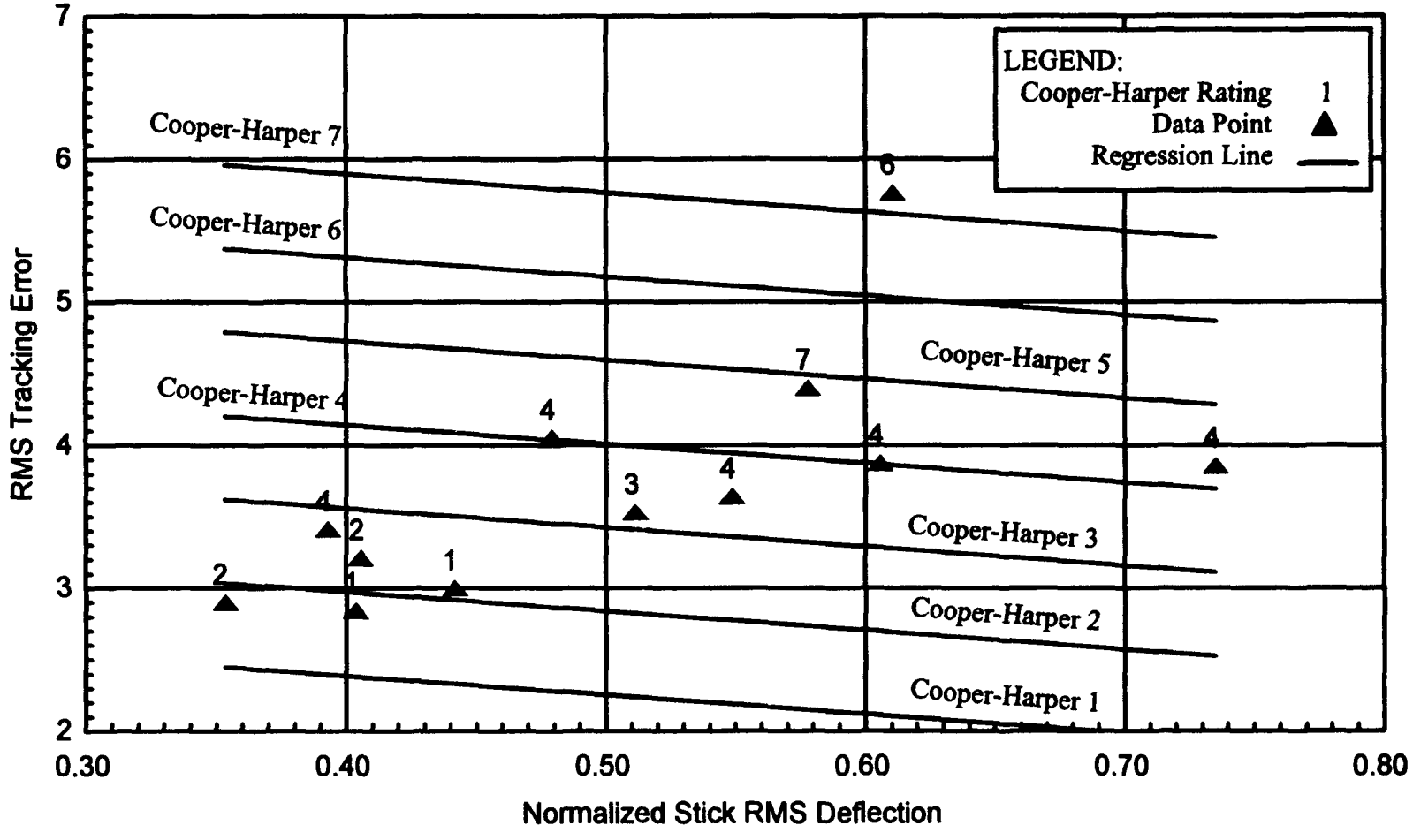

Figure C-9. Optimal Pilot Model Weightings -- Roll Axis

Pilot Model Analysis

The dynamics simulated for the flight test were evaluated using the applicable MIL-STD-1797A models and the STI optimal pilot model. The parameters given in Table C-5 were used when running the optimal pilot model.

Table C-5
Optimal Pilot Model Parameters -- Flight Test Analysis

Forcing Function, Y_w (at Aircraft Output)	$\frac{\sqrt{2}}{6.25s^2+3.54s+1}$	Motor Noise Ratio, ρ_{ua}	-20 dB
Neuro-Muscular Time Constant, T_n	0.08	Visual Indifference Thresholds, T_{y1}, T_{y2}	0
Pilot Delay, τ_p	0.25 seconds	Fractional Attention Parameter, f	1
Observation Noise Ratios, ρ_{y1} ρ_{y2}	-20 dL	Driving Noise Intensity, V_w	1

The results of this analysis are presented in Tables C-6 and C-7. Bode plots of the pilot describing functions predicted by the STI optimal pilot model for Cases 1 and 4 are shown in Figures C-10 and C-12. Bode plots of the resulting pilot-aircraft systems are shown in Figures C-11 and C-13.

Table C-6
Pitch Axis Pilot Model Predictions -- Flight Test Dynamics

Case	ζ[1]	τ_D[2]	C-H[3] Rating	CAP[4]	SP[5]	TRP[6]	BW[7] Criterion	Neal-Smith Criteria	Gibson's Criteria	OPM[8]
1	.7	.04	2-3	I	II	I	II	II	Abrupt Bobbling Tendency	3.4
2	.4	.04	1-2	I	I	I	I-II	II	Abrupt Bobbling Tendency	3.8
3	.7	.24	3-5	III	III	III	III	III	Satisfactory Response	4.3
4	.4	.24	4-5	III	III	III	III	III	Satisfactory Response	4.5

[1]Short Period Damping Ratio
[2]System Delay
[3]Cooper-Harper Ratings from Flight Test Data
[4]Control Anticipation Parameter Criterion
[5]Short Period Criterion
[6]Transient Response Parameter
[7]Bandwidth Criterion
[8]Optimal Pilot Model Rating Prediction

Table C-7
Roll Axis Pilot Model Predictions -- Flight Test Dynamics

Case	T_R[1]	τ_D[2]	C-H Rating[3]	Bandwidth Criterion[4]	Roll Constant	Spiral Constant	Delay	Step Response	OPM[5]
A	.4	.04	1-3	2	I	I	I	I	3.8
B	1	.04	2-4	3	I-II	I	I	I	5.3
C	.4	.24	4-5	4	I	I	III	I	5.2
D	1	.24	5-7	5	I-II	I	III	I	10

[1]Roll Mode Time Constant
[2]System Delay
[3]Cooper-Harper Ratings Range from Flight Test Data
[4]Bandwidth Rating is from the Regression Formula in Reference 24
[5]Optimal Pilot Model Rating Prediction

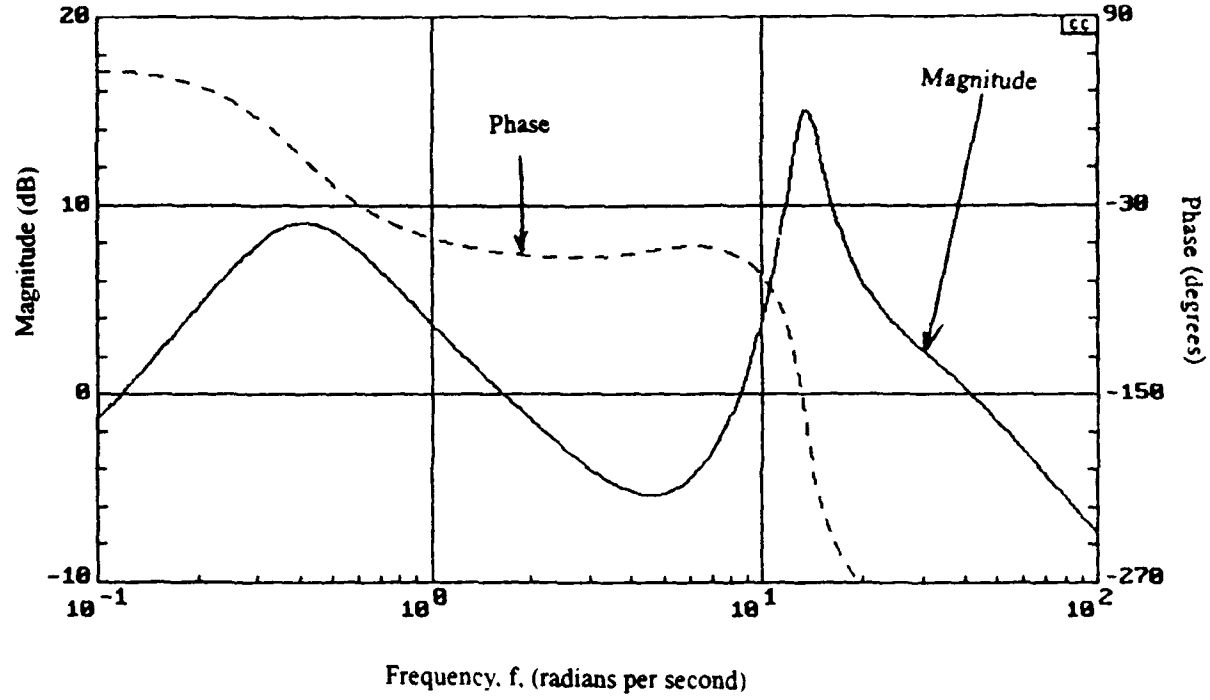

Figure C-10. Bode Plot of Predicted Pilot Transfer Function (Case 1)

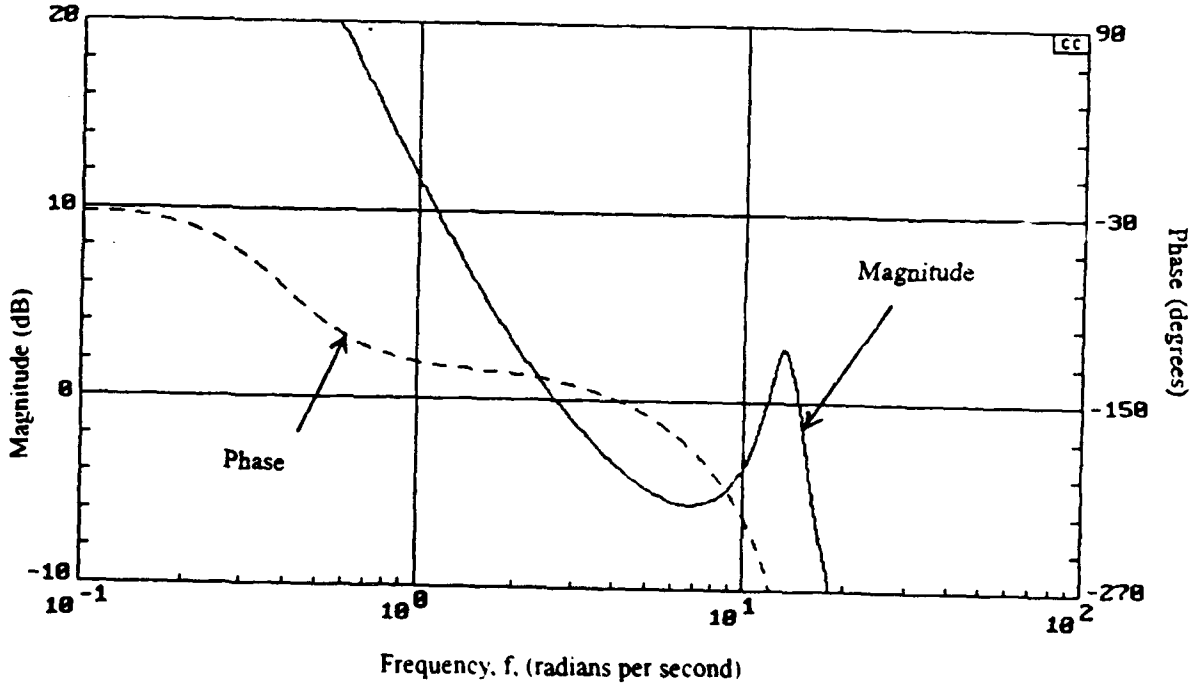

Figure C-11. Bode Plot of Predicted Pilot-Aircraft System (Case 1)

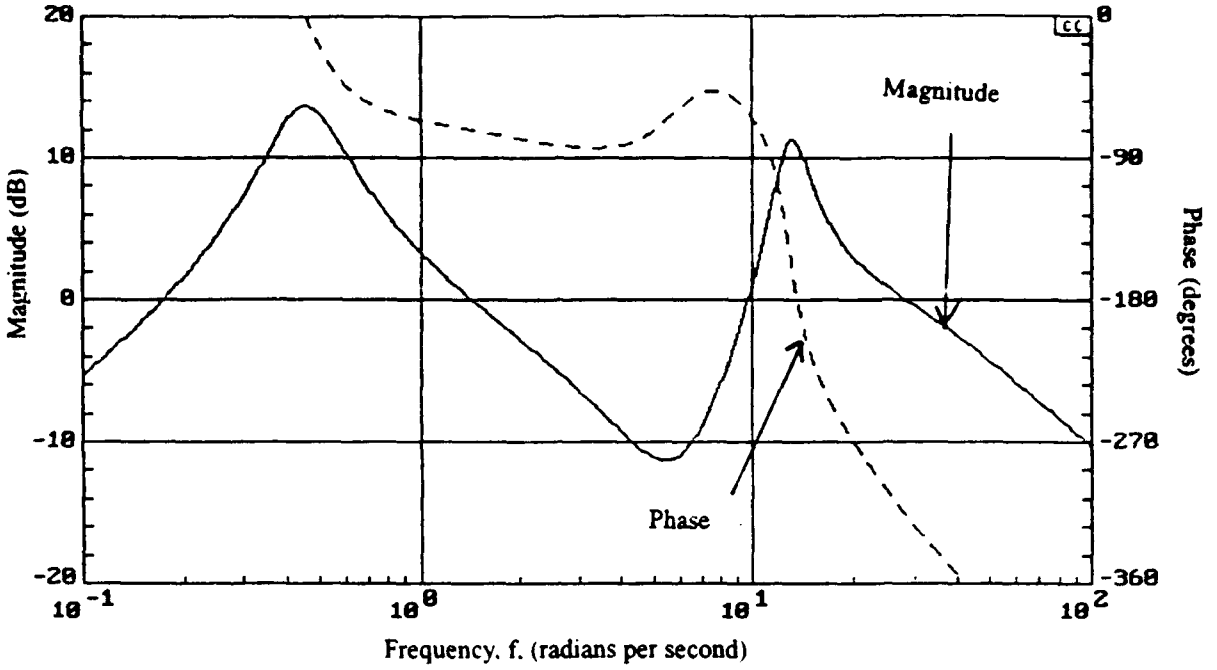

Figure C-12. Bode Plot of Predicted Pilot Transfer Function (Case 4)

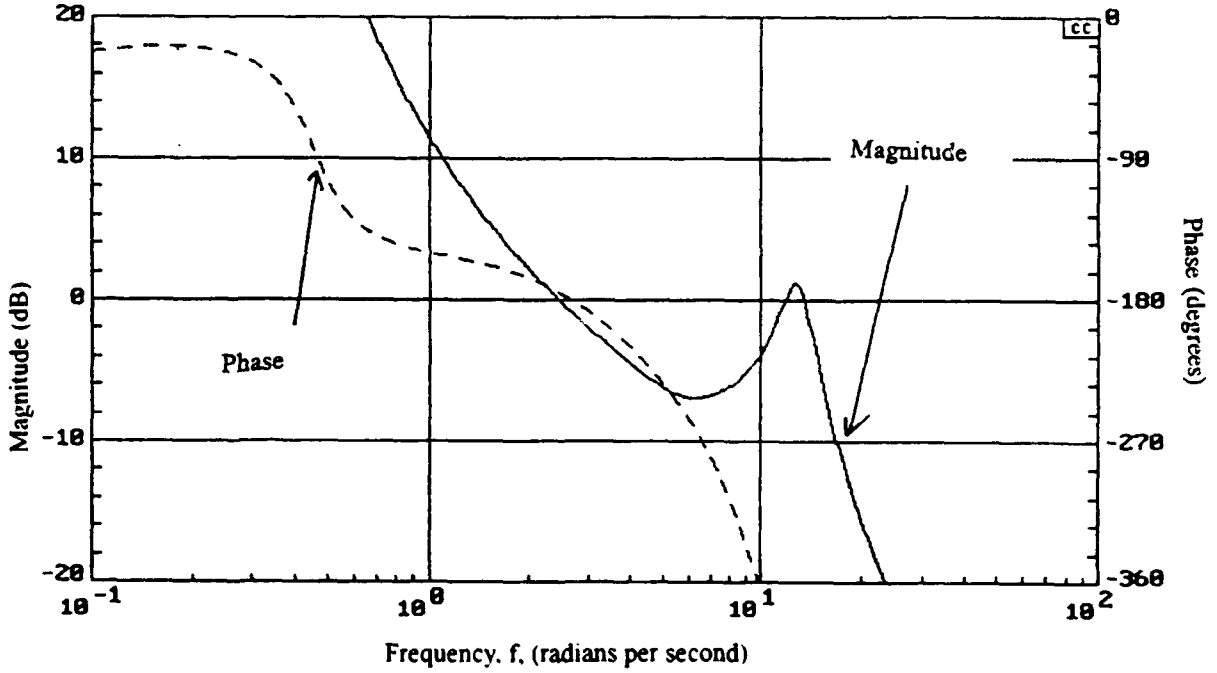

Figure C-13. Bode Plot of Predicted Pilot-Aircraft System (Case 4)

Appendix D. Frequency Response Data

This appendix contains the frequency response analysis plots referred to in Chapter 4. The first two figures display sample power spectral densities. Figures D-3 through D-10 present representative frequency responses of stick displacement to task error for each airborne sum-of-sines cases. In these figures, the top two plots represent the Bode plot of the pilot and the bottom plot presents the coherence as described in Chapter 4. For each of these figures, the data points computed by the frequency response analysis software are represented by asterisks. The dotted lines on the figures represent 95 percent confidence boundaries. Figures D-11 through D-18 present the corresponding Bode plots of the combined pilot-aircraft systems. Finally, Figures D-19 and D-22 are frequency response plots from Case 1 for the command path gain analysis described in Chapter 4.

Calspan Variable Stability Aircraft
Learjet LJ-25, Tail Number N102VS
Date: 9 - 11 Oct 93; Pilot: G; Sortie #1
Sum-of-Sines Tracking Task; Case 4; Airborne Data

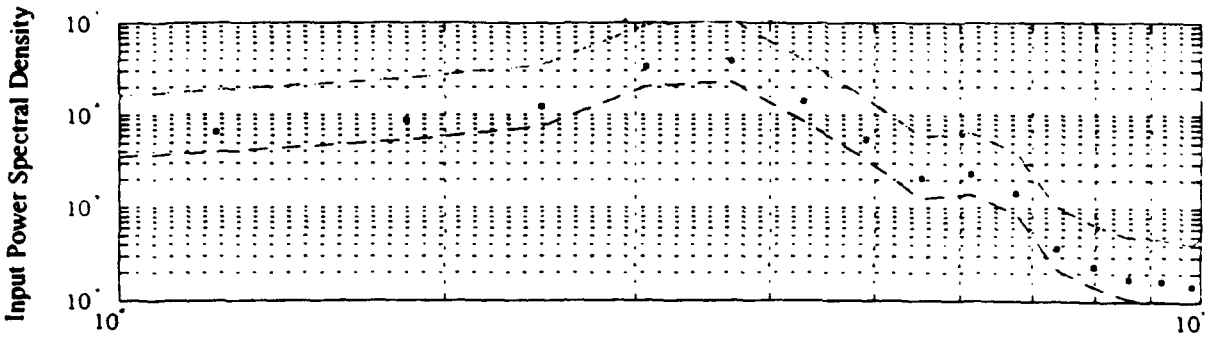

Frequency, ω (radians per second)

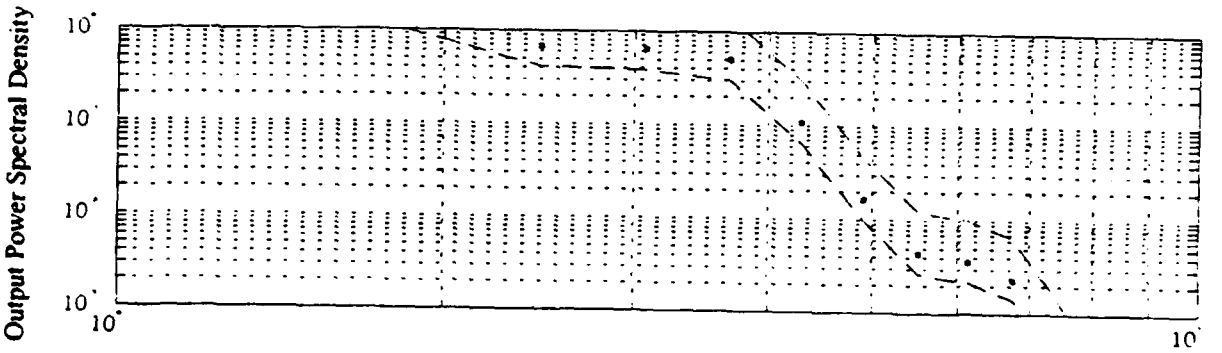

Frequency, ω (radians per second)

Figure D-1. Power Spectral Density -
Longitudinal Stick Deflection to Task Error (Case 4)

Calspan Variable Stability Aircraft
Learjet LJ-25, Tail Number N102VS
Date: 9 - 11 Oct 93; Pilot: E; Sortie #1
Sum-of-Sines Tracking Task; Case D; Airborne Data

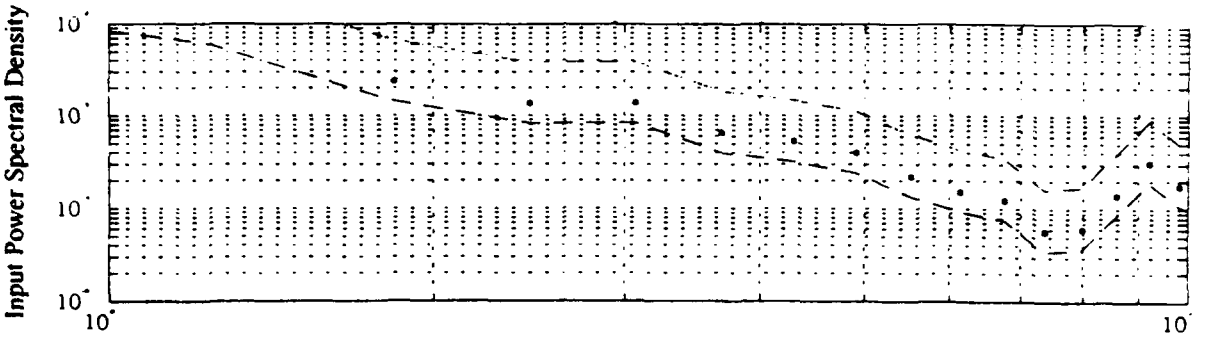

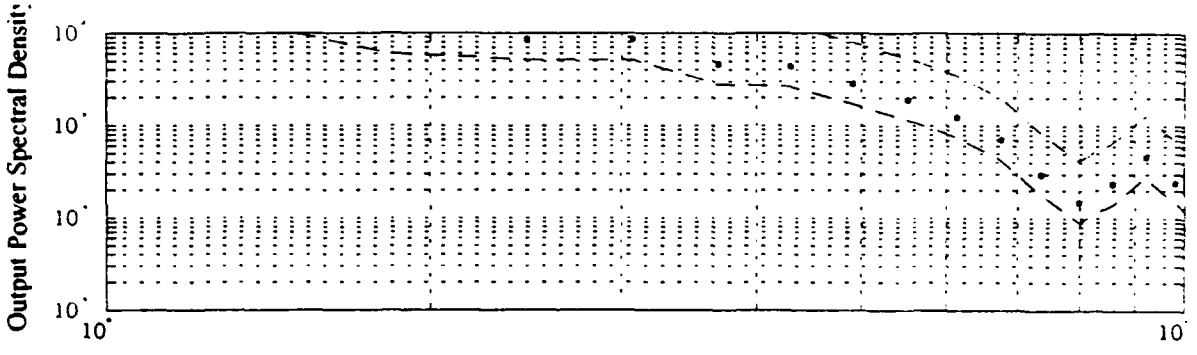

Figure D-2. Power Spectral Density -
Longitudinal Stick Deflection to Task Error (Case D)

Calspan Variable Stability Aircraft
Learjet LJ-25, Tail Number N102VS
Date: 9 - 11 Oct 93; Pilot: G; Sortie #1
Sum-of-Sines Tracking Task; Case 1; Airborne Data

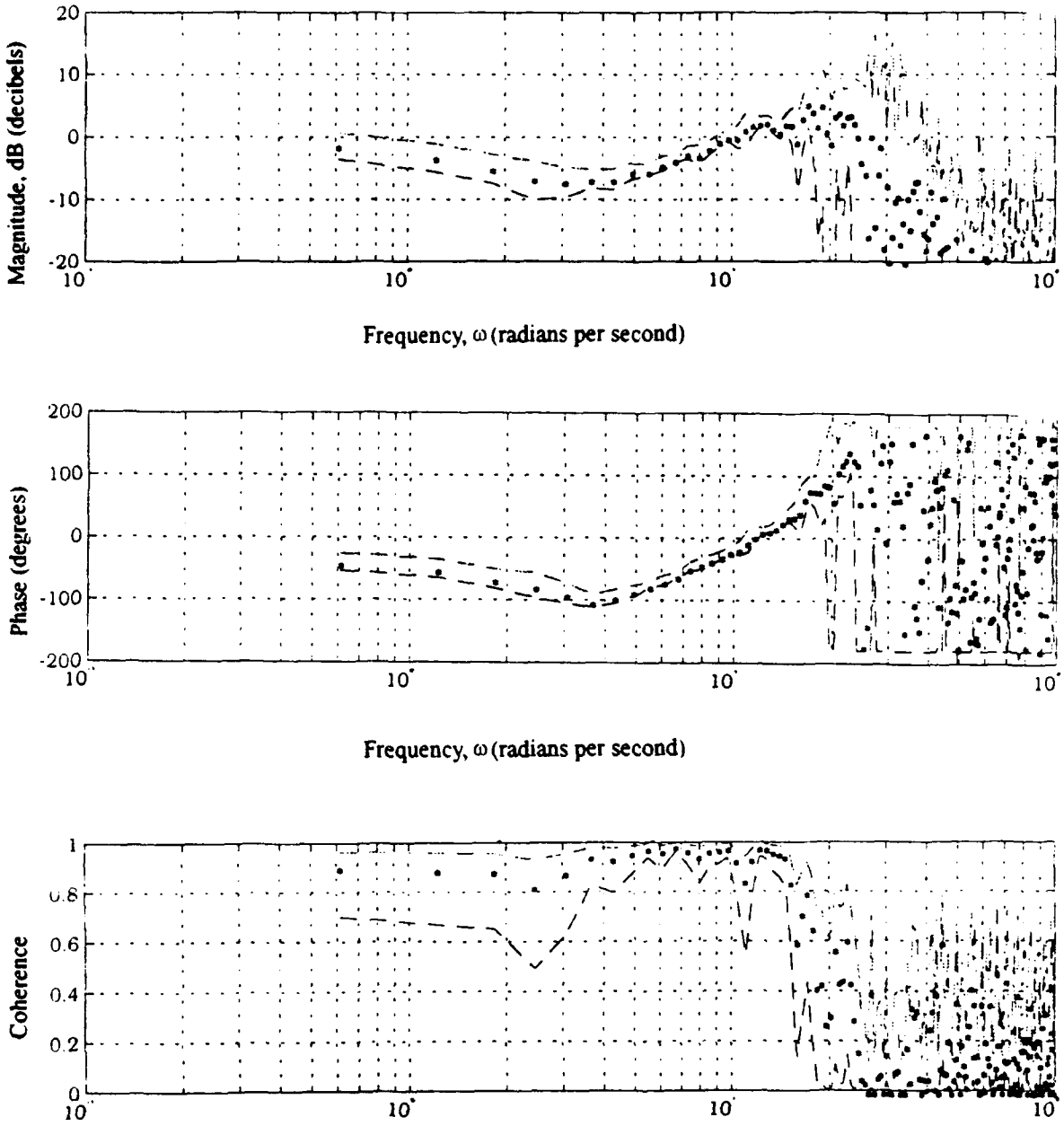

Figure D-3. Frequency Response Analysis -
Longitudinal Stick Deflection to Task Error (Case 1)

Calspan Variable Stability Aircraft
Learjet LJ-25, Tail Number N102VS
Date: 9 - 11 Oct 93; Pilot: S; Sortie #2
Sum-of-Sines Tracking Task; Case 2; Airborne Data

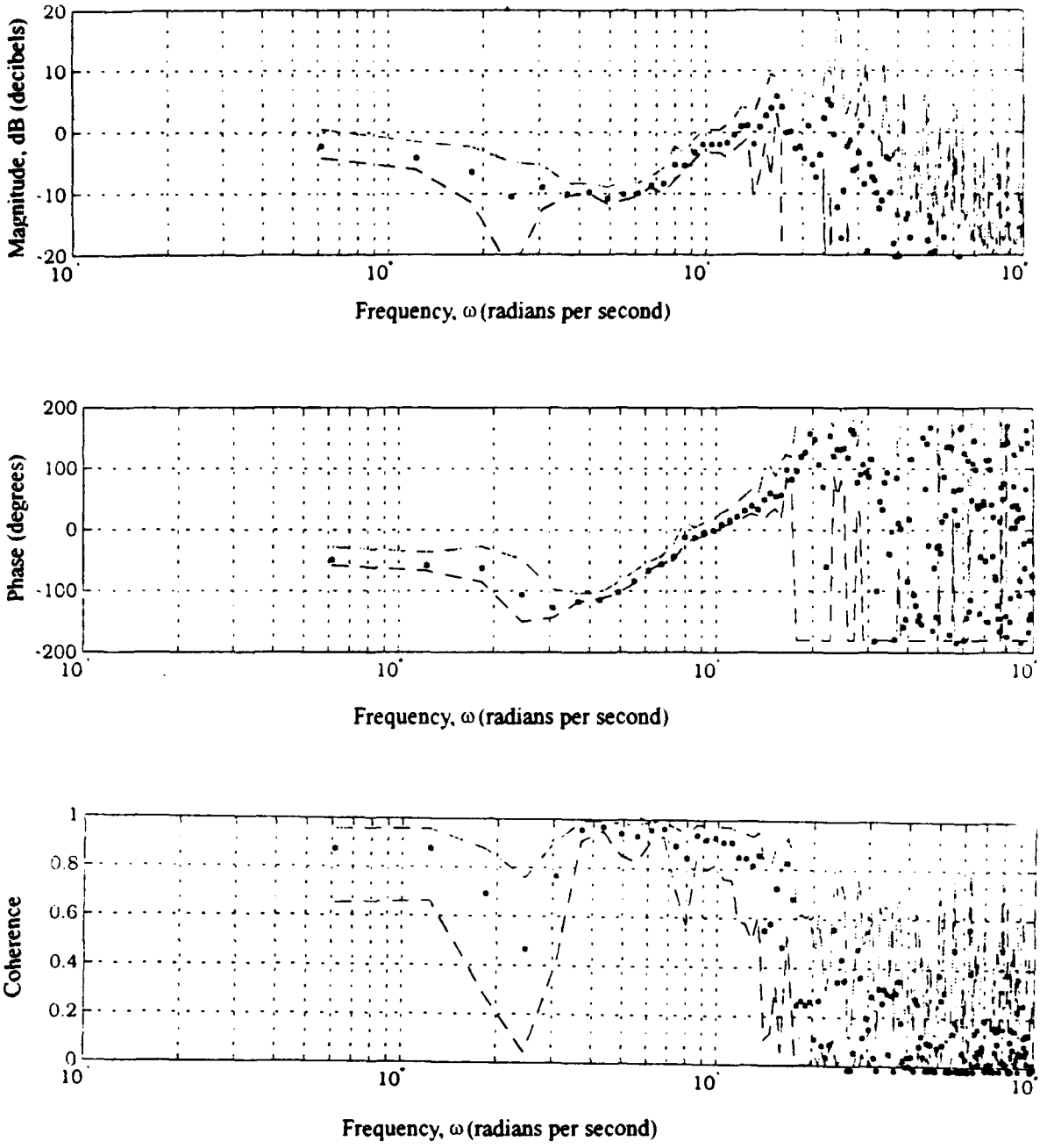

Figure D-4. Frequency Response Analysis -
Longitudinal Stick Deflection to Task Error (Case 2)

Calspan Variable Stability Aircraft
Learjet LJ-25, Tail Number N102VS
Date: 9 - 11 Oct 93; Pilot: S; Sortie #2
Sum-of-Sines Tracking Task; Case 3; Airborne Data

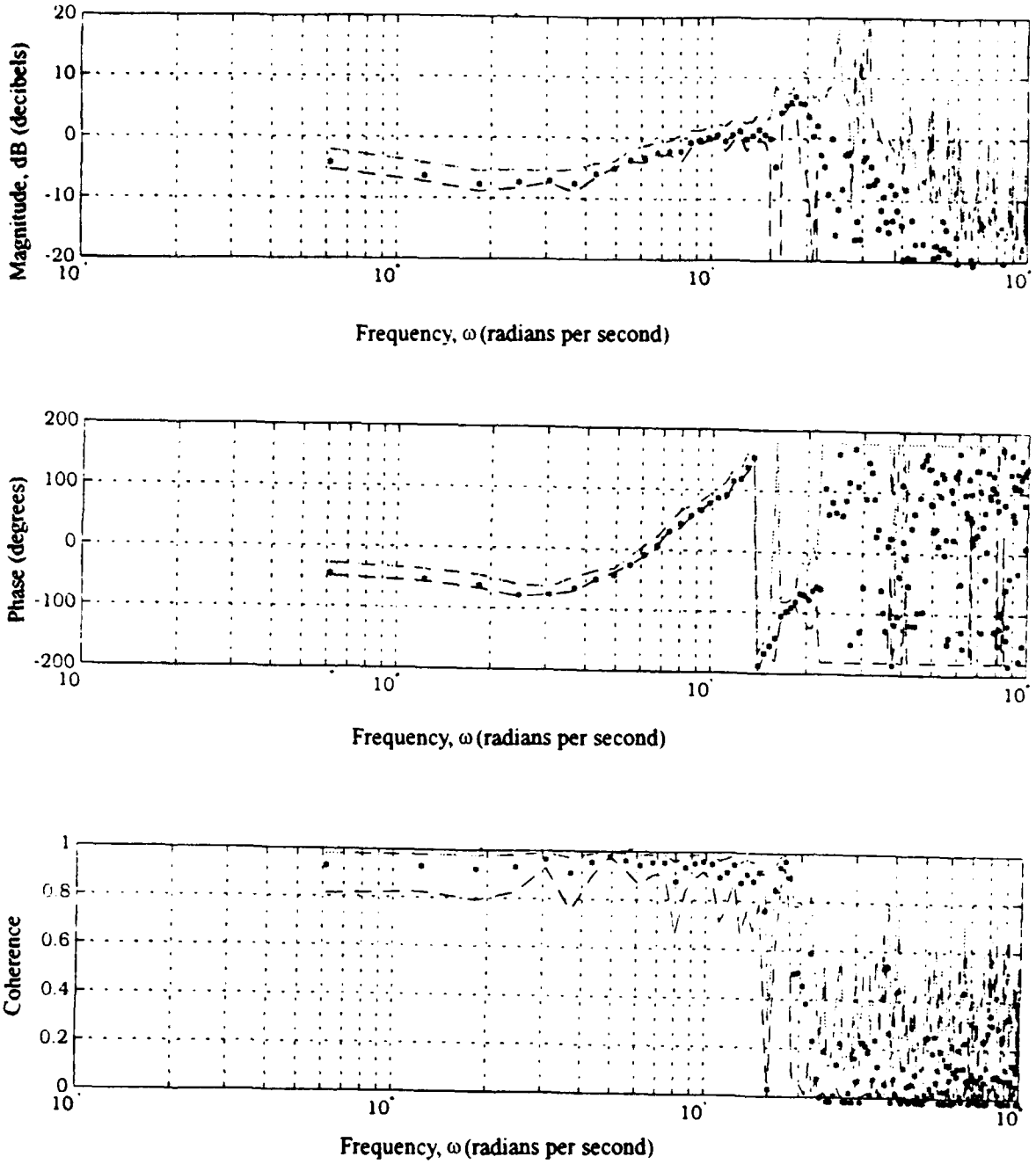

Figure D-5. Frequency Response Analysis -
Longitudinal Stick Deflection to Task Error (Case 3)

Calspan Variable Stability Aircraft
Learjet LJ-25, Tail Number N102VS
Date: 9 - 11 Oct 93; Pilot: G; Sortie #1
Sum-of-Sines Tracking Task; Case 4; Airborne Data

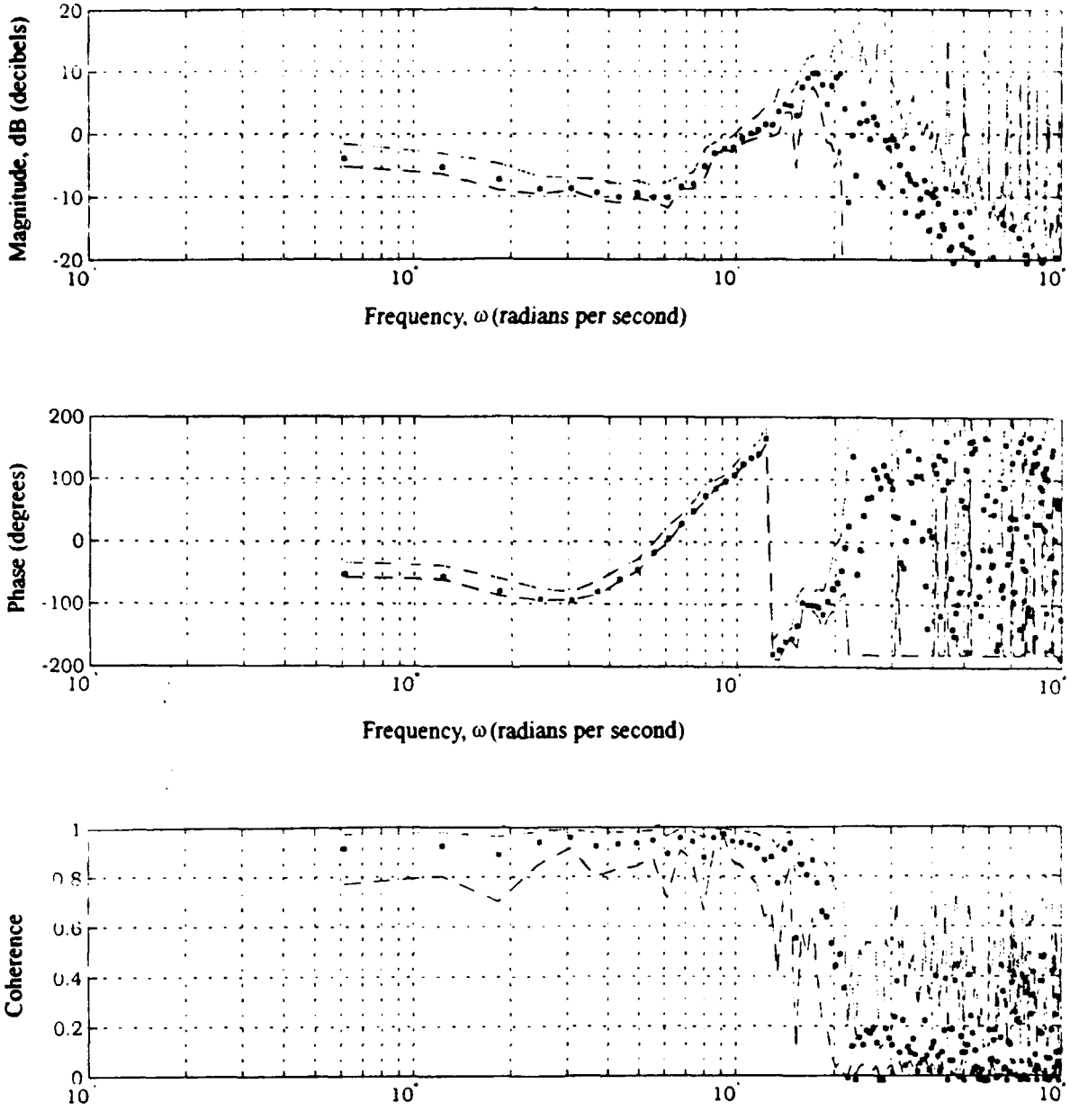

Figure D-6. Frequency Response Analysis -
Longitudinal Stick Deflection to Task Error (Case 4)

Calspan Variable Stability Aircraft
Learjet LJ-25, Tail Number N102VS
Date: 9 - 11 Oct 93; Pilot: E; Sortie #2
Sum-of-Sines Tracking Task; Case A; Airborne Data

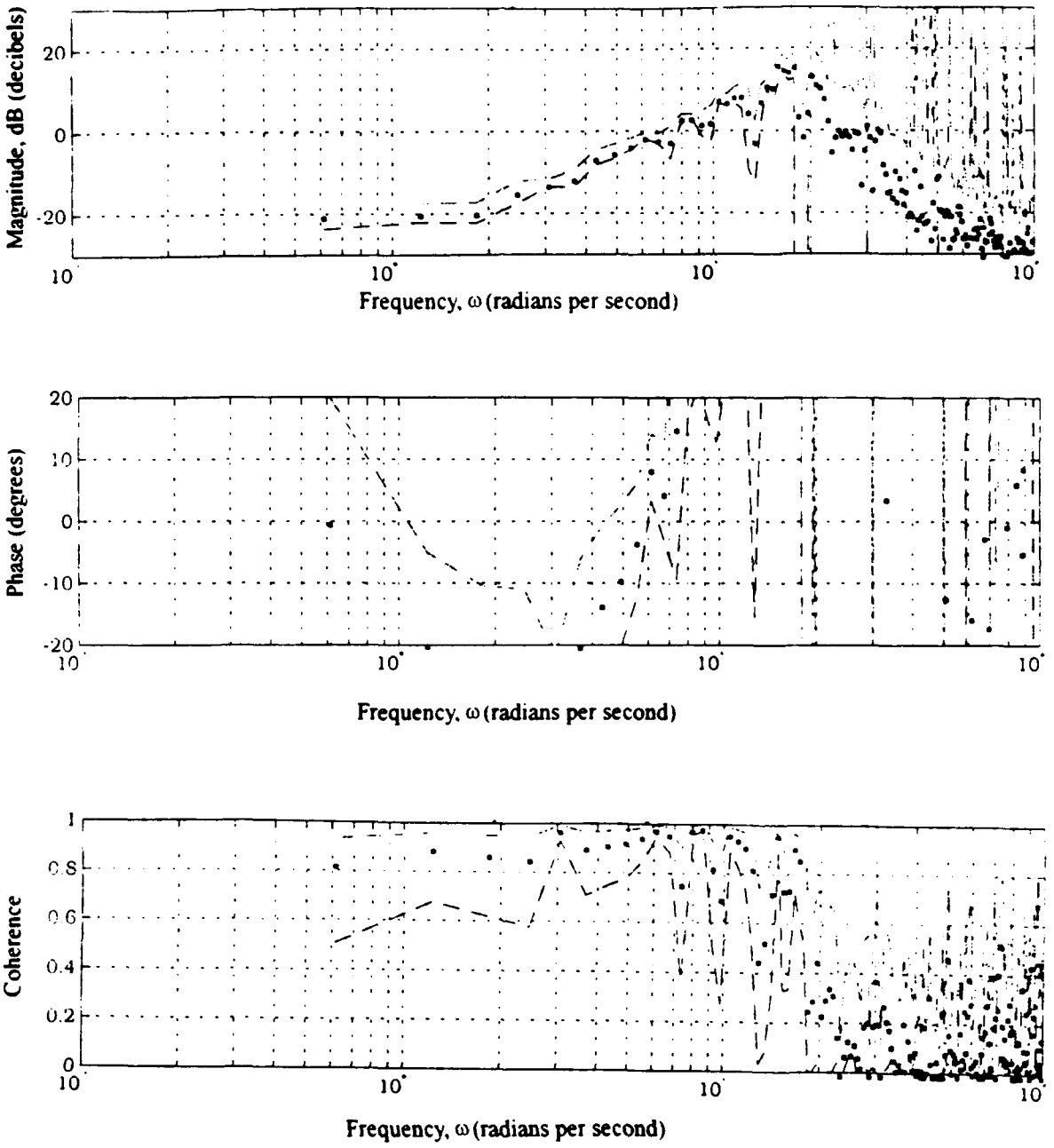

Figure D-7. Frequency Response Analysis -
Longitudinal Stick Deflection to Task Error (Case A)

Calspan Variable Stability Aircraft
Learjet LJ-25, Tail Number N102VS
Date: 9 - 11 Oct 93; Pilot: G; Sortie #5
Sum-of-Sines Tracking Task; Case B; Airborne Data

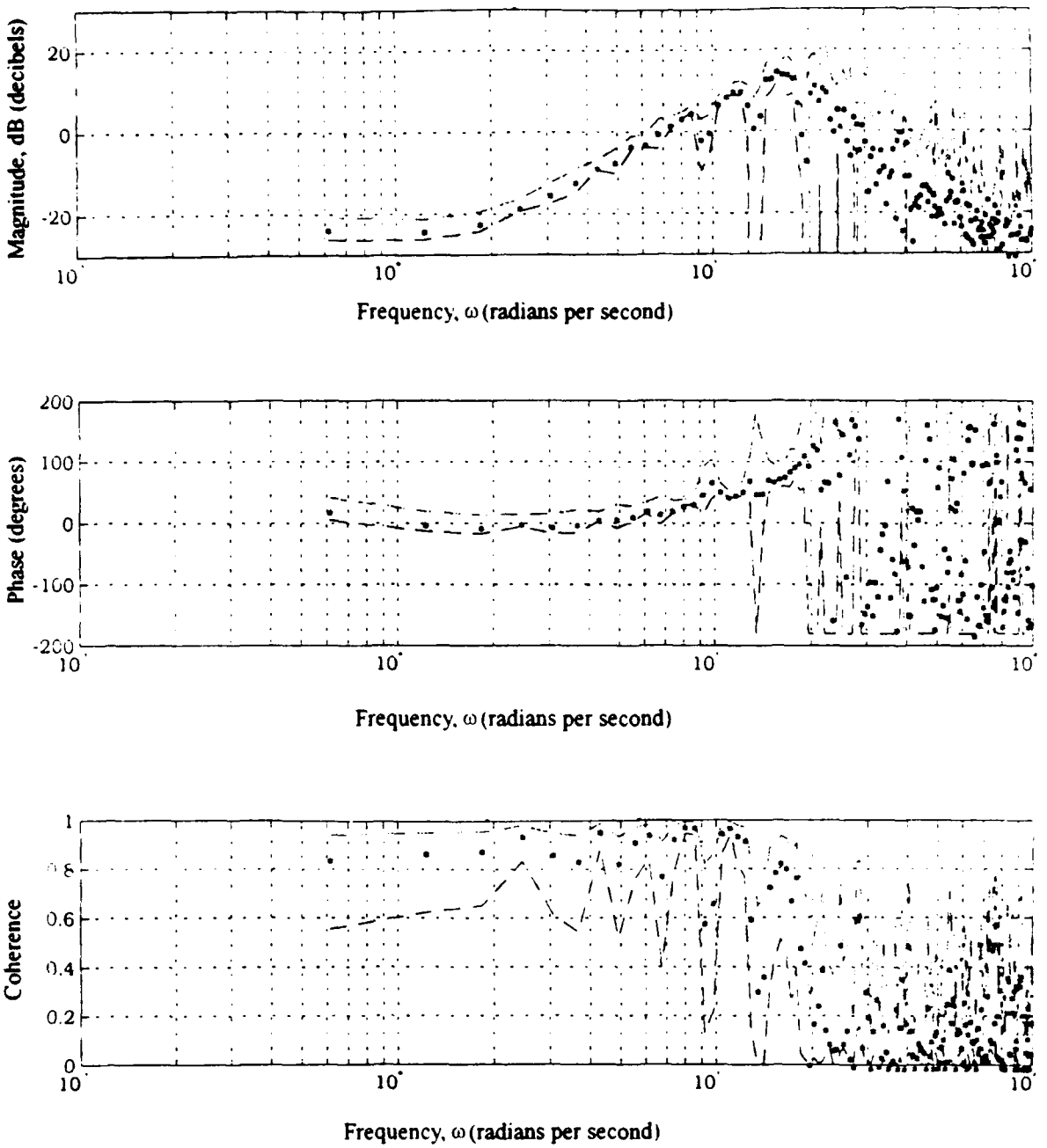

Figure D-8. Frequency Response Analysis -
Longitudinal Stick Deflection to Task Error (Case B)

Calspan Variable Stability Aircraft
Learjet LJ-25, Tail Number N102VS
Date: 9 - 11 Oct 93; Pilot: E; Sortie #2
Sum-of-Sines Tracking Task; Case C; Airborne Data

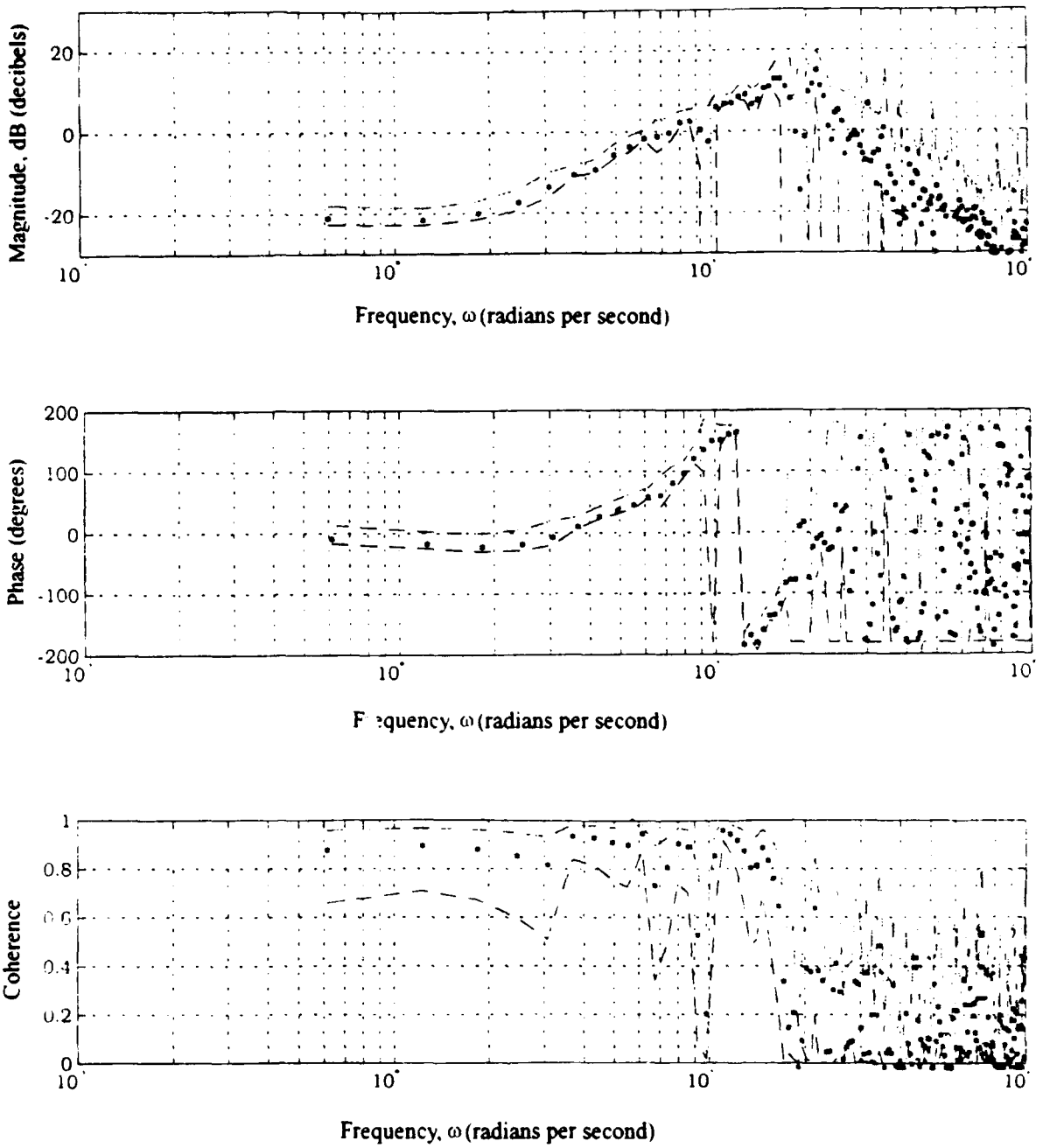

Figure D-9. Frequency Response Analysis -
Longitudinal Stick Deflection to Task Error (Case C)

Calspan Variable Stability Aircraft
Learjet LJ-25, Tail Number N102VS
Date: 9 - 11 Oct 93; Pilot: E; Sortie #1
Sum-of-Sines Tracking Task; Case D; Airborne Data

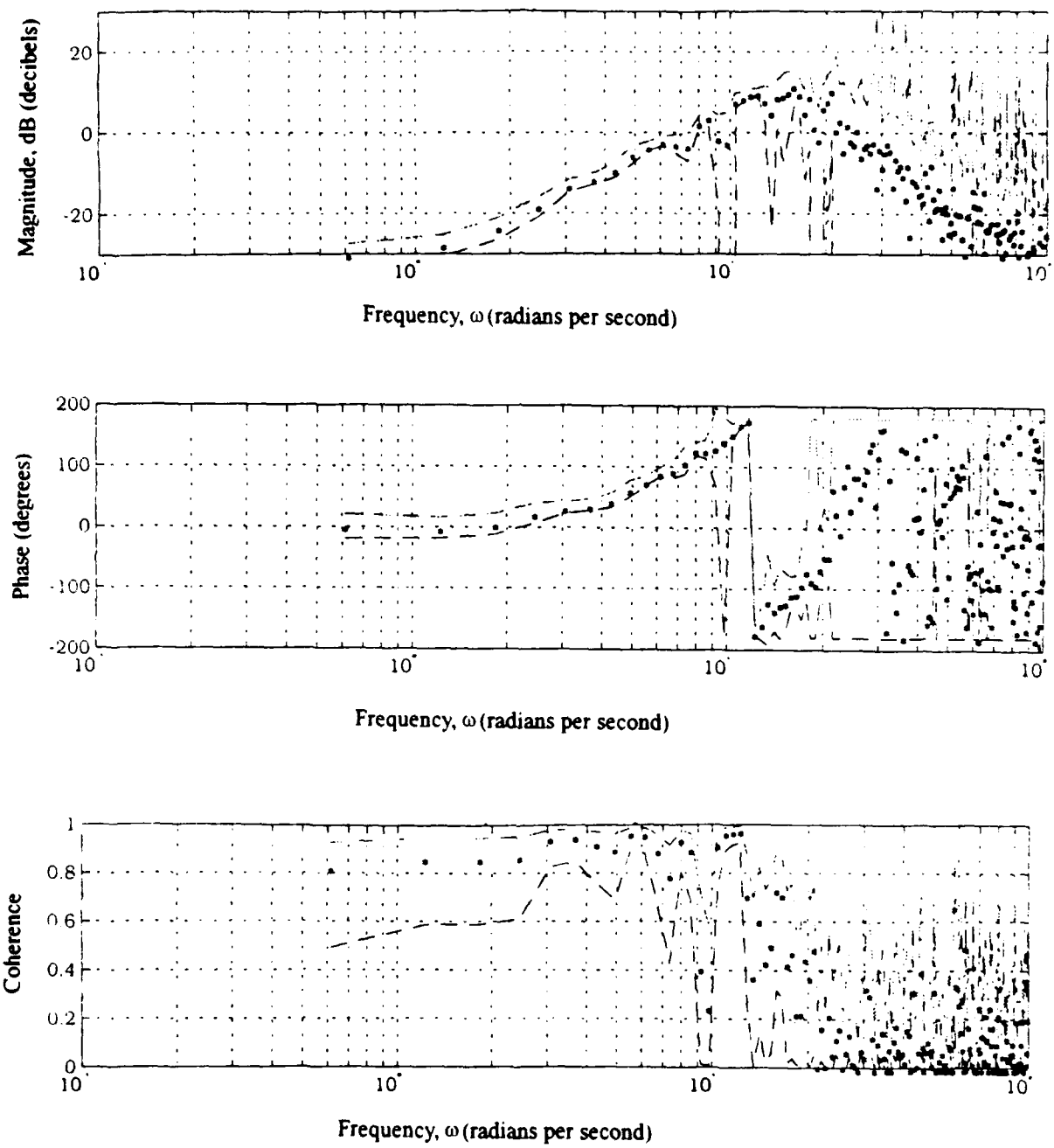

Figure D-10. Frequency Response Analysis -
Longitudinal Stick Deflection to Task Error (Case D)

Calspan Variable Stability Aircraft
Learjet LJ-25, Tail Number N102VS
Date: 9 - 11 Oct 93; Pilot: G; Sortie #1
Sum-of-Sines Tracking Task; Case 1; Airborne Data

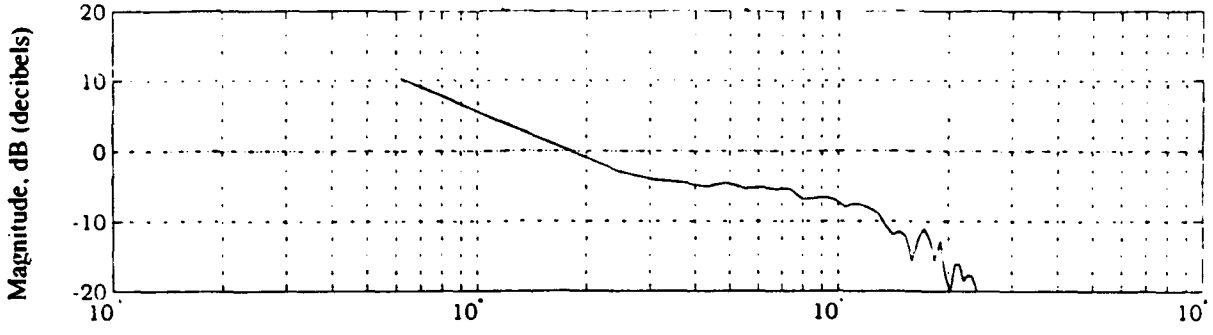

Frequency, ω (radians per second)

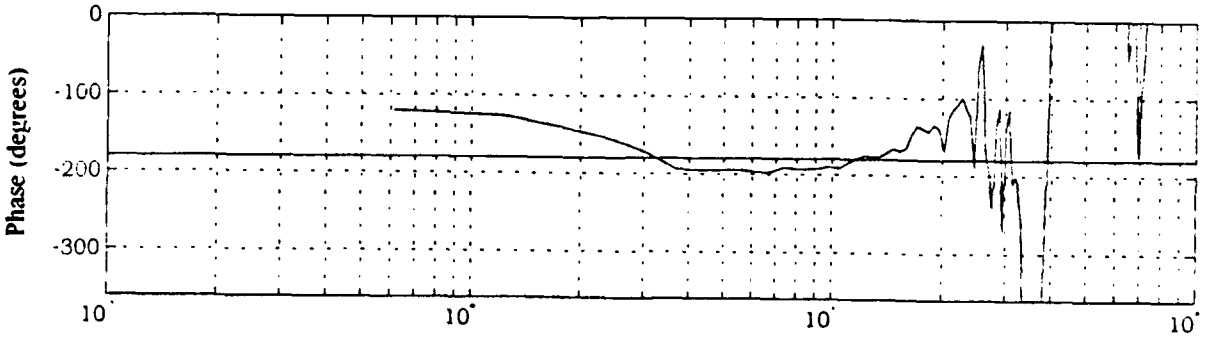

Frequency, ω (radians per second)

Figure D-11. Combined Pilot-Aircraft System (Case 1)

Calspan Variable Stability Aircraft
Learjet LJ-25, Tail Number N102VS
Date: 9 - 11 Oct 93; Pilot: S; Sortie #2
Sum-of-Sines Tracking Task; Case 2; Airborne Data

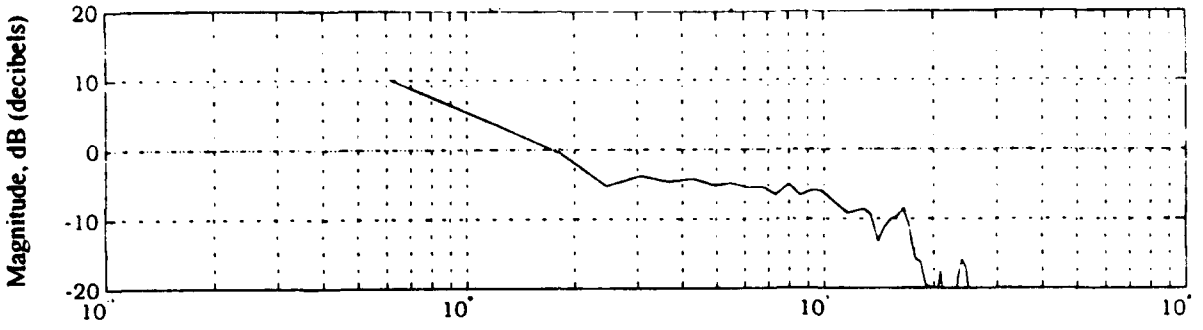

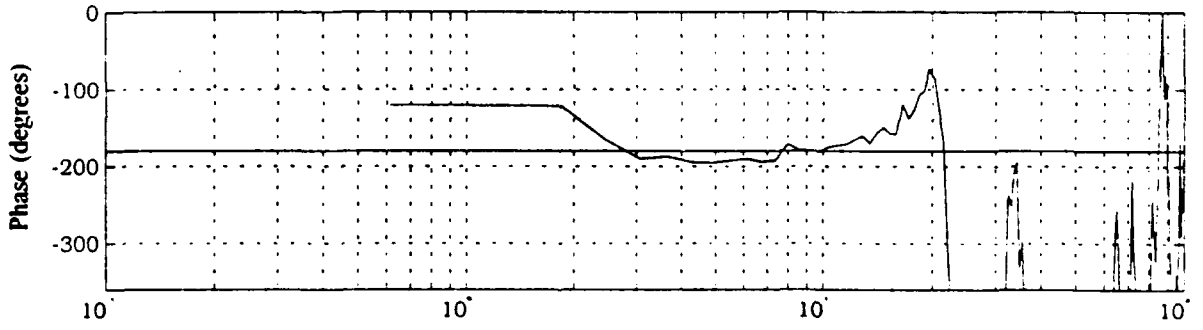

Figure D-12. Combined Pilot-Aircraft System (Case 2)

Calspan Variable Stability Aircraft
Learjet LJ-25, Tail Number N102VS
Date: 9 - 11 Oct 93; Pilot: S; Sortie #2
Sum-of-Sines Tracking Task; Case 3; Airborne Data

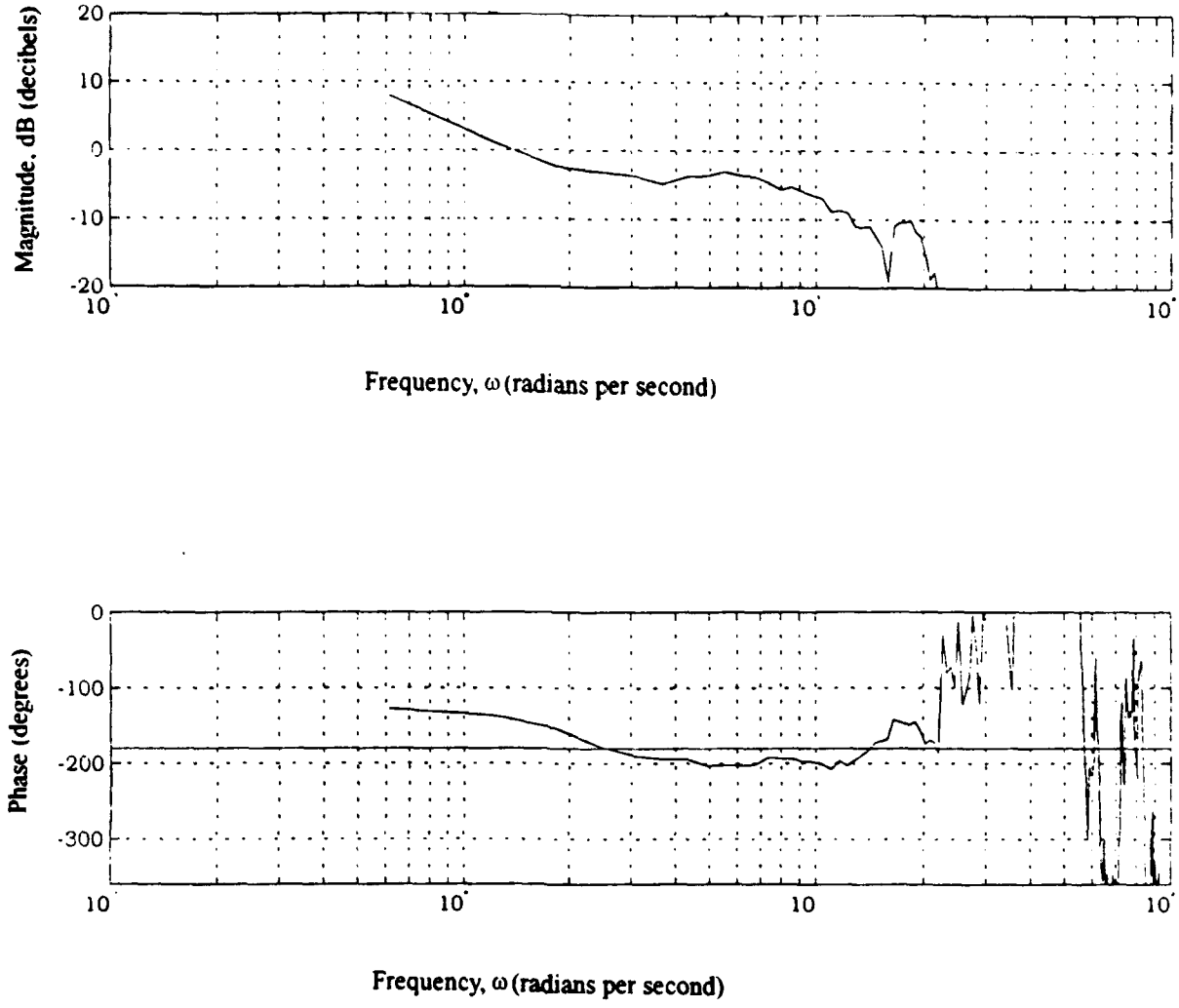

Figure D-13. Combined Pilot-Aircraft System (Case 3)

Calspan Variable Stability Aircraft
Learjet LJ-25, Tail Number N102VS
Date: 9 - 11 Oct 93; Pilot: G; Sortie #1
Sum-of-Sines Tracking Task; Case 4; Airborne Data

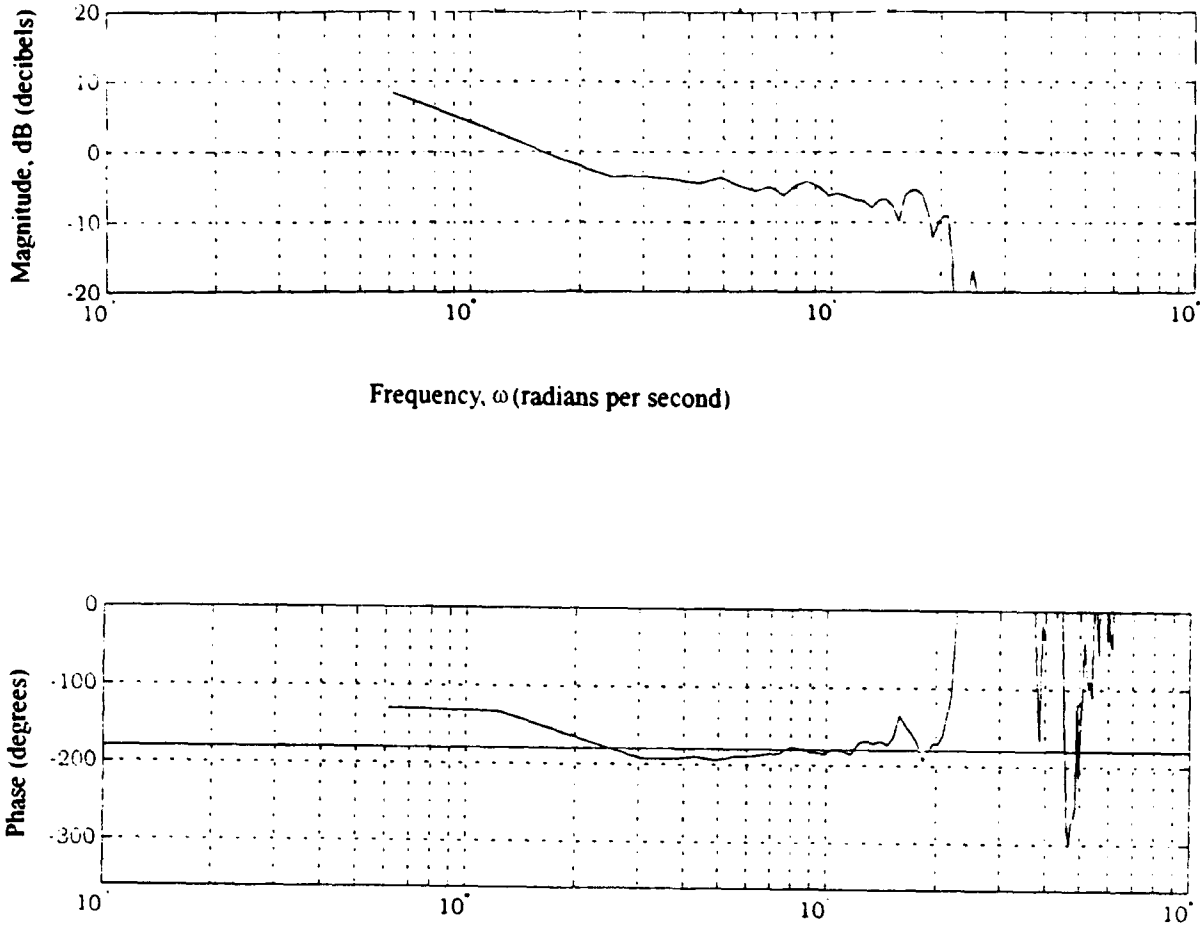

Figure D-14. Combined Pilot-Aircraft System (Case 4)

Calspan Variable Stability Aircraft
Learjet LJ-25, Tail Number N102VS
Date: 9 - 11 Oct 93; Pilot: E; Sortie #2
Sum-of-Sines Tracking Task; Case A; Airborne Data

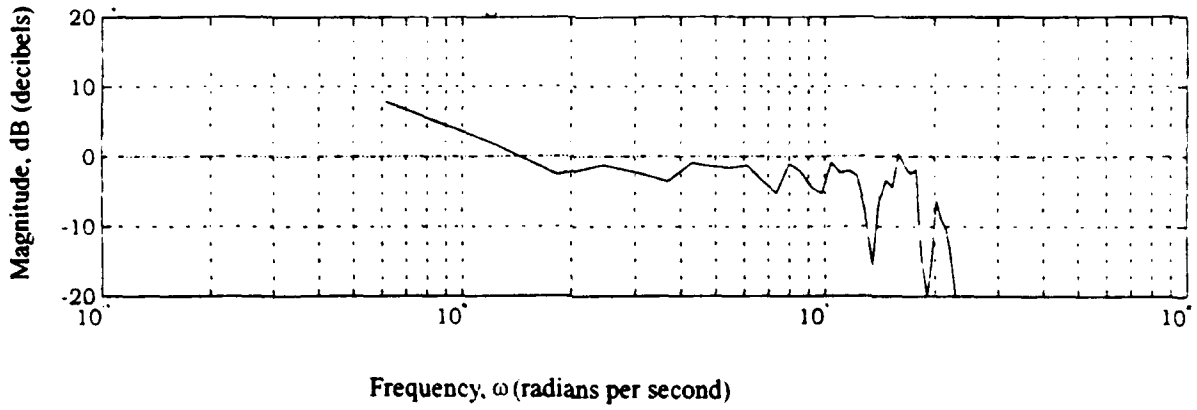

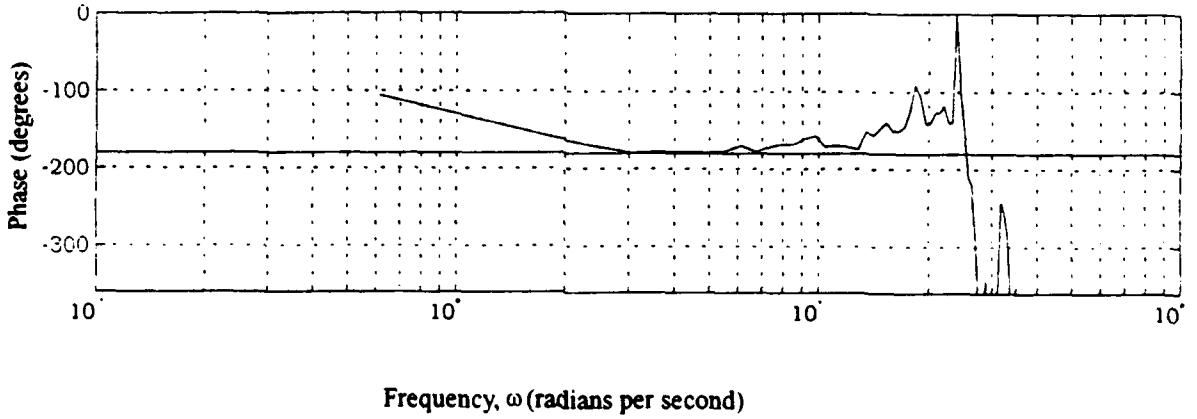

Figure D-15. Combined Pilot-Aircraft System (Case A)

Calspan Variable Stability Aircraft
Learjet LJ-25, Tail Number N102VS
Date: 9 - 11 Oct 93; Pilot: G; Sortie #5
Sum-of-Sines Tracking Task; Case B; Airborne Data

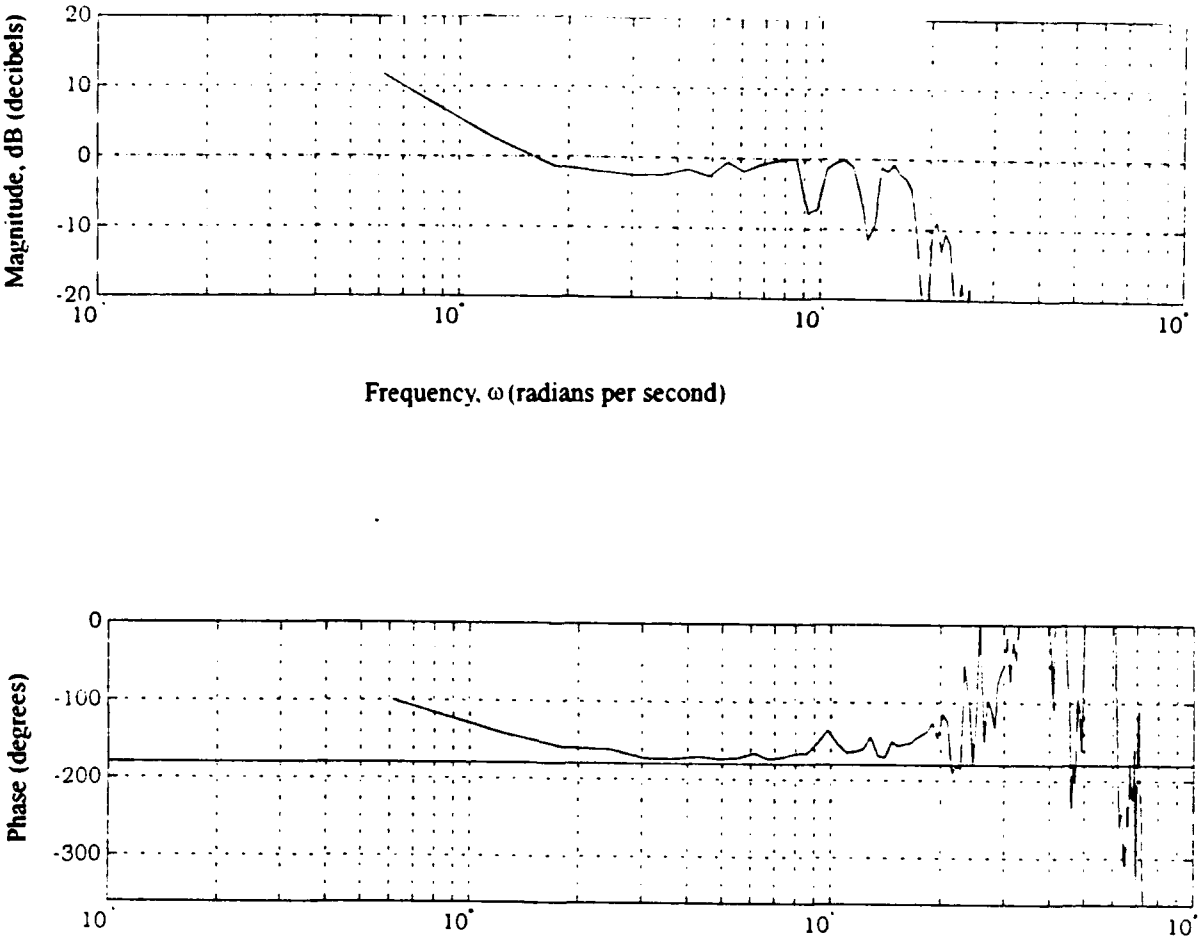

Figure D-16. Combined Pilot-Aircraft System (Case B)

Calspan Variable Stability Aircraft
Learjet LJ-25, Tail Number N102VS
Date: 9 - 11 Oct 93; Pilot: E; Sortie #2
Sum-of-Sines Tracking Task; Case C; Airborne Data

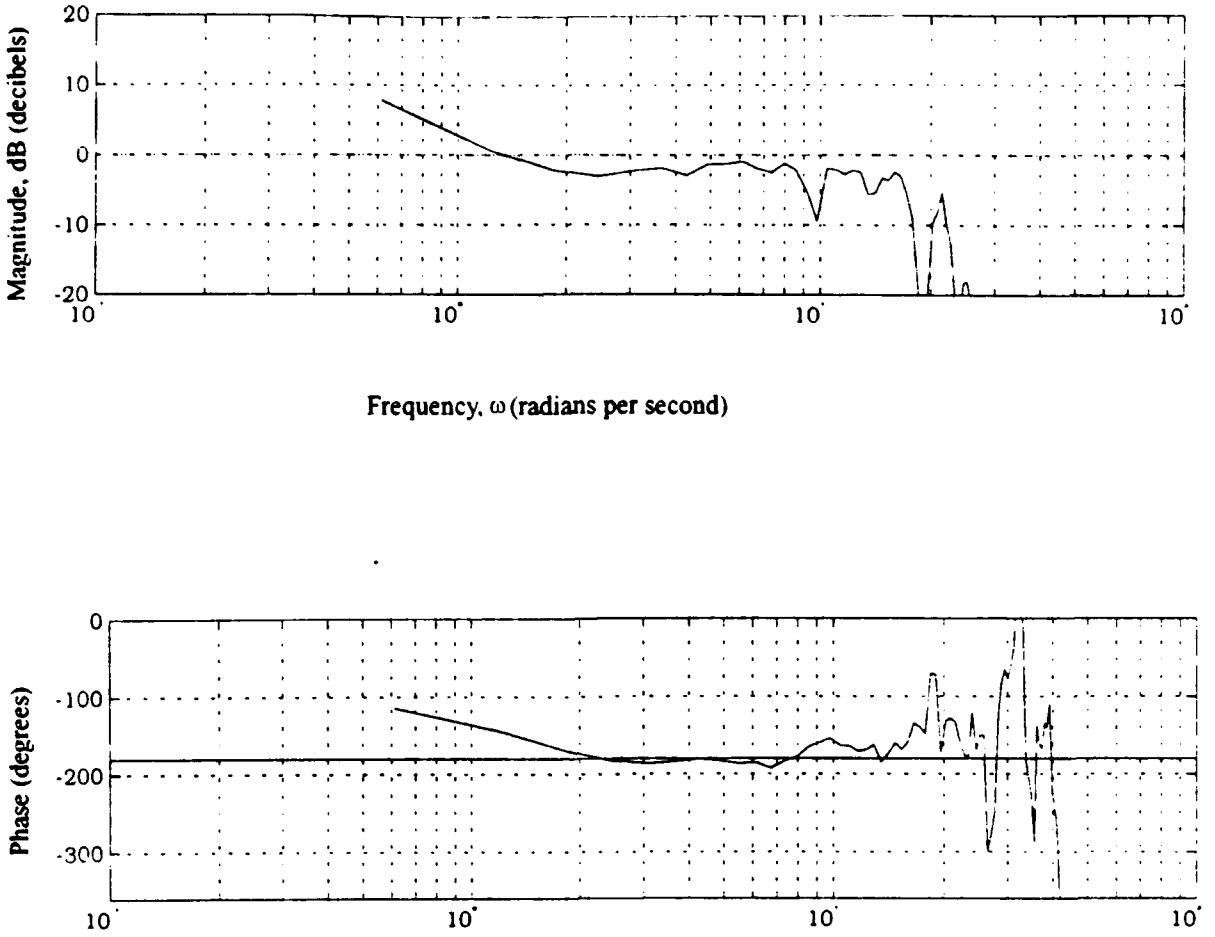

Figure D-17. Combined Pilot-Aircraft System (Case C)

Calspan Variable Stability Aircraft
Learjet LJ-25, Tail Number N102VS
Date: 9 - 11 Oct 93; Pilot: E; Sortie #1
Sum-of-Sines Tracking Task; Case D; Airborne Data

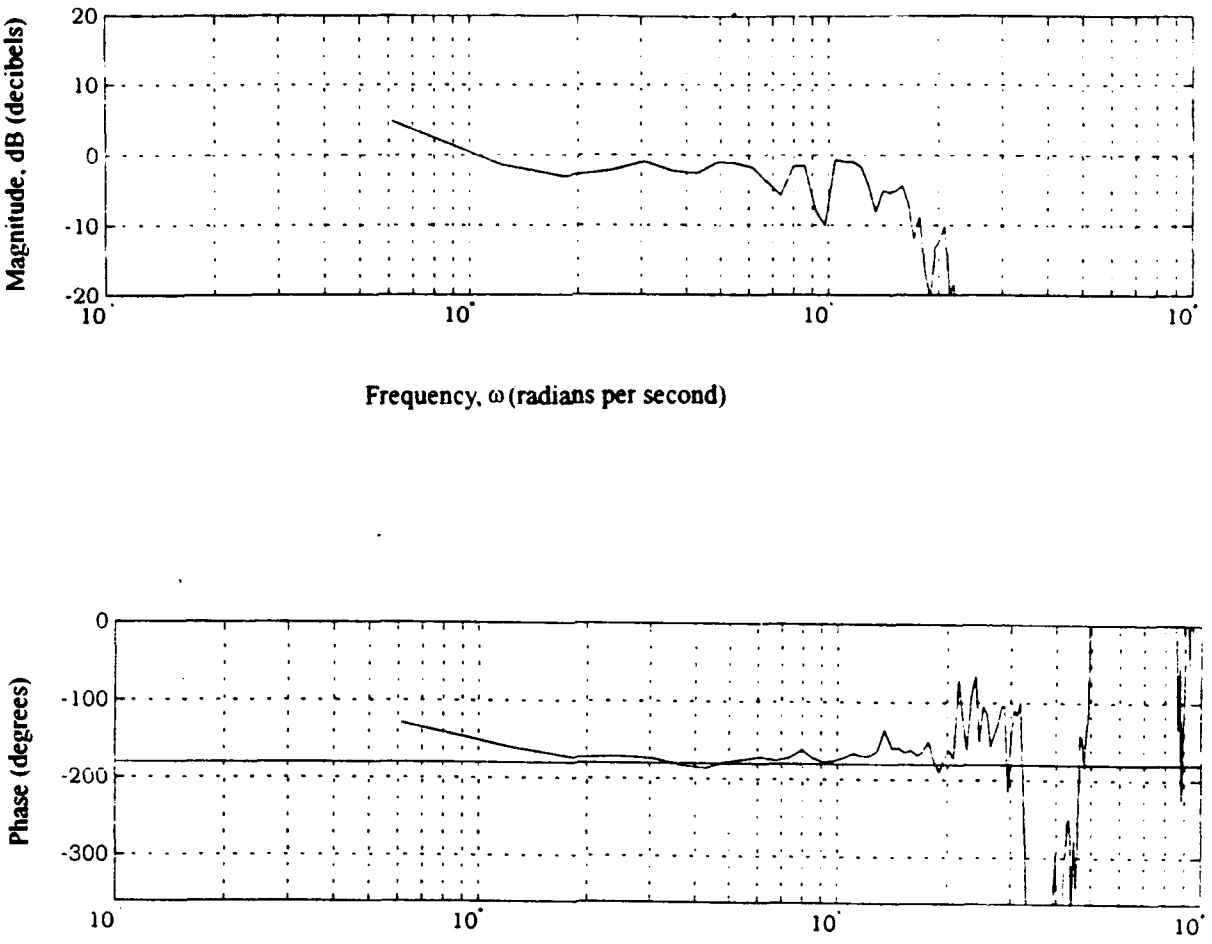

Figure D-18. Combined Pilot-Aircraft System (Case D)

Calspan Variable Stability Aircraft
Learjet LJ-25, Tail Number N102VS
Date: 9 Oct 93; Pilot: S; Sortie #8
Sum-of-Sines Tracking Task; Case 1; Ground Simulation

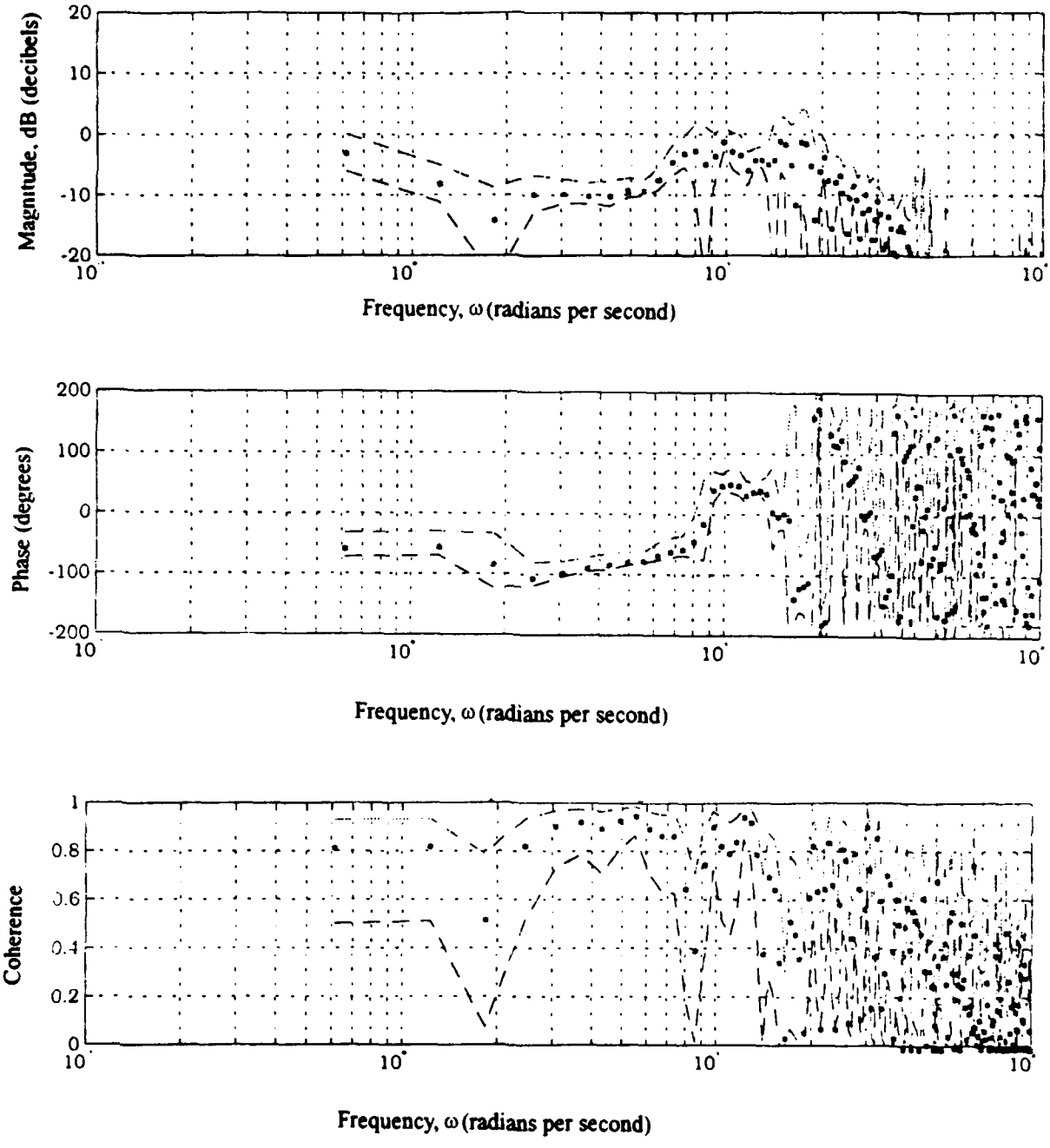

Figure D-19. Gain Investigation Baseline -
Longitudinal Stick Deflection to Task Error (Case 1)

Calspan Variable Stability Aircraft
Learjet LJ-25, Tail Number N102VS
Date: 9 Oct 93; Pilot: S; Sortie #8
Sum-of-Sines Tracking Task; Case 1; Ground Simulation

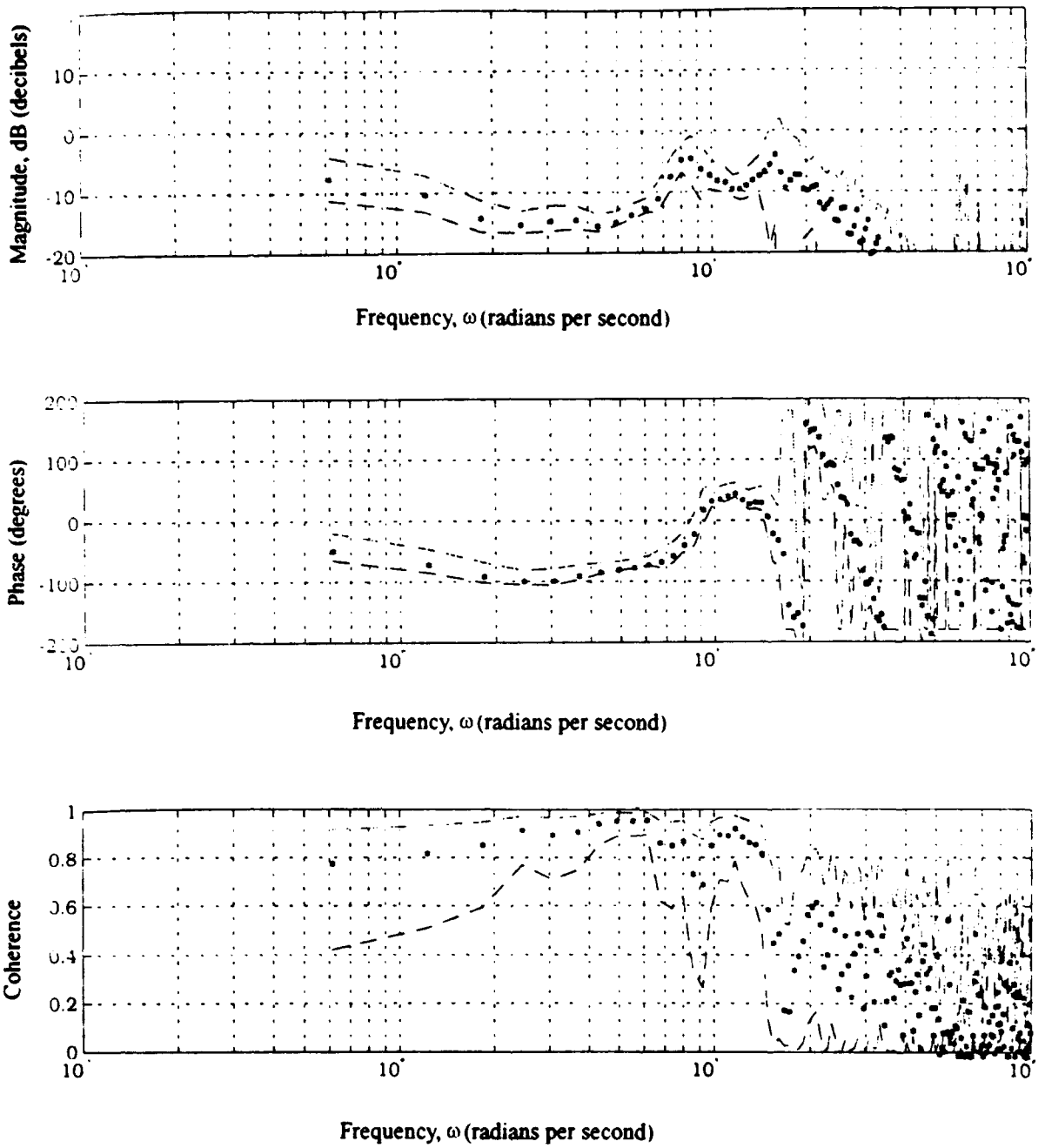

Figure D-20. Gain Investigation - Longitudinal Stick Deflection to Task Error (Case 1 with Double Gain)

Calspan Variable Stability Aircraft
Learjet LJ-25, Tail Number N102VS
Date: 9 Oct 93; Pilot: S; Sortie #8
Sum-of-Sines Tracking Task; Case 1; Ground Simulation

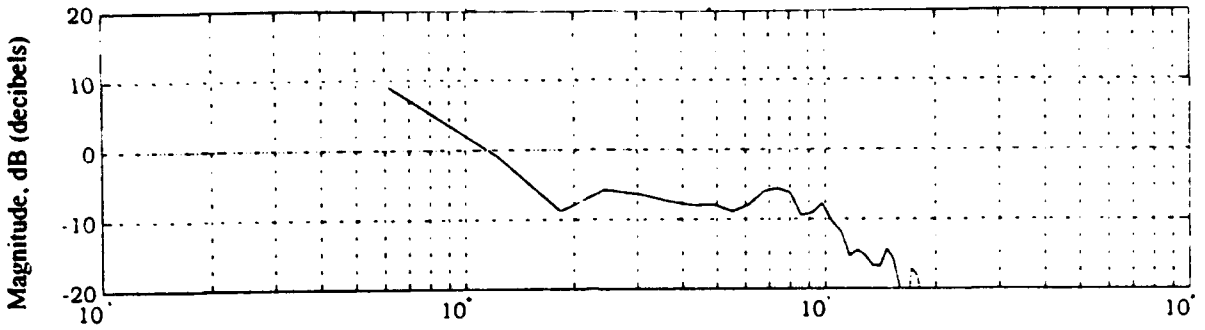

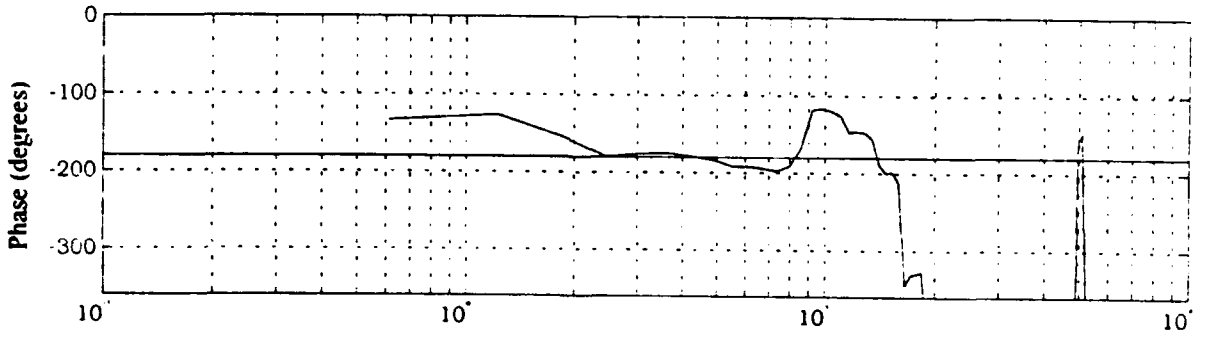

Figure D-21. Combined Pilot-Aircraft System
-- Gain Investigation Baseline (Case 1)

Calspan Variable Stability Aircraft
Learjet LJ-25, Tail Number N102VS
Date: 9 Oct 93; Pilot: S; Sortie #8
Sum-of-Sines Tracking Task; Case 1; Ground Simulation

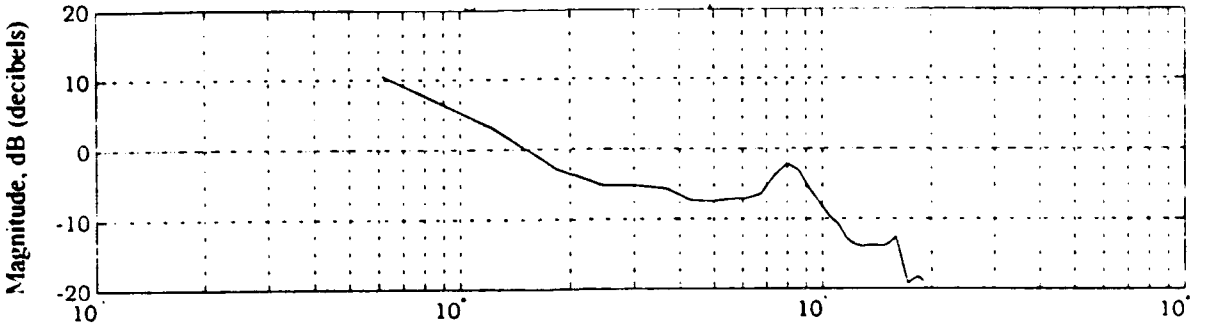

Frequency, ω (radians per second)

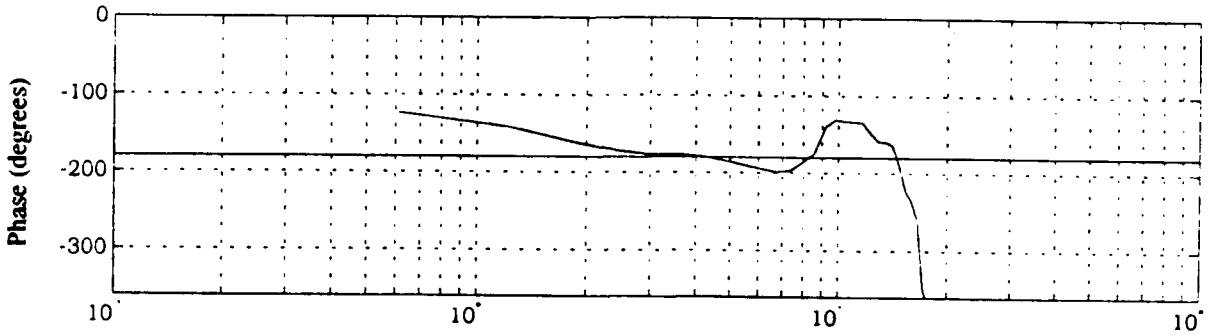

Frequency, ω (radians per second)

Figure D-22. Combined Pilot-Aircraft System
-- Gain Investigation (Case 1 with Double Gain)

Appendix E. Numerical Solution Routines and Results

PIFIND.M

```
function [J]=PIFIND(Ak,Bk,Ck,Ac,Bc,Cc,Ag,Bg,Cg,Q,R,Noise)
%
%       This File Finds the Performance Index Value for Problems
%       With Filter States
%  where
%       Ak,Bk,Ck = Compensator States
%       Ac,Bc,Cc = Aircraft States
%       Ag,Bg,Cg = Disturbanc Noise Filter States
%               Q = State Deviation Weighting
%                       (Diagonal with #Rows=#Plant+#Filter States)
%                R = Control Usage Weighting
%                       (Diagonal with #Rows=#Rows of Ck)
%            Noise = Noise Matrix
%                       |Qo 0 |   Qo = Process Noise Intensity
%                       |0  Ro|   Ro = Measurement Noise Intensity
%                        (Square with #Cols=#Cols of Bg+Bk)
%
%%%%%%%%%%%%%%%%%%%%%%%%%%%%%%%%%%%%%%%%%%%%%%%%%%%%%%%%%%%%%%%%%%%%%%%%%%%%%%%%
sizeak=size(Ak);
sizeac=size(Ac);
sizeag=size(Ag);
sizebg=size(Bg);
sizebk=size(Bk);
sizeck=size(Ck);
A=[Ac,Cg,-Bc*Ck;zeros(sizeag(1),sizeac(1)),Ag,zeros(sizeag(1),sizeak(1));Bk*Cc,zeros(sizeak(1),
sizeag(1)),Ak];
E=[zeros(sizeac(1),sizebg(2)),zeros(sizeac(1),sizebk(2));Bg,zeros(sizeag(1),sizebk(2));zeros(sizeak(1),
sizebg(2)),Bk];
L=E*Noise*E';
X=lyap(A,L);
m=sizeak(1);
n=sizeac(1)+sizeag(1);
o=sizeck(1);
term1=0;
term2=0;
for i=1:n
 term1=term1+Q(i,i)*X(i,i);
end
for h=1:o
 for i=1:m
  for j=1:m
   term2=term2+R(h,h)*Ck(h,i)*Ck(h,j)*X((n+i),(n+j));
end;end;end
J=term1+term2;
return
```

PIFINDNF.M

```
function [J]=PIFINDNF(Ak,Bk,Ck,Ac,Bc,Cc,Gamma,Q,R,Noise)
%
%       This File Finds the Performance Index Value For Problems with
%       No Filter States
%  where
%         Ak,Bk,Ck = Compensator States
%         Ac,Bc,Cc  = Aircraft States
%           Gamma = Constant Disturbance Noise Matrix
%                           (Distributes Disturbance Noise into States)
%                 Q = State Deviation Weighting
%                           (Diagonal with #Rows=#Plant+#Filter States)
%                 R = Control Usage Weighting
%                           (Diagonal with #Rows=#Rows of Ck)
%             Noise  = Noise Matrix
%                           |Qo 0 |    Qo = Process Noise Intensity
%                           |0  Ro|    Ro = Measurement Noise Intensity
%                           (Square with #Cols=#Col of Gamma+Bk)
%
%%%%%%%%%%%%%%%%%%%%%%%%%%%%%%%%%%%%%%%%%%%%%%%%%%%%%%%%%%%%%%%%%%%%%%%%
sizeak=size(Ak);
sizeac=size(Ac);
sizebk=size(Bk);
sizeg=size(Gamma);
sizeck=size(Ck);
A=[Ac,-Bc*Ck;Bk*Cc,Ak];
E=[Gamma,zeros(sizeac(1),sizebk(2));zeros(sizeak(1),sizeg(2)),Bk];
L=E*Noise*E';
X=lyap(A,L);
m=sizeak(1);
n=sizeac(1);
o=sizeck(1);
term1=0;
term2=0;
for i=1:n
 term1=term1+Q(i,i)*X(i,i);
end
for h=1:o
 for i=1:m
  for j=1:m
   term2=term2+R(h,h)*Ck(h,i)*Ck(h,j)*X((n+i),(n+j));
end;end;end
J=term1+term2;
return
```

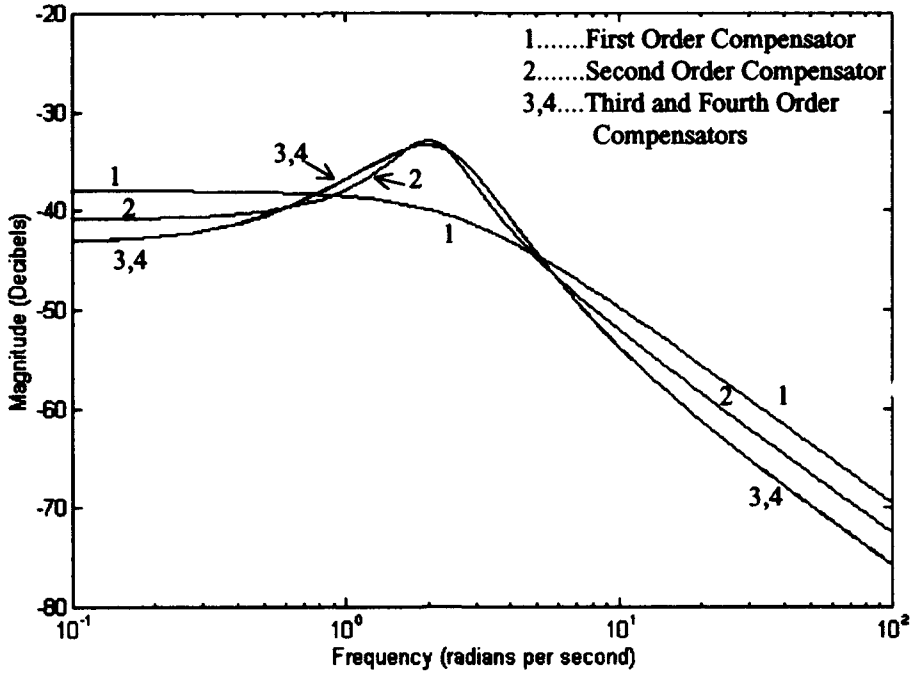

Figure E-1. Bode Magnitude Comparison Plot (First-Fourth Order Compensators)

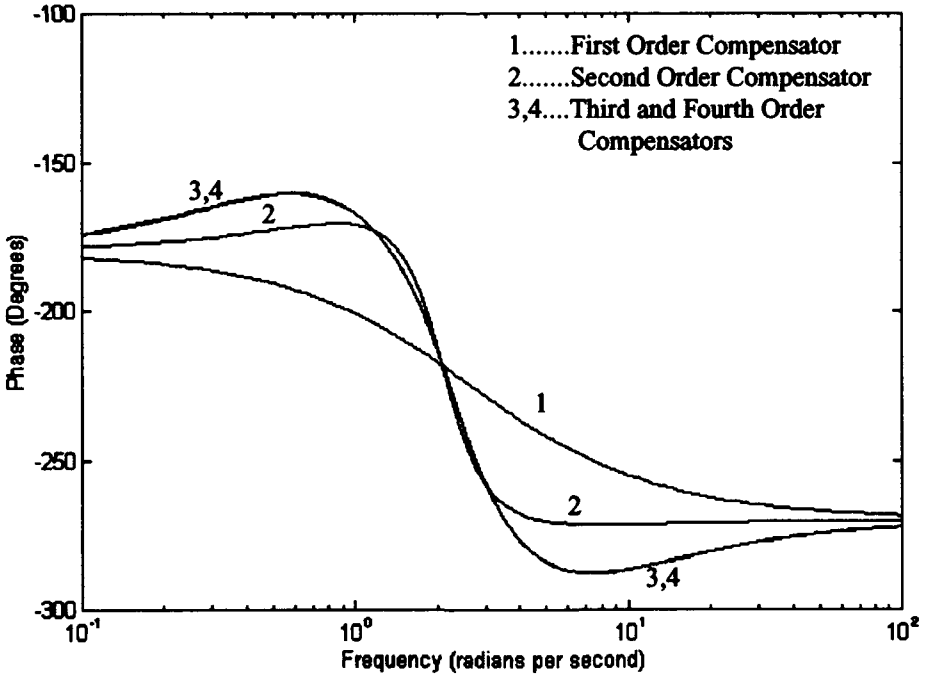

Figure E-2. Bode Phase Comparison Plot (First-Fourth Order Compensator)

Appendix F. Sub-Optimal Pilot Model Algorithm Verification

General

The numerical solution technique used in the sub-optimal pilot model is verified in this appendix. A simple example problem was solved using both the standard linear quadratic Gaussian (LQG) approach and the numerical method (Equations 6-19, 6-21, 6-22, and 6-23). As shown, the results were the same using either method.

Standard Linear Quadratic Gaussian Solution

Assume the controlled element, Y_C, and forcing function filter, Y_w, can be modeled by the following transfer functions.

$$Y_C = \frac{s+3}{s^2+2s+4} \quad and \quad Y_w = \frac{\sqrt{2}}{s+2} \tag{F-1}$$

These transfer functions have the following state space representations.

$$\begin{bmatrix} \dot{x}_{C1} \\ \dot{x}_{C2} \end{bmatrix} = \begin{bmatrix} -2 & -4 \\ 1 & 0 \end{bmatrix} \cdot \begin{bmatrix} x_{C1} \\ x_{C2} \end{bmatrix} + \begin{bmatrix} 1 \\ 0 \end{bmatrix} \cdot u$$

$$y_C = \begin{bmatrix} 1 & 3 \end{bmatrix} \cdot \begin{bmatrix} x_{C1} \\ x_{C2} \end{bmatrix} + [0] \cdot u \tag{F-2}$$

$$[\dot{x}_w] = [-2] \cdot [x_w] + [1] \cdot u$$

$$y_w = \begin{bmatrix} \sqrt{2} \end{bmatrix} \cdot [x_w] + [0] \cdot u \tag{F-3}$$

Assume this example is in the form shown in Figure 6-2, where the disturbance occurs at the controlled element output so that the error is the difference between the filter output

and the controlled element output ($e = Y_w - Y_C$). For this example, the desired weighting on error, *Q*, will be *1* and the desired weighting on control, *R*, will be *2* in accordance with the following performance index.

$$J = \int_0^\infty [e^T Q e + u^T R u] dt \tag{F-4}$$

This example will assume unit intensity forcing function driving noise, $\xi(t)$, and observation noise, $\eta(t)$, such that:

$$E\{\xi(t) \cdot \xi^T(t-\tau)\} = Q_o \cdot \delta(\tau) = \delta(\tau) \tag{F-5}$$

$$E\{\eta(t) \cdot \eta^T(t-\tau)\} = R_o \cdot \delta(\tau) = \delta(\tau) \tag{F-6}$$

To solve the standard LQG problem, the filter states must be appended to the controlled element states so that the system is in the following form.

$$\dot{x} = Ax + Bu + \Gamma\xi \quad amd \quad y = Cx + D\eta \tag{F-7}$$

For this problem, this can be accomplished using the following formula:

$$\begin{bmatrix} \dot{x}_C \\ \dot{x}_w \end{bmatrix} = \begin{bmatrix} A_C & 0 \\ 0 & A_w \end{bmatrix} \cdot \begin{bmatrix} x_C \\ x_w \end{bmatrix} + \begin{bmatrix} 0 \\ B_C \end{bmatrix} \cdot u + \begin{bmatrix} 0 \\ B_w \end{bmatrix} \cdot \xi$$

$$y = \begin{bmatrix} -C_C & C_w \end{bmatrix} \cdot \begin{bmatrix} x_C \\ x_w \end{bmatrix} + [1] \cdot \eta \tag{F-8}$$

where the optimal LQG control law is $u = -Kx$. Substituting Equations F-2 and F-3 into Equation F-8 yields the following state space representation.

$$\begin{bmatrix} \dot{x}_{C1} \\ \dot{x}_{C2} \\ \dot{x}_w \end{bmatrix} = \begin{bmatrix} -2 & -4 & 0 \\ 1 & 0 & 0 \\ 0 & 0 & -2 \end{bmatrix} \cdot \begin{bmatrix} x_{C1} \\ x_{C2} \\ x_w \end{bmatrix} + \begin{bmatrix} 1 \\ 0 \\ 0 \end{bmatrix} \cdot u + \begin{bmatrix} 0 \\ 0 \\ 1 \end{bmatrix} \cdot \xi$$

$$y = \begin{bmatrix} -1 & -3 & \sqrt{2} \end{bmatrix} \cdot \begin{bmatrix} x_{C1} \\ x_{C2} \\ x_w \end{bmatrix} + [1] \cdot \eta \qquad \text{(F-9)}$$

Error can be weighted using the following formula:

$$Q' = C^T \cdot Q \cdot C \qquad \text{(F-10)}$$

where Q is one for this example, and the new state weighting, Q', is:

$$Q' = \begin{bmatrix} 1 & 3 & -\sqrt{2} \\ 3 & 9 & -3\sqrt{2} \\ -\sqrt{2} & -3\sqrt{2} & 2 \end{bmatrix} \qquad \text{(F-11)}$$

The noise weighting matrix, Q_f, is found using the following formula.

$$Q_f = \Gamma \cdot Q_o \cdot \Gamma^T = \begin{bmatrix} 0 & 0 & 0 \\ 0 & 0 & 0 \\ 0 & 0 & 1 \end{bmatrix} \qquad \text{(F-12)}$$

Using the following MATLAB™ command will return the optimal LQG compensator:

[Ak,Bk,Ck,Dk]=lqg(A,B,C,D,W,V)

where *A, B, C,* and *D* are the state space matrices from Equation F-9, *W* contains the weighting matrices in diagonal form (*diag{Q', R}*), and V contains the noise matrices in diagonal form (*diag{Q_f, R_o}*). The optimal LQG compensator for this problem is:

$$\dot{x} = \begin{bmatrix} -2.3570 & -4.5277 & 0.2670 \\ 1 & 0 & 0 \\ 0.4313 & 1.1212 & -2.5344 \end{bmatrix} \cdot x + \begin{bmatrix} 0 \\ 0 \\ 0.3178 \end{bmatrix} \cdot u$$

$$y = \begin{bmatrix} 0.3570 & 0.5277 & -0.2670 \end{bmatrix} \cdot x \qquad \text{(F-13)}$$

or in transfer function form, the optimal LQG compensator, $K_{LQG}(s)$, is:

$$K_{LQG}(s) = \frac{-0.0849s^2 - 0.1697s - 0.3395}{s^3 + 4.8913s^2 + 10.3860s + 11.1754} \qquad \text{(F-14)}$$

The Numerical Solution

To accomplish the numerical solution the file, *PI_SOPM.M*, has to be adapted slightly. The desired compensator form is now a second over a third order transfer function as shown in the new file, *PIFINDER.M*, presented at the end of this appendix. Except for this change, *PIFINDER.M* is identical to the routine used in the sub-optimal pilot model.

For this example, the controlled element state space matrices remain as in Equations F-2 and F-3. The weightings, Q and R, are the scalar values, *1* and *2*. Finally, the *Noise* matrix is a diagonal matrix containing the noise intensities, Q_o and R_o. In this example that is a 2 by 2 identity matrix. Using an initial compensator coefficient vector, c0, of all ones, the following command will return the optimal solution.

```
cmin=fmins('pifinder',c0,[],[],Ac,Bc,Cc,Aw,Bw,Cw,Q,R,Noise)
```

The following value for cmin was computed.

```
cmin=[0.0849 0.1058 0.3218 4.0764 7.7238 10.4016]
```

Using this vector as the new initial compensator coefficient vector, c0, and running *fmins* again yielded:

cmin=[0.0849 0.1697 0.3395 4.8065 10.2163 10.8360]

This equates to the following compensator.

$$K(s) = \frac{0.0849s^2 + 0.1697s + 0.3395}{s^3 + 4.8065s^2 + 10.2163s + 10.8360} \qquad \text{(F-15)}$$

Notice that the coefficients are identical, within the tolerance of the numerical search, to those found using standard LQG methods. Also note that all of the numerator coefficients are positive while those in Equation F-14 are negative. This is because the standard LQG optimum control law is always $u = -Kx$, while the numerical method used in the sub-optimal pilot model has the control law, $u = Kx$ (see Figure 6-2, page 6-4). Thus, the numerical method used to minimize the performance index in the sub-optimal pilot model is valid.

MATLAB™ File for Disturbance at Plant Output

```
function [J]=PIFINDER(c,Ac,Bc,Cc,Ag,Bg,Cg,Q,R,Noise)
%
%       This File Finds the Minimum Performance Index Value
%       For Problems that Weight Error through Disturbance
%       Noise Injected at the Aircraft Output
%
%  where
%             c = Compensator Coefficients
%   Ac,Bc,Cc = Aircraft States
%   Ag,Bg,Cg = Disturbance Noise Filter States
%             Q = Error Weighting (scalar)
%             R = Control Usage Weighting (scalar)
%         Noise = Noise Matrix
%            |Qo 0 |    Qo = Process Noise Intensity
%            |0  Ro|    Ro = Measurement Noise Intensity
%
```

```
%%%%%%%%%%%%%%%%%%%%%%%%%%%%%%%%%%%%%%%%%%%%%%%%%%
%                    Compensator Form                    %
%%%%%%%%%%%%%%%%%%%%%%%%%%%%%%%%%%%%%%%%%%%%%%%%%%
%
%
num=[c(1) c(2) c(3)];
den=[1 c(4) c(5) c(6)];
den=abs(den);
[Ak,Bk,Ck,Dk]=tf2ss(num,den);
%
%
%%%%%%%%%%%%%%%%%%%%%%%%%%%%%%%%%%%%%%%%%%%%%%%%%%
%                    Compute J                    %
%%%%%%%%%%%%%%%%%%%%%%%%%%%%%%%%%%%%%%%%%%%%%%%%%%
%
%
sizeak=size(Ak);
sizeac=size(Ac);
sizeag=size(Ag);
A=[Ac,zeros(sizeac(1),sizeag(1)),Bc*Ck;zeros(sizeag(1),sizeac(1)),Ag,zeros(sizeag(1),sizeak(1));-Bk*Cc
,Bk*Cg,Ak];
E=[zeros(sizeac(1),2);Bg,zeros(sizeag(1),1);zeros(sizeak(1),1),Bk];
L=E*Noise*E';
X=lyap(A,L);
m=sizeak(1);
p=sizeac(1);
f=sizeag(1);
n=p+f;
term1=0;
term2a=0;
term2b=0;
term2c=0;
for i=1:m
  for j=1:m
    term1=term1+Ck(1,i)*Ck(1,j)*X((n+i),(n+j));
end;end
for i=1:f
  for j=1:f
    term2a=term2a+Cg(1,i)*Cg(1,j)*X((p+i),(p+j));
end;end
for i=1:p
  for j=1:p
    term2b=term2b+Cc(1,i)*Cc(1,j)*X(i,j);
end;end
for i=1:f
  for j=1:p
    term2c=term2c+Cg(1,i)*Cc(1,j)*X((p+i),j);
end;end
J=R*term1+Q*term2a+Q*term2b-2*Q*term2c;
return
```

Appendix G. Sub-Optimal Pilot Model Data

SOPM.M

```
function [J,Cmin,Rating]=sopm(Numc,Denc,Delay,Numg,Deng)
%
% Sub-Optimal Pilot Model
%
%       Where:
%       Numc = Numerator of Aircraft Dynamics
%       Denc = Denominator of Aircraft Dynamics
%       Delay = Delay of Aicraft Dynamics
%       Numg = Numerator of Task Forcing Function
%       Deng = Denominator of Task Forcing Function
%                       Recommend 2nd Order Butterworth:
%                       Numg=sqrt(2)
%                       Deng=[1/bw sqrt(2)/bw 1]
%                       Where 'bw' is Butterworth Filter Bandwidth
%
%%%%%%%%%%%%%%%%%%%%%%%%%%%%%%%%%%%%%%%%%%%%%%%%%%%%%%%%%%%%%%%%%%%%%%%%%%%%%%%%
%                       Input Other Variables                                   %
%%%%%%%%%%%%%%%%%%%%%%%%%%%%%%%%%%%%%%%%%%%%%%%%%%%%%%%%%%%%%%%%%%%%%%%%%%%%%%%%
%
if(nargin~=5),error('Incorrect Number of Input Arguments'),end
Q=input('Input Error Weighting (Usually 1) = ');
R=input('Input Control Weighting (Usually 4.5 Pitch, 1 Roll) = ');
rhod=input('Input Observation Noise Ratio (Usually 0.01) = ');
Tn=input('Muscular Time Constant (Usually 0.115) = ');
Pilot_Delay=input('Input Pilot Delay (sec) (Usually .35) = ');
%
%
%%%%%%%%%%%%%%%%%%%%%%%%%%%%%%%%%%%%%%%%%%%%%%%%%%%%%%%%%%%%%%%%%%%%%%%%%%%%%%%%
%                       Model Parameters are Set                                %
%%%%%%%%%%%%%%%%%%%%%%%%%%%%%%%%%%%%%%%%%%%%%%%%%%%%%%%%%%%%%%%%%%%%%%%%%%%%%%%%
%
%
Var=[Tn,Pilot_Delay+Delay];
c0=[1 1 1];
V=.5;
rhodif=1;
%
%
%%%%%%%%%%%%%%%%%%%%%%%%%%%%%%%%%%%%%%%%%%%%%%%%%%%%%%%%%%%%%%%%%%%%%%%%%%%%%%%%
%                       Performance Index is Minimized                          %
%%%%%%%%%%%%%%%%%%%%%%%%%%%%%%%%%%%%%%%%%%%%%%%%%%%%%%%%%%%%%%%%%%%%%%%%%%%%%%%%
%
[Ac,Bc,Cc,Dc]=tf2ss(Numc,Denc);
[Ag,Bg,Cg,Dg]=tf2ss(Numg,Deng);
for i=1:5
```

```
 if rhodif>0.0002          %0.1 db at rho = -20 dB (10*log10)
  disp(['Iteration  ',int2str(i)])
  Noise=[1,0;0,V]
  Cmin=fmins('pi_sopm',c0,[],[],Ac,Bc,Cc,Ag,Bg,Cg,Q,R,Noise,Var)
  [J,RMS]=RMS_sopm(Cmin,Ac,Bc,Cc,Ag,Bg,Cg,Q,R,Noise,Var)
  rho=V/pi/RMS
  rhodif=abs(rho-rhod);
  c0=Cmin;
  V=V*rhod/rho;
 end
end
%
%
%%%%%%%%%%%%%%%%%%%%%%%%%%%%%%%%%%%%%%%%%%%%%%%%%%%%%%%
%                  Cooper-Harper Rating is Computed                   %
%%%%%%%%%%%%%%%%%%%%%%%%%%%%%%%%%%%%%%%%%%%%%%%%%%%%%%%
%
x=menu('Select Axis','Pitch','Roll');
if x=1
 Rating=-30+241*log10(J);
else
 Rating=-13+117*log10(J);
end
%
%%%%%%%%%%%%%%%%%%%%%%%%%%%%%%%%%%%%%%%%%%%%%%%%%%%%%%%
%  Bode Plot and Transfer Function of Pilot are Displayed             %
%%%%%%%%%%%%%%%%%%%%%%%%%%%%%%%%%%%%%%%%%%%%%%%%%%%%%%%
%
%
Cmin=abs(Cmin);
K=Cmin(1);
A=Cmin(2)/Cmin(1);
B=Cmin(3);
C=1/Tn;
disp('')
disp('Pilot Parameters are:  ')
disp(['K =  ',num2str(K)])
disp(['A =  ',num2str(A)])
disp(['B =  ',num2str(B)])
disp(['C =  ',num2str(C)])
disp(['D =  ',num2str(Pilot_Delay)])
disp('')
disp('Where the Pilot is K(s+A)*exp(-Ds)/(S+B)*(S+C)')
%
w=logspace(-1,1,100);
num=[Cmin(1) Cmin(2)];
den=[1 Cmin(3)+1/Tn Cmin(3)*1/Tn];
[mag,phase,w]=bode(num,den,w);
mag=20*log10(mag);
phase=phase-w'*Pilot_Delay*180/pi;
hold off;
axis('normal');
```

```
subplot(211)
semilogx(w,mag,[.1 10],[0,0]);
subplot(212)
semilogx(w,phase,[.1 10],[-180 -180])
subplot(111)
title('Bode Magnitude and Phase of Pilot')
xlabel('Frequency (Rad./Sec.)')
ylabel('Phase (deg.)        Mag. (dB)')
```

PI_SOPM.M

```
function [J]=PI_SOPM(c,Ac,Bc,Cc,Ag,Bg,Cg,Q,R,Noise,Var)
%
%       This File is Called by SOPM.M to Find the Classical Pilot Model
%       Form that Produces the Minimum Performance Index Value
%
% where
%       c = Compensator Coefficients
%       Ac,Bc,Cc = Aircraft States
%       Ag,Bg,Cg = Disturbance Noise Filter States
%       Q = Error Weighting (scalar)
%       R = Control Usage Weighting (scalar)
%       Noise = Noise Matrix
%          |Qo 0 |   Qo = Process Noise Intensity
%          |0  Ro|   Ro = Measurement Noise Intensity
%       VAR = Variables -- [Muscular Time Constant, Delay]
%
%%%%%%%%%%%%%%%%%%%%%%%%%%%%%%%%%%%%%%%%%%%%%%%%%%%%%%%%
%                        Pilot Model Form                        %
%%%%%%%%%%%%%%%%%%%%%%%%%%%%%%%%%%%%%%%%%%%%%%%%%%%%%%%%
%
[num_delay,den_delay]=pade(Var(2),1);
num=conv([c(1) c(2)],num_delay);
den=conv([1 c(3)+1/Var(1) c(3)*1/Var(1)],den_delay);
den=abs(den);
[Ak,Bk,Ck,Dk]=tf2ss(num,den);
%
%
%%%%%%%%%%%%%%%%%%%%%%%%%%%%%%%%%%%%%%%%%%%%%%%%%%%%%%%%
%                        Compute J                        %
%%%%%%%%%%%%%%%%%%%%%%%%%%%%%%%%%%%%%%%%%%%%%%%%%%%%%%%%
%
sizeak=size(Ak);
sizeac=size(Ac);
sizeag=size(Ag);
A=[Ac,zeros(sizeac(1),sizeag(1)),Bc*Ck;zeros(sizeag(1),sizeac(1)),Ag,zeros(sizeag(1),sizeak(1));-Bk*Cc
,Bk*Cg,Ak];
E=[zeros(sizeac(1),2);Bg,zeros(sizeag(1),1);zeros(sizeak(1),1),Bk];
L=E*Noise*E';
X=lyap(A,L);
```

```
m=sizeak(1);
p=sizeac(1);
f=sizeag(1);
n=p+f;
term1=0;
term2a=0;
term2b=0;
term2c=0;
for i=1:m
 for j=1:m
  term1=term1+Ck(1,i)*Ck(1,j)*X((n+i),(n+j));
end;end
for i=1:f
 for j=1:f
  term2a=term2a+Cg(1,i)*Cg(1,j)*X((p+i),(p+j));
end;end
for i=1:p
 for j=1:p
  term2b=term2b+Cc(1,i)*Cc(1,j)*X(i,j);
end;end
for i=1:f
 for j=1:p
  term2c=term2c+Cg(1,i)*Cc(1,j)*X((p+i),j);
end;end
J=R*term1+Q*term2a+Q*term2b-2*Q*term2c;
return
```

RMS_SOPM.M

```
function [J,RMS]=RMS_SOPM(c,Ac,Bc,Cc,Ag,Bg,Cg,Q,R,Noise,Var)
%
%       This File is Called by SOPM.M to Find the RMS Error
%       and Performance Index Values
%
%  where
%         c = Compensator Coefficients
%       Ac,Bc,Cc = Aircraft States
%       Ag,Bg,Cg = Disturbance Noise Filter States
%       Q = Error Weighting (scalar)
%       R = Control Usage Weighting (scalar)
%       Noise = Noise Matrix
%           |Qo 0 |    Qo = Process Noise Intensity
%           |0  Ro|    Ro = Measurement Noise Intensity
%       VAR = Variables -- [Muscular Time Constant, Delay]
%
%%%%%%%%%%%%%%%%%%%%%%%%%%%%%%%%%%%%%%%%%%%%%%%%%%%%%%%%%%%%%%%%%%%%%%%%%%%%%%%%
%                                   Pilot Model Form                              %
%%%%%%%%%%%%%%%%%%%%%%%%%%%%%%%%%%%%%%%%%%%%%%%%%%%%%%%%%%%%%%%%%%%%%%%%%%%%%%%%
%
[num_delay,den_delay]=pade(Var(2),1);
```

```
num=conv([c(1) c(2)],num_delay);
den=conv([1 c(3)+1/Var(1) c(3)*1/Var(1)],den_delay);
den=abs(den);
[Ak,Bk,Ck,Dk]=tf2ss(num,den);
%
%
%%%%%%%%%%%%%%%%%%%%%%%%%%%%%%%%%%%%%%%%%%%%%%%%%%%%%%%%%%%%%%%%%%%%%%%%%%
%                              Compute J                                %
%%%%%%%%%%%%%%%%%%%%%%%%%%%%%%%%%%%%%%%%%%%%%%%%%%%%%%%%%%%%%%%%%%%%%%%%%%
%
sizeak=size(Ak);
sizeac=size(Ac);
sizeag=size(Ag);
A=[Ac,zeros(sizeac(1),sizeag(1)),Bc*Ck;zeros(sizeag(1),sizeac(1)),Ag,zeros(sizeag(1),sizeak(1));-Bk*Cc
,Bk*Cg,Ak];
E=[zeros(sizeac(1),2);Bg,zeros(sizeag(1),1);zeros(sizeak(1),1),Bk];
L=E*Noise*E';
X=lyap(A,L);
m=sizeak(1);
p=sizeac(1);
f=sizeag(1);
n=p+f;
term1=0;
term2a=0;
term2b=0;
term2c=0;
for i=1:m
 for j=1:m
  term1=term1+Ck(1,i)*Ck(1,j)*X((n+i),(n+j));
end;end
for i=1:f
 for j=1:f
  term2a=term2a+Cg(1,i)*Cg(1,j)*X((p+i),(p+j));
end;end
for i=1:p
 for j=1:p
  term2b=term2b+Cc(1,i)*Cc(1,j)*X(i,j);
end;end
for i=1:f
 for j=1:p
  term2c=term2c+Cg(1,i)*Cc(1,j)*X((p+i),j);
end;end
J=R*term1+Q*term2a+Q*term2b-2*Q*term2c;
RMS=term2a+term2b-2*term2c;
return
```

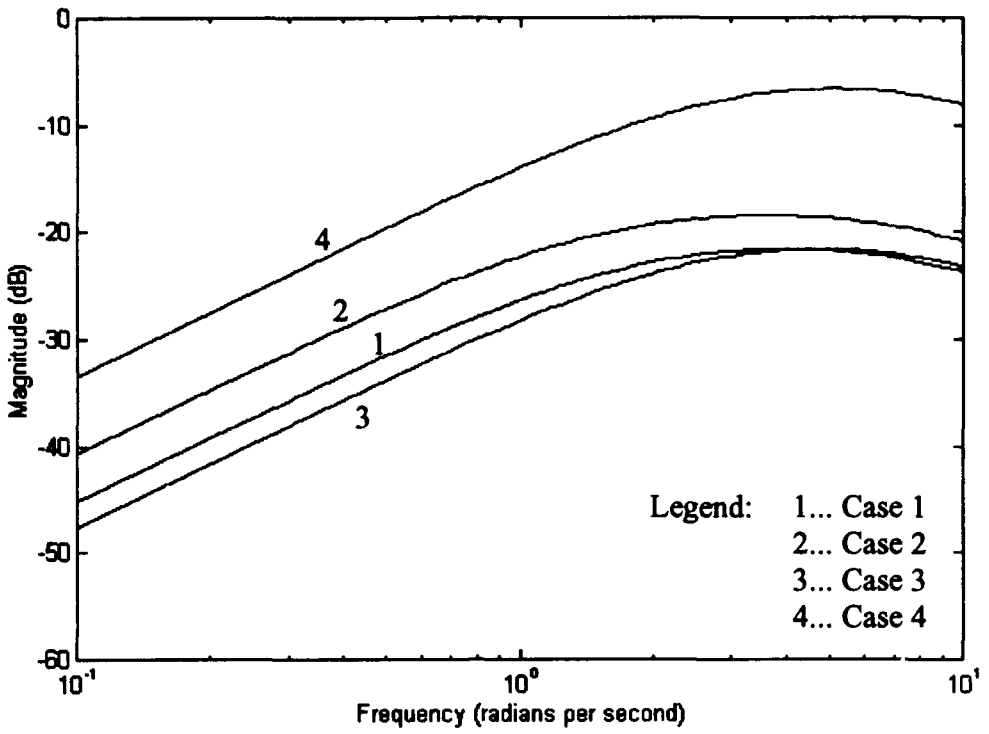

Figure G-1. Bode Magnitude Plot of Predicted Pilot Describing Functions -- Sub-Optimal Pilot Model Cases 1 Through 4

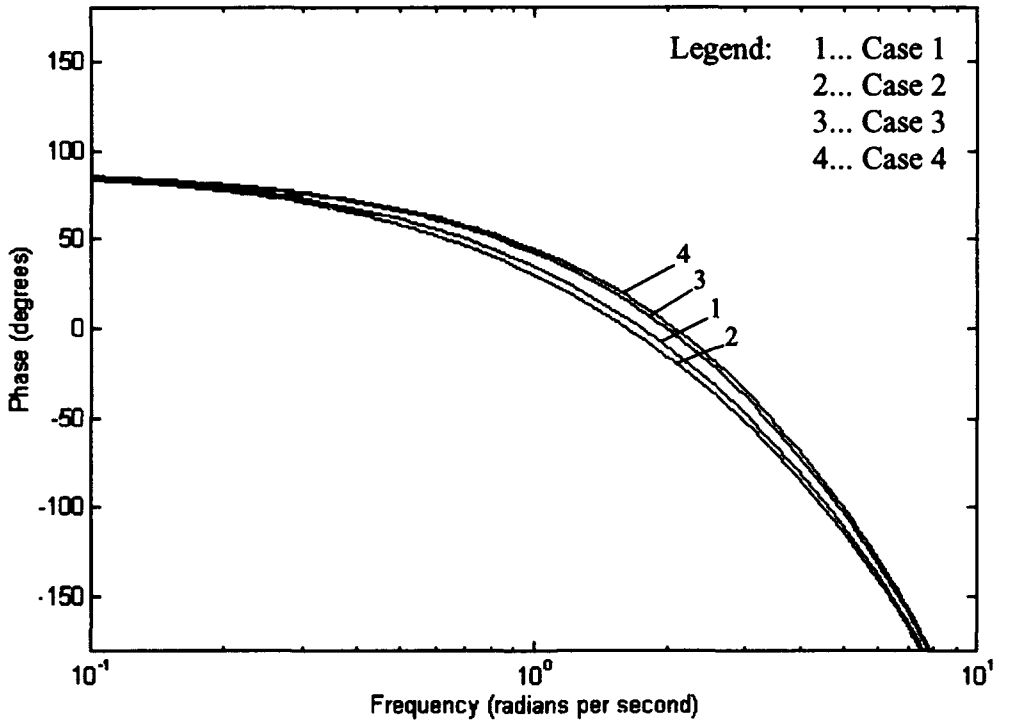

Figure G-2. Bode Phase Plot of Predicted Pilot Describing Functions -- Sub-Optimal Pilot Model Cases 1 Through 4

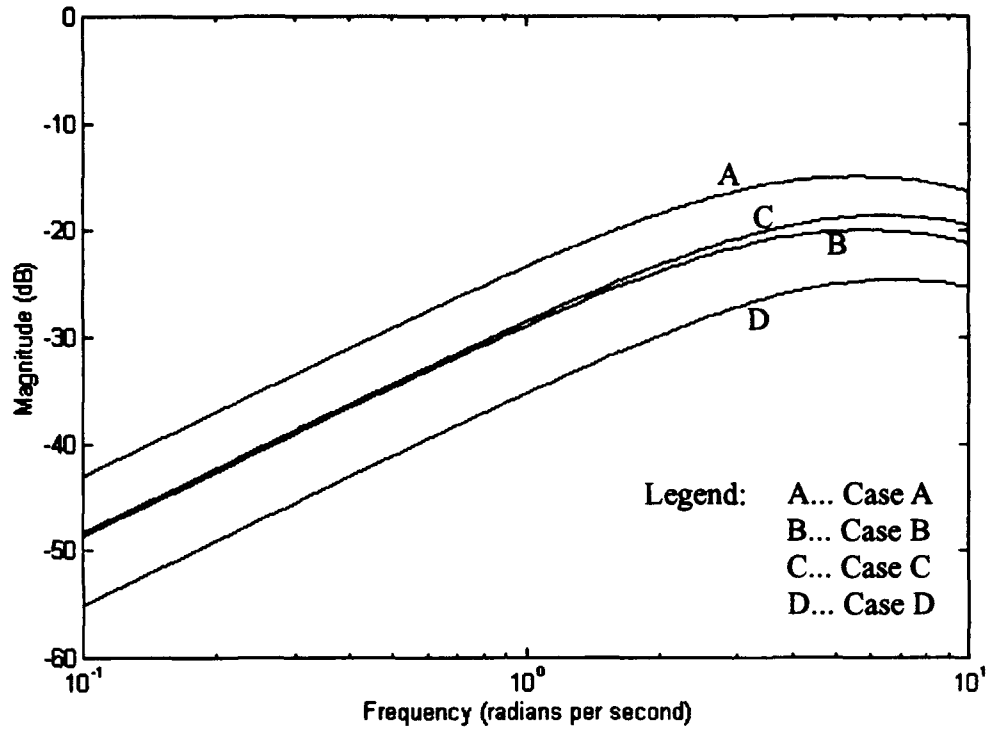

Figure G-3. Bode Magnitude Plot of Predicted Pilot Describing Functions -- Sub-Optimal Pilot Model Cases A Through D

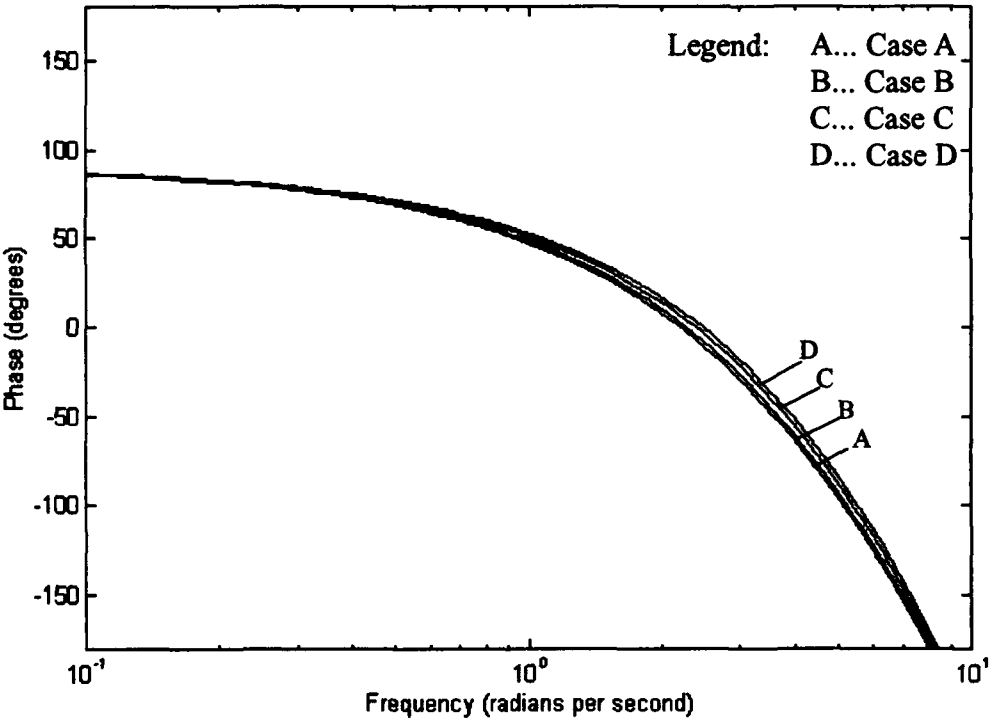

Figure G-4. Bode Phase Plot of Predicted Pilot Describing Functions -- Sub-Optimal Pilot Model Cases A Through D

Bibliography

1. Bernstein, Dennis S. and David C. Hyland. "Optimal Projection Approach to Robust Flexible Structure Control Design," in *Mechanics and Control of Large Flexible Structures.* Ed. A. Richard Seebass. Washington, DC: American Institute of Aeronautics and Astronautics, 1990.

2. Cooper, George E., and R. P. Harper, Jr. *The Use of Pilot Rating in the Evaluation of Aircraft Handling Qualities.* NASA TN D-5153. 1969 (AD-689 722).

3. Dailey, Lane R. and others. "Lecture Notes for the Workshop on H-Infinity and Mu Methods for Robust Control," *1990 American Control Conference.* San Diego: May 1990.

4. Dennis, J. E., Jr. and D. J. Woods. *New Computing Environments: Microcomputers in Large-Scale Computing,* Ed. A. Wouk. New York: SIAM, 1987.

5. Department of Defense. *Military Standard, Flying Qualities of Piloted Vehicles.* MIL-STD-1797A. Washington: GPO, January 1990.

6. Dillow, James D. and Douglas G. Picha. *Application of the Optimal Pilot Model to the Analysis of Aircraft Handling Qualities.* AFIT-TR-75-4. Wright-Patterson AFB OH: Air Force Institute of Technology, August 1975 (AD-B086 200).

7. Edkins, Craig R. and others. *Human Pilot Response During Single and Multi-Axis Tracking Tasks.* AFFTC-TLR-93-41. Edwards AFB CA: Air Force Flight Test Center, December 1993 (AD-A275 080).

8. Hess, Ronald A. "Prediction of Pilot Opinion Ratings Using an Optimal Pilot Model," *Human Factors,* 19: 459-475 (October 1977).

9. Jenkins and Watts. *Spectral Analysis and Its Applications.* New York: Holden-Day, 1968.

10. Kleinman, D. L., S. Baron, and W. H. Levison. "An Optimal Control Model of Human Response, Part I & II," *Automatica,* 6: 357-383 (May 1970).

11. Kwakernaak, Huibert and Raphael Sivan. *Linear Optimal Control Systems.* New York: Wiley-Interscience, 1972.

12. Liebst, B. L. Class Notes, SENG 665, Multivariable Control Theory. School of Engineering, Air Force Institute of Technology, Wright-Patterson AFB OH, Winter 1992.

13. Maciejowski, J. M. *Multivariable Feedback Design.* Wokingham, England: Addison-Wesley, 1989.

14. McRuer, Duane T. and Ezra S. Krendel. *Dynamic Response of Human Operators.* WADC-TR-56-524. Wright-Patterson AFB OH: Wright Air Development Center, October 1957 (AD-110-693).

15. McRuer, Duane, Ezra Krendel, and William Reisener, Jr. *Human Pilot Dynamics in Compensatory Systems: Theory, Models, and Experiments with Controlled Element and Forcing Function Variations.* AFFDL-TR-65-15. Wright-Patterson AFB OH: Air Force Flight Dynamics Laboratory, July 1965 (AD-470 337).

16. McRuer, Duane T. and E. S. Krendel. *Mathematical Models of Human Pilot Behavior.* AGARD-AG-188. January 1974 (AD-A775 905).

17. McRuer, Duane T. and H. R. Jex. "A Review of Quasi-Linear Pilot Models," *Transactions on Human Factors in Electronics,* 8: 231-248 (September 1967).

18. Mitchell, D. G. and others. *Effects of Cockpit Lateral Stick Characteristics on Handling Qualities and Pilot Dynamics.* NASA CR-4443. June 1992 (NTIS, N-92-28584).

19. Mitchell, David G., Bimal Aponso, and Roger Hoh. *Minimum Flying Qualities, Vol. I: Piloted Simulation Evaluation of Multiple Axis Flying Qualities.* WRDC-TR-89-3125. Wright-Patterson AFB OH: Air Force Flight Dynamics Laboratory, January 1990 (AD-A218 560).

20. Ridgely, D. Brett and Siva S. Banda. *Introduction to Robust Multivariable Control.* AFWAL-TR-85-3102. Wright-Patterson AFB OH: Flight Dynamics Laboratory, February 1986 (AD-A165 891).

21. Seckel, Edward and others. *Human Pilot Dynamic Response in Flight and Simulator.* WADC-TR-57-520. Wright-Patterson AFB OH: Wright Air Development Center, August 1958.

22. Smith, R.E. *Effects of Control System Dynamics on Fighter Approach and Landing Longitudinal Flying Qualities, Vol. 1.* AFFDL-TR-78-122. Wright-Patterson AFB OH: Air Force Flight Dynamics Laboratory, March 1978 (AD-A067 550).

23. Smith, R. E. and S. K. Sarrafian. "Effect of Time Delay on Flying Qualities: An Update," *Journal of Guidance, Control, and Dynamics,* 9: 578-584 (September-October 1986).

24. Smith, Ralph H. *A Theory for Handling Qualities with Applications to MIL-F-8785B.* AFFDL-TR-75-119. Wright-Patterson AFB OH: Air Force Flight Dynamics Laboratory, October 1976 (AD-A040 940).

Vita

Captain Craig R. Edkins was born in Sarasota, Florida on 15 September 1962. He graduated from high school in Fairview, Oklahoma, in 1980 and attended the U.S. Air Force Academy, graduating with a Bachelor of Science Degree in Astronautical Engineering in May of 1984. After attending Undergraduate Pilot Training, Captain Edkins served as a pilot on the KC-135 at Barksdale AFB, Louisiana. He eventually cross-trained into the KC-10, where he served as an aircraft commander and instructor pilot until his selection for the joint Air Force Institute of Technology -- Test Pilot School Course in February of 1991. While in Louisiana, he obtained a Master's Degree in Business Administration and Finance from Louisiana Tech. University. Captain Edkins has extensive operational experience in the KC-135 and KC-10, including missions in support of Desert Shield, Desert Storm, and Just Cause. He also flew missions supporting Soviet bomber intercepts over Iceland during the Cold War and in support of reconnaissance flights during the Iran-Iraq War. Captain Edkins' decorations include the Air Medal, the Aerial Achievement Medal, the Meritorious Service Medal, the Air Force Commendation Medal, and numerous campaign medals. Captain Edkins graduated from the USAF Test Pilot School in December of 1993, having flown over thirty different types of aircraft. He currently serves in the 419th Test Squadron, Edwards Air Force Base, California as an experimental test pilot on the B-1B Lancer.

Permanent Address:
C/O USAF Test Pilot School
220 S Wolfe Ave
Edwards AFB, CA 93524-6458